Adaptation Strategies to Climate Change in the Tropics: Analysis of Two Multifactorial Systems (High-Altitude Andean Ecosystems and *Plasmodium falciparum* Malaria Infections)

Daniel Ruiz Carrascal

Submitted in partial fulfillment of the
requirements for the degree of
Doctor of Philosophy
in the Graduate School of Arts and Sciences

COLUMBIA UNIVERSITY

2013

ABSTRACT

Adaptation Strategies to Climate Change in the Tropics: Analysis of Two Multifactorial Systems (High-Altitude Andean Ecosystems and *Plasmodium falciparum* Malaria Infections)

Daniel Ruiz Carrascal

In this dissertation I focus my analyses of adaptation strategies to climate change on two areas of primary concern: (i) high-altitude ecosystems of the Tropical Andes, with particular interest in the so-called *páramo* ecosystems; and (ii) mosquito-borne diseases, focusing on *Plasmodium falciparum* malaria infections. My research on páramo ecosystems follows a six-tiered approach to understand the linkages between the ongoing changes in climatic conditions and the disruptions affecting the integrity of high-altitude environments. Activities conducted herein include the analyses of changes in atmospheric stability and lifting condensation levels; the diagnosis of changes in hydrological regimes; the assessment of the extent of life zones; the analyses of increases in the occurrence and rapid spread of high-altitude fires; the assessment of the integrity of páramo ecosystems; and the analyses of increases in climatic stress. Activities are conducted for three key, strategic, protected high-altitude Andean environments of the Tropical Andes and for the full length of the Andes Cordillera. My research findings provide elements for an improved understanding of the potential responses of Andean ecosystems to the large-scale rapidly changing climate and to a strongly-influential natural interannual variability.

My research on *P. falciparum* malaria focuses on the analysis of the complexity behind the transmission dynamics of this multi-factorial disease. A deep understanding of such a complexity is possible through a holistic examination of the climatic, biological, socioeconomic, and demographic key-factors that are driving the fluctuations, changes and trends in malaria incidence. I propose a multi-model ensemble of malaria process-based models to offer useful information that could effectively guide decision-makers in risk assessment, malaria control investments and choice of interventions. I work on the integration of short-, medium- and long-term climate predictions into simulations of future changing scenarios, while helping to set up environment-informed systems at municipal level. My research thus provides a framework to: (a) compare the simulation outputs of several malaria process-based models with actual malaria morbidity profiles observed in several endemic- and epidemic-prone pilot sites in Colombia and Kenya; (b) explore the role that both climatic and non-climatic factors play in fluctuations and trends in malaria incidence, and analyze key confounders; (c) assess changing climate and future scenarios, and estimate the timing and possible magnitude of unexpected malaria outbreaks; (d) investigate current decision making processes, simulate the impact of indoor residual spraying campaigns, and provide quantitative goals for effective interventions; (e) conduct stability analysis; (f) pose and answer "what if" questions; and (g) stimulate an interactive learning environment to help decision makers learn.

Table of Contents

List of Charts, Graphs, Illustrations

Chapter 1

Chapter 2

Chapter 3

Chapter 4

Chapter 5 – Part I

Chapter 5 – Part II

Chapter 6

Acknowledgments

First of all, I would like to thank the members of my academic committee, Madeleine Thomson, Mark Cane and Douglas Martinson, for teaching me many concepts and guiding me through my research. I also would like to thank my external examiners, Arlene Fiore and Mercedes Pascual, for their critical analysis of this work. I also wish to thank the many IRI researchers and staff associates whose assistance made this research possible. In particular, I must thank Walter Baethgen, Tony Barnston, Michael Bell, Haresh Bhojwani, Lisette Braman, Pietro Ceccato, Steve Connor, Remi Cousin, John Del Corral, Michael Dervin, David DeWitt, Tufa Dinku, Katia Fernandes, Francesco Fiondella, Monica Garcia, Alessandra Giannini, Lisa Goddard, Paula Gonzalez, Arthur Greene, Brian Kahn, Bradfield Lyon, Gilma Mantilla, Ángel Muñoz, Hugo Oliveros, Andrew Robertson, Catherine Vaughan, Derek Willis, and Stephen Zebiak. Many of them honored me with a long-lasting friendship. I am also grateful to all the members of the steering committee of the InterAmerican Institute for Global Change Research and my colleagues at Escuela de Ingeniería de Antioquia and at the multiple institutions who provided me with a lot of support. Most of them are acknowledged in each of the chapters of this thesis. Many other Lamont researchers and postdocs deserve my thanks, particularly Dorothy Peteet, Anthony Del Genio, Arnold Gordon, David Rind, Laia Andreu, Kevin Anchukaitis, and Gordon Bromley. My classmates at DEES, who made my life in the US very enjoyable, are also acknowledged. In particular, I must thank Rafael Almeida, Anna Foster, Alison Hartman, Jason Jweda, Colin Kelley, Milena Marjanovic, Ivan Mihajlov, Amelia Paukert, Margaret Reitz, Sanpisa Sritrairat, Xianfeng Wang, and Wenchang Yang. And lastly, to all the members of my family, who have been always very supportive. I love you all.

Dedication

This dissertation is dedicated to the thin air of my high Andes Mountains and to the soon-to-be-a-memory of the Santa Isabel Nevado. And, of course, to you… yes, you!

Chapter 1[1]

Introduction – High-altitude Andean ecosystems and *Plasmodium falciparum* malaria infections: towards adaptation strategies to climate change

1.1. Overview

This chapter provides a general introduction to this dissertation by describing the complexities and sensitivities behind the integrity of high-altitude Andean ecosystems and the transmission dynamics of *Plasmodium falciparum* malaria infections. It also explores the potential consequences of changes in climatic conditions for ecosystem goods and services in the Tropical Andes, and for the severity and timing of *P. falciparum* malaria outbreaks. The chapter then presents the aims, objectives and methodologies of this thesis, and explains how research activities can be integrated into ongoing adaptation efforts in the Tropics, such as conservation planning of *hotspot* protected areas and malaria integrated surveillance systems. Finally, this introductory section gives a brief overview of the different chapters.

[1] This chapter merges the research articles by Ruiz et al. (2008a and b), Herzog et al. (2010) and Anderson et al. (2011). Copies of the manuscripts are available in the digital backup of this thesis.

1.2. Complexities and sensitivities behind the integrity of high-altitude Andean ecosystems and the transmission dynamics of *Plasmodium falciparum* malaria infections

Many behaviors observed in the real world are functions and outcomes of complex systems, including social structures, human economies and biological and ecological systems. Complex systems are studied by many areas of mathematics, social and natural sciences, as well as by several interdisciplinary fields such as systems theory, complexity theory and systems ecology. The challenge of understanding and predicting the behavior of complex systems has steadily risen in importance, and mathematical models have played a significant role in such a process. Models provide a holistic view of the interactions within and between the components of a given system, offer a deeper understanding of entire systems and their responses, and help to explain a wide range of system behaviors, even providing numerous insights into surprising and counterintuitive system outcomes.

Feedback mechanisms, nonlinearities, time delays, and high sensitivities (all mutually- and inter-dependent) are intrinsic characteristics of complex systems. Positive feedbacks, i.e. those that can amplify the effects of small changes in an external forcing, have gained a lot of attention. The academic community has already studied, for instance, numerous positive feedback mechanisms in the climate system, including the ice-albedo self-reinforcing cycle and the water vapor feedback (see, for instance, Hansen et al., 1993; Colman, 2003; Soden and Held, 2006; Roe and Baker, 2007). In the study of the Earth's climate system, numerous analyses have explored the nonlinearities driven by disproportional inputs and outputs, multiple equilibrium points, and episodic and abrupt changes (e.g. Boyle, 2000; Moore et al., 2000). Also, numerous research projects have focused on the role that time delays play in the function of complex

systems. For instance, the scientific community has studied time delays in the carbon cycle and their role in the context of long-term climate change (Bopp et al., 2002; Joos et al., 2003). Lastly, sensitivities have been recently explored to analyze how human activities are probably pushing the climate system to a state where the change could be potentially dangerous (e.g. Hansen et al., 2007). How positive feedbacks, nonlinearities, changes in time delays, and high sensitivities affect the dynamics or integrity of specific ecological systems is however less studied. These new areas of knowledge should be embraced if we want to move forward in the assessments of the role that human activities are playing in the current patterns of global environmental change.

In this thesis I focus my analysis on two areas of primary concern: (i) high-altitude ecosystems of the Tropical Andes, with particular interest in the so-called *páramo* ecosystems; and (ii) mosquito-borne diseases, focusing on *Plasmodium falciparum* malaria infections. A brief description of the complexities and sensitivities inherent to these two critical areas of interest is presented below. My research on páramos complements previously published research literature describing the complexity of the Andean climate and the main physical mechanisms interacting over the tropical Andes (e.g. Aceituno, 1988 and 1989; Poveda and Mesa, 1997a; Curtis and Hastenrath, 1999a and 1999b; León et al., 2000; Vuille et al., 2000a and 2000b; Falvey and Garreaud, 2005; Garreaud and Aceituno, 2007). Even though there is increasing evidence of changes in hydrological regimes in the region (e.g. Francou et al., 2003; Pabón, 2003 and 2004; Vuille et al., 2003; Buytaert et al., 2006) and an apparent upward shift in the orographic cloud band (Barry and Seimon, 2000), efforts still need to be done to study the vertical processes on the slopes of the Andes, and analyze important data from weather stations deployed in the Andean highlands. It is also important to consider that significant amounts of collected data are not available for analysis because they are still in analog format and/or have not been quality

controlled. These data, along with other sources of information such as remote sensing or palaeoclimate records, could help reconstruct the past and recent Andean climate and better understand the complex climate variability in the region. This thesis follows a six-tiered approach to understand the linkages between the ongoing changes in climatic conditions and the disruptions affecting the integrity of high-altitude environments. Activities conducted herein include the analyses of changes in atmospheric (in)stability and lifting condensation levels; the diagnosis of changes in hydrological regimes; the assessment of the extent of life zones; the analyses of increases in the occurrence and rapid spread of high-altitude fires; the assessments of the integrity of páramo ecosystems; and the analyses of increases in climatic stress. Analyses conducted herein provide some elements for an improved understanding of the potential responses, at subregional and regional spatial scales, of Andean ecosystems to the large-scale rapidly changing climate and to a strongly-influential natural interannual variability. In other timescales, analyses documented here contribute to improvements in the comprehension of convection processes in the Andean region, which might in the long run enhance our current capacities to model and predict the future climate with higher resolution.

My research on *P. falciparum* malaria focuses on the analysis of the complexity behind the transmission dynamics of this multi-factorial disease. A deep understanding of such a complexity is possible through a holistic examination of the climatic, biological, socioeconomic, and demographic key-factors that are driving the fluctuations, changes and trends in malaria incidence. In this context, numerous mathematical models have been used to try and represent the causal relationship between climatic and socio-economic drivers and malaria outcome (see a brief description of some well-known malaria process-based models in the supplementary material). Despite inherent limitations in disease transmission modeling activities due in part to

the impossibility of perfectly representing all transmission components, including initial conditions, as they occur in the real world, we may yet find value in such exercises particularly to indicate opportunities for more effective control investment and intervention both in the immediate and medium term. However, instead of using individual models in isolation we may gain more useful insights by developing 'ensembles' of different models, where biases in one model may be compensated for by biases in other models and where each model may be rerun using a different set of initial starting conditions (e.g. using different values for the initial infectious population). In this way the combined outputs (represented as probability distributions) may offer useful information to effectively guide decision-makers in risk assessment, malaria control investments and choice of interventions. This approach has been widely used in seasonal climate forecasting where it has been shown to be an effective means of improving model predictions as well as demonstrating the level of uncertainty associated with model outputs (Hagedorn et al., 2005; Doblas-Reyes et al., 2005). Such multimodel ensemble seasonal forecast outputs have already been applied to simple statistical models based on malaria incidence and rainfall (Thomson et al., 2006) for use in malaria control planning. Given the complexity of malaria transmission and the need for mathematical models for predicting the impact of interventions, I apply the same rationale for using a multimodel ensemble approach in the malaria forecasting. My research thus provides a framework to compare the simulation outputs of several malaria process-based models with actual malaria morbidity profiles observed in several endemic- and epidemic-prone regions; assess changing climate and future scenarios; simulate the impact of indoor residual spraying campaigns; conduct stability analysis; and stimulate an interactive learning environment.

1.2.1. High-altitude Andean ecosystems

The Andean complex topography, combined with elevational and latitudinal gradients, results in varied physical conditions that create unique mountain habitats. These environments harbor extraordinary biological and cultural diversity, a vast mosaic of ecosystems, and even multiple barriers for species movements. Over 45,000 plant and 3,400 vertebrate species (excluding fish) have been reported in, specifically, the tropical Andean ecosystems, representing approximately 15% and 12% of species known globally, respectively. Nearly half of these species are endemic (Myers et al., 2000). For the northern and central Andes, in particular, Josse et al. (2009) recognized 133 different ecosystem types, classified into nine major groupings: páramo in the northern Andes (in altitudes above 3,000 m); high-Andean *superpáramo* throughout the tropical and temperate Andes (>4,500 m); humid puna in northern Peru to Bolivia and Argentina (2,000-6,000 m); dry *puna* in southern Peru through Bolivia to northern Argentina (2,000-6,000 m); cloud forests throughout the tropical Andes (1,000-3,000 m); seasonal Andean forests, particularly in Peru and Bolivia (800-3,100 m); dry Andean forests in the inter-Andean valleys of Ecuador, Peru, and Bolivia (800-4,100 m); heavily human-intervened inter-Andean valleys (1,900-3,500 m); and highly diverse aquatic habitats (lakes, wetlands and peatlands) all across the tropical Andes. Today, millions of people depend on tropical Andean ecosystems as a source of fresh water, hydroenergy, timber, medicinal plants, and food (all of them provisioning services). And this dependence is not new: the well-being of Andean human populations has been linked to the functioning of these ecosystems over a history that spans more than 10,000 years. Local communities also depend on many other environmental goods and services, including climate regulation, carbon storage, flood control, down-slope safety, and water purification (regulating services); soil formation, photosynthesis, nutrient cycling, pollination,

and waste disposal (supporting services); and recreation, aesthetics, and spiritual values (cultural importance) (Millennium Ecosystem Assessment, 2005; Josse et al., 2009).

Unfortunately, the range of natural climate variability in the tropical Andes has started to exceed historically documented thresholds. Of particular concern is the general warming trend and its implications for the integrity of ecosystems and the human populations that depend on them. Climate projections using regional models suggest a more pronounced increasing trend at higher altitudes (above 4,000 m) on both the Eastern and Western slopes of the Andes (Solman et al., 2008; Marengo et al., 2009; Urrutia and Vuille, 2009). In many parts of the tropical Andes the expected magnitude of this warming is similar to that predicted for the high-latitudes in the northern hemisphere (Bradley et al., 2004 and 2006). However, the consequences of such a disruption may be felt much sooner in the Andes than those in the North Pole region, because of the diverse nature of Andean ecosystems and the effects that changes in these environments will have on a large human population, which is more directly dependent on the services they provide (Vuille et al., 2008) and more economically vulnerable.

Certain characteristics of each grouping of tropical Andean ecosystems make them uniquely vulnerable to changes in climatic conditions. Climate change will likely affect ecosystem structure and composition, both in terms of the physical environment and biological communities, as well as species and individuals within ecosystems. First, shrinking or disappearing ecosystems in terms of their geographic areas may be of concern for species in all ecosystems, but may be especially critical in páramo, superpáramo, and humid and dry puna. In the high Andean superpáramo ecosystem, in particular, warming temperatures and changing physical environments could constrict or eliminate suitable habitats, forcing species to migrate to small and distant summit areas. A 3°C-increase in temperature, commonly seen in climate

change projections, could result in a theoretical 600 m upward movement of species. The resulting loss of habitat area for species that would have to move 'up-the-hill' to keep up with their current optimum habitat could significantly affect their viability. If changes continue, several species could become critically endangered as a result of habitat reduction, or simply face extinction. Even though major changes are predicted for páramo ecosystems, based in part on their island-like distribution and highly endemic biota, cloud forest ecosystems are increasingly becoming highly vulnerable given their dependence on the level of cloud bases, which is predicted to shift with climate change. Rising cloud bases and a reduction in horizontal precipitation could lead to decreased moisture, with consequences for diverse epiphytes and the animal communities they support. Climate change could thus lead to the collapse of cloud forest populations (which are adapted to narrow elevational ranges on steep slopes) or increased their vulnerability to extinction.

In terms of biological communities, climate change could threaten species' survival and could lead to major shifts in community composition. Altitudinal migrations are already being observed, in terms of temporary shifts for breeding or more permanent colonization of higher elevation ecosystems (Seimon et al., 2007; Hardy and Hardy, 2008). Newly colonizing species can alter the identity and strength of direct and indirect biotic interactions (Levine et al., 2004; White et al., 2006), as well as change the physical structure of ecosystems (Crooks, 2002). They could also have implications for ecosystem structure (e.g., in terms of community dynamics) and function (e.g., the role of different species in maintaining ecosystem processes), and they could alter the strength of disturbance regimes (Brooks et al., 2004). Formation of no-analog communities (e.g., species assemblages that are currently unknown to occur) is also a potential outcome of climate change (Fox, 2007; le Roux and McGeoch, 2008).

Changes in climatic factors are also likely to influence abiotic functional processes of ecosystems. Changes in precipitation regimes could be accompanied by increased erosion and landslides. Páramo water retention and filtration capacity could be affected by increases in the ratio of vertical (rain) to horizontal (wind-blown mist) precipitation. Also important is a rise in the elevational level of solid (snow, graupel) precipitation, particularly in those areas with vegetation and geomorphology in equilibrium with precipitation that slowly infiltrates as it melts. A shift to liquid precipitation leads to increases in runoff and erosion. Also, páramos and their wetlands could, in the short term, shift from being sinks to sources of carbon with warmer and drier conditions. Lastly, the synergistic, interactive effects of climate change with other stressors to tropical Andean ecosystems—such as habitat modification, forest clearing, river alteration, mining, grazing, exotic species, and water pollution— may be severe and unexpected. It remains to be seen if and how changing climatic factors will interact with biotic (predation, disease, poor food supply) and abiotic (suboptimal habitat conditions) stressors to affect tropical Andean species. Beyond the species level, páramos provide an example of the potential for interactive effects of climate change with human-induced stressors at a larger scale. As climate warms, their lower margins may become more suitable to agriculture and thus more threatened by human activities. A combination of climate change and increased human influence on the páramo may also increase the spread of anthropogenic fires, considered a serious threat to integrity of this ecosystem.

As mentioned before, in the tropical Andes and elsewhere the well-being and progress of human populations depend on a typically high degree of integrity or health of ecosystems. As human demands on ecosystems increase with growth of population and consumption, and increased technology, there is greater potential for ecosystem degradation and intensification of

trade-offs related to ecosystem services. Climate change adds another dimension, as an additional driver of ecosystem change and a cause of shifts in human resource use. Climate change could threaten tropical Andean ecosystems' capacity to provide ecosystem services by causing (just to mention key disruptions): (i) vast changes in water-related services due to the effects of warming on mountain glaciers and Andean wetlands, and the degradation of vegetative cover; (ii) shifts in services related to agricultural production as a consequence of changing climatic conditions and patterns of human settlement (e.g. intensification of agriculture in existing cropland or grazing areas, expansion of the agricultural frontier both upwards to higher elevations and downslope into lowland tropical forests, and increased damage by insect herbivores and pests under warmer conditions and rises in atmospheric CO2; Pérez et al., 2010); (iii) decreased down-slope stability and safety due to shifts from solid to misty, to more liquid precipitation and increased occurrence of extreme rainfall events; (iv) changes in the ability to provide cultural services and degradation of the identity of natural areas (e.g, visual, iconic biodiversity elements); (v) changes in the contribution of Andean ecosystems to climate regulation due to decreases in the ability of páramo ecosystems and wetlands to store or sequester carbon; (vi) shifts in species distribution and abundance affecting biodiversity-related ecosystem services (Fjeldså, 2007); and (vii) exacerbation of climate change impacts on ecosystems due to shifts in human behavior (through feedbacks).

1.2.2. *Plasmodium falciparum* malaria infections

Climate change is considered to be a major global environmental problem that could have significant effects on human health (Martens, 1997; Patz et al., 2005). One of its potential,

ecologically mediated, impacts is the change in the incidence and the spatial distribution of climate-sensitive vector-borne diseases. Malaria, dengue fever, leishmaniasis, and yellow fever are among those diseases considered most likely to increase as rainfall patterns change and global temperatures increase (Epstein, 2000). Changes in climatic conditions could influence the behavior of vectors (proliferation and frequency of blood meal feedings), their geographical distribution (expansion into formerly vector-free territories), and the development rate at which pathogens inside the mosquitoes mature (Epstein, 2000).

Diseases caused by pathogens that spend part of their life cycle outside humans or other warm-blooded hosts are particularly climate-sensitive (Patz et al., 2000; WHO, 2004). Malaria, for instance, is caused by protozoan parasites (*Plasmodium*) that are transmitted by the bite of infected adult female *Anopheles* mosquitoes. The disease is widespread in tropical and subtropical regions, infects between 300 and 500 million people every year, and causes an estimated 1–3 million deaths annually, mostly among young children in Sub-Saharan Africa (WHO, 1994). The most serious forms of the disease are caused by *Plasmodium falciparum* and *P. vivax* parasites. These micro-organisms multiply within the human red blood cells, causing symptoms that include fever, anaemia, chills, flu-like illness, and in severe cases, coma and death. Malaria transmission, distribution, endemicity, and seasonality have been widely linked to prevalent climatic conditions (e.g. Aron and May, 1982; Macdonald, 1957; Dye, 1992), and frequently reported to be strongly affected by extreme weather events such as those associated with El Nino-Southern Oscillation (Poveda and Rojas, 1997b; Bouma et al., 1997; Poveda et al., 2000 and 2001). It is generally accepted that malaria transmission can be reduced by preventing mosquito bites with bed nets and insect repellents, by spraying insecticides inside houses and

draining standing water where the mosquitoes lay their eggs (Macdonald 1957), or by treating malaria primary cases.

Several articles have suggested that malaria is likely to be the vector-borne disease most sensitive to long-term climate change (Lindsay and Birley, 1996; Martens, 1997; Martens et al., 1999; Patz et al., 2000 and 2002): 'ongoing warming will have enlarged the zone of potential malaria transmission from an area containing 45% of total world's population to an area containing about 60%' by 2100 (Epstein 2000). In 2003 the WHO indicated in the summary document 'Climate change and human health – risks and responses' that increases in global temperatures of 2–3°C, already predicted by General Circulation Models, would (a) alter the geographic range (changes in both latitude and altitude) of vector-borne diseases, increasing 'the number of people who, in climatic terms, are at risk of malaria by around 3–5%'; (b) change the seasonality (timing of peaks in transmission) of the disease in many currently endemic and epidemic areas; and (c) increase the seasonal duration of malaria in epidemic-prone regions. There is now a growing body of literature arguing that global climate change could be a major driving mechanism behind increasing incidence of this disease (Patz et al., 2000). The WHO (World Health Report 2002) suggested that global warming has been causing deaths and disability-adjusted life years since the mid-1970s, and estimated that an increase of about 6% of malaria incidence, during 2000, in some middle-income countries could be attributed to climate change.

As scientific and technological advances permit better predictions of climatic conditions over the immediate term, there is 'an evident opportunity to incorporate climate forecasting capabilities into control plans' aimed at reducing the human health impacts of malaria endemicity and outbreaks (Poveda et al., 2001). Malaria, however, is not only climate-sensitive.

It is a highly complex multi-factorial disease. Changing social and economic conditions, including land use changes (which affect the local micro-climate), human migration, access to interventions (including insecticide-treated bed nets, effective medicines, effective indoor-residual spraying, environmental management and effective drugs), nutritional status and co-infection with other parasitic diseases, all have significant effects on the general epidemiology of malaria, the vulnerability of populations and on the timing and severity of disease outbreaks. The effect of global warming on malaria transmission has been generally examined, however, only in terms of increased vectorial capacity, ignoring for instance that the 'impact of temperature changes could be disproportionately higher in populations with low levels of antimalarial immunity' (Yang and Ferreira, 2000). In many tropical endemic areas the effect of increasing temperatures may be less important than changes in socioeconomic conditions (Yang and Ferreira, 2000; Thomson and Connor, 2001; Ter Veen, 2002; Hay et al., 2002). The WHO (2003) has also suggested that 'most temperate regions would remain unsuitable for transmission because either they remain climatically unsuitable or socioeconomic conditions are likely to remain unsuitable for reinvasion'.

Simulation outputs of Yang's malaria transmission model (Yang, 2000), for instance, suggest that socioeconomic factors could have greater impact on malaria incidence than relevant climatic conditions. Yang's model assesses the proportionate increase in malaria incidence that might be expected in a hypothetical population at risk under several qualitatively dissimilar climatic and socioeconomic scenarios. Yang and Ferreira (2000) conducted the analyses by assuming, initially, three levels of human exposure to the mosquito's population: RISK=0, 1 and 2, each of them reflecting representative areas of low-, intermediate- and high-risk contact, respectively. See figure 1. The social and economic conditions (SEC) were subdivided into three

major categories: SEC=0, 1, and 2, each of them representing good, intermediate, and deteriorating conditions prevailing in the communities at risk. SEC reflects, for instance, 'the health care system effectiveness in identifying promptly new malaria cases', and the sanitation conditions and economic activities of the communities at risk (Yang and Ferreira, 2000). As a final point, climatic conditions were represented in Yang's model by three major categories: low, intermediate and high ambient temperatures. The authors studied the model by analyzing its steady state equilibrium values and its dynamic state, both highly dependent on the values of the basic reproduction rate (R_o). In the steady analysis the model exhibits an equilibrium point where malaria reaches a specific endemic level. As SEC and temperature changes are both subdivided into three classes, there are nine possible combinations of the parameters of Yang's model for each level of risk. Communities living in areas with low risk of contact exhibit transitions from disease-free conditions for good and intermediate SEC, to malaria at low endemic levels for deteriorating conditions. Communities living in areas with intermediate risk of contact exhibit transitions from disease-free conditions for good SEC, to malaria at low endemic levels for intermediate and deteriorating conditions. Finally, communities living in areas with high risk of contact always experience disease at endemic levels; changes from intermediate to deteriorating SEC lead to transitions from disease at intermediate prevalence to malaria at higher endemic levels. It is observed, in general, that changes in social and economic conditions are more harmful than increases in ambient temperatures (see Yang and Ferreira, 2000 for further analyses).

In the dynamic analysis Yang and Ferreira (2000) analyzed the asymptotic equilibrium values reached by the system for three dissimilar situations. See figure 2. In the malaria-free community but potentially under low risk, the disease is eradicated during the first year after the

onset of an epidemic, despite the initial high prevalence (Yang and Ferreira, 2000). In the community where malaria is at low endemic levels but the risk of contact is intermediate, the outbreak is reached approximately a couple of years after the introduction of malaria cases. Thus, malaria can be eliminated from the community during the first days of a controlling effort by driving the Ro to values below unity. In the community where malaria is at high-endemic levels and the risk of contact is also high, the outbreak is reached more rapidly and it is more accentuated (Yang and Ferreira, 2000).

1.3. Aims, objectives and approach

As mentioned before, this thesis aims to analyze the complexities and sensitivities behind two key multi-factorial systems: high-altitude Andean ecosystems and *Plasmodium falciparum* malaria infections. I first center my attention on the self-reinforcing cycle that results from changes in atmospheric (in)stability in high-altitude environments, and the potential impacts (increased climatic stress) on the integrity of páramo ecosystems. I study near-term climate change trends derived from weather stations data and modeling simulation outputs, as well as from streamflow hydrological records, and biological data gathered in protected areas renowned for their exceptional biodiversity levels. Cloud cover conditions and sea surface temperatures data are also processed to support the analyses. Specific activities include the study of near-term and historical changes in Lifting Condensation Levels (LCL) and Convective Available Potential Energies; analysis of near-term and historical time-averaged conditions of atmospheric stability; and assessment of recent changes in the vertical profiles of water content and rainfall. All these activities are conducted at both local and regional scales.

Then I study the role that both climatic and non-climatic drivers play in the transmission dynamics of *P. falciparum* malaria infections, prevailing in various malaria-prone regions (pilot areas). I apply process-based mathematical models of environment-malaria interactions for several eco-epidemiological settings in order to examine the key-factors driving fluctuations, changes and trends in malaria incidence. Simulation runs of individual models and a multi-model ensemble include experiments for the highlands of Western Kenya and for various endemic-prone municipalities in Colombia. I also work on the development of environment-informed systems at local levels to help predict patterns of malaria risks in time (using observed weather), and I merge short-, medium- and long-term climate-based forecasts and predictions with integrated surveillance and control systems for malaria epidemic early detection and response. Along these objectives, specific activities proposed herein include the design of experiments to assess models' accuracies and predictive powers, the analysis of the role of uncertainty in the predictability of malaria outbreaks, and the validation of mathematical tools (structures, behaviors and policy-options).

1.4. Contributions to adaptation strategies

1.4.1. Adaptation measures and policy options to meet the anticipated impacts of climate change on high-altitude environments

The consequences of the loss of fundamental ecosystem services 'will be felt disproportionately by the poor, who are the most vulnerable to such environmental problem' (World Resources Institute, 2005). Colombia is a good example. Even though this nation is responsible for only 0.25% of the total global emissions of carbon dioxide to the atmosphere,

according to the First National Communication (NC1-2002) submitted to the United Nations Framework Convention on Climate Change-UNFCCC (Institute of Hydrology, Meteorology and Environmental Studies-IDEAM, 2002), Colombia is considered to be potentially one of the most seriously affected developing countries due to its high vulnerability to the negative impacts of climate change (World Bank Group, 2006). In the NC1-2002 the Colombian government identified high mountain ecosystems as one of the areas of primary concern.

Colombia is host to the largest stretch of páramos life zones in the planet (WBG, 2006). About 56% of the total extent is predicted to be seriously affected by increases in temperature by 2050 (WBG, 2006). Dramatic land use changes (i.e. clearing-off of high mountain Andean forests and páramos) caused by extensive agriculture and livestock grazing are also threatening the existence of these fragile reservoirs and ecosystems, and could be producing severe local climatic anomalies. To further complicate matters, glaciers in the areas of 'permanent' snow (above 4,500 m) are also expected to be affected by increases in temperature. In the NC1-2002, the IDEAM reported that the loss of the total Colombian glacier area had reached almost 80% since 1850, and it is expected that 78% of the remaining Colombian glaciers will be seriously affected by increases in temperature by 2050 (WBG, 2006).

The Colombian government is currently implementing policies, strategies and actions intended to ensure considerable levels of environmental goods and services in Colombian high-mountain ecosystems. The initiative aims at defining specific pilot adaptation measures and policy options to meet the anticipated impacts of climate change on these areas. Among its major goals, the initiative is strengthening the capability of the Colombian government to produce and disseminate continuous and reliable climate information relevant to high mountain ecosystems. Activities also aim to maintain high levels of biodiversity in these ecosystems, as well as to

ensure considerable levels of water supply, extremely needed to satisfy human consumption, agriculture activities, industrial processes, and hydropower generation.

Surface water supply in high-altitude watersheds has been considered an area of primary concern, not only in Colombia but also in several other Andean countries, according to priority sectors identified in the latest National Communications submitted by South American countries to the UNFCCC. Priorities include agriculture, low-lying coastal areas, water supply for human consumption, hydropower generation, and human health. See figure 3. Among many concerns, the South American governments have reported rapid shrinkage of almost all mountain glaciers, decreases in minimum and mean streamflows of rivers originated in the Andes Mountains, decreased hydro-power in highlands, and exacerbated water shortages during dry periods. Governments also address the multiple potential implications of climate change for water resources, including: lower water supply compared to demand, major increases in the number of months with hydrologic deficit, increased water needs for irrigation during longer dry periods, decreased recharge of aquifers, increased water stress and conflicts, incremental costs of water provision, and expected losses in regional hydropower generation.

1.4.2. Integrated Surveillance and Control Systems: the Colombian Initiative

In its first communication (NC1-2002) to the UNFCCC, the Colombian government also identified the human health as one of the areas of primary concern. The future climate scenario suggests a nationwide increase of 1–2°C in mean annual temperature by 2050, and variations in total annual rainfall records of about ±15%. As a consequence, Colombia is expecting a dramatic (further) increase in malaria incidence in not only its endemic-prone areas, but also in its

highlands where human populations are characterized by low immunity rates to malaria parasites. Colombia has proposed a very ambitious adaptation strategy to mitigate the possible adverse effects of climate change on human health: the National Integrated Surveillance and Control System (Instituto Nacional de Salud-INS de Colombia, 2005; Ruiz, 2005). This initiative is part of the project 'Integrated National Adaptation Pilot (INAP): High Mountain Ecosystems, Colombia's Caribbean Insular Areas, and Human Health' currently conducted and coordinated by the IDEAM. The public health strategy is based upon five linked components (see figure 4; Ruiz, 2005): an Early Warning System (EWS) Framework; climate forecast, monitoring and analysis of scenarios; epidemiological surveillance and control activities; early diagnosis and treatment of primary cases; and entomological surveillance and control activities. These components are supported by structural axes representing capacity building (primary education and local expertise) and process maintenance and continuity, and are articulated by a 'conveyor belt' representing the institutional networks and the financial strategies. The major phases of the implementation of this adaptation strategy include: the design of the EWS; the strengthening of institutional capacity; and the implementation of the knowledge management-, monitoring- and evaluation-system.

The national and international communities have been developing climate-based EWSs to provide local alerts of different magnitudes at inter-annual, annual, and seasonal timescales (Poveda et al., 2001; WHO, 2004). The major goal of these EWSs is to enhance malaria surveillance, improve control and response to epidemics, and to 'facilitate early, coupled and environmentally sound public health interventions' (Poveda et al., 2001). There has been a growing interest in developing frameworks within the EWSs that allow a continuous assessment of local risks of malaria transmission in the face of global climate change. Those frameworks,

however, have limited their focus to how climatic factors affect the transmission potential of mosquito vectors. Few efforts have explored the role both climatic and non-climatic contributors play in the dynamics of the disease and in the global increase of its incidence. Moreover, 'most tools were developed as pure research; therefore, neither the extent to which they address specific control decisions nor their utility for planning public health interventions is completely clear' (Yang, 2000).

The approach proposed for Colombia will make use of dynamical models that employ the established biological mechanisms of the transmission cycle of malaria parasites, to integrate climatic variables with demographic, epidemiological and entomological data routinely collected in malaria-prone areas. Therefore, the Integrated Surveillance and Control System will include climate forecasting capability, statistical models, eco-epidemiological mathematical models, and other promising tools to support campaigns and mitigation plans aimed at reducing human health impacts of sudden malaria outbreaks (Ruiz, 2005). Global forecasting models will be incorporated to estimate future climatic conditions with a lead time of no less than four to six months. In Colombia, the strategy will use such predictions to prevent the concomitant health effects of not only the warm phase of El Niño-Southern Oscillation (ENSO) phenomena, but also the non-ENSO climate variability. The eco-epidemiological models, on the other hand, will be used to: (a) understand the complexity of the disease, in order to evaluate spatial and temporal risks; (b) estimate the time of occurrence and severity (or possible magnitude) of unexpected malaria outbreaks; (c) analyze the major confounders of the overall driving factors that seem to be interacting to cause abrupt increases in malaria incidence (thus, interventions can be designed to address key-variables in order to reduce the vulnerability of human populations to epidemics); (d) investigate the current decision making process and provide quantitative goals for effective

interventions (timing and magnitude) adapted to the specific ecological circumstances of each endemic area (INS, 2005); (e) pose and answer "what if" questions; and (f), perhaps more important, help decision makers learn. The future goal of this eco-epidemiological initiative is to allow regional health authorities to assess the local risk of malaria transmission in the face of local and regional environmental changes, and help them to determine the most appropriate preventative actions that have to be taken in order to prevent epidemics before they begin (INS 2005). It is worth mentioning that these experiences could also be implemented for other vector-borne diseases, in which increases in incidence and prevalence are attributed to climatic forcing.

1.5. Chapters overview

Chapter 2. This chapter describes the main results of statistical and descriptive analyses that were conducted for a key protected high-altitude Andean environment in the Colombian Central Andes. Processed data included ground-truth weather station data, cloud cover conditions, streamflow hydrological records, sea surface temperatures (SSTs) observed in the tropical Indo-Pacific and Atlantic oceans, and biological (wildfires) data. Observatory and confirmatory analyses were conducted to detect statistically significant long-term linear trends, changes in the variance, and changes in the mean of observed historical time series. Spatial and altitudinal patterns of observed changes were also explored. Empirical Orthogonal Functions/Principal Component analyses were implemented to assess the major modes of spatio-temporal variability in SSTs. The chapter ends with a discussion on the changing climatic conditions faced by Colombian high-altitude ecosystems, as well as the anthropogenic stress on páramo environments and the general potential impacts on ecosystem integrity.

Chapter 3. This chapter describes the inferred historical conditions of atmospheric stability in three highly strategic high-altitude environments of the Tropical Andes, and explores the self-reinforcing cycle that results from local changes in stability conditions. Analyses include comparisons with modeling simulation outputs along the axis of the Andes Cordillera and sea surface temperature anomalies observed in the tropical Indo-Pacific and Atlantic basins. The first section discusses the hypothesis of potential changes, presents an overview of methods and data, and summarizes the evidence from near-term historical climate models' ensemble simulation runs. The second section discusses the near-term historical conditions of static instability, conditional instability and static stability in the experimental sites and their potential long-term changes. The third section assesses the historical changes in the Lifting Condensation Level and supports its discussion on the simulated changes in vertical profiles of water content and long-term changes in Convective Available Potential Energies. The last section hypothesizes the positive feedback mechanisms that are probably worsening the climatic conditions faced by high-altitude Andean environments. The chapter ends with a discussion on the research findings and the conclusions of the study.

Chapter 4. This chapter explores the role of long-term changes in climatic conditions in the increasing incidence of *Plasmodium falciparum* malaria in the highlands of Western Kenya. It starts with the main hypothesis on the potential drivers of observed changes in malaria morbidity profiles in the area under study and presents a brief overview of methods and data. The first part also provides a succinct description of various process-based models that have been proposed by the international scientific community to represent the transmission dynamics of *P. falciparum* malaria infections. Discussion includes the tools proposed by Ross-Macdonald (1957), Anderson and May (1991), Worrall, Connor, and Thomson (2007), and Alonso, Bouma

and Pascual (2010), which were all merged in a single four-model ensemble. Supplementary material includes, besides these four tools, the mathematical models proposed or discussed by Martens (1997), McKenzie et al. (1998), Yang (2000), Githeko and Ndegwa (2001), Ruiz et al. (2002a, 2002b, 2003, 2006), Ruiz and Yan (2003), Hoshen and Morse (2004), Chiyaka, Garira and Dube (2007), and Gomero (2008). Supplementary material also provides a discussion on exogenous variables and the required level of understanding of malaria transmission dynamics. The second section in this chapter characterizes the seasonality and long-term changes in *P. falciparum* malaria morbidity profiles observed in the selected highlands. The third section discusses the results of retrospective 30-year simulation experiments and provides an assessment of the impacts of changes in climatic conditions on malaria transmission dynamics. In particular, the multi-model ensemble is run with and without long-term climatic trends over the three-decade simulation period in order to address how much of a change in the size of epidemics could be attributed to changes in climatic conditions. The last section presents the advantages and limitations of the multi-model ensemble, and explores the role of uncertainty in the predictability of malaria outbreaks. The chapter ends with a discussion on the research findings and the conclusions of the study.

Chapter 5. This chapter focuses on the implementation of malaria dynamical models in four Colombian pilot sites with different eco-epidemiological settings. Activities were conducted as part of the Malaria Early Warning System framework that has been proposed in the Integrated National Adaptation Pilot project and the Colombian Integrated Surveillance and Control System. Chapter 5 has been divided into two parts: the description of study sites, and the description of preliminary results using observed weather and seasonal climate forecasts. The first part describes the main characteristics of *Plasmodium falciparum* malaria infections

observed in the endemic areas under study. Local characteristics include general profiles (natural resources and economic activities), malaria situation (predominant type of infection, malaria positive cases data, malaria incidence, and seasonality), climatic conditions (climatology, long-term trends), entomological conditions (primary and secondary vectors, mosquito densities, breeding sites, feeding frequencies, and preferences), inferred stability of malaria transmission, and key non-climatic factors (populations at risk, control campaigns and socioeconomic conditions). The second part summarizes the preliminary results of the implementation of malaria dynamical models. They include retrospective simulation experiments (base scenarios, changes in initial conditions, local settings, sensitivity analyses, and uncertainties) of at least 8-year simulation periods using observed weather data. The second part also provides a short description of the activities that were conducted to integrate short-, medium- and long-term climate predictions into simulations of future changing scenarios, and summarizes our experience in setting up environment-informed systems at municipal level. The chapter ends with a discussion on the research findings and the conclusions of our study.

Chapter 6. This chapter presents the general conclusions and final remarks of this dissertation, and describes some research activities that have resulted from the findings of this thesis.

References

Aceituno, P., 1988. On the functioning of the Southern Oscillation in the South American sector. Part I: surface climate. Monthly Weather Review 116: 505-524.

Aceituno, P., 1989. On the functioning of the Southern Oscillation in the South American sector. Part II: upper-air circulation. Journal of Climate 2: 341-355.

Anderson, E.P., J. Marengo, R. Villalba, S. Halloy, B.E. Young, D. Cordero, F. Gast, E. Jaimes, and D. Ruiz, 2011. Consequences of climate change for ecosystems and ecosystem services in the Tropical Andes. Pp. 1-18 in: Herzog S.K., R. Martínez, P.M. Jørgensen, and H. Tiessen (eds.). Climate change and biodiversity in the Tropical Andes. MacArthur Foundation, Inter-American Institute of Global Change Research (IAI) and Scientific Committee on Problems of the Environment (SCOPE), São José dos Campos and Paris, 348 pp., ISBN: 978-85-99875-05-6.

Aron, J. and R.M. May, 1982. The population dynamics of malaria. Anderson, R.M. (ed). The population dynamics of infectious diseases: theory and applications. Chapman & Hall, London, 139–179.

Barry, R., and A. Seimon, 2000. Research for mountain area development: climatic fluctuations in the mountains of the Americas and their significance. Ambio 29: 364-370.

Buytaert, W., R. Celleri, B. De Bievre, F. Cisneros, G. Wyseure, J. Deckers, and R. Hofstede, 2006. Human impact on the hydrology of the Andean páramos. Earth-Science Reviews 79: 53-72.

Bopp, L., C. Le Quéré, M. Heimann, and A.C. Manning, 2002. Climate-induced oceanic oxygen fluxes: implications for the contemporary carbon budget. Global Biogeochemical Cycles 16(2): 1022-30.

Bouma, M., G. Poveda, W. Rojas, M.L. Quiñones, J. Cox, and J. Patz, 1997. Predicting high-risk years for malaria in Colombia using parameters of El Niño-Southern Oscillation. Trop Med Int Health 2:1122–1127.

Boyle, E.A., 2000. Is ocean thermohaline circulation linked to abrupt stadial/interstadial transitions? Quaternary Science Reviews 19: 255-272.

Bradley, R.S., F.T. Keimig, and H.F. Díaz, 2004. Projected temperature changes along the American Cordillera and the planned GCOS network. Geophysical Research Letters 31, L16210. doi:10.1029/2004GL020229.

Bradley, R.S., M. Vuille, H.F. Díaz, and W. Vergara, 2006. Threats to water supplies in the Tropical Andes. Science 312:1755–1756.

Brooks, M.L., C.M. D'Antonio, D.M. Richardson, J.B. Grace, J.E. Keeley, J.M. Di Tomaso, R.J. Hobbs, M. Pellant, and D. Pyke, 2004. Effects of invasive alien plants on fire regimes. BioScience 54:677-688.

Colman, R., 2003. A comparison of climate feedbacks in general circulation models. Climate Dynamics 20: 865–873.

Crooks, J.A., 2002. Characterizing ecosystem-level consequences of biological invasions: the role of ecosystem engineers. Oikos 97:153-166.

Curtis, S., and S. Hastenrath, 1999a. Trends of upper-air circulation and water vapour over equatorial South America and adjacent oceans. International Journal of Climatology 19: 863-876.

Curtis, S., and S. Hastenrath, 1999b. Long-term trends and forcing mechanisms of circulation and climate in the Equatorial Pacific. Journal of Climate 12: 1134-1144.

Doblas-Reyes, F.J., R. Hagedorn and T.N. Palmer, 2005. The rationale behind the success of multi-model ensembles in seasonal forecasting. Part II: calibration and combination. Tellus 57A: 234–252.

Dye, C., 1992. The analysis of parasite transmission by blood-sucking insects. Annu Rev Entomol 37: 1–19.

Epstein, P.R., 2000. Is global warming harmful to health? Scientific American, August 2000.

Falvey, M., and R. D. Garreaud, 2005. Moisture variability over the South American Altiplano during the South American Low Level Jet Experiment (SALLJEX) observing season. Journal of Geophysical Research 110(D2): 2105.

Fjeldså, J., 2007. The relationship between biodiversity and population centres: the high Andes region as an example. Biodiversity and Conservation 16:2739-2751.

Fox, D., 2007. Back to the no-analog future. Science 316:823-825.

Francou, B., M. Vuille, P. Wagnon, J. Mendoza, and J.-E. Sicart, 2003. Tropical climate change recorded by a glacier in the central Andes during the last decades of the twentieth century: Chacaltaya, Bolivia, 16°S. Journal of Geophysical Research 108(D5): 4154.

Garreaud, R. D., and P. Aceituno, 2007. Atmospheric circulation over South America: mean features and variability. Pp. 45-59 in The Physical Geography of South America, edited by T. T. Veblen, K. R. Young, and A. R. Orme. Oxford: Oxford University Press.

Hagedorn, R., F.J. Doblas-Reyes and T.N. Palmer, 2005. The rationale behind the success of multi-model ensembles in seasonal forecasting. Part I: basic concept. Tellus, 57A: 219–233.

Hansen, J., A. Lacis, R. Ruedy, Mki. Sato, and H. Wilson, 1993. How sensitive is the world's climate? Natl. Geog. Soc. Res. Exploration, 9, 142-158.

Hansen, J., M. Sato, R. Ruedy, P. Kharecha, A. Lacis, R. Miller, L. Nazarenko, K. Lo, G.A. Schmidt, G. Russell, I. Aleinov, S. Bauer, E. Baum, B. Cairns, V. Canuto, M. Chandler, Y. Cheng, A. Cohen, A. Del Genio, G. Faluvegi, E. Fleming, A. Friend, T. Hall, C. Jackman, J. Jonas, M. Kelley, N.Y. Kiang, D. Koch, G. Labow, J. Lerner, S. Menon, T. Novakov, V. Oinas, Ja. Perlwitz, Ju. Perlwitz, D. Rind, A. Romanou, R. Schmunk, D. Shindell, P. Stone, S. Sun, D. Streets, N. Tausnev, D. Thresher, N. Unger, M. Yao, and S. Zhang, 2007. Dangerous human-made interference with climate: a GISS modelE study. Atmos. Chem. Phys. 7: 2287–2312.

Hardy, D. R. and S. P. Hardy, 2008. White-winged Diuca Finch (*Diuca speculifera*) nesting on Quelccaya ice-cap, Peru. Wilson Journal of Ornithology, 120: 613-617.

Hay, S.I., J. Cox, D.J. Rogers, S.E. Randolph, D.I. Stern, G.D. Shanks, M.F. Myers, and R.W. Snow, 2002. Climate change and the resurgence of malaria in the East African highlands. Nature 415: 905–909.

Herzog, S.K., P.M. Jorgensen, R. Martínez, C. Martius, E.P. Anderson, D.G. Hole, T.H. Larsen, J.A. Marengo, D. Ruiz, and H. Tiessen, 2010. Efectos del cambio climático en la biodiversidad de los Andes tropicales: el estado del conocimiento científico. Resumen para tomadores de decisiones y responsables de la formulación de políticas públicas. Inter-American Institute of Global Change Research (IAI), São José dos Campos, Brazil, 30 pp.

Instituto de Hidrología, Meteorología y Estudios Ambientales-IDEAM, 2002. Executive summary of Colombia's First National Communication to the United Nations Framework Convention on Climate Change, 22 pp.

Instituto Nacional de Salud de Colombia, 2005. Sistema Integrado de Vigilancia y Control de Malaria y Dengue en Colombia.

Joos, F., G-K. Plattner, T.F. Stocker, A. Körtzinger, and D.W.R. Wallace, 2003. Trends in marine dissolved oxygen: implications for ocean circulation changes and the carbon budget. EOS 84 (21): 197–204.

Josse, C., F. Cuesta, G. Navarro, V. Barrena, E. Cabrera, E. Chacón-Moreno, W. Ferreira, M. Peralvo, J. Saito, and A. Tovar, 2009. Ecosistemas de los Andes del norte y centro. Bolivia, Colombia, Ecuador, Perú y Venezuela. Lima: Secretaría General de la Comunidad Andina, Programa Regional ECOBONA-Intercooperation, CONDESAN-Proyecto Páramo Andino, Programa BioAndes, EcoCiencia, NatureServe, IAvH, LTA-UNALM, ICAE-ULA, CDC-UNALM, and RUMBOL SRL.

León, G.E., J.A. Zea, and J.A. Eslava, 2000. Circulación general del trópico y la Zona de Confluencia Intertropical en Colombia. Meteorología Colombiana 1: 31-38.

le Roux, P.C., and M.A. McGeoch, 2008. Rapid range expansion and community reorganization in response to warming. Global Change Biology 14:2950-2962.

Levine, J.M., P.B. Adler, and S.G. Yelenik, 2004. A meta-analysis of biotic resistance to exotic plant invasions. Ecology Letters 7:975-989.

Lindsay, S.W. and M.H. Birley, 1996. Climate change and malaria transmission. Ann Trop Med Parasitol 90: 573–588.

Macdonald, G., 1957. The epidemiology and control of malaria. Oxford University Press, London.

Marengo, J.A., J.D. Pabón, A. Díaz, G. Rosas, G. Avalos, E. Montealegre, M. Villacís, S. Solman, and M. Rojas, 2009. Cambio climático, evidencias y escenarios futuros en la Región Andina. Chapter 26.

Martens, W.J.M., 1997. Health impacts of climate change and ozone depletion. An eco-epidemiological modelling approach. Maastricht, The Netherlands.

Martens, P., R.S. Kovats, S. Nijhof, P. de Vries, M.T.J. Livermore, D.J. Bradley, J. Cox, and A.J. McMichael, 1999. Climate change and future populations at risk of malaria. Glob Environ Change 9: 89–107.

Millennium Ecosystem Assessment, 2005. Millennium Ecosystem Assessment synthesis report. Washington, DC: Island Press.

Moore, T.C., J.C.G. Walker, D.K. Rea, C.F.M. Lewis, L.C.K. Shane, and A.J. Smith, 2000. Younger Dryas interval and outflow from the Laurentide ice sheet. Paleoceanography 15(1): 4-18.

Myers, N., R.A. Mittermeier, C.G. Mittermeier, G.A.B. da Fonseca, and J. Kent, 2000. Biodiversity hotspots for conservation priorities. Nature 403:853-58.

Pabón, J.D., 2003. El cambio climático global y su manifestación en Colombia. Cuadernos de Geografía 12(1-2): 111-119.

Pabón, J.D., 2004. El cambio climático y sus manifestaciones en Colombia. Innovación y Ciencia 11(3-4): 68-73.

Patz, J.A., T.K. Graczyk, N. Geller, and A.Y. Vittor, 2000. Effects of environmental change on emerging parasitic diseases. Int J Parasitol 30(12–13): 1395–405.

Patz, J.A., M. Hulme, C. Rosenzweig, T.D. Mitchell, R.A. Goldberg, A.K. Githeko, S. Lele, A.J. McMichael, and D. Le Sueur, 2002. Regional warming and malaria resurgence. Nature 420:627–628.

Patz, J.A., D. Campbell-Lendrum, T. Holloway, and J.A. Foley, 2005. Impact of regional climate change on human health. Nature 438: 310–317.

Pérez, C., C. Nicklin, O. Dangles, S. Vanek, S. Sherwood, S. Halloy, K. Garrett, and G. Forbes, 2010. Climate change in the high Andes: implications and adaptation strategies for smallscale farmers. International Journal of Environmental, Cultural, Economic and Social Sustainability 6:1-16.

Poveda, G., and O.J. Mesa, 1997a. Feedbacks between hydrological processes in tropical South America and large-scale oceanic and atmospheric phenomena. Journal of Climate 10: 2690-2702.

Poveda, G. and W. Rojas, 1997b. Evidencias de la asociación entre brotes epidémicos de malaria en Colombia y el fenómeno El Niño-Oscilación del Sur. Revista de la Academia Colombiana de Ciencia 21:421–429.

Poveda, G., N.E. Graham, P.R. Epstein, W. Rojas, M.L. Quiñones, I.D. Vélez, and W.J.M. Martens, 2000. Climate and ENSO variability associated with vector-borne diseases in Colombia. In: El Niño and the Southern Oscillation, multi-scale variability and global and regional impacts. 1st edn. Díaz H.F. and Markgraf V. (eds). Cambridge University Press, Cambridge/New York, pp 183–204.

Poveda, G., W. Rojas, M.L. Quiñones, I.D. Vélez, R.I. Mantilla, D. Ruiz, J.S. Zuluaga, and G.L. Rúa, 2001. Coupling between annual and ENSO timescales in the malaria-climate association in Colombia. Environ Health Perspect 109: 489–493.

Roe, G.H., and M.B. Baker, 2007. Why is climate sensitivity so unpredictable? Science 318 (5850): 629-632.

Ruiz, D., G. Poveda, M.L. Quiñones, I.D. Vélez, G. Rúa, W. Rojas, and J.S. Zuluaga, 2002a. Modelación sistémica para el diagnóstico de la interacción clima-malaria en Colombia. Aplicación durante El Niño 1997–1998 y La Niña 1998–2000. Meteorología Colombiana 5: 41–48.

Ruiz, D., G. Poveda, M.L. Quiñones, I.D. Vélez, G. Rúa, W. Rojas, and J.S. Zuluaga, 2002b. Modeling entomological-climatic interaction of malaria transmission at Nuquí (Colombian Pacific Coast). Case of study: El Niño 1997–1998 and La Niña 1998–2000. In: Conference Climate Variability and Change and their Health Effects in the Caribbean: Information for

Climate Variability and Change Adaptation Planning in the Health Sector. PAHO/WHO. Bridgetown, Barbados.

Ruiz, D., G. Poveda, R.I. Mantilla, M.L. Quiñones, I.D. Vélez, G. Rúa, W. Rojas, and J.S. Zuluaga, 2003. Modelación de la interacción entomológica-climática de la transmisión de la malaria mediante Dinámica de Sistemas. Revista Colombiana Entomología 29: 191–201.

Ruiz, D. and G. Yan, 2003. Biology of African Highland Malaria: report. Department of Biological Sciences, State University of New York at Buffalo, 60 pp.

Ruiz, D., 2005. Fase de Preparación (PDF-B) del proyecto Integrated National Adaptation Pilot (INAP): High Mountain Ecosystems, Colombia's Caribbean Insular Areas, and Human Health – Sub-actividad 'Modelación Biológica', Actividad 'Evaluación del Riesgo', Área temática 'Sistema de Alerta Temprana', Componente 'Salud Humana'. Grupo de Profundización en Hidroclimatología, Programa en Ingeniería Ambiental, Escuela de Ingeniería de Antioquia. Final report, 210 pp.

Ruiz, D., G. Poveda, I.D. Vélez, M.L. Quiñones, G.L. Rúa, L.E. Velásquez, and J.S. Zuluaga, 2006. Modelling entomological-climatic interactions of *Plasmodium falciparum* malaria transmission in two Colombian endemic-regions: contributions to a National Malaria Early Warning System. Malaria Journal 5:66, doi:10.1186/1475-2875-5-66 (http://www.malariajournal.com/content/5/1/66).

Ruiz, D., H.A. Moreno, M.E. Gutiérrez, and P.A. Zapata, 2008a. Changing climate and endangered high mountain ecosystems in Colombia. Science of the Total Environment 398 (1-3): 122-132.

Ruiz, D., S. Connor, and M. Thomson, 2008b. A multimodel framework in support of malaria surveillance and control. Chapter VII (pp. 101-125) in: Seasonal Forecasts, Climatic Change, and Human Health – Health and Climate / Advances in Global Change Research Vol. 30; Madeleine C. Thomson, Ricardo García Herrera and Martin Beniston (ed.), Springer Science + Business Media, Dordrecht; Publisher: Springer Netherlands, ISBN 978-1-4020-6876-8, The Netherlands.

Seimon, T.A., A. Seimon, P. Daszak, S.R.P. Halloy, L.M. Schloegel, C.A. Aguilar, P. Sowell, A.D. Hyatt, B. Konecky, and J.E. Simmons, 2007. Upward range extension of Andean anurans and chytridiomycosis to extreme elevations in response to tropical deglaciation. Global Change Biology 13: 288-299.

Soden, B.J, and I.M. Held, 2006. An assessment of climate feedbacks in Coupled Ocean–Atmosphere Models. Journal of Climate 19: 3354-3360.

Solman, S., M. Nuñez, and M.F. Cabré, 2007. Regional climate change experiments over southern South America. I: present climate. Climate Dynamics 30:533-552.

Ter Veen, J.M.L., 2002. The effect of climate, economics and environment on the transmission of malaria in the USA between 1900 and 1946. London School of Hygiene and Tropical Medicine, 72 pp.

Thomson, M.C. and S.J. Connor, 2001. The development of Malaria Early Warning Systems for Africa. Trends Parasitol 17(9): 438–445.

Thomson, M.C., F.J. Doblas-Reyes, S.J. Mason, R. Hagedorn, S.J. Connor, T. Phindela, A.P. Morse, and T.N. Palmer, 2006. Malaria early warnings based on seasonal climate forecasts from multi-model ensembles. Nature 439: 576–579.

Urrutia, R., and M. Vuille, 2009. Climate change projections for the Tropical Andes using a regional climate model: temperature and precipitation simulations for the end of the 21st century. Journal of Geophysical Research D02108, doi:10.1029/ 2008JD011021.

Vuille, M., R.S. Bradley, and F. Keimig, 2000a. Climate variability in the Andes of Ecuador and its relation to tropical Pacific and Atlantic sea surface temperature anomalies. Journal of Climate 13: 2520-2535.

Vuille, M., R.S. Bradley, and F. Keimig, 2000b. Interannual climate variability in the central Andes and its relation to tropical Pacific and Atlantic forcing. Journal of Geophysical Research 105: 12447-12460.

Vuille, M., R. Bradley, M. Werner, and F. Keimig, 2003. 20th century climate change in the tropical Andes: observations and model results. Climatic Change 59: 75-99.

Vuille, M., B. Francou, P. Wagnon, I. Juen, G. Kaser, B.G. Mark, and R.S. Bradley, 2008. Climate change and tropical Andean glaciers: past, present and future. Earth Science Reviews 89:79-96.

White, E.M., J.C. Wilson, and A.R. Clarke, 2006. Biotic indirect effects: a neglected concept in invasion biology. Diversity and Distributions 12:443-455.

The World Bank Group, 2006. Colombia-Integrated National Adaptation Program Project. Documents & Reports.

World Health Organization, 1994. World malaria situation in Part I. Wkly Epidemiol Rec 72:269–274.

World Health Organization, 2002. World Health Report 2002: Reducing risks, promoting healthy life. Publications of the World Health Organization, Geneva.

World Health Organization, 2003. Climate change and human health – Risks and responses: summary. Publications of the World Health Organization, ISBN 92 4 159081 5, Geneva, Switzerland, 38 pp.

World Health Organization, 2004. Using climate to predict infectious disease outbreaks: a review. Geneva: World Health Organization. (WHO/SDE/OEH/04.01).

Yang, H., 2000. Malaria transmission model for different levels of acquired immunity and temperature-dependent parameters (vector). Rev Saúde Pública 34(3): 223–231.

Yang, H. and M. Ferreira, 2000. Assessing the effects of global warming and local social and economic conditions on the malaria transmission. Rev Saúde Pública 34(3): 214–222.

World Resources Institute. Millennium ecosystem assessment—ecosystems and human well-being: biodiversity synthesis; 2005. Island Press, Washington D.C., 86 pp. ISBN: 1-59726-040-1.

National communications submitted to the United Nations Framework Convention on the Climatic Change (UNFCCC):

2da Comunicación Nacional de la República Argentina a la Convención Marco de las Naciones Unidas sobre Cambio Climático. March 7, 2008. 201 pages.

Plurinational State of Bolivia - Second National Communication - Executive Summary. December 2, 2009. 24 pages.

Second National Communication of Brazil to the United Nations Framework Convention on Climate Change - Brasília: Ministério da Ciência e Tecnologia. November 30, 2010. 60 pages.

Second National Communication of Chile to the United Nations Framework Convention on Climate Change – Executive summary. October 24, 2011. 25 pages.

República de Colombia - Segunda Comunicación Nacional ante la Convención Marco de las Naciones Unidas sobre Cambio Climático. Executive summary. December 7, 2010. 26 pages.

First National Communication of the Republic of Ecuador to the United Nations Framework Convention on Climate Change. November 15, 2000. 129 pages.

Guyana Initial National Communication in response to its commitments to the United Nations Framework Convention on Climate Change. May 16, 2002. 192 pages.

Segunda Comunicación Nacional – Cambio Climático – Paraguay. December 8, 2011. 181 pages.

El Perú y el cambio climático – Segunda Comunicación Nacional del Perú a la Convención Marco de las Naciones Unidas sobre Cambio Climático 2010. Septiembre 28, 2010. 204 pages.

Republic of Suriname – First National Communication under the United Nations Framework Convention on Climate Change. March 27, 2006. 94 pages.

Uruguay – Segunda Comunicación Nacional a la Conferencia de las Partes en la Convención Marco de las Naciones Unidas sobre Cambio Climático – Resumen Ejecutivo. May 11, 2004. 49 pages.

Primera Comunicación Nacional en Cambio Climático de Venezuela. October 13, 2005. 164 pages.

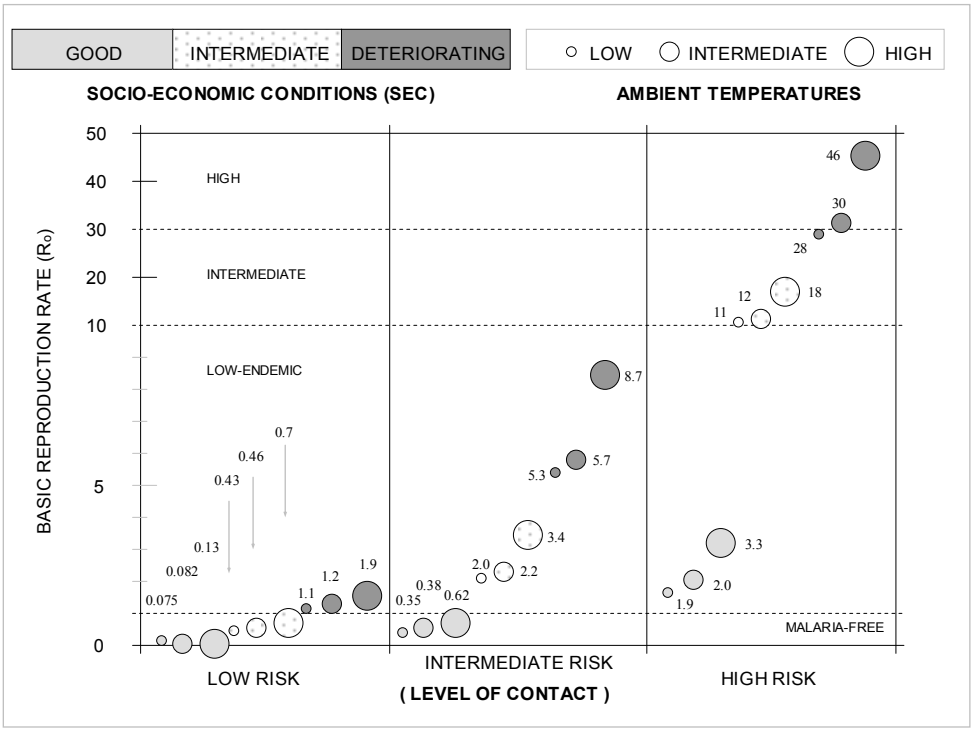

Figure 1. Steady analysis of the Yang's model for different levels of risk, socioeconomic (SEC) and ambient conditions. The basic reproduction rate (R_o) is an estimate of the average number of secondary cases arising in a very large population at risk of completely susceptible humans following the introduction of a single primary case. R_o defined by this model involves several exogenous variables, including the average period of time delayed from the infection (infective bite) until the appearance of malaria gametocytes in the blood of a human host ($1/\gamma_1$), the natural resistance rate against malaria (θ), the natural and disease-induced mortality rates for human hosts (μ and α), the transmission rate from human hosts to vectors (f), the average period to build up an effective immune response in a human host ($1/\gamma$), the duration of sporogony ($1/\sigma_2(T)$), the natural and induced (for instance, by insecticides) mortality rates of mosquitoes (μ' and α'), and the inoculation rate from vectors to humans (h). Other exogenous variables included in this tool are the rates π_1, π_2 and π_3 at which protective immunity, partial immunity and immunologic memory decrease in human hosts, the rate of oviposition φ, the rate of eggs becoming non-

viable $\mu_e(T)$, and the cycle duration from the egg to the mature adult ($1/\sigma_1(T)$). R_o=1 is defined as the transmission threshold: for values below, the disease cannot develop itself in the community at risk and will recede; for values above, malaria cases will propagate. If R_o>1, but still at low values, the disease can develop itself in the community but at low endemic levels. Lower values of R_o mean that small efforts can lead to the eradication of the disease. On the contrary, higher values of R_o mean that only greater efforts can lead to its eradication. The level of contact, RISK, is represented by the parameters h (inoculation rate) and f (transmission rate), which can be dependent on environmental conditions. Parameters θ, $1/\gamma_1$, $1/\gamma$, π_1, π_2, π_3, μ, and φ are those profoundly influenced by social and economic conditions. Parameters that are strongly affected by temperature are $\mu_e(T)$, $1/\sigma_1(T)$ and $1/\sigma_2(T)$.

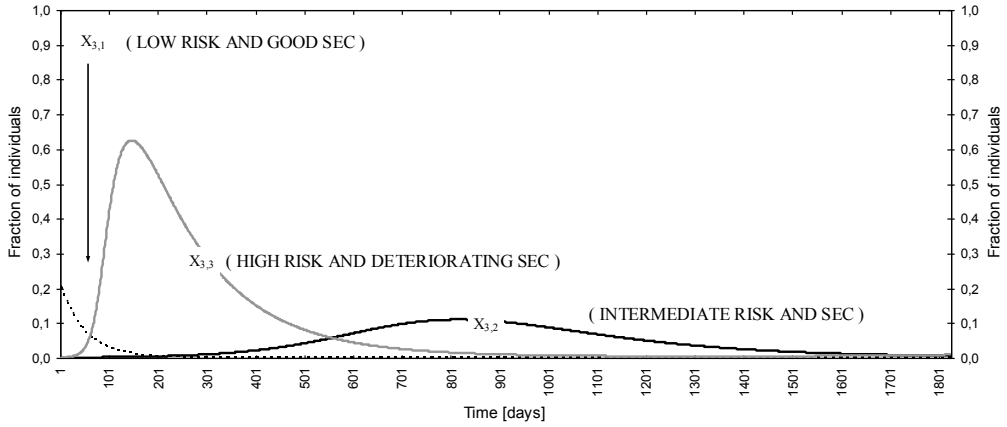

Figure 2. Time series of Yang's model results for the low risk, intermediate risk and high risk epidemiological scenarios. In the mathematical model proposed by Yang (2000) the fraction of individuals at a given time *t* who are susceptible is represented by the variable $X_1(t)$, the fraction of incubating individuals by $X_2(t)$, the fraction of infectious people by $X_3(t)$, the fraction of immune individuals by $X_4(t)$, the fraction of partially immune hosts by $X_5(t)$, the fraction of non-immune hosts but with immunologic memory by $X_6(t)$, and the fraction of incubating people after re-infection by $X_7(t)$. The fractions of susceptible, incubating and infectious mosquitoes at time *t* are represented by the variables $y_1(t)$, $y_2(t)$ and $y_3(t)$, respectively. Asymptotic equilibrium values reached by the system are analyzed for three dissimilar situations: ($X_{3,1}$) a disease-free community but potentially under low risk (RISK=0, SEC=0, T=20°C, R_o=0.075); ($X_{3,2}$) disease at low endemic levels and intermediate risk of malaria (RISK=1, SEC=1, T=21.5°C, R_o=2.172); and ($X_{3,3}$) disease at high endemic levels and under high-risk of malaria (RISK=2, SEC=2, T=31°C, R_o=46.100). The initial values for this analysis are: $X_1(0)$=(0.10; 0.998; 0.998), $X_2(0)$=(0.20; 0.001; 0.001), $X_3(0)$=(0.20; 0.001; 0.001), $X_4(0)$=(0.15; 0; 0), $X_5(0)$=(0.15; 0; 0), $X_6(0)$=(0.10; 0; 0), $X_7(0)$=(0.10; 0; 0), $y_1(0)$=(60%; 100%; 100%), $y_2(0)$=(20%; 0%; 0%), and $y_3(0)$=(20%; 0%; 0%). The Yang's model is run for a simulation period of 1,825 days (5 years).

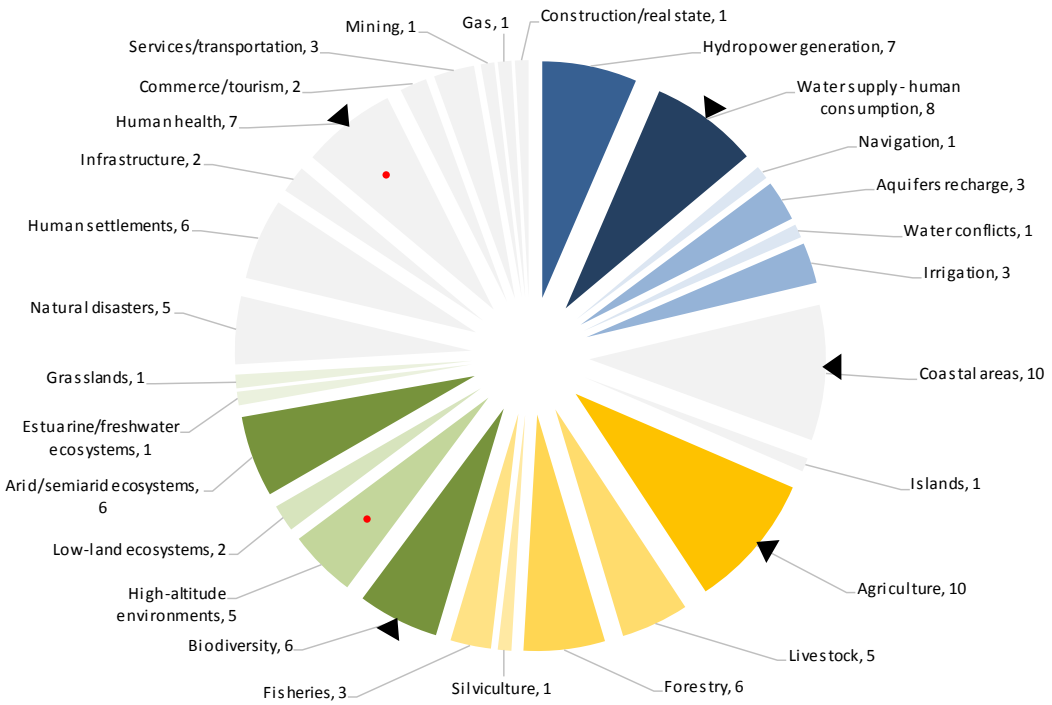

Figure 3. Priority sectors in the latest South American National Communications to the United Nations Framework Convention on Climate Change. Next to each label is the total number of countries (out of 12: Argentina, Bolivia, Brazil, Chile, Colombia, Ecuador, Guyana, Paraguay, Peru, Suriname, Uruguay, and Venezuela) identifying each sector as a critical priority. Blue, orange and olive green sectors are directly related to water resources, productive activities (consumption and revenue) and biodiversity, respectively. Other priority sectors are depicted by grey pies. Sectors of primary concern are highlighted with black solid triangles. Red dots pinpoint the themes of interest of this PhD dissertation.

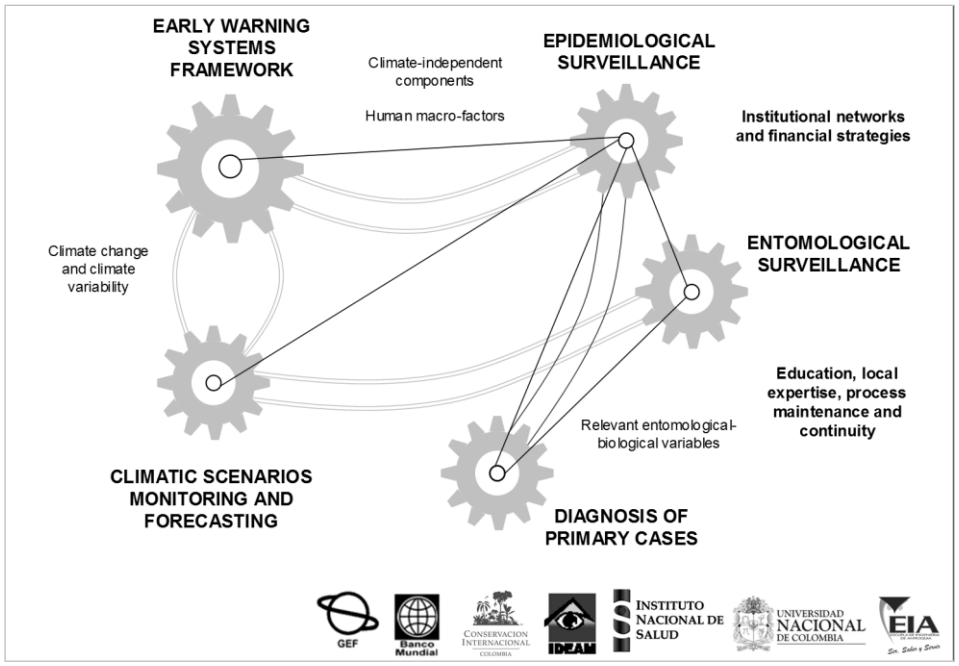

(A)

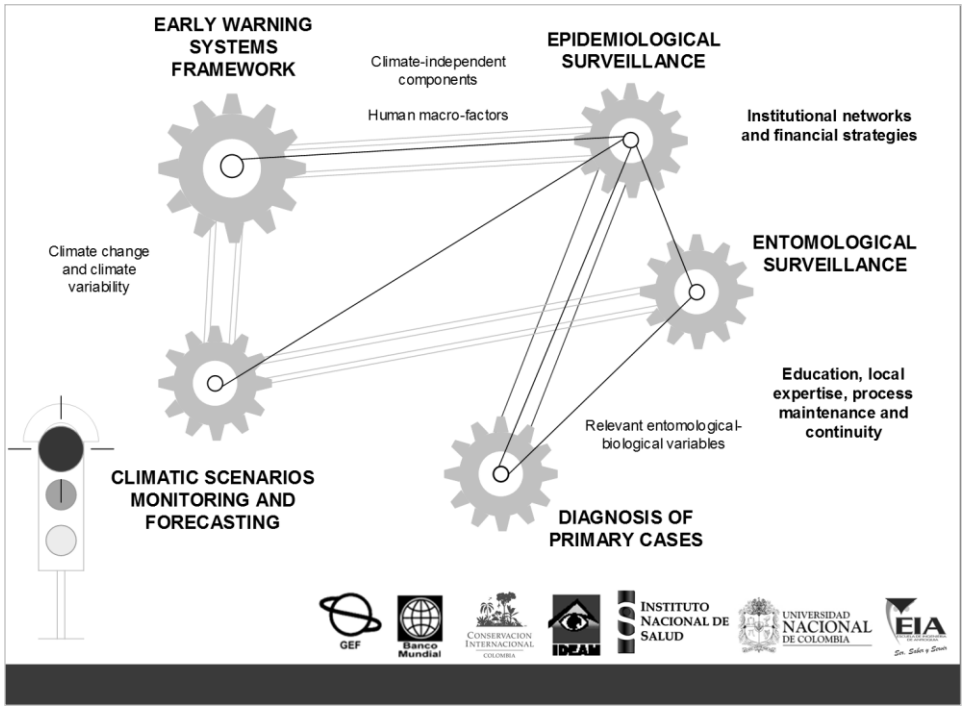

(B)

Figure 4. Integrated surveillance and control system under 'normal' conditions (A) and during the onset of epidemics (B). Major components are supported by axes and conveyor belts representing capacity building, institutional networks and financial strategies (from Ruiz, 2005).

Chapter 2[2]

Climatic stress on high-altitude Andean ecosystems

2.1. Introduction and scopes

The upper range of the northern Andes harbors unique neotropical alpine wetland ecosystems locally known as páramos. They constitute exceptional grassland regions inhabiting the narrow elevational belt above the Andean cloud forests (the so-called *bosque montano*; ca. 2,000-3,500 m) and below the areas of "permanent" snow (above ca. 4,500 m) (Castaño, 2002; Gutiérrez et al., 2006; Ruiz et al., 2008). Páramos constitute one of the most important natural features of the northern Andes (Buytaert et al., 2006) and one of the most essential Colombian climatic zones (IDEAM, 2001; Díaz-Granados et al., 2005). They provide numerous and valuable environmental goods and services including high biodiversity and a sustained ("regulated") water supply for domestic, agricultural and industrial use (Buytaert et al., 2006), as well as for hydro-power generation in the region. For example, in Colombia, 80% of the water demand of its capital city, Bogotá, is supplied by a nearby páramo and 67% of the installed power capacity is hydro-based.

The historical climatic conditions of these high-elevation environments are characterized by average temperatures below 10°C, large diurnal temperature range, cloudy skies, foggy days, high UV radiation amounts, low atmospheric pressure, strong winds, and precipitation in the

[2] This chapter merges the articles by Ruiz et al. (2011, 2012) and Ruiz (2010). Copies of the manuscripts are available in the digital backup of this thesis.

form of drizzle (Castano, 2002; Gutiérrez et al., 2006; Ruiz et al., 2008). Some of these conditions have changed dramatically over recent decades. Even though biophysical factors show considerable natural variability in the Andes, human activities occurring at local, regional and global scales have begun to introduce anthropogenic stress on high-altitude environments (Foster, 2001; Díaz et al., 2003; Bradley et al., 2006). Rapid environmental changes and important disruptions of the integrity of páramo ecosystems have been observed over recent years in Colombia (Castaño, 2002; Gutiérrez et al., 2006; WBG, 2006; Ruiz et al., 2008; WBG, 2008). Likely anthropogenically-induced changes include, among others, water stress during dry seasons due to receding glaciers and the disappearance of high-altitude water bodies, changes in patterns and abrupt loss of biodiversity, frequent occurrence and rapid spread of natural and human-induced high-altitude fires, and increased erosion. And all these alterations seem to worsen during dry seasons.

Although our understanding of glacier retreat and its consequences has significantly increased, the assessment of the consequences of climate change on the functioning of páramos and Andean forests requires additional work. In particular, improved knowledge of rapid spatial and temporal changes in their climatic patterns and hydrological regimes has become a critical priority (WBG, 2008). In this chapter I aim to investigate the recent changing climatic conditions experienced by the high mountain ecosystems inhabiting the Northern Andes, specifically the Colombian Central Andes (Colombia is host to one of the largest stretch of páramos life zones in the planet; WBG, 2006). I analyze historical time series of local climatic variables to detect statistically significant trends that occurred over recent years and explore the degree of association between the year-to-year variability of SSTs, particularly those observed in the tropical Indo-Pacific and Atlantic regions, and the year-to-year changes in regional cloud cover

conditions observed over the northwestern portion of South America. Although four 'dry' months (January, February, July, and August) are critical to the high-altitude ecosystems occupying these latitudes, I focus the analyses of cloud cover conditions on the month of January, when these environments are exposed to sunshine maxima (Ruiz et al., 2009).

My goal is to have a better picture of the conditions prevailing in the high-altitude areas of the Colombian Central mountain range in order to, in the foreseeable future, assess the stress that these fragile ecosystems could further face due to regional and global climate-induced changes. My work on cloudiness over the North Andes, in particular, is not intended to be an in-depth discussion on the physical mechanisms driving the normal variability in cloud cover over the northwestern portion of South America. Rather, it is my interest to explore the signals that the normal year-to-year variability of SSTs in the nearby ocean basins have in the cloud cover conditions prevailing over the area of Los Nevados Natural Park. I hope that my findings contribute to the ongoing design and implementation of the Colombian adaptation strategy, an effort that aims to preserve these unique, fragile, and strategic high-altitude environments that today provide valuable services, essential to the economy of the nation.

2.2. The páramos of Los Nevados Natural Park

One of the most representative Colombian páramos is located in the highly-strategic protected area of Los Nevados Natural Park, which lies in the spatial domain 04°25'to 05°15'N and 75°00' to 76°00'W (UAESPNN, 2000), on the El Ruiz-Tolima Volcanic Massif, in the Colombian Central Cordillera or Colombian Andean Central Mountain Range-ACMR. See figure 1. Los Nevados is located in the Alto Cauca hydroclimatic region (DG-UNAL, 2005), and

more specifically, in the 04°36'N-04°59'N and 75°12'W-75°33'W domain. This protected area used to have several snow-covered and ice-capped mountains and a dense network of high-altitude water bodies and aquatic-microhabitats, and also used to be the perfect environment for unique high-altitude plant species (Castaño, 2002). Climatic conditions of Los Nevados Natural Park provide ideal settings for preserving the integrity of these fragile high-altitude environments.

More specifically, my analyses focus on the climatic conditions prevailing in the surroundings of the Claro River high-altitude basin, which is located in the domain 04°48'N-04°58'N and 75°19'W-75°30'W and has a drainage area of about 191 km^2, to approximately 1,800 m where the watercourse meets the Los Molinos River. See figures 1 and 2. The watershed is currently fed by numerous mountain streams originating high in the snowfields of the El Ruiz (5,321 m) and the Santa Isabel (5,100 m) ice-capped mountains of the Central Cordillera. The Claro River watershed, along with the Otún and Chinchiná rivers, provide a continuous water supply to several communities in the adjacent lowlands.

The orography of the El Ruiz-Tolima volcanic massif (see figure 3) and the two inter-Andean Cauca and Magdalena river valleys extends from tropical to nival elevational belts. Historical climatic conditions allow the presence of eleven Holdridge (1987) life zones in such a small spatial domain: from tropical moist forest (Tmf) to alpine rain tundra (Art). In terms of the Cuatrecasas (1934) system, historical climatic conditions in the area of the Claro River watershed support moist Andean forest, wet high Andean forest, rainy subpáramo, wet subpáramo, rainy páramo, and rainy superpáramo. Data from elevational experimental plots (see Ruiz et al., 2009) show that many unique plant species inhabit the headwaters of the Claro River basin. Key species and potential bio-indicators of likely changes in the elevational location and

distribution of life zones include (see figures 4 and 5): *Miconia salicifolia* (Melastomataceae) and *Berberis rigidifolia* (Berberidaceae) in the subpáramo; *Espeletia hartwegiana* (Asteraceae), *Plantago rigida* (Plantaginaceae), and *Valeriana plantaginae* (Valerianaceae) in the páramo; and *Senecio canescens* (Asteraceae), *Loricaria colombiana* (Asteraceae), and *Lycopodium crassum* (Lycopodiaceae) in the superpáramo. A detailed dataset of high-altitude flora inhabiting Los Nevados Natural Park is presented at: http://catalogofloraparamo.eia.edu.co/flora.php?page=inicio.

2.3. Data

Analyzed records included ground meteorological, sea surface temperatures and satellite (cloud characteristics) data, as well as streamflow hydrological records and wildfires data. A brief description of the available datasets is presented below.

Weather station (ground truth) data. A total number of 37 weather stations, located in the spatial domain 04°25'N-05°15'N and 75°00'W-76°00'W, were considered to assess local changing climatic conditions. Their datasets comprise daily, monthly and annual records of sunshine, rainfall, minimum and maximum temperatures, diurnal temperature range, and relative humidity. Data were provided by the Colombian Institute of Hydrology, Meteorology and Environmental Studies – IDEAM, the Central Hidroeléctrica de Caldas – CHEC, and the Centro Nacional de Investigaciones de Café – CENICAFE. Table 1 summarizes all the climatic datasets. The available historical periods of weather station data are presented in the supplementary material. A detailed description of these records can be found in Ruiz (2009).

Sea surface temperature (SST) data. Two regions in the tropical belt 30°S-30°N were considered for the analyses of SSTs: the Indo-Pacific region, which extends from 30°E to 70°W,

and the Tropical Atlantic Ocean, which extends from 60°W to almost 16°E (see figure 6). Monthly SSTs observed in the spatial domain [30°S-30°N, 30°E-90°W] of the tropical Indo-Pacific region over the time period spanning from January, 1942 to December, 2007 (Kaplan et al., 1998; Reynolds and Smith, 1994) were selected for the study. Analyses also include a narrower region, the spatial domain [15°S-15°N, 30°E-90°W] of the tropical Indo-Pacific region. During the available time period strong La Niña events, observed in particular during the years 1973-74 and 1975-76, were accompanied by unusual cooling of the Tropical Eastern Pacific. Very strong unusual warming of SSTs, associated with strong El Niño events, were observed in the Tropical Eastern Pacific in, particularly, the years 1982-83 and 1997-98, and mainly during the months of January of Niño [+1] year (see figure 6 for one of the seven most significant El Niño events: 1991–92; Wang, 2005).

Historical time series of mean monthly SSTs observed in the Niño 3.4 region of the equatorial Pacific (5°S-5°N, 120°W-170°W; Barnston et al., 1997) over the period from January, 1950 through August, 2005 were also processed to support the analyses. SSTs in this region exhibit an intra-annual cycle with a peak occurring during the months of April, May, and June, when sea surface temperatures reach values of about 27.5°C. In January, in particular, SSTs tend to reach values of about 26.5°C under normal conditions, below the minimum threshold of ca. 26.9°C (or 300 K) necessary to initiate deep convection (Ramanathan and Collins, 1991). During El Niño events, an increase of almost 0.6°C is generally observed throughout the year, with a maximum change of +0.8°C in the month of January.

Monthly SSTs observed in the spatial domain [19°S-29°N, 60°W-16°E] of the Tropical Atlantic Ocean over the time period spanning from January, 1964 to December, 2007 were also

included. In this region, according to Zebiak (1993) and Wang (2005), 'an interannual phenomenon similar to but weaker and more frequent than the Pacific El Niño' also takes place. The largest SST anomalies occur in the eastern equatorial Atlantic (see figure 6) and are mostly observed during the summer months of the Northern Hemisphere, although some events have also occurred in the boreal winter (Wang, 2005).

Satellite data. All-type cloud characteristics (cloud amount, top pressure, top temperature, and optical thickness) observed over the spatial domain [5°S-15°N, 80°W-70°W] during the period from July, 1983 through August, 2001 were included in the analyses (see figure 6). In January, the all-type cloud amounts observed over the selected spatial domain range from 25-40% on the Colombian Caribbean Sea to 70-85% along the Colombian Andes and near the equator. The all-type top pressures observed in the same month range, in turn, from 300-400 mb on the Colombian and Peruvian Amazon regions to 750-850 mb on the Colombian Caribbean Sea. These data can be downloaded from the Data Library of the International Research Institute for Climate and Society, IRI (http://iri.columbia.edu/; source: Rossow et al., 1996) and are discussed in Ruiz (2010).

Over the grid point 03°45'N-76°15'W, where the Andean high-altitude area (Los Nevados Natural Park and its surroundings) is located, the January all-type cloud amount and top pressure, averaged over the period 1984-2001, reach values slightly above 75% and 500 mb, respectively (see previous discussion in Ruiz et al. 2008). Cloud cover patterns exhibit an intra-annual cycle with two peaks, which generally occur during the trimesters March-April-May and September-October-November and whose average cloud amounts reach values of about 84 and 83%, respectively. During the trimesters December-January-February (DJF) and June-July-August, the all-type cloud amounts over the region decrease and reach values as low as 76%,

particularly in January. Cloud top temperatures and top pressures during the trimester DJF increase consistently to values of 260-265 K and 450-500 mb, respectively, changing from average values of 250-255 K and 400-450 mb normally observed during the wettest months of May, September and October. Increases in the total monthly sunshine and the daily maximum, mean and minimum sunshine, as well as decreases in the total number of foggy days are normally observed in the high-altitude region during dry seasons, and more critically, in El Niño years. This normal climate variability is driven by the interactions between the Walker and the Hadley circulation cells, and the resulting latitudinal displacement of the Inter-Tropical Convergence Zone (Cane and Zebiak, 1985; Poveda et al., 2001; Wang, 2005). During the warm phase of ENSO, in particular, the Pacific Walker circulation weakens (Wang, 2005) and such a change in normal atmospheric circulation generally results in increased rainfall along the coast of Peru, but is associated with a significant decrease in cloud cover and rainfall over extensive areas of the Colombian region (Poveda et al., 2001).

Streamflow hydrological records. Minimum, mean and maximum streamflow records, gathered at the limnigraphic stations 2615708 Chupaderos (Chinchiná River) and 2613711 La Bananera 6-909 (Otún River), as well as at the limnimetric stations 2613721 La Pastora (Otún River), 2613719 Buenos Aires (Otún River), 2615706 Río Claro (Claro River), and 6-958 Río Claro (Claro River), were processed for the analysis of hydrological conditions. All these stations are located in the lowlands (at 2,040 m; 1,530 m; 2,450 m; 1,920 m; 1,530 m; and 1,486 m above sea level, respectively) and their historical periods span 18 years (from 1988 through 2005), 35 years (1971-2005), 2 years (1994-1995), 9 years (1994-2002), 4 years (1990-1993), and 25 years (1983-2007), respectively. Only records gathered at the limnigraphic stations were processed for the analysis of long-term trends.

Wildfires data. Lastly, forty three (43) high-altitude fires, registered in the area and surroundings of the Los Nevados Natural Park (source: Unidad Administrativa Especial del Sistema de Parques Nacionales Naturales/UAESPNN - Colombian National Natural Parks Unit), were included in the analysis. Records are available for the historical period 1994 – 2007 and include: town, locality and date of occurrence, coordinates, duration, causes, affected area, observations, and people/organization who attended. Only two (2) events were linked to unfavorable climatic conditions or power cords in contact with vegetation. Forty one (41) events were purposely set by tourists, arsonists, illegal armed groups, and hunters, or during grass and crop renovations (UAESPNN, 2008).

2.4. Methods

Weather stations, satellite and streamflow data. Daily time series (not all the datasets are available at a daily timescale) were checked for inconsistencies. Potential outliers were detected through simple run sequence plots. Anomalous records were expunged from the data before estimating monthly values only when there was strong evidence that they were erroneous (i.e. they were not reflecting the very nature of the climatic variable). However, a very small fraction of the available dataset was removed, as presented in the supplementary material of this chapter. Monthly time series were calculated for each of the climatic variables. The sample mean, median, mode, standard deviation, sample variance, standard error, kurtosis, skewness coefficient, range, minimum and maximum values, sample size, and confidence interval (95%) of each of the monthly time series were calculated using the Data Analysis Tool of Microsoft Excel. Annual cycles of cloud amount, top pressure and top temperature, optical thickness,

sunshine, rainfall, minimum and maximum temperatures, diurnal temperature range, and relative humidity were calculated using the longest time series. Annual time series were calculated for each of the climatic variables. Exploratory analyses, including time series plots and box-plots, were conducted to detect non-homogeneities in annual (free of seasonality) time series. Confirmatory analyses were then implemented to assess the significance of the observed long-term linear trends. Trend magnitudes (slope parameters) were calculated by the method of least squares. Upper and lower confidence limits were also assessed for the simple linear regression models. Four statistical tests, namely the Student's t-test, the Hotelling-Pabst test, the non-parametric Mann-Kendall test (Kendall, 1975), and the aligned rank Sen's t-test (Sen, 1968), were all used to assess (at a α=0.05) the null hypothesis of zero slope parameters in the annual time series. A historical time series was considered to have a statistically significant long-term linear trend in the mean at a α=0.05 significance level when at least three of the hypothesis tests rejected the null hypothesis of a zero slope parameter. Serially independent yearly time series were assumed when implementing the non-parametric Mann-Kendall test. December-January-February, March-April-May, June-July-August, and September-October-November time series (see supplementary material for the case of total sunshine and minimum temperatures on the coldest days), as well as monthly records of sunshine, rainfall, minimum, mean and maximum temperature, diurnal temperature range, and relative humidity gathered at the weather station XII (ID 2615502), were also processed to support the analysis (see supplementary material). Weather station XII was chosen because its observational periods span the longest historical periods of the available dataset. All hypothesis tests were run using the Analysis of Historical Time Series (ASH) software developed by J.D. Salas and R.A. Smith at the Hydrology and Water Resources Program, Colorado State University, and recently modified at the Water Resources Graduate

Program, National University of Colombia at Medellin. Finally, long-term trends, statistically significant at a α=0.05, were plotted on a map of the 04°25'N-05°15'N and 75°00'W-76°00'W spatial domain, and in the vertical profiles of sunshine, rainfall, temperature, and water content.

Conditions of atmospheric stability. Topographic profiles of the Claro River were created using a high-resolution digital terrain model produced from 1:25.000 scaled digital elevation contour maps (Ruiz et al., 2008). Average values of mean and minimum annual temperatures, annual dew point, actual and saturation vapor pressures, atmospheric pressure, actual and saturation mixing ratios, relative humidity, and potential temperature were computed for different altitudes (see spatial distributions in Ruiz et al., 2008). Saturation and actual mixing ratios were estimated through the Clausius-Clapeyron equation for the inferred spatial distributions of mean annual temperature and mean annual dew point, respectively. The Lifting Condensation Levels (LCLs) were estimated by comparing the vertical profiles of mixing and saturation mixing ratios. Finally, the vertical profile of mean annual temperature (environmental lapse rate) was compared to the theoretical paths of dry and moist adiabatic lapse rates and to the trends in minimum and maximum local temperatures, to characterize local climatic conditions and to define the regions of static instability, static stability, and conditional instability. A statically unstable atmosphere is characterized by vertical motions, the formation of convective currents, turbulence and mixing of air layers. In a statically stable atmosphere, vertical motions are inhibited, air layers are stratified and consequently free from convection, and air masses exhibit a low degree of turbulence. In a conditional unstable atmosphere, the air is unsaturated and could become unstable on the condition it becomes saturated.

Sea surface temperature data. Empirical Orthogonal Function (EOF) modes and Principal Components (PCs) were determined for January, February, July, and August SST

anomalies. The EOF analysis decomposes the spatial-temporal variations of the large SST gridded datasets into combinations of orthogonal spatial patterns with corresponding PCs in linear fashions (Lorenz, 1956; Wang and An, 2005). Finally, simple correlation analyses between Niño 3.4 SST anomalies, the first two PCs of SST anomalies, and the all-type cloud amount/top pressure records were conducted. Linear trends that are statistically significant at a 0.05 significance level were removed from the time series before estimating the correlation coefficients. Only the first PCs are discussed since they explain most of the spatio-temporal variability of SST anomalies.

2.5. Results

Some key aspects of the observed changes in historical climatic conditions are presented below. Discussion includes only those long-term linear trends that are statistically significant at a 0.05 significance level. It is worth to mention that observed changes appear to be consistent with changes occurring worldwide (see figure 7) and at national and regional spatial scales.

2.5.1. Cloud characteristics and sunshine

The mean annual values of all-type cloud amount, top pressure, top temperature, and optical thickness, observed over the grid point 03°45'N - 76°15'W during the period 1983-2001, reached 80.6%, 438 mb, 256 K, and 7.56, respectively. The annual values of sunshine variables are presented in Table 2. A decrease in all-type cloud cover of about 1.9% per decade (homogeneous, not geometric) was detected over the observing period. Trends in the mean of the

historical time series of mean annual cloud top pressure, top temperature and optical depth were not observed over the available historical period. As for sunshine, the top left panel of figure 8 depicts the annual values and long-term trends of the total annual sunshine (SR1) observed in the selected spatial domain. SR1 values gathered at most of the weather stations located on the western flank of the ACMR at altitudes around the so-called *pluviometric optimum* (ca. 1,500 m; Hastenrath, 1991; Oster, 1979) exhibited statistically significant decreasing trends ranging from –3.7 to –8.5% per decade, i.e. from –65 to –120 hours per decade, approximately. Weather stations located above that optimum did not experience increasing/decreasing trends. The strongest changes in the total sunshine occurred during the December-January-February season, as presented in the supplementary material. Decreases in SR1 are consistent with statistically significant increases in the total number of foggy days (or decreases in the total number of sunny days) of about +1.0 to +2.3 days per decade that were observed at the same weather stations. Daily maximum, mean and minimum sunshine values observed at lower altitudes also exhibited decreases of about –0.1 to –0.4, –0.2 to –0.4, and –0.08 to –0.1 hours/day/decade, respectively.

2.5.2. Rainfall

The annual values of rainfall variables are presented in Table 3. The top right panel of Figure 2 depicts the annual values and long-term trends of the total annual rainfall (R1) observed in the selected spatial domain. R1 amounts showed statistically significant decreasing trends ranging from –7 to –11% per decade (homogeneous, not geometric), i.e. –135 to –180 mm per decade, in some met stations located at altitudes above the pluviometric optimum and particularly over the western flank of the ACMR. Below this level, the historical time series of

only two weather stations exhibited increasing trends of about +3 to +4% per decade; i.e. +63 to +87 mm per decade. Most of the weather stations gathering the total number of dry days did not show statistically significant increasing/decreasing trends. Finally, maximum daily precipitation records suggested an increased occurrence of unusually heavy rainfall events, particularly over the western flank of the ACMR, with trends in the mean of about +1 to +4% per decade, equivalent to +0.7 to +2 mm per decade.

2.5.3. Minimum and maximum temperatures

The annual values of minimum and maximum temperature variables are shown in Table 4. Minimum temperatures on the warmest days (MTmin) exhibited statistically significant trends at lower altitudes that range from +0.1 to +0.2°C per decade. MTmin records gathered at higher altitudes did not show significant trends. Average minimum temperatures (ATmin) gathered at weather stations located at lower altitudes exhibited increasing trends that range from +0.1 to +0.3°C per decade. ATmin records observed at higher altitudes did not show significant trends. Minimum temperatures on the coldest days exhibited statistically significant increasing trends at all altitudes that range from +0.1 to +0.6°C per decade (see bottom left panel of figure 8; see also figure 9). Increases in these extreme temperatures at higher altitudes were almost twice of what was observed in average at lower altitudes. Also, the strongest changes in the minimum temperatures on the coldest days occurred during the December-January-February and June-July-August dry seasons, as presented in the supplementary material.

Maximum temperatures on the warmest days exhibited statistically significant trends at all altitudes that ranged from +0.2 to +1.1°C per decade (see bottom right panel of figure 8).

Increases at higher altitudes were more than three times what was observed in average at lower altitudes. Average maximum temperatures exhibited increasing trends that range from +0.2 in average at lower altitudes to +1.0°C per decade at higher altitudes. Maximum temperatures on the coldest days exhibited statistically significant increasing trends in only three weather stations; their increasing trends in the mean reached +0.2, +0.3, and +0.9°C per decade, respectively.

2.5.4. Diurnal temperature range

The annual values of diurnal temperature range (DTR) variables are shown in Table 4. Statistically significant increasing trends of about +0.4 to +1.2°C per decade were observed in maximum DTRs at higher altitudes, whereas at lower altitudes decreasing trends of about –0.2 to –0.4°C per decade were detected. Average DTRs showed increasing trends of +0.3 and +1.3°C per decade at altitudes above 2,000 m, and decreasing trends of about –0.2 and –0.3°C per decade at altitudes in the range [1,000-2,000 m]. Minimum DTRs exhibited statistically significant trends of about +1.0°C per decade at higher altitudes and decreasing trends of about –0.1 to –0.3°C per decade at altitudes below 2,000 m.

2.5.5. Relative humidity

The annual values of relative humidity (RH) variables are shown in Table 4. Statistically significant trends in maximum RH were only seen in the records of three weather stations, whose historical trends reached –2.2% per decade at higher altitudes, and +3.0 and +2.4% per decade at lower altitudes. Average RH records exhibited statistically significant decreasing trends at

altitudes above the pluviometric optimum ranging from –1.5 to –3.6% per decade. Some weather stations located at altitudes around and below this threshold showed statistically significant increasing trends of about +0.6 to +0.7% per decade. Minimum RH records exhibited statistically significant decreasing trends that range from –3.2 to –8.7% per decade; only one weather station showed records with an increasing trend of about +1.2% per decade.

2.5.6. Atmospheric stability in the area of the Claro River watershed

Table 5 summarizes the estimated climatic conditions along the mainstream of the Claro River watershed. Figure 10 depicts the estimated regions of static instability, conditional instability, and static stability in the area of this high-altitude watershed. As mentioned before, increasing trends in extreme temperatures at higher altitudes (which would be depicted by right-ward shifts in the mean values of each box-plot in figure 10) are significantly greater than those observed at lower altitudes. Particularly, minimum temperatures on the coldest days in the headwaters have increased at a rate greater than +0.6°C per decade, whereas at lower altitudes the increasing trend only reaches +0.2 to +0.3°C per decade over the same period of time. Maximum temperatures on the warmest days have increased over the past two decades at an extraordinary rate of +1.5°C per decade in the headwaters, whereas at lower altitudes the trend only reaches +0.2 to +0.3°C per decade. Also, changes in the variance (which would be depicted by broadening/contraction of range in each box-plot) are significantly greater at higher altitudes: the day-to-day standard deviation of maximum temperatures observed in the headwaters of the Claro River have increased at a rate of +0.3°C per decade, whereas in the lowlands the increasing trend reaches +0.1°C per decade.

2.5.7. Sea surface temperatures and cloud cover

EOF modes and PCs. Figure 11 depicts the first two Empirical Orthogonal Function modes of January SST anomalies observed in the 30°S-30°N and 15°S-15°N Indo-Pacific tropical regions over the period 1942-2007, as well as in the 30°S-30°N Tropical Atlantic region over the period 1964-2007. The first EOF modes of January SST anomalies observed in the selected Indo-Pacific regions represent the mature phase of ENSO. The leading EOF mode of January SST anomalies observed in the Tropical Atlantic region depicts the equatorial monopole structure (Li, 2001). The second important mode observed in this latter region is the north-south inter-hemispheric gradient of SST anomalies, or so-called meridional inter-hemispheric dipole mode (Li, 2001). Table 6 shows the percentages of the spatio-temporal variability of SST anomalies explained by the first and second modes for all the analyzed regions.

Figure 12 depicts the first two Principal Components of January, February, July, and August SST anomalies observed in the same spatial domains. The first principal components (PC1s) of January, February, July, and August SST anomalies observed in the 30°S-30°N and 15°S-15°N Indo-Pacific regions exhibit statistically significant trends over the period 1942-2007. The corresponding PC1s observed in the 30°S-30°N Tropical Atlantic region over the period 1964-2007 also show statistically significant trends. Time series associated with the first principal components of tropical Atlantic SST anomalies exhibit steeper long-term trends than their tropical Indo-Pacific PC1s counterparts, which are influenced by the long-term cooling of some parts of the eastern equatorial Pacific (Cane et al., 1997) and the zonal SST gradient in the tropical Pacific (Karnauskas et al., 2012). The slope of the linear trend exhibited by the PC1 of

January SST anomalies observed in the 30°S-to-30°N Indo-Pacific region reaches –0.1756/year (decreasing trend, toward El Niño). 15.3% of the variance of this PC1 can be explained by the fitted linear trend. PC1 values exceeded the +1.0 standard deviation (SD) envelopes during the strong 1955-56, 1973-74, 1975-76, and 1988-89 La Niña events. PC1 values during the strong 1972-73, 1982-83, and 1997-98 El Niño events exceeded, in turn, the –1.0 SD envelopes. Over the period from 1951 to 1976, nine La Niña events (three weak, three normal, and three strong) and only three El Niño events (two normal and one strong) took place. Over the period 1977-2004 only three La Niña events (two normal and one strong) and eight El Niño events (five normal and three strong) occurred. If the first PC of January SST anomalies were to be divided into two sub-series, the fitted linear trend would exhibit an increasing (positive, toward La Niña) trend with a slope of about +0.1643/year over the period 1951-1976, and a small decreasing (negative, toward El Niño) trend with a slope of about –0.0405/year over the period 1977-2007.

Correlation coefficients. Figure 13 depicts the correlation coefficients between January all-type cloud amounts observed over the spatial domain [5°S-15°N, 80°W-70°W] during the period from 1984 through 2001, and (a) the January SST anomalies observed in the Niño 3.4 region, (b) the first principal component of January SST anomalies observed in the 30°S-30°N-belt of the Indo-Pacific region, (c) the first principal component of January SST anomalies observed in the 15°S-15°N-belt of the Indo-Pacific region, and (d) the first principal component of January SST observed in the Tropical Atlantic Ocean. January SST anomalies in the Niño 3.4 region explain between 22% and 59% of the year-to-year variability of January all-type cloud amounts observed over the Colombian Andean and Pacific regions. The strongest correlation coefficient of –0.770 is observed in the grid point where the Andean high-altitude area is located. The PC1 of January SST anomalies observed in the 30°S-to-30°N-belt of the Indo-Pacific region

explains, in turn, between 26% and 72% of that year-to-year variability. Again, the highest correlation coefficient of +0.848 is observed in the same grid point. The PC1 of January SST anomalies observed in the 15°S-15°N-belt of the Indo-Pacific region explains between 26% and 71% of that year-to-year variability. The highest correlation coefficient also lies in the same grid point.

Lastly, the PC1 of January SST observed in the Tropical Atlantic Ocean explains between 18% and 32% of the year-to-year variability of January all-type cloud amounts observed over the northeastern portion of the Colombian Andean region. This PC1 explains almost 28% of the year-to-year variability of January all-type cloud amounts observed over the grid point where the Andean high-altitude area is located. Only a few dispersed grid points in the selected spatial domain [5°S-15°N, 80°W-70°W] exhibit statistically significant correlation coefficients in the months of February, July and August (figures not shown).

2.5.8. Water balance, high-elevation water bodies and ice caps

Changes have also occurred in hydrological regimes. Besides rainfall, water inputs to the hydrological cycle in high-elevation watersheds include outflow from water bodies and aquatic micro-habitats, mist (see figure 5), glaciers, and snowmelt. My analysis of intra-annual cycles of the mean streamflow of the Claro, Otún, and Chinchiná rivers suggest that water discharges follow the bi-modal annual cycles of rainfall observed in the surroundings of Los Nevados Natural Park, but with a one-month time lag (see figure 14). Periods of high mean water discharge are usually observed during April-May-June and October-November-December. Periods of low streamflow tend to occur during January-February and July-August. Although

minimum streamflows show similar intra-annual distributions, observed records exhibit important differences during the dry periods January-February and July-August. During these months meltwater runoff from snowfields and glaciers, as well as water inputs from high-altitude water bodies and *turberas* (bogs) increase surface streamflow (i.e., streamflow is greater than would be expected from rainfall amounts alone due to meltwater runoff). This effect is particularly pronounced in the Claro and Otún river basins. By contrast, in the Chinchiná River, which does not receive meltwater runoff, and where aquatic microhabitats are limited to a few areas at its headwaters, reductions in streamflow during the critical dry months are considerable.

Decreases in annual rainfall observed at elevations above the pluviometric optimum and increases in near-surface temperatures, particularly at higher elevations, are likely to decrease streamflow. Exploratory analyses suggest decreasing trends in annual maximum and mean streamflow values in the Otún and the Chinchiná rivers over the past 40 and 20 years, respectively, although these trends are not statistically significant. Minimum discharges during the critical months January-February and July-August show changes in the available historical time series that are statistically significant. In the Otún River, minimum water discharges and minimum streamflows during the driest period January-February exhibit decreases of ca. 1.0% and >6.0% per decade, respectively, over the past 40 years.

Are these trends related to changes in the extent of high-elevation water bodies and ice-caps? Water bodies in the Los Nevados Natural Park have experienced reductions in surface area over recent years, and some have already experienced natural sediment-filling and drying processes, accompanied by a gradual colonization by local vegetation (see figure 15). However, water bodies also exhibit a marked seasonality driven by regional climatic conditions (see figure 16). Increases in their water levels are common during April-May and October-November,

whereas decreases typically occur during December-January-February and July-August-September. On inter-annual timescales, high-elevation water bodies show dynamics related to the warm and cold events of the El Niño–Southern Oscillation. Specifically, significant drought-induced shrinkages with respect to "past" reference shorelines are observed after above-normal summers that commonly accompany the El Niño warm events.

On the other hand, the Molinos glacier on the western flank of El Ruiz Nevado and the Conejeras glacier tongue on the western flank of the Santa Isabel Nevado have retreated dramatically over recent years (Euscátegui, 2002; Ceballos et al., 2008; IDEAM, 2008). These retreats have been forced by volcanic activity, changes in climatic conditions, and changes in local surface albedo. Although there is limited information to infer the potential impacts of the changes in the extent of high-elevation water bodies and ice-caps on the ecosystem as a whole, the disappearance of water bodies and turberas and the retreat of mountain glaciers are probably undermining the integrity of páramo ecosystems. It is likely that the change in water availability has and will continue to have a sizable effect.

2.5.9. High-elevation fires

Fire events are one of the most serious threats to the integrity of high-Andean ecosystems and one of the most critical challenges for the conservation of protected areas. At higher elevations, fires cause numerous and almost-irreversible damage to páramo soils, wetlands, fauna, and flora (see figure 17). Fire-induced changes in the structure and composition of páramo ecosystems affect their provision of several environmental goods and services. In the surroundings of Los Nevados, lower-elevation areas and buffer zones are inhabited by

smallholder farmers whose main productive activities include grazing dairy cattle and the cultivation of potato crops. Fires are usually set to regenerate grass for livestock, prepare land after harvesting crops, and expand cultivated land areas. These burns are not controlled appropriately and often spread into "non-target" natural vegetation in páramo zones. Fires are particularly hazardous during the dry season given the high to very high vulnerability of páramo habitats to the occurrence and rapid spread of fires during this period.

As previously mentioned, historical records of fires in Los Nevados extend back to 1994 (see figure 18). These records include the worst ecological disaster that has occurred in protected Colombian high-elevation ecosystems, namely the fire of unprecedented severity that took place in the surroundings of the Laguna del Otún in July 2006 (Lotero et al., 2007). This event lasted for almost eight days and affected more than 4% of the park. Sadly, since 1994 the annual number of fire events, the total area affected per year and the average fire duration show strong increasing trends. This is the result of several factors such as a weak institutional capacity to react to fires, more combustible material in the area, and climatic conditions more favorable to the spread of fires. Most events have been induced by or are related to human activities, but it is likely that changing climatic conditions have favored their rapid spread. Increases in the number of events and affected areas seem to correlate with the increasing and decreasing trends observed in temperature and relative humidity records, respectively, gathered at nearby weather stations.

This link does not appear to be a coincidence. Testimonies of local experts and park guards support the links between the current rapid spread of fire events and the observed changes in climatic conditions in the area. Also, an association between the timing of fire events, the total area affected per month, and the intra-annual cycles of climatic conditions in the area of Los Nevados has been observed. Most fire events occur during the dry seasons June-July-August

(JJA) and December-January-February (DJF). Higher values of maximum temperatures linked to lower relative humidity and rainfall set the stage for a potential increase in the spread of "small-scale" fire events during these trimesters. The maximum number of events and greatest area affected per month are observed during the trimester JJA. However, when excluding the unprecedented fire event of July 2006, the highest value of total area affected per month occurs during DJF. In summary, although changing conditions are not directly causing an increase in high-elevation fires, drier conditions may favor their rapid spread. Thus, larger affected areas and greater duration of fires are early warnings of the páramo ecosystems' increasing vulnerability.

2.5.10. Model projections

Model projections consistently suggest future climatic conditions will be unfavorable for páramo life zones (Vuille et al., 2003; Díaz et al., 2003). Hulme and Sheard (1999) used the outputs of six Global Climate Models (GCMs) to propose future climate scenarios for the Northern Andes. According to their results, the total annual rainfall in the central region of the Cordillera Central is expected to be above the 1961-1990 normal annual value for all emission scenarios. They also suggest that increases in mean annual temperatures are expected throughout the region. Giorgi and Bi (2005) used atmosphere-ocean coupled GCM simulations for northern South America to predict increases in rainfall during future wet seasons and decreases during dry seasons. Also, near-surface temperatures are predicted to be above historical normal conditions. Bradley et al. (2006) used GCM results to suggest that, at 5°N and at elevations of 3,000-5,000 m, mean annual temperatures are expected to increase over this century under emission scenario A2 of Meehl et al. (2007). For Colombia recent statistical downscaling techniques of GCM

outputs were used to estimate future climatic conditions under a $2xCO_2$ emission scenario (Departamento de Geografía–Universidad Nacional de Colombia, 2005). On a national scale and for the Alto Cauca hydroclimatic region, total annual rainfall is expected to change up or down depending on the model, but mean annual ambient temperatures are consistently expected to be above the past mean.

GCM outputs indicate an increase in the elevation of clouds under a future warmer world (Meehl et al., 2007). They also suggest that most tropical areas will experience a decrease in net cloud cover over all layers. Based on my analyses of January SST anomalies (see Ruiz et al., 2009), I suggest that a significant decrease in cloud cover in the high-elevation region is likely to occur over the next 50 years under normal conditions. My predicted decrease of 6.8% in total cloud cover, relative to the period 1984-2001, is 1.4 times greater than (but consistent with) the -2.0% annual mean change suggested by Meehl et al. (2007) for the period 2080 to 2099, relative to 1980 to 1999. I also argue that if a strong El Niño event were to occur by 2050, the reduction in January monthly average cloud cover could be more critical.

Changes in the structure, composition, integrity, and extension of high-elevation ecosystems inhabiting the Claro River watershed and nearby areas are likely to occur over the first half of this century. Ongoing changes in climatic conditions could force upward shifts in the transitions between life zones, which would lead to the appearance of new environments, the expansion of some others, and reductions in the extent of the subalpine (páramo), alpine (superpáramo), and nival (glacial) elevational belts. The future distribution of these ecosystems will depend on their capacity to adapt to the expected climatic changes. My analyses (see chapter 3 on life zones in Ruiz et al., 2009) suggest that by 2050 climatic conditions in the watershed and the region will likely be suitable for the colonization of lower montane dry forest (LMdf) and

montane moist forest (Mmf). A 56% increase in the montane wet forest (Mwf) surface area could also occur. On the other hand, subalpine rain páramo (SArp), alpine rain tundra (Art) and nival (N) life zones could experience reductions of about 31%, 53%, and 80%, respectively, by 2050. In terms of the Cuatrecasas classification, reductions in the areas of subpáramo, páramo, superpáramo, and nival zones could be 83%, 22%, 53%, and 80%, respectively. With respect to the entire páramo zone, such reductions correspond to a total decrease in area of about 54%.

2.6. Discussion

Climatic patterns have changed in the central region of the ACMR. Observed trends in several climatic variables (minimum and maximum near-surface temperatures, rainfall amounts, relative humidity, cloud characteristics, sunshine, and diurnal temperature range) and inferred conditions of atmospheric (in)stability suggest that climatic stress is increasing in the high-altitude Andean ecosystems of the Central Cordillera. In the areas surrounding Los Nevados Natural Park, specifically, most of the climatic variables that control the integrity of high-elevation ecosystems also show statistically significant changes (see local scale in Ruiz et al., 2009 for specific rates of change). These variables include total annual rainfall, maximum daily rainfall, minimum temperatures during the coldest days, maximum temperatures during the warmest days, and minimum relative humidity. Some key aspects of the inferred and observed changes are discussed below.

2.6.1. Changes in atmospheric stability

Atmospheric stability conditions in the area of the Claro River watershed are characterized by the following factors: (a) cloud and fog formation in montane cloud forests, (b) moist advection over the western flank of the ACMR during day-time uplifting thermodynamic processes, and (c) cooling and drying processes driven by nighttime down-slope winds (nocturnal subsidence dynamics). Air masses' daytime motions play a significant role in the integrity of high-altitude ecosystems and are considered key to the preservation of high-altitude environments (Ruiz et al., 2008). The process seems to be simple: in the early morning when the lower atmosphere is statically stable, low- and middle-level clouds are clearly differentiated from their high-level counterparts. With solar insolation heating the ground surface during the first hours of the day, enough convective potential energy is accumulated in the lower altitudes of the atmosphere to destabilize this condition (Vernekar et al., 2003). In the late morning and early afternoon, statically unstable conditions prevail, producing turbulence and vertical mixing. The induced atmospheric motions transport significant amounts of water vapor from lower to higher altitudes in the lower atmosphere, increasing the relative humidity in high-altitude environments, forming fog and middle-level clouds, and initiating convective cloud clusters. Fog and middle-level clouds 'protect' the vegetation, ice-caps, high-altitude water bodies, and aquatic microhabitats from direct sunlight. Differences in temperature and humidity between higher and lower altitudes control the diurnal dynamics, and would likely continue to drive future climate conditions in this high mountain environment.

My analyses indicate that ambient temperatures at higher altitudes are increasing significantly faster than those observed in lowland weather stations, a difference that is consistent with the outputs of several General Circulation Models (Trenberth et al., 2007; Meehl

et al., 2007). Also, relative humidity records in higher altitudes exhibited strong reductions, compared to the weak but significant increasing trends observed at lower altitudes. Even though several other factors, such as changes in circulation dynamics and land conversion on the west flank of the Cordillera Central must be also considered for the analyses of alterations in atmospheric stability in the area, it can be argued that the observed increases in near-surface temperatures at higher altitudes are strongly affecting the relationship between the environmental lapse rate and the dry and moist adiabatic lapse rates. The current scenario suggests that this section of the atmosphere is increasingly becoming conditionally unstable or statically stable. Hence, currents of uplifting air, commonly occurring in the area during the late morning and early afternoon, could be progressively weakening. As a consequence of this disruptive process, less water vapor is being produced over Andean cloud forests and less fog could be reaching higher altitudes on these mountains (Ruiz et al., 2008).

Changes in the amount of cloud and fog cover, driven by changes in atmospheric stability, have significant impacts on the net radiation balance, and consequently on glacier masses, high altitude water bodies and mountain species. My analyses suggest important reductions in the amount of all-type clouds over the observing period. As satellite data only capture information from the highest cloud tops, only those changes that have occurred in the amount of low-level clouds that are not obscured by higher clouds can be addressed (A. Del Genio, personal communication). This limitation indicates that the observed decreasing trend is a lower limit of what has been happening in the area; thus, low-level clouds might have decreased even more. My previous study (see Ruiz et al., 2008) reported that in higher altitudes (ca. 4,150 m) the total number of foggy days per month has slightly decreased over the past two decades, and hence, the total number of sunny days per month has increased. Analyses presented here

suggest that decreases in the total annual sunshine, the total number of sunny days, and the maximum, minimum, and mean daily sunshine values have occurred at lower altitudes. Also, I detect increases in the total number of days of null sunshine. Again, these evidences suggest that the mechanism that moves water vapor to higher altitudes has probably weakened over recent decades. In lower altitudes fog is more and more often getting "trapped", increasing the occurrence of foggy days there. In higher altitudes, decreases in fog, evidenced by decreases in relative humidity, could be the mechanism behind the increases in the number of sunny days. This scenario is particularly harmful to páramo life zones because without fog they are "protected" from direct sunlight only by high-level clouds, which have the net effect of increasing surface temperatures. Although deep convective events are expected to become less frequent (A. Del Genio, personal communication), analyses of minimum monthly temperatures at higher altitudes suggest that they have not changed as dramatically as maximum monthly temperatures, thus the reason why the atmosphere still exhibits strong movements of uplifting air in several instances. Thus, deep convective events could occur when conditions at the ground become favorable moisture-wise.

2.6.2. Observed trends in rainfall and temperature

Although studies on changing climatic conditions in páramo life zones are limited due to the lack of long-term historical records, there is considerable evidence suggesting that significant changes in annual rainfall and near-surface ambient temperatures have occurred in these tropical environments. Bradley et al. (2006) analyzed temperature records gathered at several climatic stations along the Tropical Andes and indicated that the rate of increase in air temperatures

reached +0.11°C per decade over the period from 1939 to 1998. If continued, this trend suggests that mean annual ambient temperatures in the headwaters of the Claro River could reach 5.4°C by 2050 (i.e. an increase of almost 0.6°C over the mean value of 4.9°C observed during the period 1981-2003). For Colombia, Pabón (2003 and 2004) analyzed weather stations data and indicated that total annual rainfall over the period 1961-1990 changed (increased or decreased) at rates of 4 to 6% per decade, and mean annual ambient temperatures increased at rates of about +0.1 to +0.2°C per decade over the same period. By assuming the maximum observed trend (+0.2°C per decade) mean annual temperatures in the headwaters of the Claro River could reach 5.9°C by 2050. More recent analyses (Departamento de Geografía–Universidad Nacional de Colombia, 2005) have suggested that changes in precipitation in the Alto Cauca hydroclimatic region exceeded –2.4%, with respect to the 1961-1990 normal annual rainfall, and increases in near-surface temperatures reached +0.12°C per decade over the same period. Extrapolations of such detected trends suggest a decrease in total annual rainfall in the area of 14% and an increase in temperature of about +0.7°C by 2050, both with respect to the total and mean values observed over the period 1961-1990. Consequently, mean annual ambient temperatures in the headwaters could reach 5.5°C in 50 years. In summary, previous estimates suggest that near-surface air temperatures in the high mountain basin of the Claro River are likely to reach from 5.4 to 5.9°C by 2050.

My study has produced evidence supporting these findings: (i) analysis of weather station data (see nationwide scale in Ruiz et al., 2010) suggests increases of up to +0.3°C/decade in mean near-surface temperatures along the Andean mountain ranges; (ii) On a regional scale, most historical time series of mean annual near-surface temperatures observed at weather

stations located along a 5°N latitudinal transect, show increasing trends that could reach 0.4°C/decade on all mountain flanks (see nationwide scale in Ruiz et al., 2010); and (iii) temperature data observed in the surroundings of the Claro River watershed suggest that mean annual temperatures have increased coherently at rates ranging between +0.2 and +0.4°C per decade, while minimum and maximum annual temperatures have increased at rates of about +0.4 to +0.6°C per decade. Under these conditions, I suggest that mean annual ambient temperatures in the headwaters of the Claro River could reach an extremely high value for these environments of 7.0°C by 2050.

With regard to rainfall (see nationwide scale in Ruiz et al., 2009), most stations along the mountain ranges show decreasing trends over the past 25 years. Stations located in the inter-Andean valleys exhibit increasing trends. Regional rainfall also shows important changes: increases have been observed over recent years on the western flank of the Cordillera Occidental, where total annual rainfall is strongly influenced by the orographic uplift of the westerly Chocó low-level jet (Poveda and Mesa, 2000; Vernekar et al., 2003). By contrast, historical time series over the eastern flank of the Cordillera Central, where rainfall amounts are influenced by the behavior of the easterlies and the low-level jet to the east of the Cordillera Oriental (Vernekar et al., 2003), show general tendencies toward drier conditions. In the inter-Andean valleys some stations exhibit increasing trends in rainfall while others have seen decreases. Along these valleys rainfall amounts are affected by elevation and show influences of the northeasterly trade winds, which in the area become valley currents that blow southward.

2.6.3. Changes in sea surface temperatures and likely impacts on cloud cover

The base state change in average Tropical Pacific SSTs (Yamaguchi and Noda, 2006; Meehl et al., 2007) is defined by the spatial anomaly pattern correlation coefficient between the linear trend of SSTs in the 1%/year CO_2 increase climate change experiment and the first EOF of SSTs in the control experiment over the spatial domain [10°S-10°N, 120°E-80°W]. Positive correlation coefficients indicate that the mean climate change has an El Niño-like pattern, and negative values are La Niña-like. Based on the output of 13 out of 16 Coupled Atmosphere-Ocean General Circulation Models, and taking into account the skill of the present-day El Niño – Southern Oscillation phenomenon (ENSO) simulations, it can be argued that more El Niño-like conditions are expected in the trend-ENSO pattern correlation (van Oldenborgh et al., 2005; Yamaguchi and Noda, 2006; Meehl et al., 2007). My analyses suggest that the PC1s of January SST anomalies observed in the 30°S-to-30°N and 15°S-to-15°N Indo-Pacific regions exhibit statistically significant trends over the period 1951-2007 that were accompanied by more El Niño-like conditions over the last 28 years of this observational period. Even though it became more La Niña-like after 1998, the trend over the period 1951-2007 is dominated by the El Niño conditions in the last decades of the 20th century. The PC1s of January SST anomalies also exhibit statistically significant changes in the mean, related to changes in the slopes of the 'long-term' linear trends, that occurred around 1976. This abrupt change is consistent with the observed and previously discussed natural mode shift that occurred in the Tropical Pacific in that year (Fedorov and Philander, 2001; Gordon and Giulivi, 2008).

Outputs from General Circulation Model ensembles suggest that increases in cloud cover in the vicinity of the tropopause (and decreases below) are very likely to occur at all latitudes – more consistent outside the Tropics– under a future warmer world (Meehl et al., 2007). In

general, simulation outputs indicate an increase in the altitude of clouds overall. Much of the low latitudes are expected to experience a decrease in net cloud cover over all the layers, after allowance for the overlap of clouds. Extrapolation of my estimated trends suggest that the PC1 of January SST anomalies for the 30°S-30°N Indo-Pacific Region could reach an expected value of –15.45, in the range [–7.99; –22.92], by 2050. If a strong El Niño event were to occur in that year, the expected PC1 would likely reach a value of –29.26. If a strong La Niña event were to occur, the expected PC1 would likely increase to –3.12. The January all-type cloud amount would likely decrease to 68.7%, in the range [63.8%; 73.6%], under normal or non-El Niño conditions. A strong El Niño event would reduce this monthly average value to almost 60%; a strong La Niña event would increase it to 76.8%. The decrease of 6.8% under normal conditions, relative to the period 1984-2001 (i.e. a rate of decrease of about 0.14%/year), is 1.4 times greater than (but consistent with) the –2.0% annual mean change in total cloud area cover expected for the period 2080 to 2099, relative to 1980 to 1999, under the SRES A1B scenario (Meehl et al., 2007).

2.6.4. Other changes

Previous studies have reported that, due to increases in tropospheric aerosol concentrations in the atmosphere, the diurnal temperature range (DTR) is decreasing in several places around the world. My analyses suggest that maximum, mean, and minimum DTRs at higher altitudes have increased over the past decades. This upward trend is a consequence of the difference between the rates of increase in minimum and maximum temperatures. Also, below-freezing temperatures and cold days are becoming less frequent in the area. Analyses of available

records suggest that minimum and maximum temperatures during the coldest days have significantly increased over recent decades. Furthermore, I observed changes in the variability of extreme temperatures. Historical time series of minimum temperatures exhibited a decrease in the variance, whereas maximum temperatures showed an increase. All these changes could favor the colonization of several mountain species, but might have a devastating impact on those individuals that have adapted to extreme conditions and now require them.

2.7. Conclusions and potential impacts on ecosystem integrity

Actionable and verifiable adaptation strategies to long-term climate change have a lot in common with strategies for anticipating and managing current climate variability. In other words, an effective way for assisting our society to be better prepared for the ongoing global change is by assisting it to cope better with current climate variability and climate-related events. Many of the climatic conditions that could be expected in the selected high-altitude environment in a future warmer world –increases in sunshine, diurnal temperature range, and minimum, mean and maximum temperatures, as well as decreases in relative humidity and the total number of foggy days (i.e. increases in the total number of sunny, clear-sky days)– are quasi-periodically realized in the warm events of ENSO. ENSO is the strongest signal in the inter-annual variability of the ocean-atmosphere coupled system and is the main forcing mechanism of Colombia's hydroclimatology at that timescale. ENSO plays out every two to seven years and has numerous impacts on many sectors globally (water resources, agriculture, health, among many others), and therefore has been drawing great scientific attention and has prompted a strong observational system.

My analyses suggest that 72% of the variance of cloud cover conditions over the area and the surroundings of Los Nevados Natural Park in the month of sunshine maxima is explained by the first principal component of SST anomalies observed in the 30°S-to-30°N belt of the Indo-Pacific region in that month, the latter representing the mature phase of ENSO. Assuming that long-term trends in SST anomalies observed over the time period 1942-2007 will continue, my analyses also indicate that more El Niño-like conditions are likely to occur in the years to come. Thus, these results combined with the observed impacts of ENSO allow me to think that the warm phase of this phenomenon can be used as a proxy for future climate scenarios in the high-altitude ecosystems within the selected region, and how harsh conditions might affect these highly strategic environments. I have to say that although I have obtained high levels of statistical significance, my analyses have several caveats, most of them derived from the use of remote sensing data, causing reason to be taken with caution. In particular, the spatial resolution of the satellite-derived records is a main obstacle to thoroughly predicting the potential impacts of changes in regional cloud cover on páramos and other high-altitude environments. The spatial extent of each pixel is so large that it covers not only páramos, but a large array of tropical systems ranging from tropical dry forests in the inter-Andean valleys of the Cauca and Magdalena rivers, to even tropical wet forests on the Pacific lowlands.

Previous analyses suggest that changes or trends in time series of temperatures and pressures of all type cloud tops have not occurred in the area over recent years (Ruiz et al., 2008), but reductions in the amount of all type clouds took place over the observing period. It was also reported that in higher altitudes (ca. 4,150 m) the total number of foggy days per month has slightly decreased over the past two decades, and hence, the total number of sunny days per month has increased. Based on my analysis, I can argue that there is likely to be a decrease in the

net cloud cover over this area of the Colombian Central mountain range over the next 50 years. These expected changes could affect several physical processes, including the water cycle and the net radiative balance. Decreases in cloud and fog cover directly imply higher incoming solar radiation amounts, higher near-surface ambient temperatures and increased evaporation, which combined could contribute to a further retreat of local mountain glaciers and snowfields, and an accelerated disappearance of high-altitude water bodies and aquatic microhabitats.

Expected changes could also have numerous ecologically-related effects such as increases in the rate of desertification of mountain habitats and shifts in species ranges (species will be forced to adapt to new climatic conditions, move towards new climatic niches or become extinct). They could also induce shifts in major vegetation zones or biomes: e.g. higher incoming solar radiation would probably enhance the temperature of páramo topsoil and hence would induce upward displacements of the upper forest line (Körner and Paulsen, 2004). Finally, changes in incoming solar irradiance could produce drier and warmer vegetation layers and soil conditions, which in turn could set the conditions for a rapid spread of high-altitude fires and could directly and indirectly (e.g. faster decomposition rates of organic matter) lead to a decrease in organic carbon storage in both below-ground soils and peat accumulations, causing a net release of carbon to the atmosphere (Buytaert et al., 2010).

Changing climatic conditions are now seriously contributing to increased stress on the high mountain ecosystems of the Colombian Central Mountain Range. The observed changes 'are currently occurring region-wide, are cumulative, and are likely to be irreversible' (WBG, 2008). Although their impacts on the integrity of high-altitude habitats are very difficult to assess, my analyses suggest that changing climatic conditions are likely to lead to the disruption of páramo and cloud forest ecosystems. Some of the expected impacts include:

- Upward migrations of low-elevation plant species and upward shifts of ecosystem boundaries (Gutiérrez, 2002) are expected to occur, reducing the extent of páramo habitats. As the climate warms and ice caps melt a shift in life zones to higher elevations could be expected as, over long time intervals, these zones would maintain their relationships to the snow line. However, the inferred rapid upward changes in the Lifting Condensation Level (not discussed in this chapter) and field-observed retreats of snowline, both considered good approximations of upward shifts in the transitions between life zones, suggest that several high-elevation plant species will most likely be unable to migrate upward. Changes in temperature could favor the upslope migration of many montane species, but might also have a devastating impact on those species that have adapted to and become dependent on extreme conditions at high altitudes.
- Elevational changes in sunshine and rainfall could contribute to an increase in the rate of desertification of montane habitats, which today house an important fraction of global biodiversity.
- Areas where only snow or drizzle used to fall could be experiencing heavy rain due to the rapid upward shift of the freezing level. Glacier margins may be at increasing risk of retreat, contributing to a continued diminution of the self-regulation capacity of the hydrological system.
- Decreases in the amount of cloud and fog cover, driven by changes in atmospheric stability, will have significant impacts on the net radiation balance. As a consequence, glacier mass, high-elevation water bodies and mountain species could be further affected.

- Lastly, higher solar energy is expected to accelerate the hydrological cycle and increase evapotranspiration, having strong effects on water bodies and aquatic microhabitats.

Combined, these impacts constitute a serious threat to unique páramo habitats and, consequently, to the water supply in the region. A reduction in water availability for human consumption in urban centers, agricultural and industrial use, and hydro-power generation could affect vital elements of the economy and welfare of the nation. In the foreseeable future it will be more expensive to supply water for these demands (Vergara et al., 2007; Vergara, 2009).

I think that the analyses and results presented here can help us better understand and predict the consequences of expected changes in cloud and fog cover in the Andes, and could give us some insights into the choice of local climate-informed conservation practices, adaptation strategies and general decision-making processes. I claim that ambitious sustainable management strategies are now urgently required to protect these unique, rich, fragile, and highly endangered high-altitude environments.

References

Barnston, A.G., M. Chelliah, and S.B. Goldenberg, 1997. Documentation of a highly ENSO-related SST region in the equatorial Pacific. Atmosphere-Ocean 35: 367-683.

Bradley R.S., M. Vuille, H.F. Diaz, and W. Vergara, 2006. Threats to water supplies in the Tropical Andes. Science 312: 1755-1756.

Buytaert W., R. Célleri, B. De Bièvre, F. Cisneros, G. Wyseure, J. Deckers, and R. Hofstede, 2006. Human impact on the hydrology of the Andean páramos. Earth-Science Reviews 79: 53-72.

Buytaert, W., F. Cuesta-Camacho, and C. Tobón, 2010. Research review: Potential impacts of climate change on the environmental services of humid tropical alpine regions. Global Ecology and Biogeography; DOI information: 10.1111/j.1466-8238.2010.00585.x

Cane, M. and S.E. Zebiak, 1985. A Theory for El Niño and the Southern Oscillation. Science 228 (4703): 1085 – 1087.

Cane, M.A., A.C. Clement, A. Kaplan, Y. Kushnir, R. Murtugudde, D. Pozdnyakov, R. Seager, and S.E. Zebiak., 1997. 20th century sea surface temperature trends. Science 275: 957-960.

Castaño, C., 2002. Páramos y ecosistemas alto andinos de Colombia en condición hotspot & global climatic tensor. Bogotá (Colombia): Ministerio del Medio Ambiente e Instituto de Hidrología, Meteorología y Estudios Ambientales. 387pp. In: http://www.ideam.gov.co/publica/index4.htm

Ceballos, J.L., C. Euscátegui, J. Ramírez, M. Canon, C. Huggel, W. Haeberli, and H. Machguth, 2006. Fast shrinkage of tropical glaciers in Colombia. Annals of Glaciology 43:194-201.

Cuatrecasas, J., 1934. Observaciones geobotánicas en Colombia. Trabajos del Museo Nacional de Ciencias Naturales, Serie Botanica 27:1-144.

Departamento de Geografía–Universidad Nacional de Colombia, 2005. Escenarios de cambio climático para el territorio colombiano. Fase PDF-B, Integrated National Adaptation Pilot (INAP) - Informe Ejecutivo. Bogotá, Colombia, 19 pp.

Díaz-Granados, M. A., J.D. Navarrete, and T. Suárez, 2005. Páramos: hidrosistemas sensibles. Revista de Ingeniería Vol. 22. Departamento de Ingeniería Civil y Ambiental, Universidad de los Andes, Bogotá, Colombia. p. 64-75.

Diaz, H. F., M. Grosjean, and L. Graumlich, 2003. Climate variability and change in high elevation regions: past, present and future. Climatic Change 59(1-4). doi: 10.1023/A:1024416227887

Euscátegui, Ch., 2002. Estado de los glaciares en Colombia y análisis de la dinámica glaciar en el Parque Los Nevados, asociada al cambio climático global. Thesis of Master in Meteorology. Universidad Nacional de Colombia. Facultad de Ciencias. Departamento de Geociencias, Bogotá, Colombia. In: http://www.ideam.gov.co/biblio/paginaabierta/galaciarparquenevados.pdf

Fedorov, A.V. and S.G. Philander, 2001. A stability analysis of tropical ocean-atmosphere interactions: Bridging measurements and theory for El Niño. J. Clim. 14: 3086–3101.

Foster, P., 2001. The potential negative impacts of global climate change on tropical montane cloud forests. Earth-Science Reviews 55: 73-106.

Giorgi, F. and X. Bi, 2005. Updated regional precipitation and temperature changes for the 21 century from ensembles of recent AOGCM simulations. Geophysical Research Letters 32, L21715.

Gordon, A.L., and C.F. Giulivi, 2008. Sea surface salinity trends – over fifty years within the subtropical North Atlantic. Oceanography 21 (1): 22-31.

Gutiérrez, H., 2002. Aproximación a un modelo para la evaluación de la vulnerabilidad de las coberturas vegetales de Colombia ante un posible cambio climático utilizando Sistemas de Información Geográfica con énfasis en la vulnerabilidad de las coberturas nival y de páramo de Colombia. In: Castaño C (ed.) Páramos y ecosistemas alto andinos de Colombia en condición Hotspot y Global Climatic Tensor. Instituto de Hidrología, Meteorología y Estudios Ambientales (IDEAM), Bogotá, pp. 335–377.

Gutiérrez, M.E., P.A. Zapata, and D. Ruiz, 2006. Entendimiento de las señales de cambio climático y variabilidad climática en la oferta hídrica superficial de cuencas hidrográficas en zonas de alta montaña. Envigado, Antioquia (Colombia): Environmental Engineering Program, Antioquia School of Engineering. 160 pp.

Hastenrath, S., 1991. Climate dynamics of the tropics, Kluwer, Dordrecht, The Netherlands.

Holdridge, L.R., 1987. Ecología basada en zonas de vida. Instituto Interamericano de Cooperación para la Agricultura, San José, Costa Rica.

Hulme, M. and N. Sheard, 1999. Escenarios de cambio climático para países de los Andes del Norte. Unidad de Investigación Climática, Norwich, Reino Unido, 6 pp.

Instituto de Hidrología, Meteorología y Estudios Ambientales – IDEAM, 2001. Colombia: Primera Comunicación Nacional ante la Convención Marco de las Naciones Unidas sobre el Cambio Climático, Bogotá, Colombia.

In: http://www.ideam.gov.co/publica/cambioclimatico/PrimeraComunicacionColombia.pdf

Instituto de Hidrología, Meteorología y Estudios Ambientales – IDEAM, 2008. Los glaciares colombianos: expresión del cambio climático global. In: www.ideam.gov.co/publica/glaciares/glaciares.pdf

IPCC, 2001. Climate Change 2001: The Scientific Basis. Contribution of Working Group I to the Third Assessment Report of the Intergovernmental Panel on Climate Change [Houghton, J.T.,Y. Ding, D.J. Griggs, M. Noguer, P.J. van der Linden, X. Dai, K. Maskell, and C.A. Johnson (eds.)]. Cambridge University Press, Cambridge, United Kingdom and New York, NY, USA, 881 pp.

Kaplan, A., M. Cane, Y. Kushnir, A. Clement, M. Blumenthal, and B. Rajagopalan, 1998. Analyses of global sea surface temperature 1856-1991. Journal of Geophysical Research, 103(18): 567-589.

Karnauskas, K.B., J.E. Smerdon, R. Seager, and J.F. González-Rouco, 2012. A Pacific centennial oscillation predicted by coupled GCMs. Journal of Climate 25: 5943-5961.

Kendall, M.G., 1975. Rank Correlation Methods. Charles Griffin, London.

Körner, C. and J. Paulsen, 2004. A world-wide study of high altitude treeline temperatures. Journal of Biogeography, 31: 713–732.

Li, Z.X., 2001. Thermodynamic air-sea interactions and Tropical Atlantic SST dipole pattern. Phys. Chem. Earth (B), Vol. 26, No. 2, pp. 155-157.

Lorenz, E.N., 1956. Empirical orthogonal functions and statistical weather prediction. Sci. Rep. 1, 49 pp., Mass. Inst. of Technol., Cambridge.

Lotero, J.H., L.N. Trujillo, W.G. Vargas, and O. Castellanos, 2007. Restauración ecológica en páramos del Parque Nacional Natural Los Nevados: experiencias de restauración ecológica en páramos luego de incendios forestales en la cuenca alta del río Otún. Unidad Administrativa Especial del Sistema de Parques Nacionales Naturales de Colombia (UAESPNN) and Corporación Autónoma Regional de Risaralda (CARDER). Editorial Andina, 152 pages.

Meehl, G.A., T.F. Stocker, W.D. Collins, P. Friedlingstein, A.T. Gaye, J.M. Gregory, A. Kitoh, R. Knutti, J.M. Murphy, A. Noda, S.C.B. Raper, I.G. Watterson, A.J. Weaver, and Z-C. Zhao, 2007. Global Climate Projections. In: Climate Change 2007: The Physical Science Basis. Contribution of Working Group I to the Fourth Assessment Report of the Intergovernmental Panel on Climate Change [Solomon, S., D. Qin, M. Manning, Z. Chen, M. Marquis, K.B. Averyt, M. Tignor and H.L. Miller (eds.)]. Cambridge University Press, Cambridge, United Kingdom and New York, NY, USA, pp. 764-765.

Oster, R., 1979. Precipitation in Colombia (in Spanish). Revista Colombia Geográfica, 6.

Pabón, J.D., 2003. El cambio climático global y su manifestación en Colombia. Cuadernos de Geografia, v XII (1-2): 111-119.

Pabón, J.D., 2004. El cambio climático y sus manifestaciones en Colombia. Innovación y Ciencia, v XI (3-4): 68-73.

Poveda, G., and O.J. Mesa, 2000. On the existence of Lloró (the rainiest locality on Earth): enhanced ocean–land–atmosphere interaction by a low level jet. Geophys. Res. Lett., 27, 1675–1678.

Poveda, G., O.J. Mesa, and J.I. Vélez, 2001. Balances hidrológicos de Colombia. Universidad Nacional de Colombia Sede Medellín: Publicaciones Postgrado en Aprovechamiento de Recursos Hidráulicos; 150 pp.

Ramanathan, V. and W. Collins, 1991. Thermodynamic regulation of ocean warming by cirrus clouds deduced from observations of the 1987 El Niño. Nature 351: 27 – 32.

Reynolds, R.W. and T.M. Smith, 1994. Improved global sea surface temperature analyses, J. Climate 7.

Rossow, W.B., A.W. Walker, D.E. Beuschel, and M.D. Roiter, 1996. International Satellite Cloud Climatology Project (ISCCP) - Documentation of New Cloud Datasets. WMO/TD-No. 737, World Meteorological Organization, 115 pp.

Ruiz, D., H.A. Moreno, M.E. Gutiérrez, and P.A. Zapata, 2008. Changing climate and endangered high mountain ecosystems in Colombia. Science of the Total Environment 398 (1-3): 122-132; DOI: 10.1016/j.scitotenv.2008.02.038.

Ruiz, D., M.P. Arroyave, A.M. Molina, J.F. Barros, M.E. Gutiérrez, and P.A. Zapata, 2009. Signals of climate variability/change in surface water supply of high-mountain watersheds - Case study: Claro River high mountain basin, Los Nevados Natural Park, Andean Central

Mountain Range, Colombia. World Bank Group / School of Engineering (Medellin, Colombia), 207 pages.

Ruiz, D., 2010. Indo-Pacific and Tropical Atlantic EOF modes: contributions to the analyses of cloud cover conditions in the Los Nevados Natural Park, Colombian Central Mountain Range. Revista Escuela de Ingeniería de Antioquia (EIA), ISSN 1794-1237, No. 14: 39-52.

Ruiz, D., M.P. Arroyave, M.E. Gutiérrez, and P.A. Zapata, 2011. Increased climatic stress on high-Andean ecosystems in the Cordillera Central of Colombia. Pp. 182-191 in: Herzog SK, Martínez R, Jørgensen PM, Tiessen H (eds.). Climate change and biodiversity in the Tropical Andes. MacArthur Foundation, Inter-American Institute of Global Change Research (IAI) and Scientific Committee on Problems of the Environment (SCOPE), São José dos Campos and Paris, 348 pp., ISBN: 978-85-99875-05-6.

Ruiz, D., D.G. Martinson, and W. Vergara, 2012. Trends, stability and stress in the Colombian Central Andes. Climatic Change 112 (3): 717-732, doi: 10.1007/s10584-011-0228-0.

Sen, P.K., 1968. On a class of aligned rank order tests in two-way layouts. Annals of Mathematical Statistics 39, pp. 1115–1124.

The World Bank Group, 2006. Colombia-Integrated National Adaptation Program Project. Documents & Reports.

The World Bank Group, 2008. Assessing the potential consequences of climate destabilization in Latin America. Latin America and Caribbean Region Sustainable Development Working Paper 32 [W. Vergara (ed.)], 115 pp.

Trenberth, K.E., P.D. Jones, P. Ambenje, R. Bojariu, D. Easterling, A. Klein Tank, D. Parker, F. Rahimzadeh, J.A. Renwick, M. Rusticucci, B. Soden, and P. Zhai, 2007. Observations: Surface and Atmospheric Climate Change. In: Climate Change 2007: The Physical Science Basis. Contribution of Working Group I to the Fourth Assessment Report of the Intergovernmental Panel on Climate Change [Solomon, S., D. Qin, M. Manning, Z. Chen, M. Marquis, K.B. Averyt, M. Tignor and H.L. Miller (eds.)]. Cambridge University Press, Cambridge, United Kingdom and New York, NY, USA, pp. 265-271.

Unidad Administrativa Especial del Sistema de Parques Nacionales Naturales - UAESPNN, 2000. Información General del Parque Nacional Natural Los Nevados. Programa de Conservación y Manejo del Parque Nacional Natural Los Nevados. Manizales, Colombia.

van Oldenborgh, G.J., S.Y. Philip, and M. Collins, 2005. El Niño in a changing climate: a multi-model study. Ocean Sci., 1, 81–95.

Vergara, W., A.M. Deeb, A.M. Valencia, R.S. Bradley, B. Francou, A. Zarzar, A. Grünwaldt, and S.M. Haeussling, 2007. Economic impacts of rapid glacier retreat in the Andes. EOS, Transactions, American Geophysical Union 88(25): 261-264.

Vergara, W. (ed.), 2009. Assessing the potential consequences of climate destabilization in Latin America. Latin America and Caribbean Region Sustainable Development Working Paper 32. The World Bank. 115 pp. Available at: http://go.worldbank.org/RV4VNYC2U0.

Vernekar A.D., B.P. Kirtman, and M.J. Fennessy, 2003. Low-level jets and their effects on the South American summer climate as simulated by the NCEP Eta model. J Climate 16(2): 297–311.

Vuille, M., R.S. Bradley, M. Werner, and F. Keimig, 2003. 20th century climate change in the Tropical Andes: observations and model results. J Climatic Change;59 (1-2):75-99.

In: http://www.ingentaconnect.com/content/klu/clim/2003/00000059/F0020001/05117726

Wang, C., 2005. ENSO, Atlantic climate variability, and the Walker and Hadley circulations. In: The Hadley Circulation: Present, Past and Future, H.F. Diaz and R.S. Bradley (eds.): Kluwer Academic Publishers, The Netherlands, pp. 173-202.

Wang, B. and An S-I., 2005. A method for detecting season-dependent modes of climate variability: S-EOF analysis. Geophysical Research Letters, Vol. 32, L15710, doi:10.1029/2005GL022709.

Yamaguchi, K., and A. Noda, 2006. Global warming patterns over the North Pacific: ENSO versus AO. J. Meteorol. Soc. Japan, 84, 221–241.

Zebiak, S.E., 1993. Air-sea interaction in the equatorial Atlantic region. Journal of Climate 6: 1567–1586.

Table 1. Summary of available ground meteorological data. The available historical periods of weather station data are presented in the supplementary material.

Climatic variable	Climatic sub-variable		Longest historical period
Sunshine	SR1	Total sunshine [hrs]	1955-2005
	SR2	Total number of foggy days/null sunshine [days]	
	TSD	Total number of sunny days [days]	
	SR4	Daily maximum sunshine [hrs]	
	SR5	Daily mean sunshine [hrs]	
	SR6	Daily minimum sunshine [hrs]	
	SR7	Day-to-day standard deviation of daily sunshine [hrs]	
Rainfall	R1	Total rainfall [mm]	1942-2006
	R2	Total number of dry days [days]	
	R3	Maximum daily rainfall [mm]	
Minimum temperature	MTmin	Minimum temperatures during the warmest days [°C]	1950-2007
	ATmin	Average minimum temperatures [°C]	
	mTmin2	Minimum temperatures during the coldest days [°C]	
	SDTmin	Day-to-day standard deviation of minimum temperatures [°C]	
Maximum temperature	MTmax	Maximum temperatures during the warmest days [°C]	1950-2007
	ATmax	Average maximum temperatures [°C]	
	mTmax2	Maximum temperatures during the coldest days [°C]	
	SDTmax	Day-to-day standard deviation of maximum temperatures [°C]	
Diurnal temperature range	MDTR	Maximum diurnal temperature range [°C]	1950-2007
	ADTR	Mean diurnal temperature range [°C]	
	mDTR2	Minimum diurnal temperature range [°C]	
	SDDTR	Day-to-day standard deviation of diurnal temperature range [°C]	
Relative humidity	MRH	Maximum relative humidity [%]	1950-2007
	ARH	Mean relative humidity [%]	
	mRH2	Minimum relative humidity [%]	
	SDRH	Day-to-day standard deviation of relative humidity [%]	

Table 2. Annual historical values of sunshine variables

Area	SR1 [hrs/year]	SR2 [days/year]	TSD [days/year]	SR4 [hrs/day]	SR5 [hrs/day]	SR6 [hrs/day]	SR7 [hrs/day]
Lower altitudes on the W flank of the ACMR	1,330 to 1,750	8 to 11	344 to 357	8.9 to 9.5	4.1 to 4.9	0.27 to 0.38	2.4 to 2.6
Higher altitudes on the W flank of the ACMR	760	53	268	8.1	2.5	0.01	2.3
Lower altitudes on the E flank of the ACMR	1,550 to 1,600	12	341 to 351	9.4 to 9.6	4.3 to 4.6	0.22 to 0.27	2.6 to 2.7

Table 3. Annual historical values of rainfall variables

Area	R1 [mm/year]	R2 [days/year]	R3 [mm/day]
Lower altitudes on the W flank of the ACMR	1,800 to 2,700	106 to 187	42.7 to 48.0
Higher altitudes on the W flank of the ACMR	1,100 to 2,000	120 to 173	19.5 to 31.7
Lower altitudes on the E flank of the ACMR	1,900 to 2,300	153	45.7
Higher altitudes on the E flank of the ACMR	990 to 1,800	193 to 199	18.1 to 32.3

Table 4. Annual historical values of temperature, diurnal temperature range and relative humidity variables. The Greek letter 'Γ' represents the adjusted lapse rates (changes in temperature with increases in altitude); see also the R-squared coefficient, which depicts the measure of the fit.

Climatic variable	Sub-variable	Min	Max	Climatic variable	Sub-variable	Min	Max
Minimum temperatures [°C]	MTmin Γ= - 4.9 K/km (R^2=0.88)	+3.0	+18.6	Maximum temperatures [°C]	MTmax Γ= - 5.9 K/km (R^2=0.84)	+11.6	+30.6
	ATmin	+1.2	+17.2		ATmax	+8.4	+27.7
	mTmin2 Γ= - 5.0 K/km (R^2=0.88)	-1.5	+15.3		mTmax2 Γ= - 5.5 K/km (R^2=0.86)	+5.5	+23.5
	SDTmin	+0.8	+1.0		SDTmax	+1.2	+1.9
Diurnal temperature range [°C]	MDTR	9.3	14.7	Relative humidity [%]	MRH	90.2	98.2
	ADTR	6.6	11.0		ARH	74.5	91.6
	mDTR2	3.6	6.3		mRH2	62.7	77.1
	SDDTR	1.4	2.1		SDRH	4.8	7.2

Table 5. Climatic conditions along the mainstream of the Claro River watershed

Climatic variable	Lower altitudes, ~1,800m (Claro River–Molino River confluence)	Higher altitudes, ~4,450m (Visible headwaters)
Mean annual temperature [°C]	+19.9	+3.2
Minimum annual temperature [°C]	+13.1	-2.3
Mean annual dew point [°C]	+14.6	+0.9
Annual actual vapor pressure [hPa]	16.6	6.5
Annual saturation vapor pressure [hPa]	20.5	7.7
Mean annual relative humidity [%]	81.5	85.1
Atmospheric pressure [mb]	814.6	602.6
Actual mixing ratio	0.0127	0.0067
Saturation mixing ratio	0.0156	0.0079
Potential temperature [K]	274.1	239.1

Table 6. Percentage of the variance of SST anomalies explained by EOF modes

Month	Region	First EOF mode	Second EOF mode
January	30°S to 30°N Indo-Pacific	30.7	13.7
February		28.9	13.4
July		22.7	13.3
August		24.3	14.6
January	Tropical Atlantic	32.0	23.6
February		34.8	25.4
July		40.6	16.0
August		42.8	16.0
January	15°S to 15°N Indo-Pacific	44.3	15.6
February		41.1	14.4
July		31.0	17.5
August		32.8	18.9

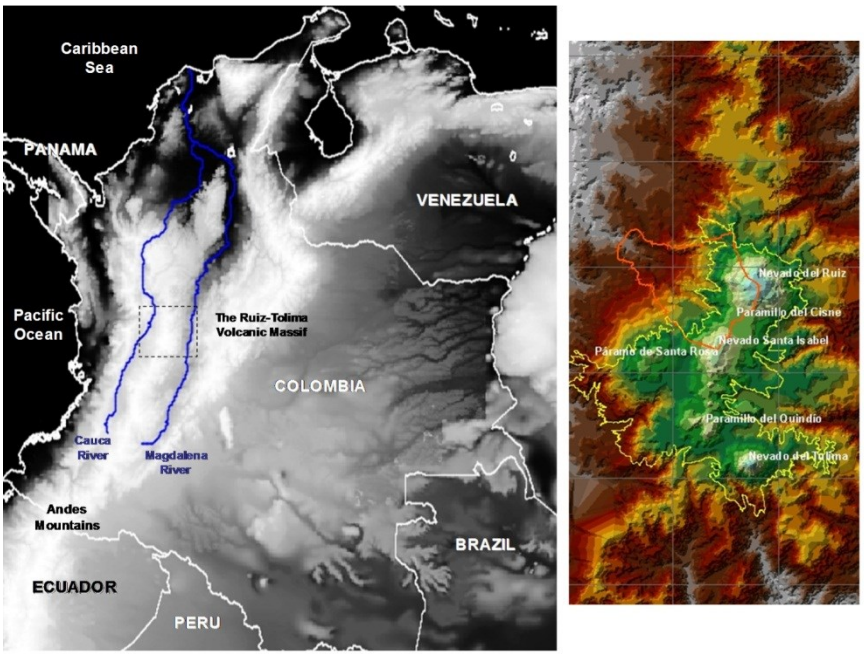

Figure 1. Study site. Left panel: general location of the El Ruiz-Tolima Volcanic Massif, on the Colombian Andean Central Mountain Range (source of Digital Elevation Model: HidroSig Java; Copyright: Postgrado en Aprovechamiento de Recursos Hidráulicos, Universidad Nacional de Colombia Sede Medellín). Right panel: Claro River high-altitude basin (orange line) and Los Nevados Natural Park (yellow line) (source: Ruiz et al., 2008).

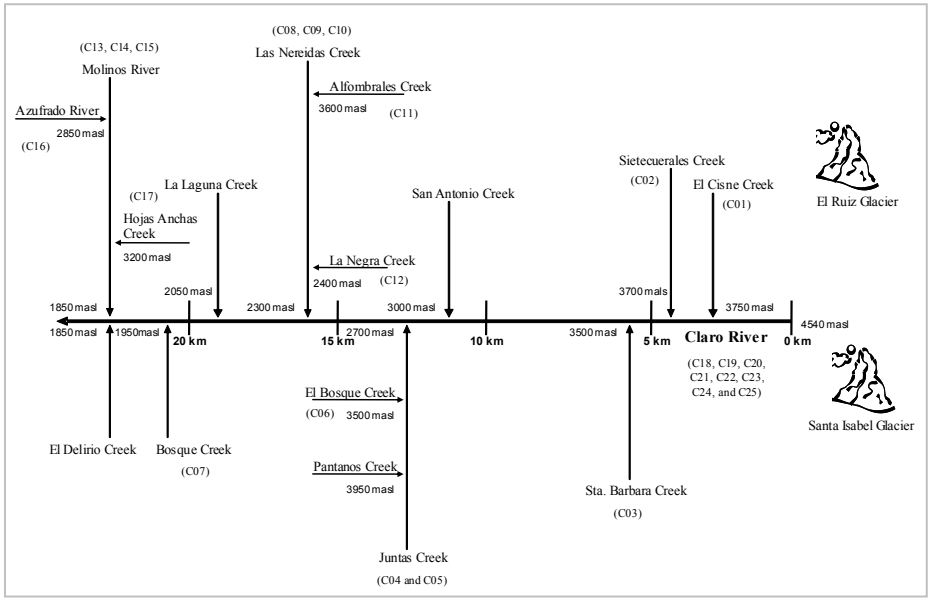

Figure 2. Systemic representation of the Claro River basin: mainstream (central axis) and main tributaries (arrows). See altitudes of stream joints and distances (along the main channel) from the Claro River headwaters.

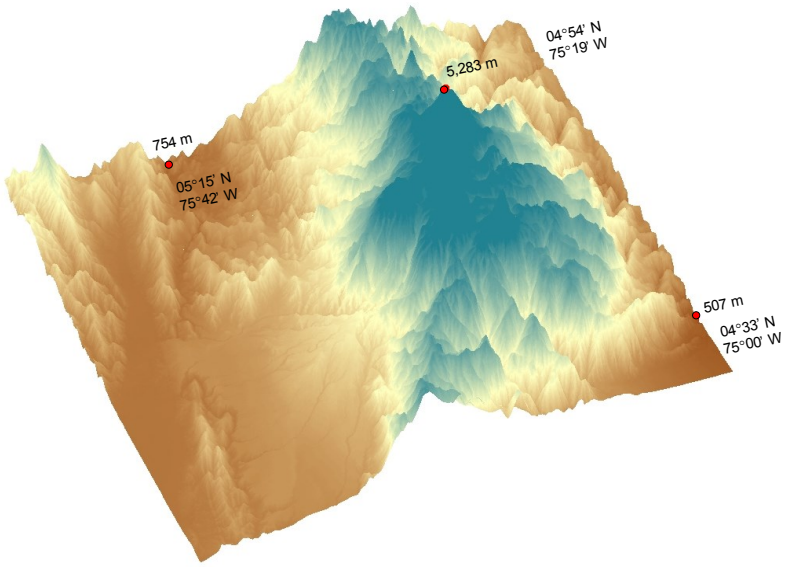

Figure 3. Digital Elevation Model (DEM) of the El Ruiz–Tolima volcanic massif, in the Cordillera Central of the Colombian Andes. Red dots denote points of reference over the ground: lowest point along the Cauca River valley (left); approximate summit of El Ruiz ice-capped mountain (center), and lowest point along the Magdalena River valley (right).

Figure 4. Key and characteristic species in the subpáramo (top panels; from left to right: *Miconia salicifolia*, *Berberis rigidifolia* and *Monnina aff. salicifolia*), proper páramo (middle panels; from left to right: *Gentianella* sp., *Plantago rigida* and *Diplostephium* sp.), and superpáramo (bottom panels; from left to right: *Lycopodium crassum*, *Draba pennell-hazenii* and *Loricaria colombiana*) life zones, in the Claro River high-altitude basin. For further information, visit the virtual catalog of high-altitude flora of Los Nevados Natural Park at: http://catalogofloraparamo.eia.edu.co/flora.php?page=inicio.

Figure 5. Interception of atmospheric water in Velón de páramo (*Lupinus alopecuroides*; left picture) and Frailejón (*Espeletia hartwegiana*; right picture).

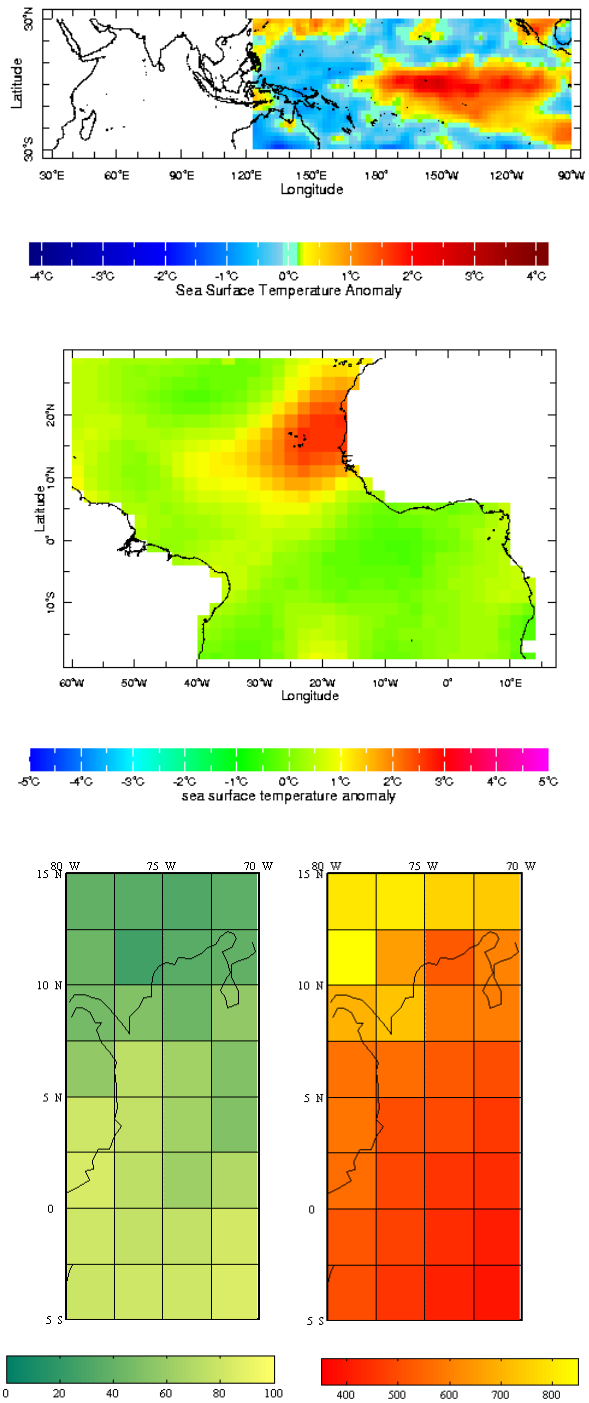

Figure 6. Areas of interest. Top panel: SST anomalies [°C] observed in January, 1992 in the spatial domain [30°S-30°N, 120°E-90°W] of the Pacific Ocean (source of info: Kaplan Extended v2). Central panel: SST anomalies [°C] observed in January, 1992 in the spatial domain [20°S-30°N, 60°W-10°E] of the Atlantic Ocean (source of info: Fundação Cearense de Meteorologia e Recursos Hídricos -

FUNCEME). Bottom panels: January average all-type cloud amounts [%] (left) and top pressures [mb] (right) observed over the spatial domain [5°S-15°N, 80°W-70°W] during the period 1984-2001 (source of info: NASA ISCCP D2).

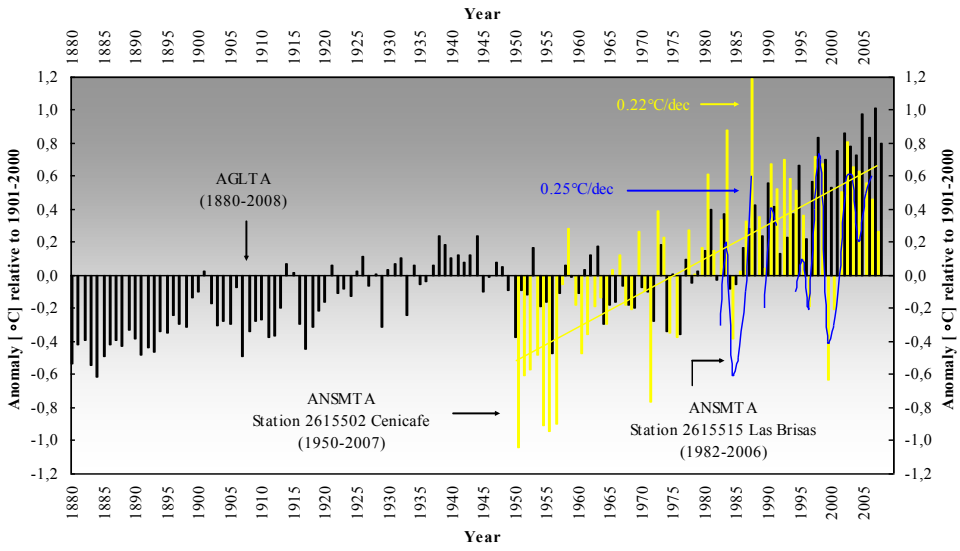

Figure 7. Annual global land temperature anomalies (AGLTA; source: NOAA Satellite and Information Service-National Environmental Satellite, Data and Information Service) and annual local near-surface mean temperature anomalies (ANSMTA, observed at stations XII-2615502 Cenicafé and I-2615515 Las Brisas). Anomalies are defined as departures from the 20th-century average (1901-2000). Linear trends in near-surface ambient temperatures observed in the area of the Claro River watershed exhibit rates of increase of about 0.22-0.25°C/decade.

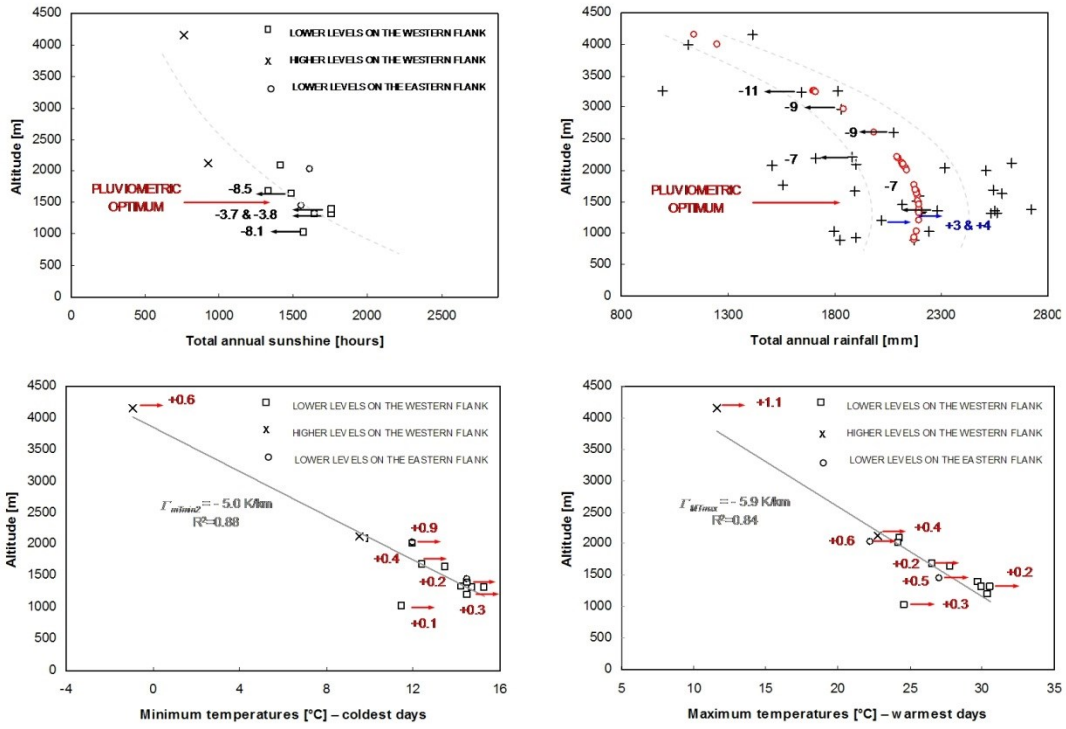

Figure 8. Historical annual values (boxes, crosses and circles) of sunshine (top left panel), rainfall (top right panel), minimum temperatures on the coldest days (bottom left panel), and maximum temperatures on the warmest days (bottom right panel) observed in the spatial domain 04°25'N-05°15'N and 75°00'W-76°00'W. Grey dashed and solid lines in top left, bottom left and bottom right panels depict the observed patterns in vertical profiles. Γ_{mTmin2} and Γ_{MTmax} in bottom left and right panels represent the adjusted lapse rates; see also the R-squared coefficient, which depicts the measure of the fit. Red circles in the top right panel depict the observed pattern of total annual rainfall with altitude. Grey dashed lines in the top right panel represent the observed envelopes. Arrows on top of all panels represent the observed long-term linear trends that were statistically significant at a 95% confidence level (boxes, crosses and circles without arrows depict those weather stations that reported climatic records with long-term trends that were not statistically significant at a 0.05 significance level). Trends in sunshine and rainfall (values next to arrows) are expressed in %/decade; trends in temperature (values next to arrows) are expressed in

°C/decade. Black arrows pointing to the left in top left and right panels depict decreasing trends. Blue arrows pointing to the right in top right panel depict increasing trends. Red arrows pointing to the right in bottom left and right panels represent increasing trends.

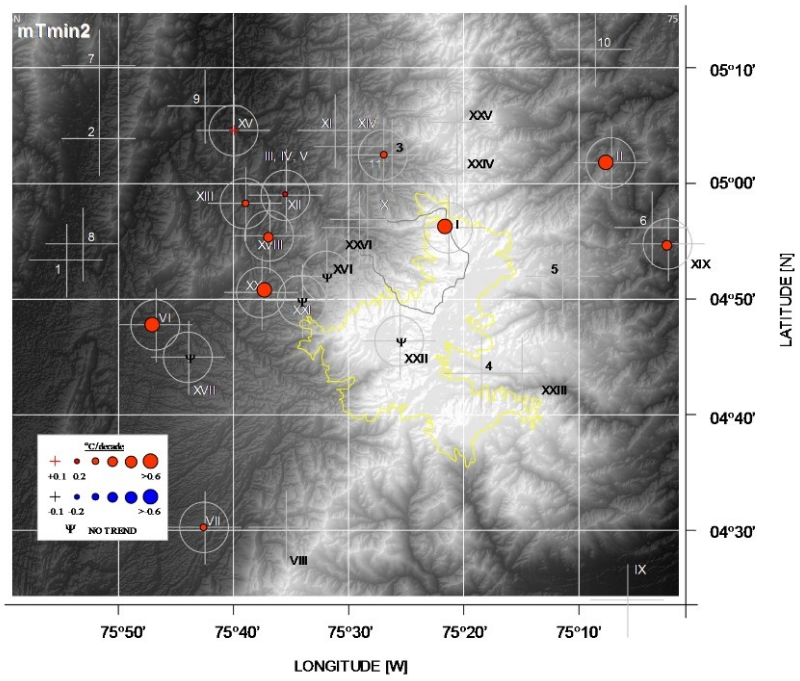

Figure 9. Estimated long-term trends in the mean (confirmatory analysis) of minimum temperatures observed on the coldest days in the selected spatial domain (04°25'N-05°15'N and 75°00'W-76°00'W). Crosses represent the location of meteorological stations. Grey circles around crosses denote those weather stations with available records of minimum temperatures. Trends plotted with red and blue circles are significant at a 95% confidence level. The size of these circles depicts the rate of change (see labels). Greek letter Ψ depicts those weather stations that reported climatic records with long-term trends that were not statistically significant at a 0.05 significance level. Yellow solid line delineates the perimeter of the Los Nevados Natural Park; grey solid line shows the Claro River high-altitude basin.

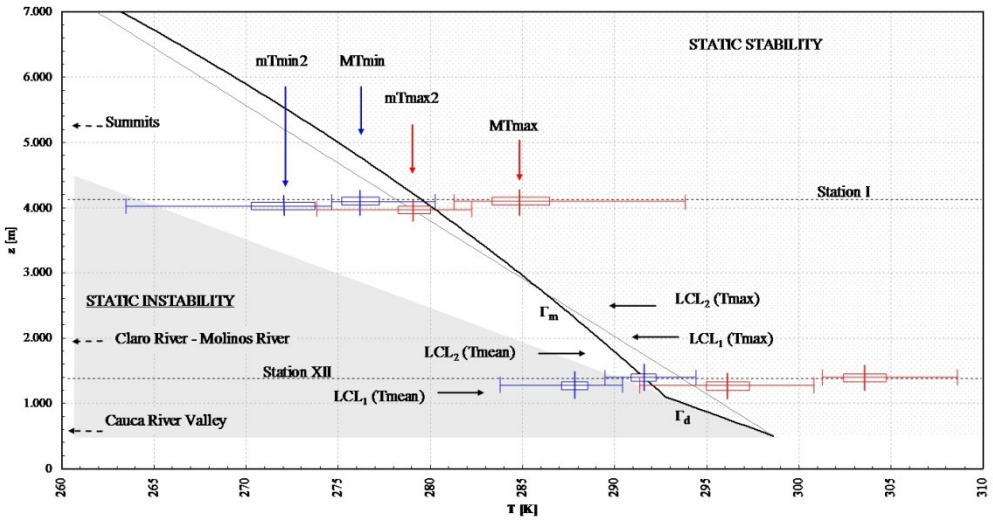

Figure 10. Estimated regions of static instability, conditional instability, and static stability in the area of the Claro River watershed. Γ_d and Γ_m represent the dry and moist (saturated) adiabatic lapse rates, respectively. LCL_1 and LCL_2 denote the estimated Lifting Condensation Levels for air parcels located at altitudes of around 700 m (Cauca River Valley) and 1,310 m (foothills of the ACMR or around met station XII), respectively. Shaded and dotted areas represent, respectively, the regions of static instability (environmental lapse rate is greater than Γ_d) and static stability (environmental lapse rate is smaller than Γ_d and Γ_m). The white area between the abovementioned areas depicts the region of conditional (in)stability (environmental lapse rate is between Γ_d and Γ_m). In this graph, regions of static instability, conditional instability and static stability are delimited assuming a LCL at an altitude of LCL_1(Tmean). Observed temperatures are represented by box-plots: blue for minimum monthly temperatures; red for maximum monthly temperatures. In each box-plot, vertical lines depict, from left to right, the minimum, mean and maximum observed values; boxes represent +1.0 standard deviations. mTmin2 and MTmin represent the minimum monthly temperatures during the coldest days and the warmest days, respectively; mTmax2 and MTmax represent the maximum monthly temperatures during the coldest and the warmest days, respectively.

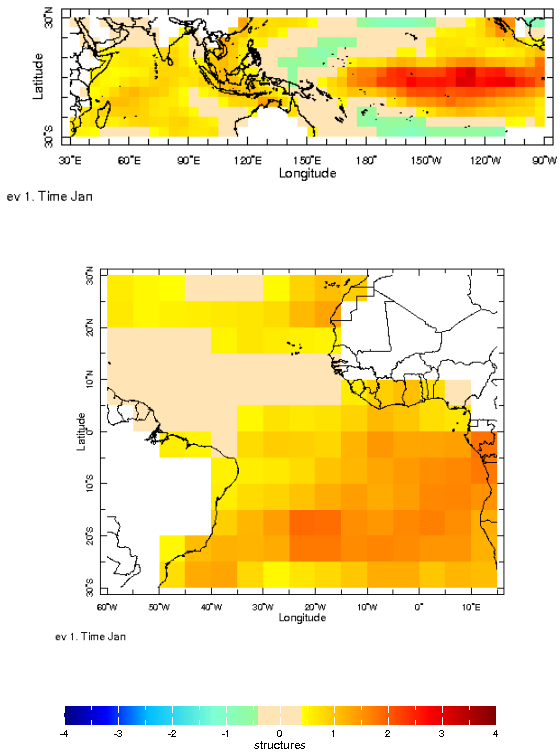

Figure 11. Spatial patterns of the Empirical Orthogonal Function modes of January SST anomalies observed in the Indo-Pacific and Tropical Atlantic oceans. Top panel: first loading pattern observed in the 30°S to 30°N Indo-Pacific region. Bottom panel: first loading pattern observed in the 30°S to 30°N Tropical Atlantic region. The first EOF modes of January SST anomalies observed in the 30°S to 30°N and 15°S to 15°N Indo-Pacific ocean basins represent the mature phase of ENSO and account for, respectively, 30.7% and 44.3% of the total variance of January SST anomalies (see Table 1).

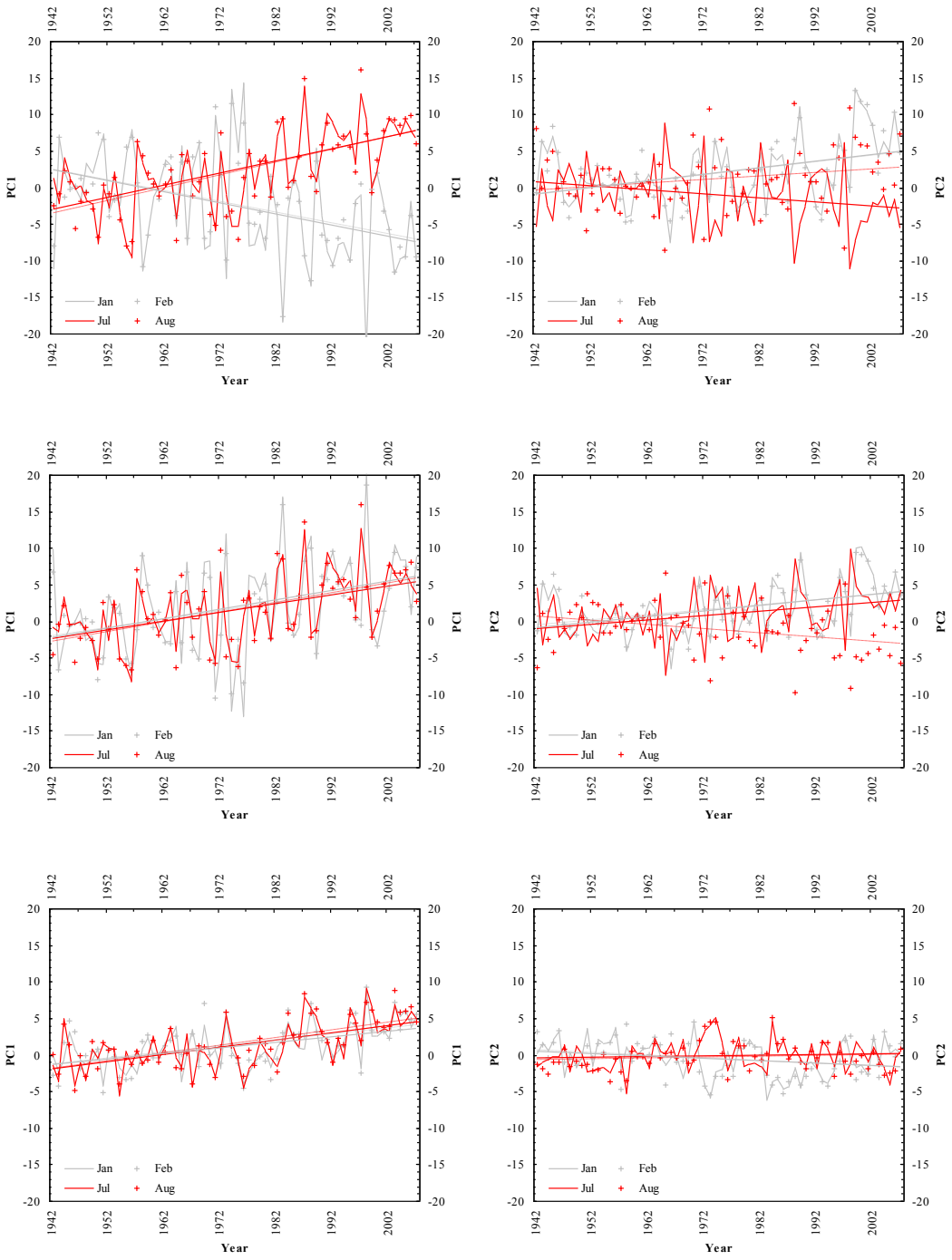

Figure 12. Principal components of SST anomalies observed in the Indo-Pacific and Tropical Atlantic oceans. Months of January, February, July, and August are represented, respectively, by the gray solid line, the gray pluses, the red solid line, and the red pluses. Top left and right panels: first and second PCs, Indo-Pacific region extending from 30°S to 30°N. Central left and right panels: first and second PCs,

Indo-Pacific region extending from 15°S to 15°N. Bottom left and right panels: first and second PCs, Tropical Atlantic.

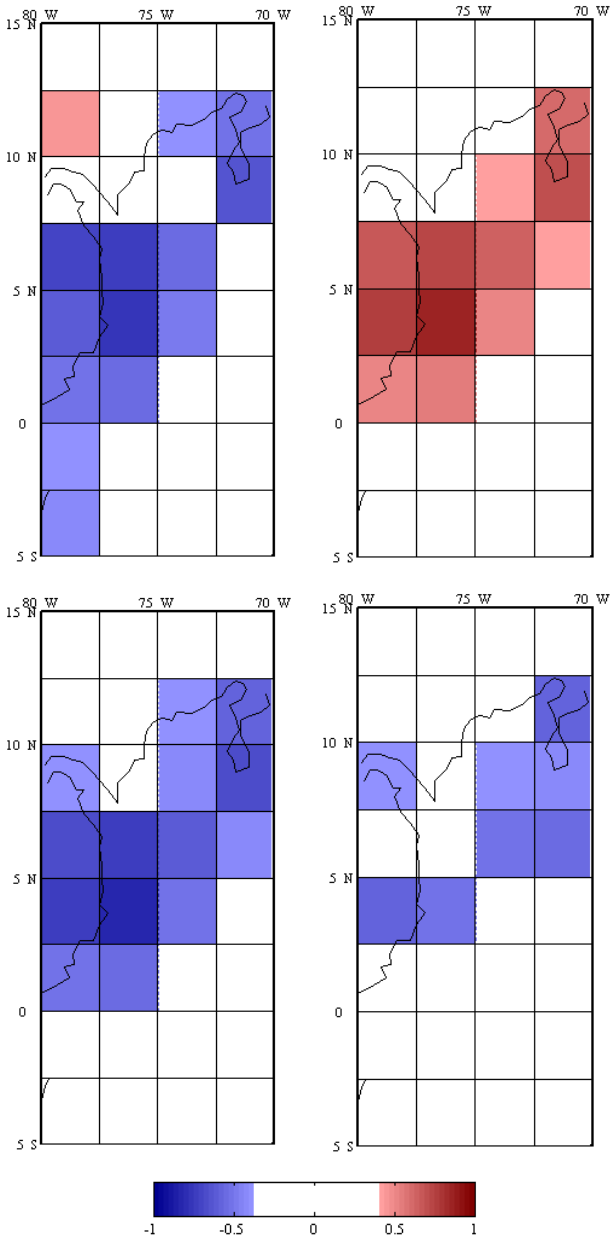

Figure 13. Correlation coefficients between January all-type cloud amounts observed over the spatial domain [5°S-15°N, 80°W-70°W] during the period from 1984 through 2001 and the January SST

anomalies observed in the Niño 3.4 region (top left), the first principal component of January SST anomalies observed in the 30°S to 30°N-belt of the Indo-Pacific region (top right), the first principal component of January SST anomalies observed in the 15°S to 15°N-belt of the Indo-Pacific region (bottom left), and the first principal component of January SST observed in the Tropical Atlantic Ocean (bottom right). Only those correlation coefficients that are statistically significant at a 95% confidence level are displayed.

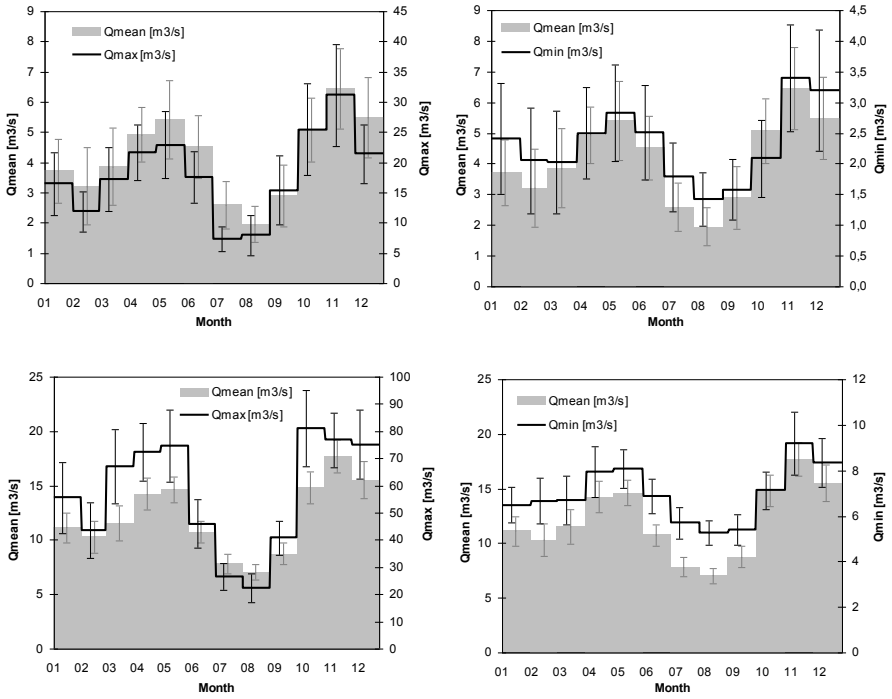

Figure 14. Annual cycles of minimum, mean and maximum streamflows observed at Chupaderos (Chinchiná River; 1988- 2005; top left and right panels) and La Bananera 6-909 (Otún River; 1971-2005; bottom left and right panels) limnigraphic stations.

Figure 15. Dried water bodies in the Los Nevados Natural Park.

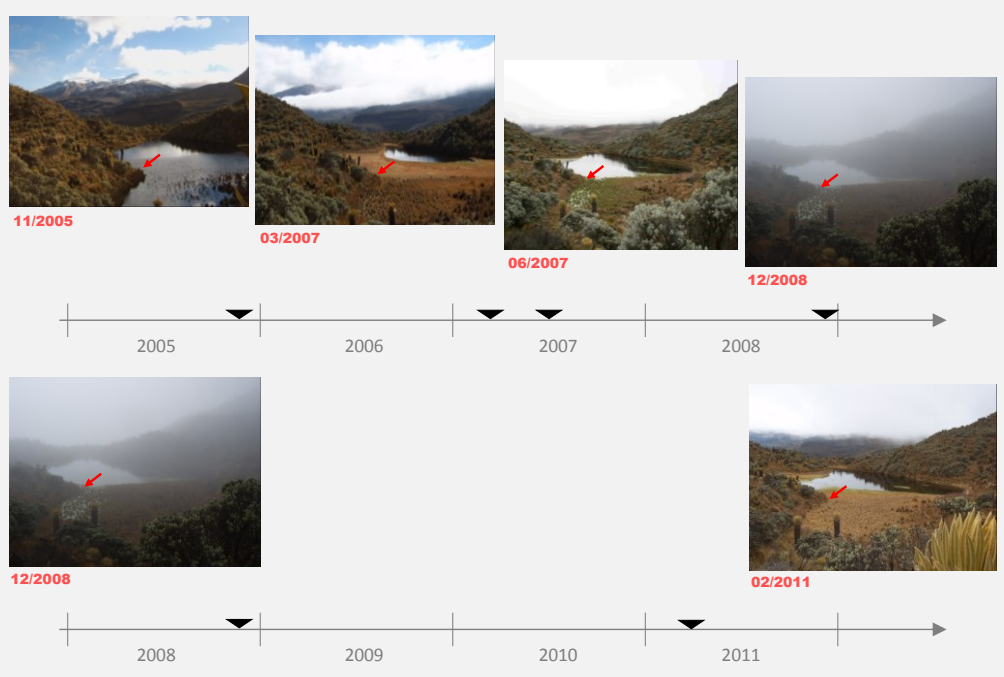

Figure 16. Fluctuations of high-altitude water body ID#01, linked to GPS mark 052, over the period 2005-2011.

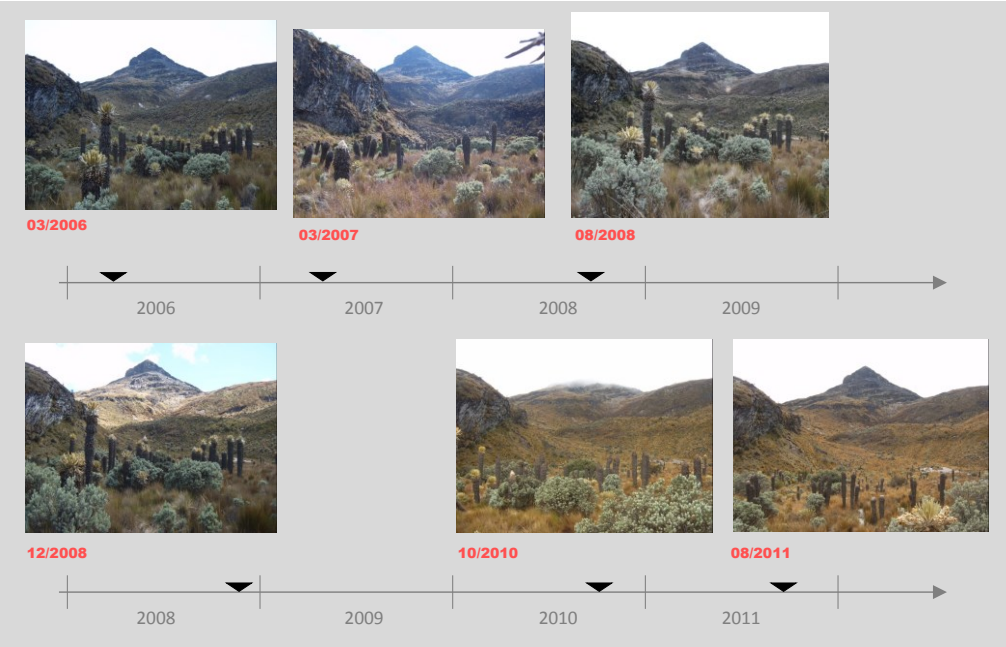

Figure 17. Recovery process of the area in the Los Frailejones Valley, on the track to Laguna Verde, Los Nevados Natural Park. The fire event took place in August, 2006. See the gradual disappearance of *Espeletia hartwegiana* individuals.

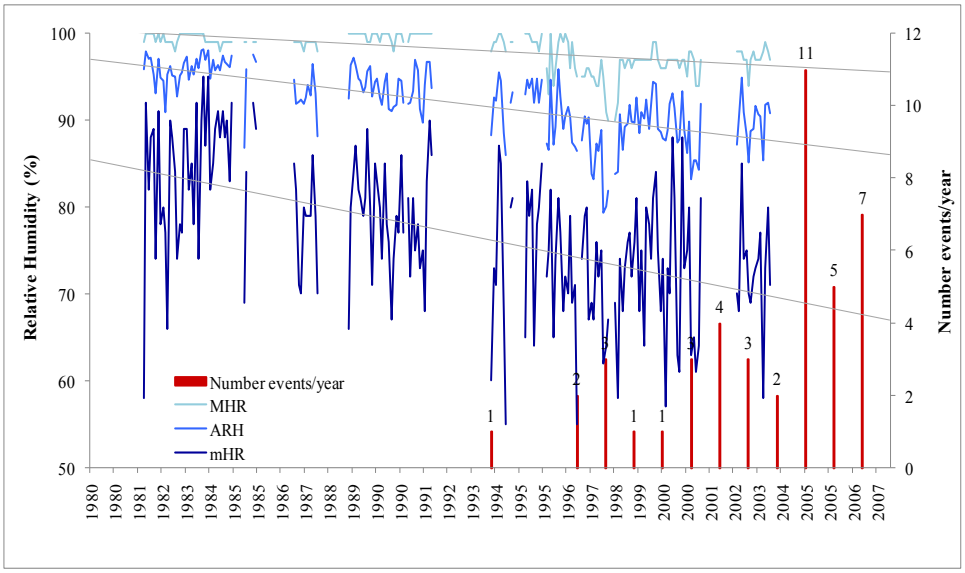

Figure 18. Monthly mean relative humidity values gathered at Las Brisas weather station over the period 1981-2003 along with the annual total number of fire events registered in the Los Nevados Natural Park over the period 1994-2007 (source: Unidad Administrativa Especial del Sistema de Parques Nacionales Naturales). MRH, ARH and mRH represent, respectively, the maximum, mean and minimum relative humidity values.

Chapter 3[3]

Atmospheric instability, feedback mechanisms and climatic stress on high-altitude Andean ecosystems

3.1. Introduction

Tropical upper-tropospheric warming (Fu et al., 2004; Fu and Johanson, 2005; Karl et al., 2006; Fu et al., 2011), as simulated for the A1B emission scenario (Meehl et al., 2007), is likely to have negative impacts on the integrity of high-altitude Andean ecosystems and thus on the vast number of environmental goods and services they provide (Foster, 2001; Ruiz et al., 2008; Vergara, 2009; Buytaert et al., 2010). A faster warming of the upper troposphere is likely to worsen the already rapid shrinkage of tropical mountain glaciers (Bradley et al., 2006; Ceballos et al., 2006). It could also have a sizable impact on key regional and local circulation dynamics (Butler et al., 2010) that will, more indirectly, exacerbate the climatic stress faced by these unique environments (Ruiz et al., 2011; Ruiz et al., 2012). In particular, a radiative positive feedback mechanism, which could result from changes in the environmental lapse rate and atmospheric conditional instability in the tropical troposphere, could cause further disruptions in the integrity of Andean biodiversity hotspots. Several convergent factors seem to be the critical drivers behind these changes: (i) the adjustment of the atmosphere to the radiative forcing of increasing greenhouse gases (Meehl et al., 2007); (ii) the rapid upward shifts in freezing levels,

[3] This chapter merges the research article by Ruiz et al. (to be submitted to the journal 'Advances in Geosciences') with the Mountain Research Initiative outreach newsletter by Ruiz et al. (2012). Copies of the manuscripts are available in the digital backup of this thesis.

which drive changes in surface albedo in upper levels; (iii) the decreases in the amount of fog and cloud cover in high-elevation regions where radiation is very intense; and (iv) the rapid decrease in the extent of Andean montane moist forests due to deforestation. They all interplay in a very complex fashion and our knowledge of these environmental problems, their physical mechanisms and concomitant impacts is still very limited.

In this chapter the self-reinforcing cycle that could result from changes in atmospheric stability in the tropical Andes is explored by studying both regional and local spatial scales. Discussions for the former comprise the full length of the Andes Cordillera, i.e. from its northernmost tip in the Colombia-Venezuela border region to Tierra del Fuego in southern Argentina, and are based on evidence from near-term historical climate models' ensemble simulation runs. Specifically, long-term trends and changes in mean annual near-surface and free air temperatures, environmental lapse rates, dew points, specific humidity, squared moist and dry Brunt-Väisälä frequencies, Lifting Condensation Levels, and Convective Available Potential Energies are studied. Analyses of the local scale are focused on three highly strategic high-altitude environments of the Tropical Andes: (a) the already discussed Los Nevados Natural Park on the El Ruiz-Tolima volcanic massif in the Colombian central Andean region (see chapter 2); (b) the protected complex 'El Angel Ecological Reserve – El Golondrinas Protected Forests – Awa Indian Preserve', on the Pacific slope of the Northern Andes in the Colombia-Ecuador transboundary region; and (c) the Madidi – Apolobamba – Bahuaja-Sonene – Tambopata protected area complex, which connects the Pacific and Amazonian slopes of the Central Andes in the border region between Bolivia and Peru. All these sites span elevational gradients of about 4,500 m, are renowned for their exceptional biodiversity and endemism, and have been considered key Andean biodiversity hotspots. For these experimental sites analyses include the

assessment of near-term historical conditions of static instability, conditional instability, and static stability using observed weather station and data logger data, where available.

3.2. Data

ECHAM4.5 mean monthly near-surface and free air temperatures (T_a) and specific humidities (q_s) (Roeckner et al., 1996), from ensemble simulation runs[4] and for the grid points located along the axis of the Andes Cordillera, were selected for the analysis of regional conditions. T_a and q_s values are available for the period spanning from January, 1950 through October, 2011, and for nine (9) pressure levels[5]. Environmental lapse rates, dew points, squared moist and dry Brunt-Väisälä frequencies, Lifting Condensation Levels, and Convective Available Potential Energies, estimated using T_a and q_s ensemble simulation runs, were also included in the analysis. Monthly sea surface temperature anomalies (SSTa) observed in the spatial domains [30°S-30°N, 30°E-90°W] of the tropical Indo-Pacific region and [30°S-30°N, 60°W-15°E] of the tropical Atlantic Ocean were considered to support the study. SSTa are available for the period spanning from January, 1942 to October, 2011 (source: Kaplan et al. 1998; see figure 6 in Chapter 2).

Daily minimum and maximum temperatures gathered at several weather stations were processed for the assessment of historical stability conditions at local level. In the Colombian Central Andean region, specifically, temperature data included records from eight (8) ordinary climatological or principal synoptic stations that are located on the western flank of the

[4] Freely downloadable at: http://iridl.ldeo.columbia.edu/SOURCES/.IRI/.FD/.ECHAM4p5/.History/.MONTHLY/.PressureLevel-SF/.

[5] 1000, 950, 850, 700, 500, 400, 300, 200, and 100 mb.

Colombian Central Cordillera, in the surroundings of the ca. 3,000 m altitudinal transect that follows the mainstream of the Claro River watershed. See table 1. These weather stations are all part of the network of thirty seven (37) weather stations available in the surroundings of the El Ruiz-Tolima volcanic massif (see table A-1 in Chapter 2 supplementary material). For the assessment of current conditions of atmospheric stability in the surroundings of the Claro River high-altitude basin, five (5) temperature and relative humidity (T/RH) data loggers were installed on its headwaters. See figure 1. Records gathered at these digital sensors allow to characterize: (i) local climatic conditions in the upper levels; (ii) the time of occurrence of minimum and maximum temperatures in the headwaters; and (iii) the actual environmental lapse rates along the Claro River basin, which were originally assumed to be close to the moist adiabatic lapse rate (see methods section and grey solid line in figure 10, chapter 2). Up to date, hourly temperature, relative humidity and dew point records comprise the historical periods spanning from mid-December, 2008 through the end of January, 2012, except for the highest digital sensor deployed in the *Lupinus* Valley which was installed on January 29, 2012. See table 2.

In the Colombian/Ecuadorian transboundary region a total number of seventy five (75) weather stations, most of them on the Pacific slope of the Andes Cordillera, were selected for the analysis. They include forty six (46) meteorological stations on the Colombian side of the border (see table SM-1(a) in supplementary material), and twenty nine (29) stations on the Ecuadorian side (see table SM-1(b) the supplementary material). In Colombia, ordinary climatological stations 5206502 Barbacoas and 5205502 El Paraíso, located at [01°40'N, 78°08'W and 32 m] and [01°05'N, 77°37'W and 3,120 m], respectively, are representative of the altitudinal gradient that runs from the Pacific lowlands into the Colombian highlands. In Ecuador, weather stations M025 La Concordia and M105 Otavalo, which are located at [00°01'N, 79°22'W and 360 m] and

[00°14'N, 78°15'W and 2,556 m], respectively, exemplify the path that connects the Pacific lowlands to the Ecuadorian upper Andes. In the Bolivian/Peruvian transboundary region a total number of seventeen (17) weather stations were selected for the analysis. They include seven (7) stations on the Bolivian side of the border, and ten (10) weather stations on the Peruvian side (see tables SM-1(c) and SM-1(d) in supplementary material). Records are part of a daily dataset for climate extreme analyses in Latin America (Martínez et al., 2012)[6]. Since stations on the Amazonian lowlands were not available, analyses conducted here are restricted to the Pacific slope of Bolivian/Peruvian transect. In particular, weather stations Tacna and Ayo Ayo, located at [18°03'S, 70°16'W and 452 m] and [17°05'S, 68°00'W and 3,880 m], respectively, are considered to be representative of this transect.

3.3. Methods

Correlation coefficients between observed near-surface temperatures anomalies, total rainfall anomalies and corresponding simulation outputs from CCM3.6 (Hack et al., 1998; Hurrell et al., 1998; Kiehl et al., 1998), COLA (Kinter et al., 1997), ECHAM4.5 (Roeckner et al., 1996), ECPC (Roads et al., 2001), GFDL (Delworth et al., 2006), and NSIPP (Bacmeister et al., 2000) for the historical period 1950-2000[7] were initially analyzed to select the climate model that better represents climatic conditions across South America. The best results in the area under study are obtained with the ECHAM4.5 model. For the December-January-February trimester, for instance, ECHAM4.5 near-surface temperature anomaly correlation coefficients range from +0.55 to +0.85 in most of the tropical belt 15°S-12°N, except in the spatial domains [10°S-5°S

[6] Data and metadata available at: http://ciifen.knmi.nl

[7] See model skill comparison at: http://iri.columbia.edu/forecast/climate/skill/Skill_comp.html.

and 70°W-75°W] and [15°S-10°S and 40°W-47°W] where values drop to almost +0.1 to +0.3. ECHAM4.5 rainfall anomaly correlation coefficients for the same trimester show, on the other hand, values as low as +0.1 except in the Northern Andes where they reach from +0.40 to +0.55.

ECHAM4.5 grid points located along the axis of the Andes Cordillera were obtained by masking the quality controlled NOAA NGDC GLOBE gridded 1-km global Digital Elevation Model (Hastings and Dunbar, 1999) with the ECHAM4.5 grid. See figure 2. The resulting dataset thus comprised a matrix of 26 latitudinal grid points by 9 pressure levels per month and per climatic variable. ECHAM4.5 mean annual free air temperature (T_a), specific humidity (q_s), environmental lapse rate (Γ), free air temperature and dew point difference (T_a-T_d) were obtained by averaging T_a, q_s, Γ and (T_a-T_d) monthly values, respectively. Four statistical tests were then used to assess the null hypothesis of zero slope parameters in T_a, q_s, Γ and (T_a-T_d) annual time series. They included the Student's t-test, the Hotelling–Pabst test, the non-parametric Mann–Kendall test (Kendall, 1975), and the aligned rank Sen's t-test (Sen, 1968). For further details, see methods section in Chapter 2. A historical time series was considered to have a statistically significant long-term linear trend in the mean at a α=0.05 significance level when at least three of these hypothesis tests rejected the null hypothesis of a zero slope parameter.

Also, exploratory and confirmatory analyses were conducted to detect statistically significant changes in the mean and the variance of T_a, q_s, Γ and (T_a-T_d) annual time series. The Bayesian Analysis (Lee and Heghinian, 1977; Salas and Boes, 1980) was used to determine the mean and the mode of the strongest point of change in the historical annual time series, as well as the mean of the total amount of change. Ten hypothesis tests, namely the Mann-Whitney/Wilcoxon rank sum test (Wilcoxon, 1945; Mann and Whitney, 1947), the simple t-test

assuming change and no change in the variance, the modified t-test (Matalas and Langbein, 1962) assuming change and no change in the variance, the simple t-test with corrections for dependence (Lettenmaier, 1975) assuming change and no change in the variance, and the Kruskal-Wallis test (Kruskal and Wallis, 1952) were used to detect statistically significant changes in the mean of the historical time series, using the point of change estimated through the Bayesian Analysis. A historical time series was considered to have a statistically significant change in the mean at a α=0.05 significance level when at least six of these hypothesis tests rejected the null hypothesis of equal means. Six hypothesis tests were then used to assess the significance of a change in the variance of T_a, q_s, and Γ annual time series. They included the simple F-test (Devore, 1982), the simple F-test with corrections for dependence (Lettenmaier, 1975), the modified F-test (Bayley and Hammersley, 1946) using Chi-square and F distributions, the Ansari-Bradley test (Hollander and Wolfe, 1973), the Bartlett test (Snedecor and Cochran, 1980), and the Levene test (Snedecor and Cochran, 1980). The point of change was also estimated through the Bayesian Analysis. A historical time series was considered to have a statistically significant change in the variance at a α=0.05 significance level when at least four of these hypothesis tests rejected the null hypothesis of equal variances.

Principal Component (PC) analyses were then conducted on January through December ECHAM4.5 simulated (ensemble runs) mean monthly T_a and q_s anomalies, and for the historical period 1950-2010. PC analyses were also conducted on the January through December monthly SSTa observed in the Indo-Pacific and Atlantic tropical ocean basins and for the historical period 1942-2010 (see figures 11 and 12 in chapter 2). First *eigenvalues* of monthly ECHAM4.5 mean T_a and q_s ensemble simulation outputs were then compared to the main modes of spatio-temporal variability of SSTa in the Indo-Pacific and Atlantic tropical belts.

The historical conditions of atmospheric stability were assessed through the analysis of the squared dry (N^2) and moist (N_m^2) Brunt-Väisälä frequencies. The former is given by:

$$N^2 = \frac{g}{T}(\Gamma_d - \Gamma),$$

where g denotes the gravitational acceleration, T the sensible temperature of the atmosphere, Γ_d the dry adiabatic lapse rate ($\Gamma_d = 9.8\, K/km$), and Γ the environmental lapse rate.

As a first approximation, the squared Brunt-Väisälä frequency in a saturated atmosphere, N_m^2, was determined using an analogous expression to the formula for the squared dry Brunt-Väisälä frequency (Durran and Klemp, 1982; Fraser et al., 1973), as follows:

$$N_m{}^2 = \frac{g}{T}(\Gamma_m - \Gamma),$$

where Γ_m denotes the moist adiabatic lapse rate, which is given by:

$$\Gamma_m = \frac{d\,lnT}{d\,lnp} = \Gamma_d \left[\frac{1+\frac{L\omega_S}{R_d T}}{1+\frac{L^2 \omega_S}{c_{pd} R_v T^2}} \right].$$

In the equation above L represents the latent heat of evaporation (for water at 0°C, $L=2.5x10^6\ J/kg$), R_d the ideal gas constant for dry air ($R_d=287\ J/K\text{-}kg$), R_v the gas constant for water vapor ($R_v=461\ J/K\text{-}kg$), and c_{pd} the specific heat for dry air ($c_{pd}=1004.5\ J/K\text{-}kg$). Since usually p>>e, the saturation mixing ratio, ω_s, is obtained using $\omega_s \cong \frac{\varepsilon e_s}{p}$, where $\varepsilon = \frac{R_d}{R_v} = 0.622$. The saturation vapor pressure $e_s(T)$ is calculated through the Clausius-Clapeyron equation:

$$e_s(T) = e_s(T_o) exp\left[\frac{L}{R_v}\left(\frac{1}{T_o} - \frac{1}{T}\right) \right],$$

where $T_o=273.15\ K$ (or 0°C) is the triple point of water, at which $e_s=6.11\ mb=611\ Pa$.

It is worth noting that in an unsaturated atmosphere a parcel of air that is lifted adiabatically cools by adiabatic expansion. If the atmosphere is saturated, however, upward displacements are accompanied by condensation and latent heating, which partially compensate for the cooling produced by adiabatic expansion (Durran and Klemp, 1982). Thus, two additional terms (not calculated here) have been proposed for estimating the squared Brunt-Väisälä frequency in a saturated atmosphere (Dudis, 1972; Lalas and Einaudi, 1974), as follows:

$$N_m{}^2 = \frac{g}{T}\left(\Gamma_m - \Gamma\right)\left(1 + \frac{L\omega_s}{R_d T}\right) - \frac{g}{1+\omega_w}\frac{d\omega_w}{dz},$$

where ω_w, the total water mixing ratio, is the sum of ω_s and the liquid water mixing ratio ω_L.

The squared dry and (approximated) moist Brunt-Väisälä frequencies were calculated for minimum, mean and maximum temperatures, depending on their availability. For the analysis of atmospheric stability along the axis of the Andes Cordillera, only ECHAM4.5 simulated (ensemble runs) mean annual air temperatures were used. Statistically significant long-term trends and changes in the mean and the variance of squared dry and moist Brunt-Väisälä frequencies were then assessed through the implementation of the abovementioned hypothesis tests. For the analysis of atmospheric stability on the west flank of the El Ruiz-Tolima volcanic massif and the Colombia-Ecuador and Bolivia-Peru transboundary regions, daily squared dry and moist Brunt-Väisälä frequencies were calculated using daily weather station minimum and maximum temperature records. Minimum, mean and maximum monthly squared dry and moist Brunt-Väisälä frequencies were then obtained and plotted on time series graphs.

The monthly Lifting Condensation Levels (LCLs) were determined by comparing the vertical profiles of free air temperature and dew point in Skew-T diagrams. Annual LCLs for all grid points along the axis of the Andes Cordillera were calculated by averaging monthly values and then tested for homogeneity using the hypothesis tests described above. Finally, monthly Convective Available Potential Energy (CAPE) for each grid point was calculated by integrating vertically the local buoyancy of an air parcel from the Level of Free Convection (LFC) to the Equilibrium Level (EL, neutral buoyancy), through the equation (Moncrieff and Miller, 1976):

$$CAPE = \int_{z_f}^{z_e} g\left(\frac{T_{v,parcel} - T_{v,env}}{T_{v,env}}\right) dz,$$

where z_f and z_e denote the heights of the LFC and the EL, respectively. Variables $T_{v,parcel}$ and $T_{v,env}$ represent the virtual temperatures of the air parcel and the surrounding air, respectively, and refer to the temperature that dry air would have if its pressure and specific volume (or 1/ρ, where ρ denotes the air density) were equal to those of a given sample of moist air. For the case of surrounding air the virtual temperature is given by:

$$T_{v,env} = T_{env}\left(\frac{1+\frac{\omega}{\varepsilon}}{1+\omega}\right),$$

where T_{env} and ω represent, respectively, the air temperature and the mixing ratio. Annual CAPE values for all grid points along the axis of the Andes Cordillera were calculated by averaging monthly values and then tested for homogeneity.

3.4. Results

3.4.1. Near-term climate change trends derived from simulation outputs

The top panel in figure 3 depicts the statistically significant long-term linear trends in mean annual air temperatures that took place along the axis of the Andes Cordillera over the period 1950-2010, according to ECHAM4.5 ensemble simulation runs. Outputs are consistent with the warming of the troposphere that has been discussed in Meehl et al. (2007), but do not agree with the cooling of the lower layers of the stratosphere suggested by their multi-model mean. Analyses of ECHAM4.5 simulation runs indicate, in particular, that air temperatures increased in all latitudes and in all pressure levels at a rate ranging from +0.03 to +0.40 °C per decade. Between 15°N and 15°S and at higher elevations [100-400 mb], air temperatures increased at a maximum rate ranging from +0.27 to +0.40 °C per decade. This rate of warming in the upper troposphere in the 15°N to 15°S latitudinal range exceeded 1.8 times what was simulated for the lower troposphere over the available 61-year historical period.

These long-term linear trends reflect, however, a non-uniform warming over time of all pressure levels in the troposphere. According to the years of occurrence of statistically significant changes in the mean of 1950-2010 ECHAM4.5 mean annual air temperatures along the axis of the Andes Cordillera (see top panel in figure SM-1(a) in the online supplementary material), most of the abrupt changes took place in the last two decades of the 20th century and particularly in the 1980-1990 period. However, they did not include strong changes in the variance (see the bottom panel of figure SM-1(a) in the online supplementary material), which were only observed in the 45°S to 55°S latitudinal range, in pressure levels in the range 200-950 mb, and in the early years of the 1980-1990 decade.

The upper-tropospheric warming affects the environmental lapse rate and will likely have an impact on atmospheric conditional instability in the tropical troposphere. Analyses of long-term linear trends in ECHAM4.5 mean annual environmental lapse rates (Γ) over the period 1950-2010 (see bottom panel in figure 3) suggest that most of the pressure levels in the tropical troposphere decreased their Γ values at a rate ranging from 0.01 to 0.03 K/km/decade, except in the 0° to 10°N tropical belt and in altitudes below 850 mb, where environmental lapse rates increased at almost 0.01 to 0.03 K/km/decade. By assuming an unmodified moist adiabatic lapse rate (equivalent to assess long-term trends in squared mean annual dry Brunt-Väisälä frequencies), these results would suggest that in altitudes above ca. 3,000 m the tropical troposphere could be slowly becoming static stable, whereas in altitudes below ca. 1,500 m it could be turning even more conditionally unstable or static unstable.

Statistically significant changes in the mean of annual time series of environmental lapse rates occurred primarily during the period from 1965 through 2004, according to the results of the implemented hypothesis tests (see top panel in figure SM-1(b) in the online supplementary material). Changes in the variance were not statistically significant, expect for the case of a few dispersed grid boxes which show abrupt changes in the 1967-2002 historical period (see bottom panel in figure SM-1(b) in the online supplementary material).

Figure 4 depicts the statistically significant long-term linear trends in squared mean annual moist Brunt-Väisälä frequencies (N_m^2) that are calculated for the axis of the Andes Cordillera and for the period 1950-2011, according to ECHAM4.5 ensemble simulation runs. Grid boxes labeled with the letter 'S' depict the ECHAM4.5 pressure levels where the air has been historically absolutely stable ($N_m^2>0$ or $\Gamma<\Gamma_m$), i.e. above 850 mb in the latitudinal range 35°S to 60°S, and above 500 mb in the latitudinal range 15°N to 35°S. ECHAM4.5 results

indicate that N_m^2 values changed along the Andes Cordillera at rates ranging from -0.0300E-04 to +0.0200E-04 s^{-2} per decade. Between 15°N and 15°S and at higher elevations (above 500 mb), N_m^2 historical time series show decreasing long-term linear trends, i.e. towards conditional instability, of about -0.0300E-04 to -0.0100E-04 s^{-2} per decade over the period 1950-2011. In the lower levels (below 500 mb), N_m^2 time series show slow, but statistically significant, increasing and decreasing trends in the range [-0.0100E-04;+0.0200E-04] s^{-2} per decade. ECHAM4.5 simulation results do not fully support the hypothesis of a long-term shift to static stable conditions in the tropical troposphere when the moist adiabatic lapse rate is also allowed to change over time, except in the lower levels of the Per/Bol transect and the northern tip of the Andes Cordillera.

3.4.2. Near-term historical time-averaged conditions of local atmospheric stability

Analyses of near-term historical time-averaged conditions of atmospheric stability on the west flank of the El Ruiz-Tolima volcanic massif included the assessment of the time of occurrence of vertical motions (see further information in the online supplementary material), and the calculation of squared monthly mean and minimum dry Brunt-Väisälä frequencies, as well as squared monthly maximum moist Brunt-Väisälä frequencies. Analyses of near-term historical time-averaged conditions of atmospheric stability in the Colombia-Ecuador and Bolivia-Peru transboundary regions only included the assessment of the aforementioned squared Brunt-Väisälä frequencies; i.e. the assessment of the time of occurrence of vertical motions was not conducted.

Time of occurrence of vertical motions on the west flank of the El Ruiz-Tolima volcanic massif. Figure 5 shows the time of occurrence of minimum and maximum near-surface air temperatures and relative humidity observed in the headwaters and the lowlands of the Claro River watershed. Minimum and maximum temperatures at the altitudes of T/RH data loggers, i.e. from 3,790 m to 4,260 m, usually take place (more than 20% of the total number of available days) at 06:00 am and 02:00 pm, respectively. See top panel. In the lowlands, in turn, near-surface minimum and maximum air temperatures commonly occur at 06:00 am and 03:00 pm, according to the records observed at the weather station 2615502 Cenicafé. See bottom panel. Hence, for the analysis of vertical motions minimum and maximum temperatures in the study site can be assumed to occur at 06:00 and 14:00, respectively. Figure 6 shows the inferred monthly states of convective stability in the headwaters of the Claro River watershed. Historical records (see top panel) confirm that the lower local atmosphere in the area and surroundings of the selected high-altitude basin could be either conditionally unstable or absolutely stable in the early morning, and hence air layers tend to be stratified and consequently free from convection. In the early afternoon (see bottom panel for conditions at 14:00) conditionally unstable conditions prevail, and vertical motions, turbulence and mixing of air layers occur when the air becomes saturated.

Near-term historical conditions of atmospheric stability in the proposed altitudinal transects. Figures 7(a) and 7(b) show the conditions of atmospheric stability inferred for the altitudinal transects proposed in the Colombian central Andean region (Los Nevados), the Colombia-Ecuador transboundary region (northwestern Ecuador and southwestern Colombia), and the Bolivia-Peru transboundary region (central Pacific slope). The top panel in Figure 7(a) presents, in particular, the squared early morning monthly mean dry Brunt-Väisälä frequencies

($_{EMM\mu}N^2$), based on historical records of local weather stations. The bottom panel in Figure 7(a) shows the squared early afternoon monthly mean dry Brunt-Väisälä frequencies, $_{EAM\mu}N^2$. The top panel in Figure 7(b) depicts the squared early afternoon monthly minimum dry Brunt-Väisälä frequencies, $_{EAMm}N^2$. And the bottom panel in Figure 7(b) presents the squared early afternoon monthly maximum moist Brunt-Väisälä frequencies, $_{EAMM}N_m^2$.

3.4.3. Regional near-term historical changes in the Lifting Condensation Levels (LCL)

According to ECHAM4.5 ensemble simulation runs, the historical mean free air temperature and dew point difference (T_a-T_d) in the region of moist convection (i.e. in the 20°S to 15°N latitudinal range, where strong uplifting processes of warm, moist air take place), reaches 6.4, 6.4, 8.0, and 6.2 °C in the trimesters December-January-February (DJF), March-April-May (MAM), June-July-August (JJA), and September-October-November (SON), respectively. The minimum T_a-T_d difference in the same latitudinal belt reaches, in turn, 1.0, 0.9, 1.8, and 1.1 °C in DJF, MAM, JJA, and SON, respectively.

The top panel in figure 8 shows the statistically significant long-term linear trends in (T_a-T_d) observed in the 20°S to 15°N latitudinal range during the trimester DJF and over the period 1950-2010, according to ECHAM4.5 ensemble simulation runs. (T_a-T_d) values have changed at rates ranging from -0.25 to +0.43 °C per decade over the studied historical period. The top panel in figure 8 also shows the historical annual Lifting Condensation Levels (LCLs) suggested by ECHAM4.5 simulation results for all the latitudes along the axis of the Andes Cordillera and for the period 1950-2011, as well as the statistically significant long-term linear trends in LCL annual time series. In the latitudinal range [60°S-30°S], LCLs reached annual values in the range

from 790 to 960 mb, with decreasing trends of about -0.11 to -1.09 mb per decade. In the tropical belt [5°S-15°N], LCLs reached average values of about 890 to 940 mb and exhibited long-term trends in the range from -1.40 to +0.30 mb per decade. In the 30°S to 5°S region ECHAM4.5 ensemble simulation runs suggest LCLs below the ground surface. The fastest upward shifts in LCLs along the Andes Cordillera have taken place in the ECHAM4.5 grid points centered at 34.88°S, 6.98°N and 9.77°N, where rates of change reached -1.09, -1.11 and -1.40 mb per decade.

3.4.4. Recent changes in the vertical profiles of water content

Figure 9 depicts the statistically significant long-term linear trends in ECHAM4.5 mean annual specific humidity that occurred along the Andes Cordillera over the period 1950-2010. ECHAM4.5 ensemble simulation outputs indicate that specific humidity has increased through much of the troposphere at a rate ranging from +1E-05 to +19E-05 per decade. Major increases took place in the middle to lower levels [500-850 mb] between 5°N and 15°S. Figure 9 also shows the historical annual Convective Available Potential Energies (CAPEs) for all the latitudes along the axis of the Andes Cordillera and for the period 1950-2011, as well as the statistically significant long-term trends in CAPE annual time series observed over the same historical period. Historical annual CAPE values range from 2 to almost 145 Joules/kg in the southern Andes (or in the latitudinal range [60°S-25°S]). In the central and northern Andes, CAPE values reach [44 to 1,374 Joules/kg] and [822 to 2,084 Joules/kg], respectively. Over the period 1950-2011 the rates of change in CAPE historical annual values range from -0.80 Joules/kg per decade

in the southern Andes, to +14.54 in the central Andes, and to almost +41.00 Joules/kg/decade in the Tropics.

3.5. Discussion

Figure 10 depicts a schematic, simplified diagram of the large-scale atmospheric circulation pattern that usually takes place along the studied latitudes, plotted on top of the axis of the Andes Cordillera. For the sake of simplicity, the north-south migration of the Inter-Tropical Convergence Zone (ITCZ) is not presented[8], and the ongoing poleward widening of the northern and southern hemisphere Hadley cells (Seidel et al., 2008) is ignored. Figure 10 also shows the 1950-2010 long-term linear trends in ECHAM4.5 simulated mean annual air temperatures and specific humidity, as well as the inferred long-term trends in atmospheric stability conditions in the proposed altitudinal transects. ECHAM4.5 ensemble simulation runs and inferred changes in stability conditions support the hypothesis of an ongoing strengthening of the ascending branches of the Hadley circulation cells (and the concomitant lifting of the tropopause; Williams, 2006) only if a southward migration of the ITCZ occurs.

The strengthening of the ascending branches of Hadley circulation cells causes a general increase in the amount of rainfall in the tropical belt and an increased occurrence of unusually heavy rainfall events in the latitudes where the ITCZ is placed. It also increases the release of latent heat in upper levels, which in turn produces and/or enhances the upper-tropospheric warming, particularly in the 15°N to 15°S latitudinal range. This near-tropopause warming alters

[8] ECHAM4.5 air temperature and dew point difference suggest that the ascending branches of Hadley circulation cells are located at almost 0°N during the trimester December-January-February, at almost 5°N in March-April-May, above 5°N in June-July-August, and at almost 5°N in September-October-November.

the conditions of atmospheric instability in the upper range of the tropical Andes, predominantly in latitudes within the Hadley cell that are distant from the ascending branches. These latitudes experience, in the long-term, an increased difference between free-air temperatures and dew points, a faster upward shift of Lifting Condensation Levels and a general decrease in moist convection. In fact, if the air were dry in pressure levels above 800 mb, latitudes within the Hadley circulation cells that are distant from the ascending branches would become static stable, according to ECHAM4.5 ensemble simulation runs. The amount of convective potential energy, water vapor and momentum that is being trapped in lower levels (below ca. 1,500 m, particularly in the northern hemisphere Hadley circulation cell) and that contributes to increase static or conditional instability in those latitudes, is being transported to the 0 to 10°S latitudinal range. An increase in specific humidity is taking place in tropical latitudes south of the Equator, specifically in lower levels (below 700 mb), and is accompanied by a decreased difference between free-air temperatures and dew points in pressure levels below 500 mb.

This process, although beneficial to some high-altitude environments located in areas surrounding the ascending branches of Hadley cells, could be very disruptive to key environments located in upper levels right in the heart of these circulation cells. High-altitude environments in the northern Andes, for instance, would benefit from moist convection[9] only if the lower atmosphere is saturated. Long-term periods of warmer and drier conditions in the upper Andes, particularly in the center of Hadley circulation cells, have occurred several times since the Last Glacial Maximum (see Muñoz et al., 2009), and could be a response to the non-linear dynamics (see Bush et al., 2010) that characterize the self-reinforcing cycle that results from local changes in stability conditions.

[9] According to ECHAM4.5 ensemble simulation runs all latitudes experienced increased conditional instability in pressure levels above 500 mb over the period 1950-2011.

3.5.1. Changes in atmospheric instability and positive feedbacks

Soden and Held (2006) forced coupled Atmosphere–Ocean General Circulation Models with increasing CO_2 concentrations to explore various feedbacks in the climate system and to study the potential feedbacks that could arise from uniform and non-uniform temperature changes in the troposphere. They argued that in low latitudes, where a greater reduction in the environmental lapse rate takes place due to a faster warming of the upper troposphere, the resulting feedback that could arise from a non-uniform temperature change, or environmental lapse rate feedback, could be more negative and, hence, larger climate change stabilization should be expected. From a systemic point of view, the feedback taking place in high-altitude Andean environments is the result of a coupled system that is composed of two interrelated opposite feedback loops: a positive, mostly hydrological/radiative loop that is driven by the dynamics of fog, middle-level clouds, ice caps and high-altitude water bodies; and a negative, thermodynamic feedback mechanism that is driven by changes in the environmental lapse rate and moist convection. See figure 11.

In upper levels of latitudes within the northern hemisphere Hadley circulation cell that are distant from its ascending branch, the resulting feedback that arises from the interactions of these two linked mechanisms is becoming positive and will only be reversed by external forcing. Changes in sea surface temperatures (SSTs) in both the Eastern Equatorial Pacific and the Tropical Atlantic oceans control the altitude of the 0°C isotherm and drive the location of the ITCZ. Positive anomalies in, particularly, the Eastern equatorial Pacific SSTs decrease all-type cloud and fog cover over extensive areas of the northern Andes, and therefore increase sunshine

and incoming sunlight reaching high-altitude Alto-Andean and páramo environments. Positive anomalies in Eastern Equatorial Pacific SSTs also increase upper-tropospheric temperatures through the release of latent heat due to convective processes in the ascending branches of the Hadley cells and the eastward-shifted ascending branch of the Walker circulation cell. Increases in the amount of direct sunlight and incoming short-wave radiation in high-altitude environments increase evaporation and reduce the extent of high-altitude water bodies, aquatic microhabitats and ice caps. They also increase near-surface and free-air temperatures in mountain habitats, drying the environment and exacerbating the effect through a positive, self-reinforcing hydrological/radiative feedback mechanism (reduced humidity, warmer temperatures and increased evaporation in a cloudless setting).

Positive anomalies in the Eastern Equatorial Pacific SSTs also increase lower-, high-level- and upper-tropospheric temperatures in the northern Andes. These changes in temperature increase the altitudes of the Lifting Condensation Level (LCL), the Level of Free Convection (which in turn affects convective available potential energy) and the 0°C isotherm, and generally decrease fog cover in all pressure levels. A faster warming of upper levels, in particular, decreases the environmental and moist adiabatic lapse rates. Decreases in the former reduce moist convection, thus increasing cloud cover in lower altitudes and driving long-term decreases in sunshine and sunny days, all these key aspects of a negative feedback[10]. Upward shifts in the 0°C isotherm also decrease the environmental lapse rate because katabatic winds coming down from the mountain ice caps (subsidence dynamics) decrease their microclimatic influence. Decreases in the moist adiabatic lapse rate would make the atmosphere more conditionally unstable and would favor moist convection only if the lower levels were saturated. Increases in

[10] At higher altitudes, on the contrary, decreases in moist convection reduce fog and cloud cover, causing increases in sunshine, more sunny days and producing the positive feedback mechanism described before.

specific humidity in Andean moist forests, which are influenced by the altitudinal shifts of the LCL, would also favor moist convection. Thus, the system could be driven back into a stable state because uplifting processes could increase cloud and fog cover in high altitudes, and could bring fog and mist to the surroundings of high altitude water bodies and ice caps (i.e. cloudy skies, reduced incoming sunlight and evaporation, and increased humidity).

Under the current scenario of global environmental change, however, it is unlikely that the system could recover its steady state. Human-induced increases in greenhouse gases have forced the adjustment of the atmosphere to the radiative forcing (Meehl et al., 2007) and have further increased upper-tropospheric temperatures (and will continue to do so). Deforestation rates, particularly in the northern Andes, have significantly reduced the extent of cloud and Alto-Andean forests (this environmental problem is also likely to continue), diminishing the source of humidity in lower levels (Spracklen et al., 2012; Suárez et al., 2011). Combined decreases in the environmental lapse rate and water vapor sources in lower levels are therefore reducing the role that moist convection plays in balancing the weights of the interrelated feedback loops of the high-altitude Andean climate system. Under these conditions, the external indirect and direct shocks that we are exerting on high-altitude environments could only be counteracted by the system's response in longer time periods.

3.5.2. Drivers

As mentioned, the high-altitude Andean climate system is influenced by external forcing associated with changes in El Niño Southern Oscillation (ENSO) dynamics and/or Tropical

Atlantic Ocean regimes. What is the signature of changes in SSTs in the spatio-temporal patterns of ambient temperatures and specific humidity along the axis of the Andes Cordillera? Figure 12 depicts the spatial patterns of the first *eigenvalues* or Empirical Orthogonal Function (EOF) modes of ECHAM4.5 December, January and February mean air temperature (T_a) and specific humidity (q_s) anomalies, along the axis of the Andes Cordillera and for the historical period spanning from January, 1950 through October, 2011. EOF modes for the rest of the months are available in the digital backup of these analyses. Figure 13 shows, in turn, the Principal Components (PCs) of February and August SST anomalies (SSTa) observed in the Atlantic [15°E-60°W and 30°S-30°N] and the Indo-Pacific [90°W-30°E and 30°S-30°N] tropical belts over the period spanning from January, 1942 to October, 2011, along with the time series of the first *eigenvalues* of ECHAM4.5 February and August mean air temperature and specific humidity anomalies (ensemble simulation outputs) along the axis of the Andes Cordillera and for the historical period spanning from January, 1950 through October, 2011. PCs for the rest of the months are available in the digital backup of these analyses. The first EOF modes of December, January and February T_a anomalies explain 76.4%, 78.9% and 78.8% of the total spatio-temporal variability of mean air temperature anomalies along the axis of the Andes Cordillera. The leading EOF modes of December, January and February q_s anomalies explain, in turn, 79.3%, 71.7% and 70.6% of the total spatio-temporal variability of specific humidity anomalies.

Leading December, January and February T_a EOF modes suggest a monopole structure centered in the upper levels (above 500 mb approximately) of the 15°S to 15°N latitudinal range. The first December, January and February q_s EOF modes also indicate another monopole structure that is centered in the lower levels (below 600 mb) of the 15°S to 5°N latitudinal range. Air temperatures and specific humidity anomalies along the axis of the Andes Cordillera show a

coupled behavior with SSTa in the Indo-Pacific and Atlantic tropical belts, particularly in the winter of the northern hemisphere (NH), as shown in the time series of first eigenvalues. More specifically, T_a and q_s monopole structures seem to respond to the first EOF modes observed in SSTa in the Indo-Pacific and Tropical Atlantic belts during the NH winter months, according to ECHAM4.5 ensemble simulation runs. As discussed in Chapter 2, these first EOF modes observed in SSTa depict, respectively, the mature phase of ENSO in the Indo-Pacific ocean and the equatorial monopole structure in the Tropical Atlantic belt. It could be argued that long-term changes in ambient temperatures in the upper levels of the 15°S to 15°N latitudinal range are, in particular, strongly dependent on changes (long-term warming and normal variability) in sea surface temperatures in both the Indo-Pacific and Tropical Atlantic oceans. Although not discussed here, long-term changes in air temperatures in the upper levels of the 15°S to 15°N latitudinal range could also respond to synergistic effects of ENSO and Tropical Atlantic dynamics.

3.6. Conclusions

According to ECHAM4.5 ensemble simulation runs, changes in climatic conditions along the Andes Cordillera over the period 1950 to present were characterized by: (a) faster increases in mean annual upper tropospheric free-air temperatures in the 15°N to 15°S latitudinal range, compared to their corresponding lower tropospheric counterparts; (b) major increases in mean annual specific humidity in middle to lower levels of the 15°S to 5°N tropical belt; (c) decreases in historical air temperature and dew point difference in lower levels of the 0 to 10°S latitudinal range; (d) faster upward shifts in Lifting Condensation Levels in the northern Andes; (e) major

increases in convective available potential energy in the Tropics; (f) increases in static or conditional instability in lower levels (altitudes below ca. 1,500 m) of the northern hemisphere Hadley circulation cell, particularly in the 0° to 10°N latitudinal range; (g) increases in static stability (for dry air) in the tropical troposphere in altitudes above ca. 3,000 m; and (h) shifts towards conditional instability (for moist air) in higher elevations (above 500 mb) of the 15°S to 15°N latitudinal range.

The tropical near-tropopause faster warming alters the conditions of atmospheric conditional instability in the upper range of the tropical Andes. On the ground weather data suggest that, along the altitudinal transect in Los Nevados Natural Park in central Colombia, conditionally unstable conditions are in the long-term shifting towards static stability, according to historical squared early afternoon monthly maximum moist Brunt-Väisälä frequencies. Along the altitudinal gradient that runs from the Pacific lowlands into the Colombian highlands in Southwestern Colombia, conditionally unstable to low-frequency static stable conditions are in the long run pointing towards more static stable conditions. Along the path that connects the Pacific lowlands to the Ecuadorian upper Andes, static stable conditions have prevailed and show, historically, to become even more prevalent. On the contrary, on the Pacific slope of the Central Andes in the Bolivia-Peru transboundary region, historical static stable conditions are shifting towards conditional instability. These opposite behaviors suggest ongoing disruptive processes in the northern hemisphere Hadley circulation cell.

The upper range of the northern Andes is rapidly experiencing the imbalance of the coupled thermodynamic and hydrological/radiative mechanisms that characterize the dynamics of the Andean high-altitude climate. Combined decreases in the environmental lapse rate due to faster upper tropospheric warming and rapid reduction of water vapor sources in lower levels due

to deforestation are lessening the role that moist convection plays in balancing the weights of these interrelated, opposite feedback loops. The ongoing strengthening of the ascending branches of the Hadley circulation cells and the potential southward migration of the Inter-Tropical Convergence Zone are causing a positive feedback towards drier conditions in latitudes within the northern hemisphere Hadley cell that are distant from its uplifting path. Ongoing changes in environmental conditions are driving the northern Andean climate away from its steady state and would probably result in a severe, long-lasting drought in the region. The consequences of this rapid destabilization of the Andean climate are manifold and have serious implications for water, energy supply, agriculture, and ecosystem integrity (IDB–WWF–ECLAC, 2012).

Acknowledgments

The research group thank the Colombian Institute of Hydrology, Meteorology and Environmental Studies – IDEAM, the Centro Nacional de Investigaciones de Café – CENICAFE, the Unidad Administrativa Especial del Sistema de Parques Nacionales Naturales de Colombia – UAESPNN, the Ecuadorian National Institute of Meteorology and Hydrology – INAMHI, the Bolivian National Service of Meteorology and Hydrology – SENAMHI, the Peruvian National Service of Meteorology and Hydrology – SENAMHI, and the International Research Centre on El Niño – CIIFEN for providing data and continuous support. We also acknowledge the helpful suggestions made by three anonymous peer-reviewers who read and commented this manuscript. This study forms part of the multidisciplinary project “Impacts of climate change on biodiversity in the tropical Andes” funded by the John D. and Catherine T. MacArthur Foundation through a grant to the Inter-American Institute for Global Change

Research. D. Ruiz was partially supported by the Department of Earth and Environmental Sciences at Columbia University in the City of New York, the International Research Institute for Climate and Society, Lamont-Doherty Earth Observatory, and the Antioquia School of Engineering (Colombia).

References

Bacmeister, J., P.J. Pegion, S.D. Schubert, and M.J. Suarez, 2000. Atlas of seasonal means simulated by the NSIPP 1 Atmospheric GCM. NASA/TM-2000- 104505, Vol. 17, 194 pp.

Bayley, G.V., and J.M. Hammersley, 1946. The effective number of independent observations in an autocorrelated time series. Journal of the Royal Statistical Society 8(1B): 184–197.

Bradley, R.S., M. Vuille, H.F. Diaz, and W. Vergara, 2006. Threats to water supplies in the Tropical Andes. Science 312: 1755-1756.

Bush, M.B., J.A. Hanselman, and W.D. Gosling, 2010. Nonlinear climate change and Andean feedbacks: an imminent turning point? Global Change Biology 16: 3223–3232, doi: 10.1111/j.1365-2486.2010.02203.x.

Butler, A.H., D.W.J. Thompson, and R. Heikes, 2010. The steady-state atmospheric circulation response to climate change-like thermal forcings in a simple general circulation model, J. Clim. 23: 3474–3496.

Buytaert, W., F. Cuesta-Camacho, and C. Tobón, 2010. Research review: Potential impacts of climate change on the environmental services of humid tropical alpine regions. Global Ecology and Biogeography; doi: 10.1111/j.1466-8238.2010.00585.x

Ceballos, J.L., C. Euscátegui, J. Ramírez, M. Canon, C. Huggel, W. Haeberli, and H. Machguth, 2006. Fast shrinkage of tropical glaciers in Colombia. Annals of Glaciology 43:194-201.

Delworth, T.L., A.J. Broccoli, A. Rosati, R.J. Stouffer, V. Balaji, J.A. Beesley, W.F. Cooke, K.W. Dixon, J. Dunne, K.A. Dunne, J.W. Durachta, K.L. Findell, P. Ginoux, A. Gnanadesikan, C.T. Gordon, S.M. Griffies, R. Gudgel, M.J. Harrison, I.M. Held, R.S. Hemler, L.W. Horowitz, S.A. Klein, T.R. Knutson, P.J. Kushner, A.R. Langenhorst, H.C. Lee, S.J. Lin, J. Lu, S.L. Malyshev, P.C.D. Milly, V. Ramaswamy, J. Russell, M.D. Schwarzkopf, E. Shevliakova, J.J. Sirutis, M.J. Spelman, W.F. Stern, M. Winton, A.T. Wittenberg, B. Wyman, F. Zeng, and R. Zhang, 2006. GFDL's CM2 Global Coupled Climate Models. Part I: Formulation and simulation characteristics. J. Climate 19: 643-674.

Devore, J., 1982. Probability and statistics for engineering and the sciences. Monterey, CA: Brooks/Cole.

Dudis, J.J., 1972. The stability of a saturated, stably-stratified shear layer. J. Atmos. Sci. 29: 774-778.

Durran, D.R., and J.B. Klemp, 1982. On the effects of moisture on the Brunt-Väisälä frequency. Journal of the Atmospheric Sciences 39: 2152-2158.

Foster, P., 2001. The potential negative impacts of global climate change on tropical montane cloud forests. Earth-Science Reviews 55: 73-106.

Fraser, A.B., R.C. Easter, and P.V. Hobbs, 1973. A theoretical study of the flow of air and fallout of solid precipitation over mountainous terrain: Part I. Air flow model. Journal of Atmospheric Sciences 30: 801-812.

Fu, Q., C.M. Johanson, S.G. Warren, and D.J. Seidel, 2004. Contribution of stratospheric cooling to satellite-inferred tropospheric temperature trends. Nature 429: 55–58.

Fu, Q., and C.M. Johanson, 2005. Satellite-derived vertical dependence of tropical tropospheric temperature trends. Geophys. Res. Lett., 32, L10703.

Fu, Q., S. Manabe, and C.M. Johanson, 2011. On the warming in the tropical upper troposphere: models versus observations. Geophys. Res. Lett., 38, L15704, doi: 10.1029/2011GL048101.

Hack, J.J., J.T. Kiehl, and J.W. Hurrell, 1998. The hydrologic and thermodynamic characteristics of the NCAR CCM3. J. Climate 11: 1179–1206.

Hastings, D.A., and P.K. Dunbar, 1999. Global land one-kilometer base elevation (GLOBE) digital elevation model, Documentation, Volume 1.0. Key to Geophysical Records Documentation (KGRD) 34. National Oceanic and Atmospheric Administration, National Geophysical Data Center, 325 Broadway, Boulder, Colorado 80303, U.S.A.

Hollander, M., and D.A. Wolfe, 1973. Nonparametric statistical methods. New York: John Wiley & Sons, 83–92.

Hurrell, J.W., J.J. Hack, B.A. Boville, D.L. Williamson, and J.T. Kiehl, 1998. The dynamical simulation of the NCAR Community Climate Model version 3 (CCM3). J. Climate 11: 1207–1236.

Inter-American Development Bank – IDB, World Wildlife Fund – WWF and Economic Commission for Latin America and the Caribbean – ECLAC, 2012. The climate and

development challenge for Latin America and the Caribbean: options for climate resilient low carbon development. No 71918, IDB Publications.

Kaplan, A., M. Cane, Y. Kushnir, A. Clement, M. Blumenthal, and B. Rajagopalan, 1998. Analyses of global sea surface temperature 1856-1991. Journal of Geophysical Research 103 (18): 567-589.

Karl, T.R., S.J. Hassol, C.D. Miller, and W.L. Murray (Eds.), 2006. Temperature trends in the lower atmosphere: steps for understanding and reconciling differences. Synth. Assess. Prod. 1.1, U.S. Clim. Change Sci. Program, Washington, D.C.

Kendall, M.G., 1975. Rank correlation methods. Charles Griffin, London.

Kiehl, J.T., J.J. Hack, G.B. Bonan, B.A. Boville, D.L. Williamson, and P.J. Rasch, 1998. The National Center for Atmospheric Research Community Climate Model. J. Climate 11: 1131–1149.

Kinter, J.L. III, D. DeWitt, P.A. Dirmeyer, M.J. Fennessy, B.P. Kirtman, L. Marx, E.K. Schneider, J. Shukla, and D.M. Straus, 1997. The COLA Atmosphere-Biosphere General Circulation Model Volume 1: Formulation. COLA Technical Report No. 51.

Kruskal, W.H., and W.A. Wallis, 1952. Use of ranks in one-criterion analysis of variance. Journal of the American Statistical Association 47 (260): 583–621.

Lalas, D.P., and F. Einaudi, 1974. On the correct us of the wet adiabatic lapse rate in stability criteria of a saturated atmosphere. J. Appl. Meteor. 13: 318-324.

Lee, A.F.S., and S.M. Heghinian, 1977. A shift of the mean level in a sequence of independent normal random variables – a Bayesian approach. Technometrics 19(4): 503-506.

Lettenmaier, D.P., 1975. Detection of trends in water quality data from records with dependent observations. Water Resources Res. 12(5): 1037-1046.

Mann, H.B., and D.R. Whitney, 1947. On a test of whether one of two random variables is stochastically larger than the other. Annals of Mathematical Statistics 18 (1): 50–60.

Martínez, R., J.J. Nieto, A. Freire, E.J.M. van den Besselaar, A.M.G. Klein Tank, G. van der Schrier, 2012. Daily dataset for climate extreme analyses in Latin America. In preparation.

Matalas, N.C., and W.B. Langbein, 1962. Information content of the mean. J. Geophys. Res. 67(9): 3441–3448.

Meehl, G.A., T.F. Stocker, W.D. Collins, P. Friedlingstein, A.T. Gaye, J.M. Gregory, A. Kitoh, R. Knutti, J.M. Murphy, A. Noda, S.C.B. Raper, I.G. Watterson, A.J. Weaver, and Z.-C. Zhao, 2007. Global Climate Projections. In: Climate Change 2007: The Physical Science Basis. Contribution of Working Group I to the Fourth Assessment Report of the Intergovernmental Panel on Climate Change [Solomon, S., D. Qin, M. Manning, Z. Chen, M. Marquis, K.B. Averyt, M. Tignor and H.L. Miller (eds.)]. Cambridge University Press, Cambridge, United Kingdom and New York, NY, USA.

Moncrieff, M.W., and M.J. Miller, 1976. The dynamics and simulation of tropical cumulonimbus and squall lines. Quarterly Journal of the Royal Meteorological Society 102 (432): 373–394.

Muñoz-Uribe, P., M. Jojoa, C. Velásquez, and G.E. Gorin, 2009. Middle and late Holocene climate in the tropics: contribution of a high-resolution palynological and geochemical record in northwestern Colombia. American Geophysical Union, Fall Meeting 2009.

Roads, J.O., S-C. Chen and F. Fujioka, 2001. ECPC's weekly to seasonal global forecasts. Bull. Amer. Meteor. Soc 82(4): 639-658.

Roeckner, E., K. Arpe, L. Bengtsson, M. Christoph, M. Claussen, L. Dümenil, M. Esch, M. Giorgetta, U. Schlese, and U. Schulzweida, 1996. The atmospheric general circulation model ECHAM4: Model description and simulation of present-day climate. Max-Planck-Institut fur Meteorologie Rep. 218, Hamburg, Germany, 90 pp.

Ruiz, D., H.A. Moreno, M.E. Gutierrez, and P.A. Zapata, 2008. Changing climate and endangered high mountain ecosystems in Colombia. Science of the Total Environment 398 (1-3): 122-132; doi: 10.1016/j.scitotenv.2008.02.038.

Ruiz, D., M.P. Arroyave, M.E. Gutiérrez, and P.A. Zapata, 2011. Increased climatic stress on high-Andean ecosystems in the Cordillera Central of Colombia. Pp. 182-191 in: Herzog SK, Martínez R, Jørgensen PM, Tiessen H (eds.). Climate change and biodiversity in the Tropical Andes. MacArthur Foundation, Inter-American Institute of Global Change Research (IAI) and Scientific Committee on Problems of the Environment (SCOPE), São José dos Campos and Paris, 348 pp., ISBN: 978-85-99875-05-6.

Ruiz, D., D.G. Martinson, and W. Vergara, 2012. Trends, stability and stress in the Colombian Central Andes. Climatic Change 112 (3): 717-732; doi: 10.1007/s10584-011-0228-0.

Ruiz, D., S.K. Herzog, P.M. Jørgensen, T.H. Larsen, R. Martínez, J.J. Nieto, S.V. Poats, and M. Ohira, 2012. Five-tiered integrated climate-related biodiversity vulnerability assessment in the Tropical Andes. Mountain Research Initiative Newsletter 7: 7-11. Available online at: http://mri.scnatweb.ch/individual-articles-mri-news-no.7-high-resolution/view-category/Page-3.

Ruiz, D., M. Cane, R. Cousin, A.G. Muñoz, A. Jaramillo, and R. Martínez, (forthcoming). Shifting atmospheric stability and tropical Andean biodiversity hotspots in trouble.

Salas, J.D., and D.C. Boes, 1980. Shifting level modeling of hydrologic series. Advances in Water Resources 3: 59–63.

Seidel, D.J., Q. Fu, W.J. Randel, and T.J. Reichler, 2008. Widening of the tropical belt in a changing climate. Nature Geoscience 1: 21-24.

Sen, P.K., 1968. On a class of aligned rank order tests in two-way layouts. Ann Math Stat 39:1115–1124.

Snedecor, G.W., and W.G. Cochran, 1980. Statistical methods (7th edn.). Iowa State University Press, Ames, IA.

Soden, B.J, and I.M. Held, 2006. An assessment of climate feedbacks in Coupled Ocean–Atmosphere Models. Journal of Climate 19: 3354-3360.

Spracklen, D.V., S.R. Arnold, and C.M. Taylor, 2012. Observations of increased tropical rainfall preceded by air passage over forests. Nature 489: 282–285.

Suárez, C.F., L.G. Naranjo, J.C. Espinosa, and J. Sabogal, 2011. Land use changes and their synergies with climate change. Pp. 141-151 in: Herzog, S.K., R. Martínez, P.M. Jørgensen, and H. Tiessen (Eds.). Climate change and biodiversity in the Tropical Andes. MacArthur Foundation, Inter-American Institute of Global Change Research (IAI) and Scientific Committee on Problems of the Environment (SCOPE), São José dos Campos and Paris, 348pp., ISBN: 978-85-99875-05-6.

Vergara, W. (ed.). 2009. Assessing the potential consequences of climate destabilization in Latin America. Latin America and Caribbean Region Sustainable Development Working Paper 32. The World Bank. 115 pp.

Wilcoxon, F., 1945. Individual comparisons by ranking methods. Biometrics Bulletin 1 (6): 80–83.

Williams, G.P., 2006. Circulation sensitivity to tropopause height. J. Atmos. Sci. 63: 1954–1961.

Table 1. Colombian weather stations included in the assessment of historical stability conditions at local level

ID	Name	Altitude [m]	Historical period of temperature
2615515	Las Brisas	4,150	1981-2003
2615517	Fca Tesorito	2,200	N.A.
2615511	Apto La Nubia	2,080	1969-2006
2615502	Cenicafé	1,310	1950-2007
2613507	El Cedral	2,120	1961-2006
2613506	El Jazmín	1,635	1975-2006
2613516	San Remo	2,000	1994-2006
2613511	Veracruz	1,684	1978-2006

Table 2. Historical periods of temperature, relative humidity and dew point gathered at the installed T/RH data loggers

Serial No. and GPS mark	Altitude [m]	Historical period
2272886 Salto_Cueva - GPS mark 029	3,790	December 18, 2008, 12:00 m – January 30, 2012, 09:00 am Dataset with continuous records
2272887 Microcentral - GPS mark 078	3,910	December 18, 2008, 03:00 pm – January 30, 2012, 03:00 pm Dataset with continuous records
2272888 El Cisne - GPS mark 022	4,000	December 16, 2008, 06:00 pm – January 30, 2012, 05:00 pm Dataset with missing data: May 3, 2009, 09:00 am – February 28, 2010, 09:00 am
2272889 Nariz_Diablo - GPS mark 037	4,260	December 17, 2008, 12:00 m – January 29, 2012, 09:00 am Dataset with continuous records
10047204 Lupinus_Valley – GPS mark (TBD)	~4,600	Installed on January 29, 2012 at 12:30 m, for a delayed start: January 30, 2012, 00:00 am Records not yet available

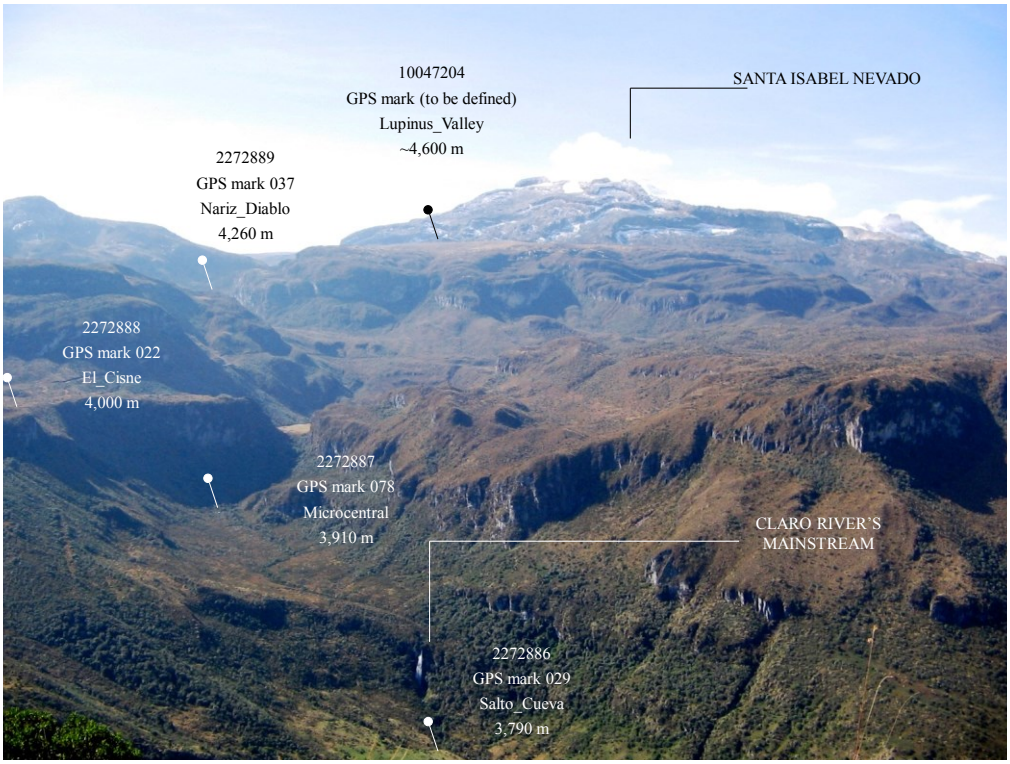

Figure 1. U23-001 HOBO® Temperature/Relative Humidity data loggers installed in the headwaters of the Claro River high-altitude watershed, in the Los Nevados Natural Park, on the El Ruiz-Tolima Volcanic Massif, Colombian Andean Central Mountain Range. See serial numbers, GPS marks, data loggers' names, and altitudes above sea level. These digital sensors have a temperature range of -40 to 70°C and a relative humidity range of 0 to 100%. Their accuracy in temperature and relative humidity readings reaches +0.18°C at an ambient temperature of 25°C, and +2.5% for values in the range from 10 to 90%, respectively. Finally, the temporal resolutions are 0.02°C at 25°C and 0.03%, respectively.

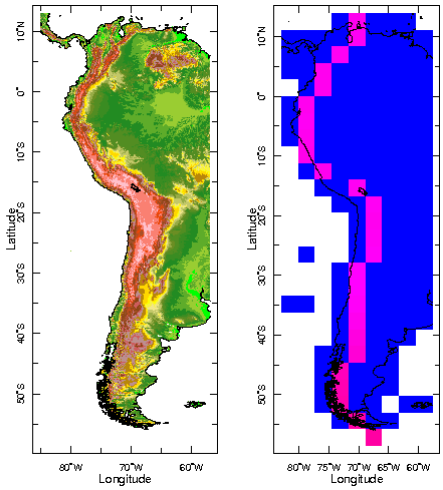

Figure 2. Axis of the Andes Cordillera selected for the analyses. (Left panel) NOAA NGDC GLOBE gridded 1-km, quality controlled global Digital Elevation Model (DEM) data[11] from the Global Land One-km Base Elevation (GLOBE) Project (Hastings and Dunbar, 1999). (Right panel) Proposed axis of the Andes Cordillera – only pink ~2.8125° pixels were considered for the analysis of ECHAM4.5 ensemble simulation outputs.

[11] Available online at: http://iridl.ldeo.columbia.edu/expert/SOURCES/.NOAA/.NGDC/.GLOBE/.topo/

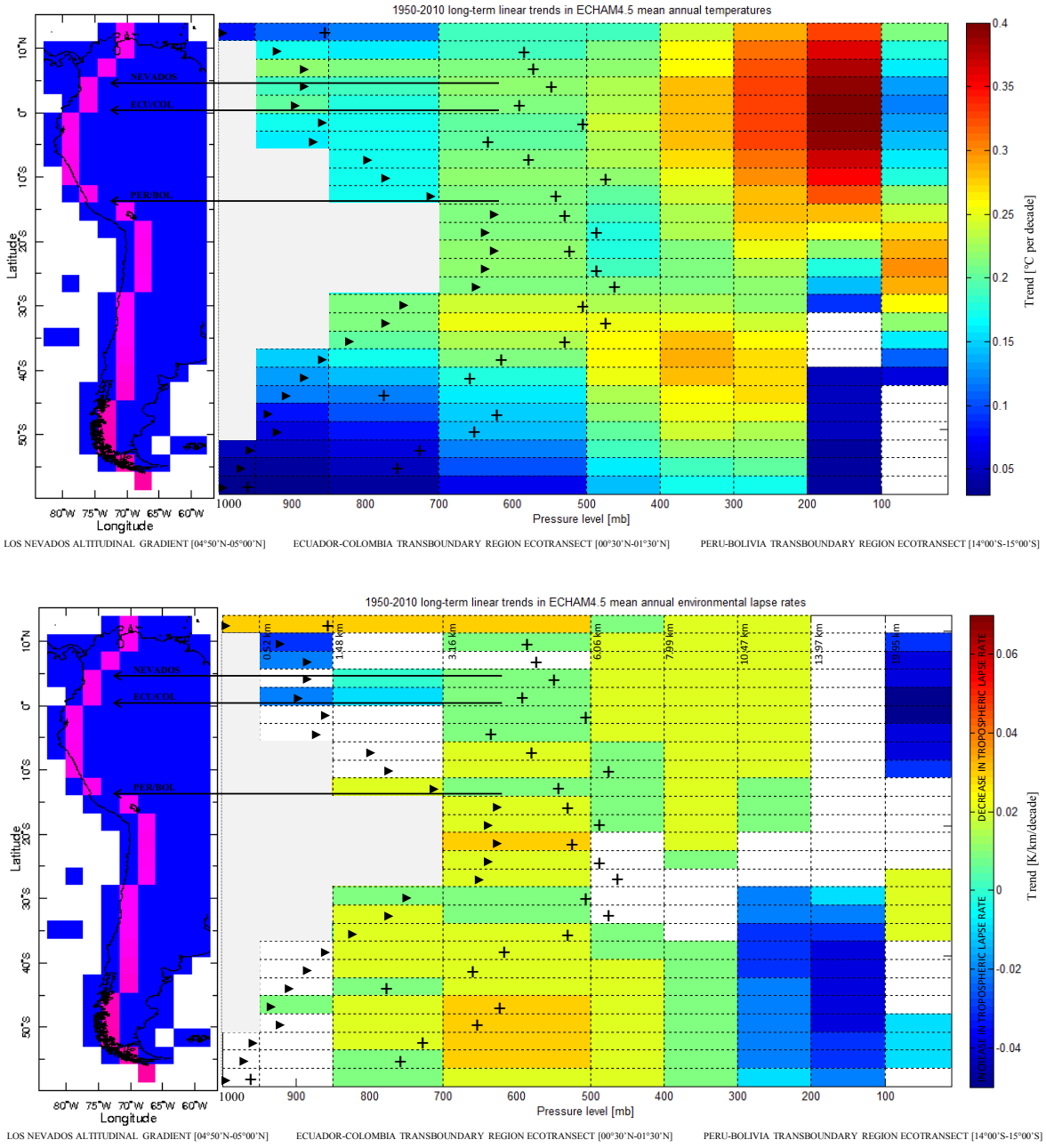

Figure 3. 1950-2010 long-term linear trends in ECHAM4.5 mean annual air temperatures (top panel) and mean annual environmental lapse rates (bottom panel) along the axis of the Andes Cordillera (see pink 2.8125°pixels on plan views), for the latitudinal range [60°S-15°N], and for 9 pressure levels [1000, 950, 850, 700, 500, 400, 300, 200, and 100 mb; see vertical profiles]. Air temperatures and environmental lapse rates are obtained through ECHAM4.5 ensemble simulation runs. Trends are expressed in °C per decade (top panel) and K/km/decade (bottom panel); see color scales. Only statistically significant (at

α=0.05) long-term linear trends are displayed; i.e. non-significant trends are depicted by white boxes. Proposed ecotransects are highlighted with arrows. Black solid triangles and crosses depict, respectively, the average and maximum altitudes (expressed in atmospheric pressures) of the NOAA NGDC GLOBE gridded 1-km, quality controlled global Digital Elevation Model (Hastings and Dunbar, 1999) in the ECHAM4.5 model gridpoints. Areas blocked in grey depict grid boxes below the ground surface. Note the differences above and below the tropopause, which is defined as 100 mb at the equator with a linear increase with latitude to 300 mb at the Poles. For reference, see the estimated altitudes above sea level (expressed in km) in the upper part of the bottom panel. In the latitude where Los Nevados Natural Park is located, which is depicted by grid boxes centered at about 4.19°N, see top panel, air temperatures increased over the period 1950-2010 at a rate ranging from 0.19 to 0.23°C per decade in altitudes below 500 mb, whereas in the upper levels (200 to 300 mb) temperatures exhibited an increasing long-term linear trend of about 0.33 to 0.39 °C per decade. In the latitude where the Colombian-Ecuadorian transect (Ecu/Col) is located, which is depicted by grid boxes centered at about 1.40°N, air temperatures increased at a rate in the range from 0.18 to 0.23°C per decade in altitudes below 500 mb, whereas in the upper levels the warming trend reached 0.33 to 0.40°C per decade. The Bolivian-Peruvian transect (Per/Bol, located at approximately 12.56°S) experienced, in turn, increasing long-term linear trends in free air temperatures of about 0.17 to 0.21°C per decade in lower levels, and of about 0.28 to 0.32°C per decade in upper levels. Mean annual environmental lapse rates in the latitude where Los Nevados Natural Park is located, see bottom panel, decreased at 0.003-0.010 K/km/decade in altitudes in the range 850-700 mb, and at 0.016-0.023 K/km/decade in the 500-400 mb altitudinal range. In the Ecu/Col transect, mean annual environmental lapse rates increased at 0.023-0.007 K/km/decade in the range 950-850 mb, and decreased at 0.015-0.024 in the 700-400 mb altitudinal range. In the Per/Bol transect, in turn, mean annual environmental lapse rates decreased at 0.011-0.019 K/km/decade in the 700-400 mb altitudinal range.

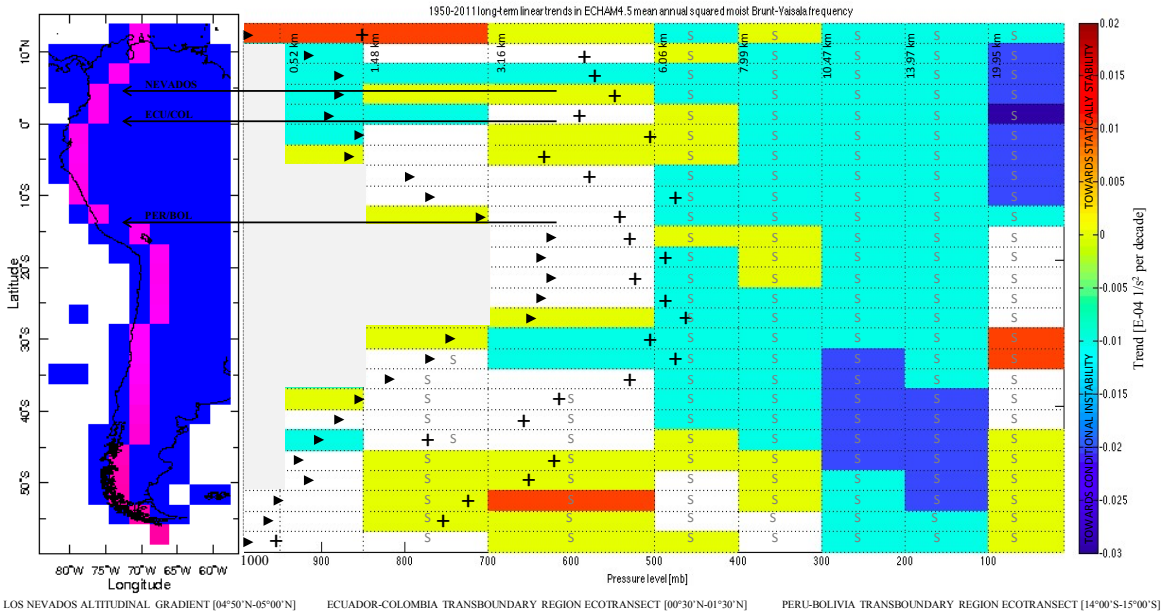

Figure 4. 1950-2011 long-term linear trends in ECHAM4.5 squared mean annual moist Brunt-Väisälä frequency along the axis of the Andes Cordillera (see pink 2.8125°pixels on plan view), for the latitudinal range [60°S-15°N], and for 9 pressure levels [1000, 950, 850, 700, 500, 400, 300, 200, and 100 mb; see vertical profile]. For these analyses, air temperatures and environmental lapse rates are obtained through ECHAM4.5 ensemble simulation runs. Trends are expressed in E-04 s^{-2} per decade; see color scale. Only statistically significant (at α=0.05) long-term linear trends are displayed; i.e. non-significant trends are depicted by white boxes. Proposed ecotransects are highlighted with arrows. Black solid triangles and crosses depict, respectively, the average and maximum altitudes (expressed in atmospheric pressures) of the NOAA NGDC GLOBE gridded 1-km, quality controlled global Digital Elevation Model (Hastings and Dunbar, 1999) in the ECHAM4.5 model gridpoints. Areas blocked in grey depict grid boxes below the ground surface. Letter 'S' denotes the ECHAM4.5 grid boxes where the air has been (historically) absolutely stable ($N_m^2>0$ or $\Gamma<\Gamma_m$). In the latitude where Los Nevados Natural Park is located, squared mean annual moist Brunt-Väisälä frequencies (N_m^2) show slow decreasing long-term linear trends (i.e. towards conditional instability) over the period 1950-2011 from about -0.0050E-04 s^{-2} per decade at 850 mb to -0.0100E-04 at 200 mb. In the Ecu/Col transect, slow decreasing long-term linear trends are also

observed in all pressure levels with values reaching from about -0.0100E-04 s^{-2} per decade at 950 mb to -0.0100E-04 at 200 mb, and a lower rate of -0.0040E-04 at 500 mb. In the Per/Bol transect, in turn, N_m^2 values show an increasing trend (i.e. towards static stability) of +0.0030E-04 s^{-2} per decade at 850 mb, and decreasing trends (i.e. towards conditional instability) in upper levels ranging from -0.0030E-04 at 700 mb to -0.0070E-04 at 200 mb.

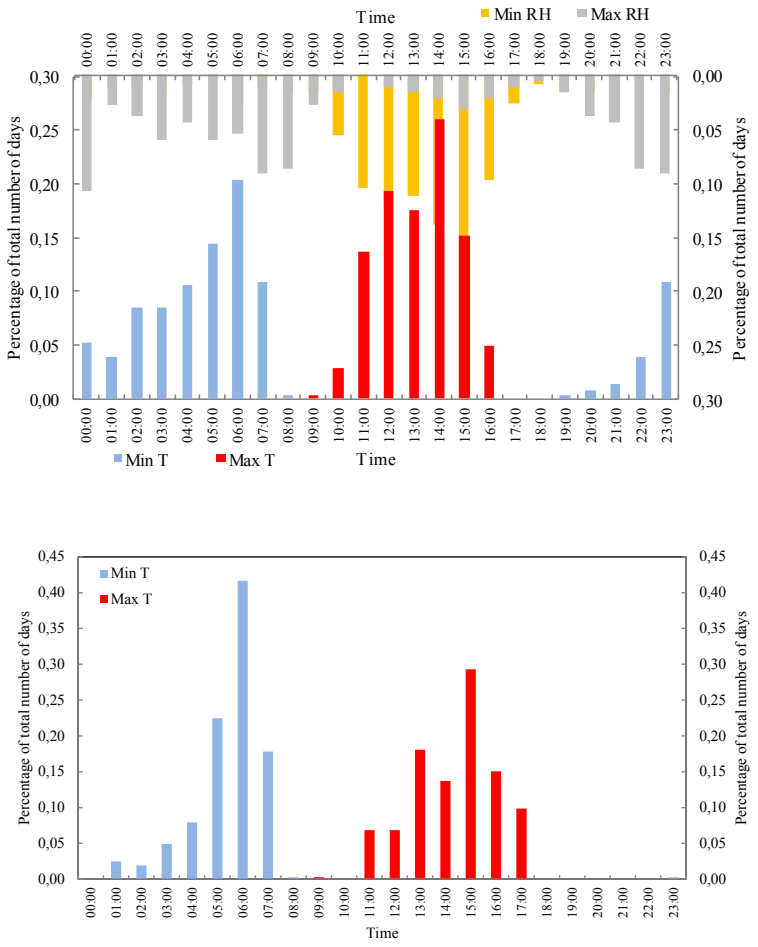

Figure 5. Time of occurrence of minimum and maximum near-surface air temperatures and relative humidity observed in the headwaters and the lowlands of the Claro River watershed, on the west flank of the El Ruiz-Tolima volcanic massif in the Colombian central Andean region. Top panel: time of occurrence of December-January-February near-surface minimum and maximum air temperatures (see Min T - blue solid bars and Max T - red solid bars on left y-axis) and relative humidity (see Min RH - orange solid bars, and Max RH - grey solid bars on right y-axis; note reverse order) gathered at the U23-001 HOBO® Temperature/Relative Humidity data logger 2272889 Nariz_Diablo (GPS mark 037, 4,260 m), installed in the proper páramo to superpáramo transition in the headwaters of the Claro River watershed. Records are available for the trimesters December-January-February of 2008-2009, 2009-2010

and 2010-2011, and for the month of December, 2011. A total number of 284 days were included in the analysis of near-surface Min T and Max T. Total 268 and 186 days were, in turn, included in the analysis of Min RH and Max RH, respectively (days with saturated conditions, RH=100%, were not included). Bottom panel: time of occurrence of near-surface minimum and maximum air temperatures gathered at the weather station 2615502 Cenicafé (1,310 m), in the lowlands of the Claro River watershed, over the year 2011. Total 365 days were included in the analysis (source: Alvaro Jaramillo – CENICAFE, personal communication).

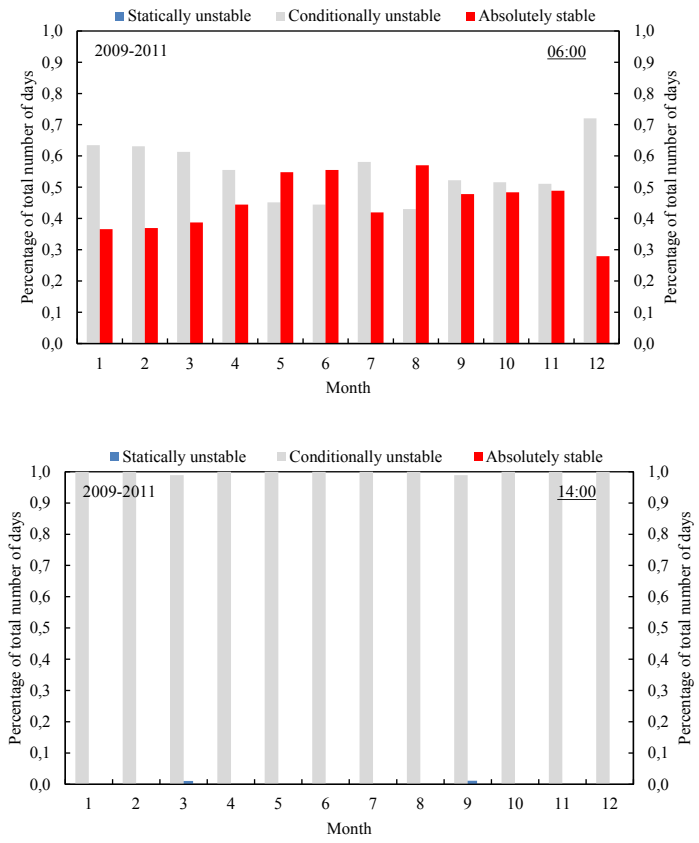

Figure 6. Inferred monthly states of convective stability at 06:00 (top panel) and 14:00 (bottom panel) in the headwaters of the Claro River watershed, on the west flank of the El Ruiz-Tolima volcanic massif in the Colombian central Andean region, according to the squared dry (N^2) and moist (N_m^2) Brunt-Väisälä frequencies observed over the period 2009-2011. Static unstable ($N^2<0$ or $\Gamma>\Gamma_d$), conditionally unstable ($N_m^2<0$, $N^2>0$ or $\Gamma_m<\Gamma<\Gamma_d$), and absolutely stable ($N_m^2>0$ or $\Gamma<\Gamma_m$) conditions are represented by blue, grey and red solid bars, respectively. Dry neutrally stable ($N^2=0$ or $\Gamma=\Gamma_d$) and moist neutrally stable ($N_m^2=0$ or $\Gamma=\Gamma_m$) conditions are not shown.

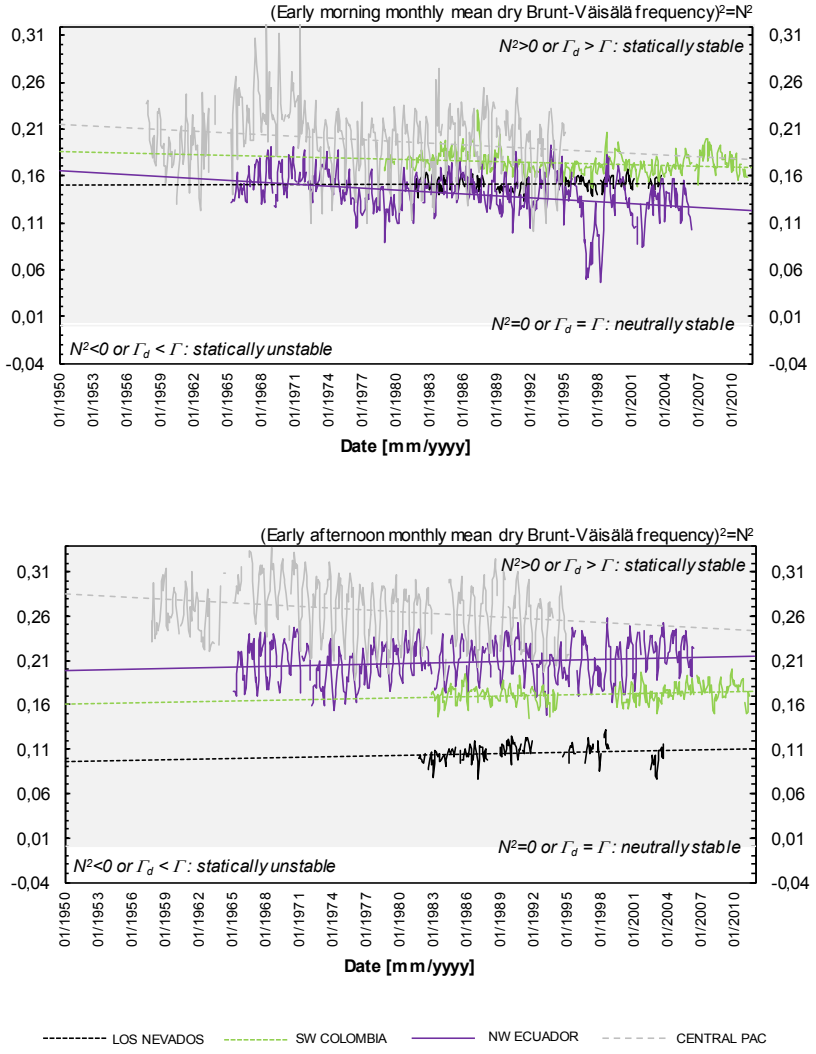

Figure 7(a). Conditions of atmospheric stability inferred for the altitudinal transects in the Colombian central Andean region (Los Nevados), the Colombia-Ecuador transboundary region (Northwestern Ecuador and Southwestern Colombia), and the Bolivia-Peru transboundary region (Central Pacific slope). Top panel: squared early morning monthly mean dry Brunt-Väisälä frequency ($_{EMM\mu}N^2$), expressed in E-03 s^{-2} [along the Claro River watershed environmental lapse rates, Γ, at approximately 06:00 reached an average value of -5.6 K/km with minimum and maximum values of -5.1 and -6.1 K/km, respectively. These values are consistent with Γ values suggested by T/RH data loggers]. According to $_{EMM\mu}N^2$ values

the local atmosphere on the west flank of the El Ruiz-Tolima volcanic massif experienced homogeneous (no trend) static stable conditions in the early morning over the period October, 1981 through December, 2003. Along the altitudinal gradient that runs from the Pacific lowlands into the Colombian highlands in Southwestern Colombia, $_{EMM\mu}N^2$ values suggest static stable conditions with a slow decreasing trend (i.e. towards static unstable conditions) over the historical period January, 1979-June, 2011. Along the path that connects the Pacific lowlands to the Ecuadorian upper Andes, in the same transboundary region, $_{EMM\mu}N^2$ values also indicate static stable conditions in the early morning over the period May, 1965-June, 2006, but with a strong decreasing trend driven by the El Niño 1997-1998 and 2001-2002 events. Lastly, on the Central Pacific slope in the Bolivia-Peru transboundary region, $_{EMM\mu}N^2$ values also suggest static stable conditions with a strong decreasing trend over the instrumental period October, 1957 through March, 1995. Bottom panel: squared early afternoon monthly mean dry Brunt-Väisälä frequency ($_{EAM\mu}N^2$), expressed in E-03 s^{-2} [along the Claro River watershed, Γ values at 14:00 reached an average of -6.8 K/km with minimum and maximum values of -6.0 and -7.6 K/km, respectively. The historical average $\Gamma_{14:00}$ is almost 8% smaller than the mean Γ obtained with the installed T/RH data loggers]. According to the inferred $_{EAM\mu}N^2$ values, the local atmospheres on the west flank of the El Ruiz-Tolima volcanic massif and along the altitudinal gradients that run from the Pacific lowlands into the Colombian and Ecuadorian Andean highlands, experienced static stable conditions with moderate increasing trends, i.e. reinforcing static stability, over the respective instrumental periods. $_{EAM\mu}N^2$ values on the Central Pacific slope in the Bolivia-Peru transboundary region suggest, conversely, a moderate decreasing trend (i.e. towards static unstable conditions) over the available historical period. For both panels: in a static stable atmosphere, an air parcel will oscillate about an initial position z=0, with buoyancy providing the restoring force. In a neutrally stable atmosphere, the air parcel will experience no net force and thus will remain at initial position. In a static unstable atmosphere, the air parcel will accelerate away from z=0, converting gravitational potential energy into kinetic energy and producing convection.

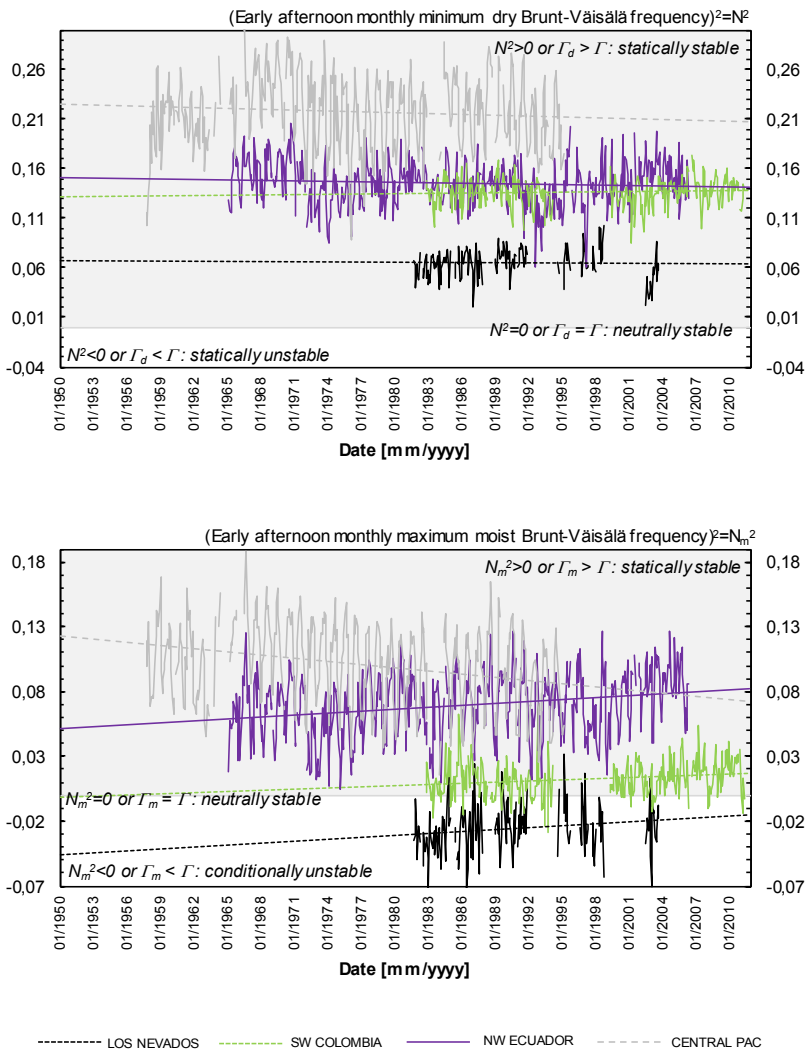

Figure 7(b). Conditions of atmospheric stability inferred for the altitudinal transects in the Colombian central Andean region (Los Nevados), the Colombia-Ecuador transboundary region (Northwestern Ecuador and Southwestern Colombia), and the Bolivia-Peru transboundary region (Central Pacific slope). Top panel: squared early afternoon monthly minimum dry Brunt-Väisälä frequency ($_{EAMm}N^2$), expressed in E-03 s^{-2}. Inferred $_{EAMm}N^2$ values for the altitudinal transects in Los Nevados and SW Colombia indicate homogeneous (no trend) static stable conditions over the available instrumental periods. In NW Ecuador and the Central Pacific slope in the Bolivia-Peru transboundary region $_{EAMm}N^2$ values show moderate decreasing trends towards static unstable conditions. Bottom panel: squared early afternoon monthly maximum moist Brunt-Väisälä frequency ($_{EAMM}N_m^2$), expressed in E-03 s^{-2}. In the Los Nevados transect,

historical 14:00 values suggest primarily conditionally unstable conditions that are, in the long-term, shifting towards static stable conditions. Along the altitudinal gradient that runs from the Pacific lowlands into the Colombian highlands in Southwestern Colombia, $_{EAMM}N_m^2$ values lie in the fringe from conditionally unstable to low-frequency static stable conditions. In the long-term, however, conditions are becoming more static stable. Along the path that connects the Pacific lowlands to the Ecuadorian upper Andes, static stable conditions have prevailed and, in the long run, show to become even more prevalent. On the Central Pacific slope in the Bolivia-Peru transboundary region, $_{EAMM}N_m^2$ values indicate historical static stable conditions shifting, on the contrary, towards conditionally instability. In a conditionally unstable state, the atmosphere is stable if unsaturated but unstable if saturated.

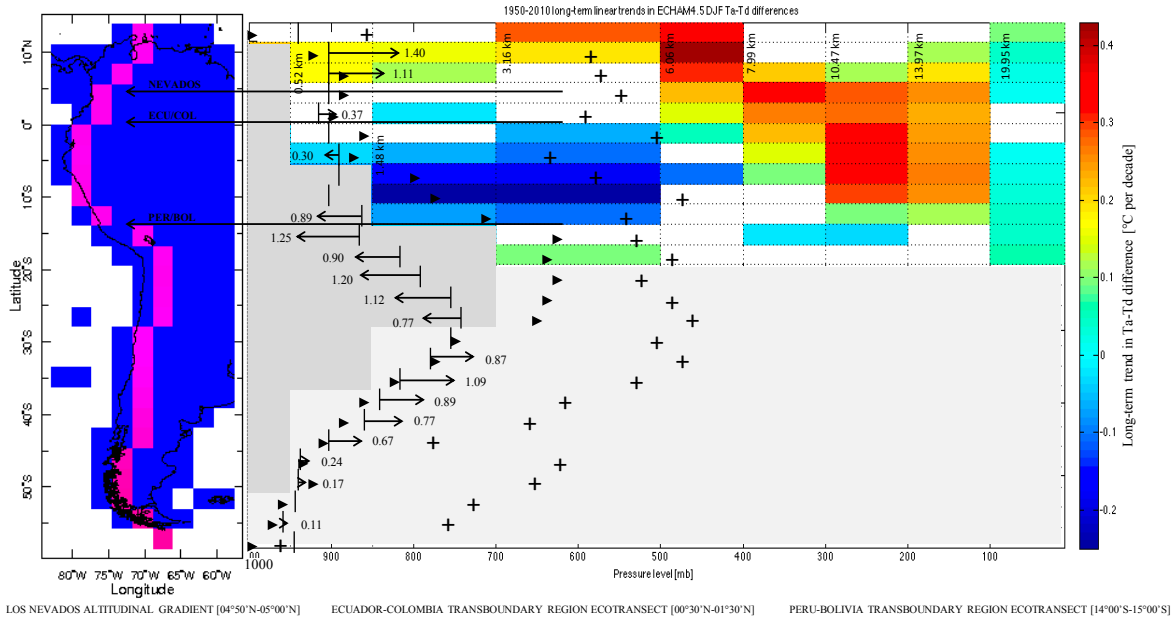

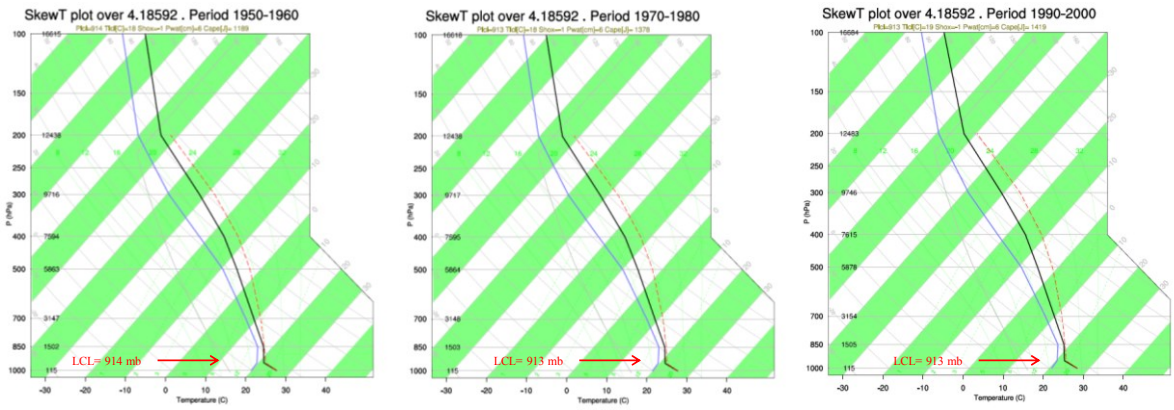

Figure 8. Top panel: 1950-2010 long-term linear trends in ECHAM4.5 December-January-February (DJF) air temperature and dew point difference (T_a-T_d) along the axis of the Andes Cordillera (see pink 2.8125°pixels on plan view), for the latitudinal range [60°S-15°N], and for 9 pressure levels [1000, 950, 850, 700, 500, 400, 300, 200, and 100 mb; see vertical profile]. Only long-term trends in DJF (T_a-T_d) in the [20°S-15°N] latitudinal range are plotted on this graph. Near-surface and free air temperatures are obtained through ECHAM4.5 ensemble simulation runs. Trends are expressed in °C per decade; see color scale. Only statistically significant (at α=0.05) long-term linear trends are displayed; i.e. non-significant

trends are depicted by white boxes. Proposed ecotransects are highlighted with arrows. Black solid triangles and crosses depict, respectively, the average and maximum altitudes (expressed in atmospheric pressures) of the NOAA NGDC GLOBE gridded 1-km, quality controlled global Digital Elevation Model (Hastings and Dunbar, 1999) in the ECHAM4.5 model gridpoints. Areas blocked in grey depict grid boxes below the ground surface. Grid boxes blocked in pale grey depict latitudes south of 20°S, which were not included in the analysis. See also historical annual Lifting Condensation Levels (LCLs) expressed in mb (short vertical lines at each latitude) and statistically significant long-term trends in LCL annual time series over the period 1950-2011. Arrow widths and numbers denote the magnitude of the rate of change in LCL historical values, expressed in mb per decade. Bottom panel: 1950-1960, 1970-1980 and 1990-2000 ECHAM4.5 simulated vertical profiles of free-air temperature (black solid lines) and dew point (blue solid lines) for the latitude where the Los Nevados altitudinal transect is located. See also the inferred LCLs (red arrows and text). At this latitude, long-term linear trends in DJF (T_a-T_d) values are not statistically significant in altitudes below 500 mb. Above this level, tropospheric DJF (T_a-T_d) values have increased in all pressure levels at a rate ranging from +0.22 to +0.32 °C per decade. In the latitude where the Ecu/Col transect is located, DJF (T_a-T_d) values do not show statistically significant trends in altitudes below 500 mb, whereas in upper levels trends are all positive and range from +0.15 to +0.28 °C per decade. In the Per/Bol transect, lower levels experienced long-term decreasing trends ranging from -0.08 to -0.11 °C per decade. Above 300 mb long-term have been positive and of about +0.10 to +0.12 °C per decade.

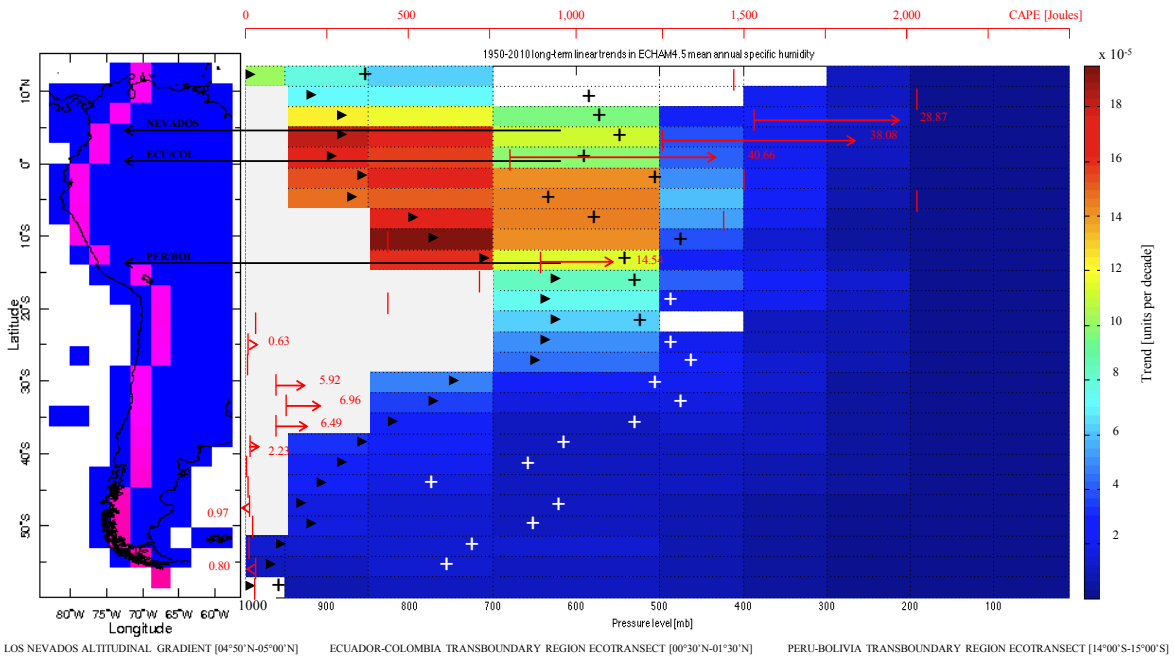

Figure 9. 1950-2010 long-term linear trends in ECHAM4.5 mean annual specific humidity along the axis of the Andes Cordillera (see pink 2.8125°pixels on left panel), for the latitudinal range [60°S-15°N], and for 9 pressure levels [1000, 950, 850, 700, 500, 400, 300, 200, and 100 mb; see right panel]. Specific humidity values are obtained through ECHAM4.5 ensemble simulation runs. Trends are expressed in grams of water vapor per kilogram of air per decade (see color scale on right panel). Only statistically significant (at α=0.05) long-term linear trends are displayed; i.e. non-significant trends are depicted by white boxes. Proposed ecotransects are highlighted with arrows. Black and white solid triangles and crosses depict, respectively, the average and maximum altitudes (expressed in atmospheric pressures) of the NOAA NGDC GLOBE gridded 1-km, quality controlled global Digital Elevation Model (Hastings and Dunbar, 1999) in the ECHAM4.5 model gridpoints. Areas blocked in grey depict grid boxes below the ground surface. See also historical annual Convective Available Potential Energies (CAPEs) expressed in Joules per kg of air (short red vertical lines at each latitude; see x-axis on top) and statistically significant long-term trends in CAPE annual time series over the period 1950-2011. Arrow

widths and numbers denote the magnitude of the rate of change in CAPE historical values, expressed in Joules per kg per decade. CAPE depicts the ‘amount of energy a parcel of air would have if lifted a certain distance vertically through the atmosphere’ and expresses the positive buoyancy (atmospheric instability) of an air parcel (Moncrieff and Miller, 1976). CAPE exists within the conditionally unstable layer of the troposphere, where an ascending air parcel is warmer than its surrounding air. Rising motions and convection can eventually lead to thunderstorms; however, if there is not enough water vapor present, there is no ability for condensation.

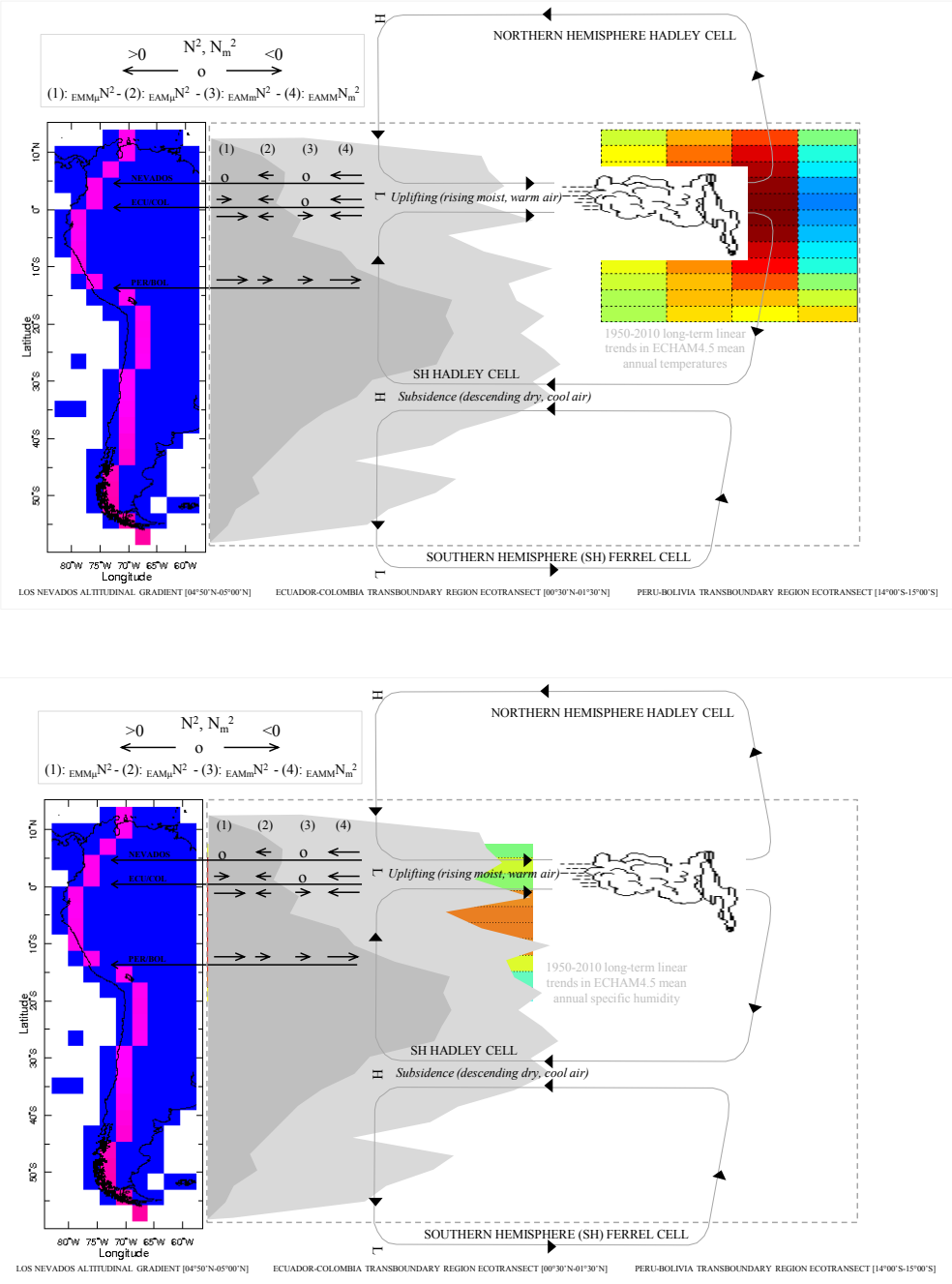

Figure 10. Idealized representation of the large-scale atmospheric circulation over the axis of the Andes Cordillera, along with the 1950-2010 long-term linear trends in ECHAM4.5 mean annual air temperatures (top panel) and specific humidity (bottom panel). Semiannual north-south migration of Hadley cells is not

represented – i.e. the thermal equator is assumed to be static at around 0-5°N, approximately. Graphs only include grid pixels with the highest increases in temperature and humidity (figures 3 and 9 display long-term trends for all latitudes and pressure levels). Dark- and light-shaded solid areas depict, respectively, the average and maximum altitudes (expressed in atmospheric pressures) of the NOAA NGDC GLOBE gridded 1-km, quality controlled global Digital Elevation Model (Hastings and Dunbar, 1999) in the ECHAM4.5 model gridpoints. Proposed ecotransects are highlighted with arrows. See also variables ${}_{EMM\mu}N^2$ and ${}_{EAM\mu}N^2$ which represent, respectively, the squared early morning and afternoon monthly mean dry Brunt-Väisälä frequencies; variables ${}_{EAMm}N^2$ and ${}_{EAMM}N_m^2$ depict, respectively, the squared early afternoon monthly minimum and maximum dry and moist Brunt-Väisälä frequencies. Long-term decreasing trends in N^2 and N_m^2 values (towards instability) are depicted by arrows pointing to the right. The size of each arrow represents the magnitude of the long-term trend.

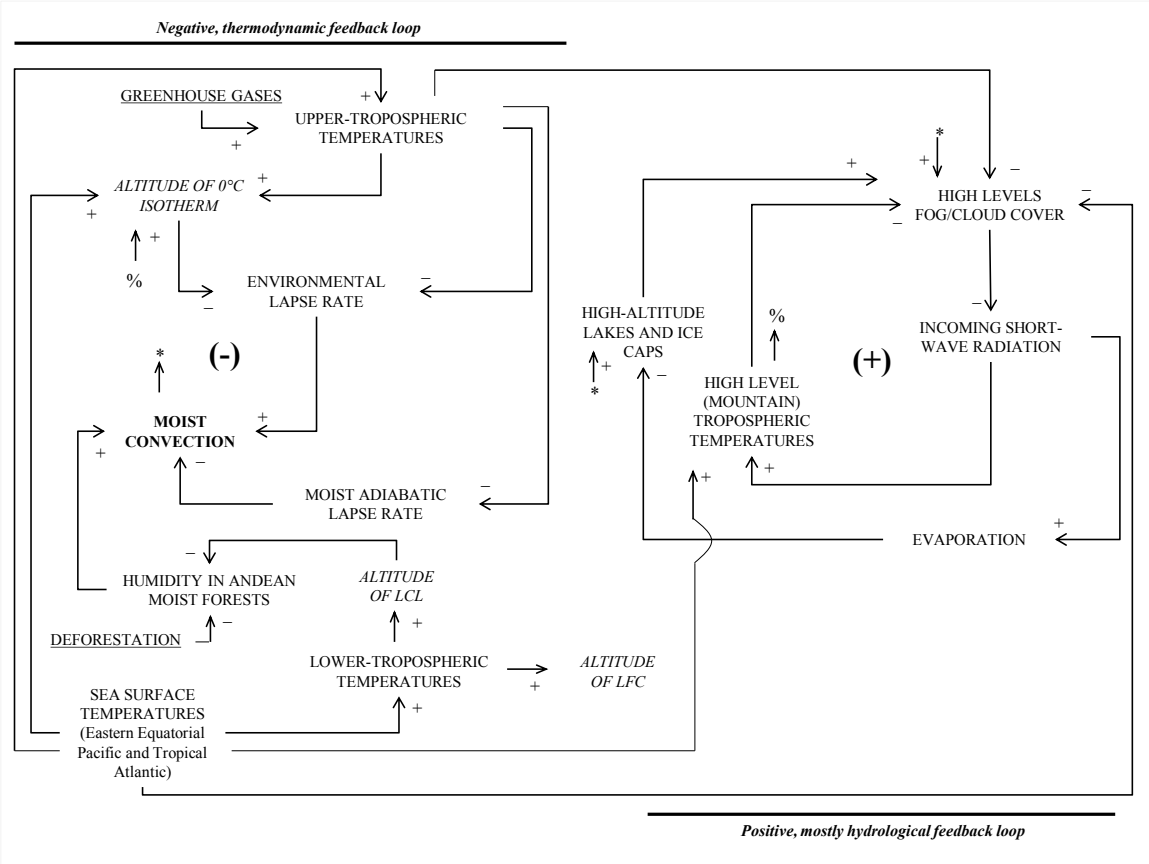

Figure 11. High-altitude Andean climate system and interrelated opposite feedback mechanisms

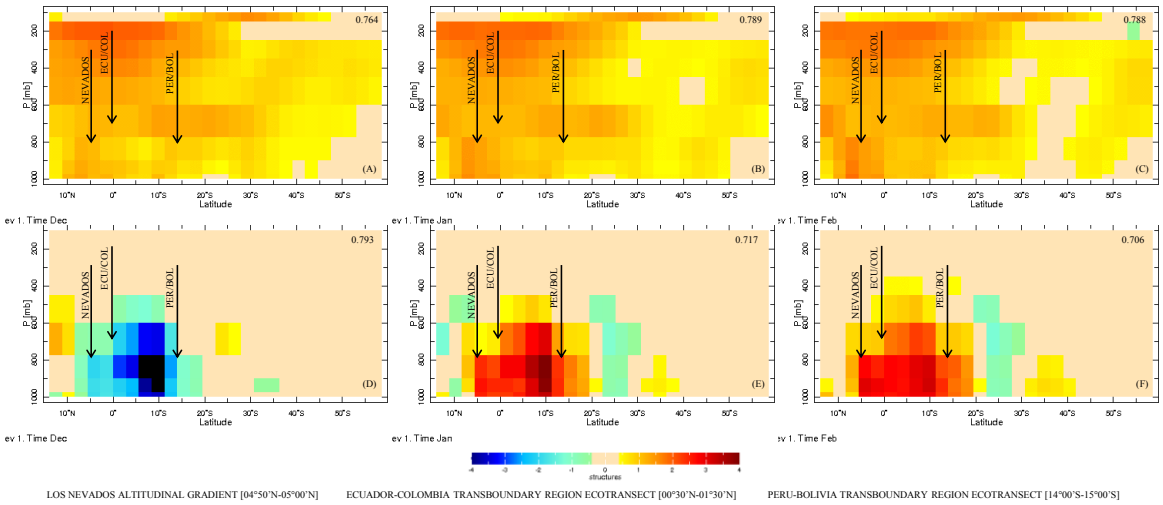

Figure 12. First *eigenvalues* (ev1) of ECHAM4.5 December, January and February mean air temperature (top panels A, B and C, respectively) and specific humidity (bottom panels D, E and F, respectively) anomalies (ensemble simulation outputs) along the axis of the Andes Cordillera and for the historical period spanning from January, 1950 to October, 2011. Proposed ecotransects are highlighted with arrows. In each panel the percentage of total variance explained by the corresponding structure is presented on the upper right corner.

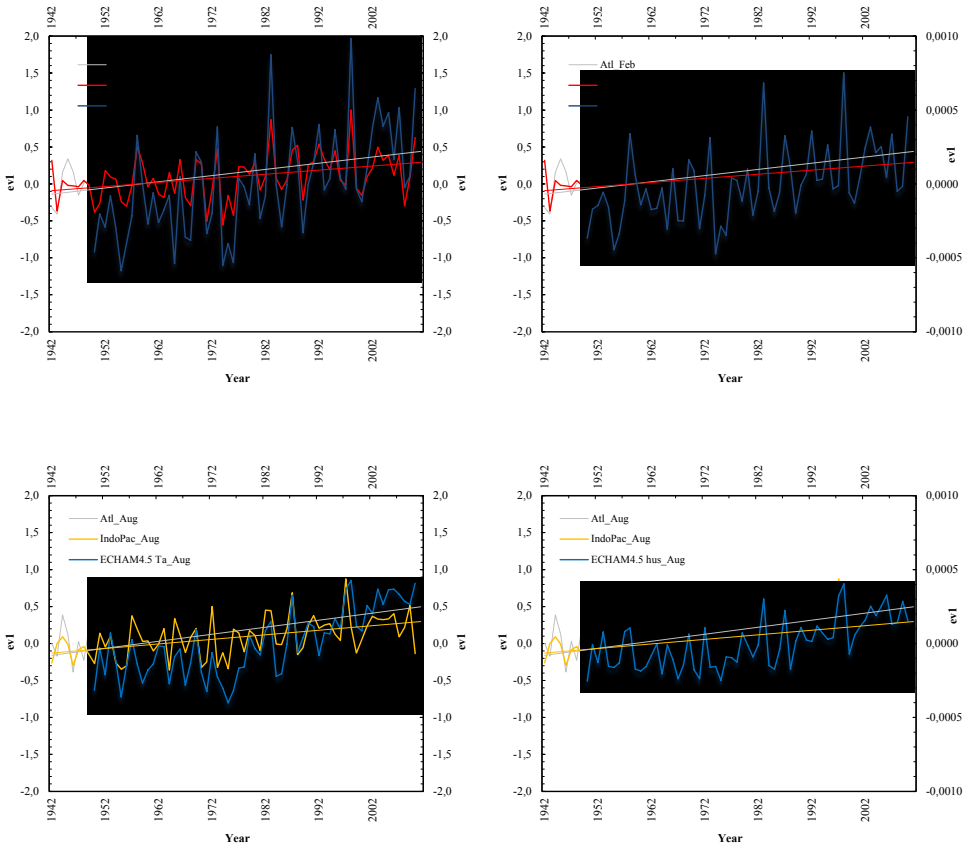

Figure 13. First *eigenvalues* (ev1) of February (top panels) and August (bottom panels) sea surface temperature anomalies (SSTa) observed in the Atlantic [15°E-60°W and 30°S-30°N] and the Indo-Pacific [90°W-30°E and 30°S-30°N] tropical belts over the period spanning from January, 1942 to October, 2011 (source: Kaplan et al. 1998), along with the first *eigenvalues* of ECHAM4.5 February and August mean air temperature (T_a, left panels) and specific humidity (q_s, right panels) anomalies (ensemble simulation outputs) along the axis of the Andes Cordillera (latitudinal range [60°S-15°N]) and for the historical period spanning from January, 1950 through October, 2011.

Chapter 4[12]

Multi-model ensemble (MME-2012) simulation experiments: exploring the role of long-term changes in climatic conditions in the increasing incidence of *Plasmodium falciparum* malaria in the highlands of Western Kenya

Abstract

In this article we implement a four process-based model ensemble to assess the impact of long-term changes in climatic conditions on *Plasmodium falciparum* malaria morbidity profiles observed in Kericho district, in the highlands of Western Kenya, over the period 1979-2009. The ensemble was run to address how much of a change in the size of epidemics could be attributed to the changing climate, and to understand whether or not climatic conditions have been less favorable to malaria transmission in recent years. Input data included quality controlled daily ground-truth records of maximum temperatures, minimum temperatures and rainfall totals, gathered at a nearby weather station over the period 1979-2009. Data also included mean

[12] Note: This chapter will be submitted to the journal Proceedings of the National Academy of Sciences as:

Daniel Ruiz Carrascal[1,2,3], Cyrille Brun[4,1], Stephen J. Connor[1], Judith A. Omumbo[1], Bradfield Lyon[1], and Madeleine C. Thomson[1]

[1] International Research Institute for Climate and Society (IRI), Columbia University in the City of New York, Lamont Doherty Earth Observatory, 61 Route 9W - PO Box 1000, Palisades, New York 10964-8000, USA; Phone number: +1(845) 680-4465; Fax number: +1(845) 680-4864; pfcarlos@iri.columbia.edu

[2] Programa de Ingeniería Ambiental, Escuela de Ingeniería de Antioquia, km 02 Variante al Aeropuerto José María Córdova, Municipio de Envigado, Antioquia, Colombia; Phone number: +57(4) 354-9090; Fax number: +57(4) 331-7851; pfcarlos@eia.edu.co

[3] Department of Earth and Environmental Sciences, Columbia University in the City of New York, 1200 Amsterdam Avenue, 556-7 Schermerhorn Extension, New York, NY 10027, USA

[4] École Polytechnique ParisTech, Route de Saclay, 91128 Palaiseau Cedex, France; Téléphone : +33 (0)1 69 33 38 93; Télécopie : +33 (0)1 69 33 38 88

monthly near-surface and free air temperatures from ensemble simulation runs of the ECHAM4.5 coupled ocean-atmosphere general circulation model, for the historical period 1950-2011. Simulations included analysis of stability conditions, sensitivities to changes in initial conditions, outputs for constant and actual climatic conditions assuming full certainty in the set of parameters, models' sensitivities to changes in the set of parameters, uncertainty in parameter values (i.e. introducing parameter ranges in simulation runs), and analysis of nonlinear changes in the mean duration of host's infectivity to vectors due to increased resistance to anti-malarial drugs. The process-based model ensemble explained from 32 to 38% of the variance of *P. falciparum* malaria incidence. Obtained R^2-values were above the results achieved with individual model simulation outputs. Up to 18.6% of the variance of malaria incidence over the period 1979-2004 could be attributed to the +0.19 to +0.25°C per decade statistically significant 1950-2009 long-term linear trend in near-surface air temperatures. Simulation outputs also suggest that climatic conditions have likely been less favorable to malaria transmission in Kericho in recent years. On top of the 18.6% increase in the variance of malaria incidence, at least 6% could be related to the increased resistance to anti-malarial drugs. Long-term changes in climatic conditions and nonlinear changes in the mean duration of host's infectivity are synergistically driving the increasing incidence of *P. falciparum* malaria in the Kenyan highlands. Simple, open source mathematical tools such as the ones presented herein could improve decision-making process of local and regional health authorities.

4.1. Introduction

The Kenya's western highlands have long been at the center of a debate on whether or not global climate change has played a significant role in the recent reemergence and increasing incidence of *Plasmodium falciparum* malaria (Hay et al., 2002a; Shanks et al., 2002; Zhou et al., 2004; Hay et al., 2005; Pascual et al., 2006; Pascual et al., 2008; Paaijmans et al., 2009; Chaves and Koenraadt, 2010; Omumbo et al., 2011; Stern et al., 2011; Waweru et al., 2011). Attention has been given to reported outbreaks in, just to mention two focal places, the Kisii District of Nyanza province and the adjacent tea plantations in Kericho State. Inpatient and outpatient data from these sites suggest that malaria patterns over the period 1980-2000 were characterized by increased incidence, expanded geographic areas, and higher case-fatality rates (Zhou et al., 2004). Malaria positive cases in Kericho State have, however, recently declined and returned to moderate levels since 2005 (Stern et al., 2011), and such marked decline has been observed across many localities in East Africa (Okiro et al., 2009). As widely discussed in the scientific literature, changes in local climatic conditions are not the only external factor driving the observed changes in malaria epidemics (Shanks et al., 2002). Antimalarial drug resistance (Rapuoda et al., 1996; Hay et al., 2002c; Sutherland et al., 2002; Shanks et al., 2005b), economic-driven two-way mobility from/to endemic-prone lowlands (Shanks et al., 2005a), changes in mosquito vector populations (Hay et al., 2003), and to a lesser extent, depletion of regional health services (Hay et al., 2002d), have also played a critical role in long-term changes in malaria morbidity. All these environmental, socioeconomic and behavioral factors thus need to be considered together (Lindsay and Martens, 1998; Reiter, 2008; Ruiz et al., 2008; Protopopoff et al., 2009) in order to understand the general epidemiology of malaria and the timing and severity of *P. falciparum* malaria epidemics. In this article we implement a simple

tool, comprising four well-known process-based models, to assess (in the foreseeable future, and holistically) the impact of changes in all these critical factors on malaria morbidity profiles in the highlands of Western Kenya. The implementation herein is focused on the role that long-term changes in climatic conditions play in the final malaria incidence, but can be expanded to the analysis of changes in non-climatic factors once related information becomes available. Simulations presented here complement previous experiments for the Kisii District Hospital of Kisii municipality (Ruiz and Yan, 2004; Ruiz et al., 2008).

4.2. Study site

Analyses are focused on Tea Plantation 1 in Kericho district, in the Kenyan western highlands (1,200-3,000 m above sea level), a region of upmost economic and political importance given its agricultural activities (Shanks et al. 2005b). Kericho district provides a good scenario for modeling the timing and severity of *P. falciparum* malaria outbreaks and the potential impacts of changes in climatic conditions on malaria morbidity profiles. According to Shanks et al. (2005a) two tea plantations, each consisting of 18 estates, employ in average 18,000–18,500 workers whose families comprise 3 to 4 dependents each. Assuming that the number of individuals has been stable over the past decades (Hay et al., 2002b), the total population at risk in Plantation 1 can be assumed to reach about 27,000 individuals.

4.3. Data

Data included weather station (ground-truth) records, ECHAM4.5 ensemble simulation outputs, and *P. falciparum* malaria positive cases. Quality controlled daily records of maximum temperatures, minimum temperatures and rainfall totals, gathered at Kericho meteorological station (Waweru et al., 2011), located at 33°21'E and 0°21.6'S in the Kenyan highlands, were processed. Temperature records are available for the period spanning from January 1, 1979 through December 31, 2009. Rainfall time series are available for the period spanning from January 1, 1980 through December 31, 2009. ECHAM4.5 mean monthly near-surface and free air temperatures (T_a) (Roeckner et al., 1996), from ensemble simulation runs[13] and for the grid points located along the Eastern African highlands, were also selected for the analysis. T_a values are available for the period spanning from January, 1950 through October, 2011, and for nine (9) pressure levels (1000, 950, 850, 700, 500, 400, 300, 200, and 100 mb). Monthly malaria positive cases from inpatient admission registers in Tea Plantation 1 in Kericho, spanning over the period from January, 1970 through October, 2004, were obtained from figures 4 and 6 in Shanks et al. (2005); see figure 1(A).

4.4. Methods

4.4.1. Multi-model ensemble

In the multi-model ensemble proposed for this set of simulations only four mathematical tools were considered: the models proposed by Ross-Macdonald (1911; 1957), Anderson and

[13] Freely downloadable at: http://iridl.ldeo.columbia.edu/SOURCES/.IRI/.FD/.ECHAM4p5/.History/.MONTHLY/.PressureLevel-SF/.

May (1991), Worrall, Connor, and Thomson (2007), and Alonso, Bouma and Pascual (2011). These four process-based models exemplify the ample spectrum of malaria modeling approaches: from a tool with a single dynamical, discrete equation to a process-based model with a system of eleven coupled ordinary differential equations. The Ross-Macdonald's model (1911; 1957), hereafter called MAC model, is based upon a system of two coupled ordinary differential equations, whose dynamical variables represent the proportion of people affected (X) and the (implicit) counterpart in the vector population (Y). These proportions do not distinguish between infected and infectious stages. The MAC model provides the formula for the Basic Reproduction Rate (R_0) of malaria, or the average number of secondary cases arising in a very large population of completely susceptible humans following the introduction of a single primary case. Anderson and May (1991) extended the Ross-Macdonald's model by considering the proportions of exposed individuals and exposed mosquitoes, and by including the latency of infection in human hosts and mosquito vectors. The hereafter called AM model is thus based on a system of four coupled ordinary differential equations with time lags. Worral, Connor and Thomson (2007) developed, in turn, a single discrete-equation, temperature- and rainfall-driven dynamical model to predict malaria epidemics in areas where brief seasonal transmission and occasional epidemics do not enable acquired immunity, and to examine the impact of indoor residual spraying (IRS) on malaria transmission intensity. The WCT tool is composed of six sub-models, which calculate the number of adult female mosquitoes feeding on human hosts, the length of the *gonotrophic* and *sporogonic* cycles, the vector survivorship in sprayed and unsprayed populations, the *sporozoite* rate, and the total number of new infections (I), super-infections and recoveries within the human population. Lastly, Alonso, Bouma and Pascual (2011) developed a coupled mosquito-human model, herein called the ABP model, based upon a system of eleven coupled

ordinary differential equations. In the human host component, level variables represent the susceptible non-infected human hosts, the infected but non-infectious individuals, the infected individuals who acquire asymptomatic infection but are nevertheless infectious and can transmit malaria parasites to mosquito vectors, the recovered individuals or those human hosts who have cleared parasitaemia, and the infected individuals who present symptoms and therefore receive some sort of clinical treatment. In the mosquito population, level variables depict the number of larvae, the larvae carrying capacity, and the total number of susceptible non-infected mosquitoes, infected non-infectious mosquitoes, and infectious mosquitoes. A full description of all these tools is presented in Ruiz et al. (2012), see the online supplementary material; their stock-flow models, built on Powersim Constructor® Version 2.51 and Powersim Studio 8 Academic®, are also shown. Community-based, *Plasmodium malaria* parasite, human host, *Anopheles* mosquito population and environmental parameters and exogenous variables of all these process-based models were initially gathered from published literature; see tables 1(a) and 1(b). (1) and (2) in the last column denote, respectively, those parameters and exogenous variables that were chosen from literature and fixed constant, and the ones that were chosen from literature and later fitted with simulations.

The following three endogenous variables of the MAC model were modified to include climate covariates: (i) the vector feeding frequency (a), represented as a function of the daily effective temperature (T_e) following the simple regression, discussed in Alonso, Bouma and Pascual (2011), between the inverse of the average gonotrophic cycle and the daily ambient temperature; (ii) the anopheline density in relation to man (m), represented as a linear function of the rainfall-to-mosquitoes constant (μ) and the monthly rainfall, following the expression for the number of mosquitoes emerging each month discussed in Worral, Connor and Thomson (2007);

and (iii) the probability of a female mosquito surviving through one whole day (p), represented as a function of the gonotrophic cycle (U), which in turn is dependent on the daily ambient temperature. Besides the three endogenous variables modified in the MAC model, the following two variables were changed in the AM model to include climate covariates: (1) the incubation period of *P. falciparum* malaria parasites (n), represented as a function of the daily ambient temperature; and (2) the duration of a host's infectivity to vectors, from the first to the final present of infective gametocytes (WN), represented as a function of time. The following four endogenous variables of the WCT model include climate covariates: (a) the number of mosquitoes emerging each month (q), represented as a linear function of the rainfall-to-mosquitoes constant (μ) and the monthly rainfall; (b) the daily survival probability of a female mosquito (p), as a function of the gonotrophic cycle (U), which in turn depends on the daily ambient temperature; (c) the incubation period of *P. falciparum* malaria parasites (n), as a function of the daily ambient temperature; and (d) the feeding frequency (a), represented as a function of the human blood index (h) and the duration of the gonotrophic cycle (U). Lastly, the following five endogenous variables of the ABP model include climate covariates: (i) the vector feeding frequency (a), represented as a function of the daily effective temperature (T_e); (ii) the larval mortality rate (δ_L), as a function of the temperature-dependent larval mortality ($\delta_L(T)$) and the rainfall-dependent increase in mortality due to heavy rain ($\delta_L(P)$); (iii) the larval development rate (d_L), as a function of the daily ambient temperature; (iv) the average lifetime of mosquitoes, ($\langle\lambda\rangle$), represented as a function of the daily ambient temperature; and (v) the per-capita rate at which new infectious mosquitoes arise (γ_P), dependent on the daily ambient temperature.

4.4.2. Set of simulations

Simulations runs proposed herein included six series of experiments, whose descriptions are presented below. Numerical simulations were run using the user-friendly, online-downloadable, open source computer software Scilab® 5.3. Codes developed for the analyses are available upon request.

Stability conditions. The first set of experiments included comparisons of simulation outputs with the results of the analytical study of equilibrium points, time to reach equilibria and time steps of the MAC and WCT models. Parameters of these two models were fixed to representative values and full certainty in their values was initially assumed.

The MAC model reaches stable equilibria, denoted by (X^*,Y^*), at (0,0), or at:

$$\left(\frac{R_0 - 1}{R_0 + \frac{a\,c}{\mu}}, \frac{R_0 - 1}{R_0 + \frac{a\,b\,m}{r}}\right),$$

where $R_0 = \frac{a^2\,b\,c\,m}{\mu\,r}$. Parameter *a* denotes the average number of men bitten by one mosquito in one night, *b* the proportion of those *Anopheles* vectors with sporozoites in their salivary glands which are actually infective, *c* the vector susceptibility, *m* the anopheline density in relation to man, μ the daily mortality rate of mosquito vectors, and *r* the proportion of affected people, who have received one infective inoculum only, who revert to the unaffected state in one day. The model requires a time to reach the equilibrium given by:

$$t^* \geq \frac{\left| X\left(t^*\right) - X(0) \right|}{a\, b\, m \left\{ max[Y(t)] \right\}}.$$

For the values of *a*, *b* and *m* usually observed in the field, it requires many time steps to reach its equilibrium. Also, simulation outputs of the MAC model suggest that a time step of Δt=1/5 day allows better results.

The WCT model, in turn, reaches equilibrium at: $I^* = \frac{R\, d}{r - r\, R + R}$, where *R* represents the probability of a human receiving an infectious bite, *d* the total human population at risk, and *r* the probability of recovery of new infected humans after time *t*. The time to be close to the equilibrium at 5% [i.e. (1±0.05) I^*] is given by:

$$t^* = -\frac{log\left(\frac{\pm 0.05\, I^*}{I_0 - I^*} \right)}{log(K_1)},$$

where $K_1 = 1 + r - r\, R + R$. Contrary to the behavior of the MAC model, the WCT tool reaches equilibrium in about 20 time steps. Also, the WCT model is not sensitive to changes in Δt.

Base scenarios. The second set of simulations included models' sensitivities to changes in initial conditions and simulation outputs for constant climatic conditions. As in the analysis of stability conditions, parameters of the four-model ensemble were fixed to fully-certain representative values. Changes in equilibrium points and time to reach equilibria were assessed for at least five different initial proportions of infected or infectious individuals. Constant mean annual temperatures and total annual rainfall amounts, as well as historical annual cycles of

mean temperature and rainfall were used to characterize local epidemiological conditions. Simulated annual cycles of malaria prevalence (once models reach their equilibria) were then compared to the historical annual cycle of *P. falciparum* malaria incidence.

Models' outputs and accuracies. The third set of experiments comprised simulations of actual climatic conditions over the retrospective period spanning from January, 1979 through October, 2004. Some parameters of the four-model ensemble, which were initially set to fully-certain values, were then modified to several values within a sensible range reported in the literature. In the MAC model, the host delay for infectivity (*HD*), the host window for immunity (*WN*) and the rainfall-to-mosquitoes constant (μ) were fitted using the full retrospective period January, 1979 - October, 2004. In the AM model, the following parameter values were fitted: the latency of infection in human hosts (t_h), *WN*, μ, and the latency of infection in mosquito vectors (t_m). In the WCT model, the following parameter values were modified within their reported range and later fitted: the human host recovery probability (r) and μ. Lastly, in the ABP model the following parameters were included in this analysis: the average time in the exposed phase ($1/\gamma$), the external force of infection (β_e), the loss of immunity basal rate (σ_0), the fraction of infections in humans that fully develops severe malaria symptoms and then receive clinical treatment (ξ), the factor that decreases the per-capita transmission rate (η), the I to R recovery basal rate (r_0), the C to I recovery rate (ν), the mosquito fecundity factor (F), the larvae mortality rate (δ_0), the washout effect for the larvae (δ_R), the carrying capacity conversion factor (k_A), and the carrying capacity loss rate (k_E).

Simulation outputs were compared through several statistical parameters such as the correlation coefficient (R-value) between simulated malaria cases and actual positive cases, the percentage of the variance of the actual malaria morbidity that is explained by simulation outputs (R^2-value), the slope of the regression of simulated cases on actual cases, and the mean square and mean absolute errors. Comparisons also included a function of likelihood that is based on the probability of observing I_o cases given the deterministic prediction I, as discussed in Alonso, Bouma and Pascual (2011). Their error function is given by:

$$P(I_o \mid I) = \frac{1}{I\left(2 - \frac{1}{e}\right)} \begin{cases} exp\left(-\frac{(I_o - I)}{I}\right) & : \quad I_o > I \\ exp\left(-\frac{(I - I_o)}{I}\right) & : \quad I_o < I \end{cases}.$$

Sets of parameters Θ of each process-based model that yield 'comparable predictions of actual malaria positive cases' (Alonso, Bouma and Pascual, 2011) were obtained by optimizing the function:

$$P\left(I_o^{(1)}, \ldots, I_o^{(n)} \mid \Theta\right) = \prod_{i=1}^{m} P\left(I_o^{(i)} \mid I^{(i)}\right),$$

where m represents the total number of data points.

The 'most likely' models (with sets of parameters that yield 'comparable predictions') were then implemented to assess the impacts of changes in climatic conditions on *P. falciparum* malaria transmission dynamics in the highlands under study. The ensemble was run with and without long-term climatic trends, inter-annual dependency and historical seasonality, in order to address how much of a change in the size of epidemics could be attributed to changes in climatic conditions.

The third set of experiments also included multi-model simulations to the end of the Kericho temperature and rainfall data (i.e. retrospective period spanning from January, 1979 through December, 2009), in order to understand whether or not climatic conditions have been less favorable to malaria transmission in recent years. A full certainty in the 'most likely' set of parameters was also assumed in these simulation runs.

Models' sensitivity. The fourth set of simulations included models' sensitivities to changes in sets of parameters. In order to assess the impacts of changes in exogenous variables on simulation outputs of the proposed dynamical tools, the following discrete gradient was used to measure the models' response to slight variations in the values of their best set of parameters, $x = (x_1, x_2, \cdots, x_i, x_{i+1}, \cdots, x_n)$:

$$S_i = \frac{\frac{F(x_1, x_2, \cdots, x_i + \Delta x_i, x_{i+1}, \cdots, x_n) - F(x_1, x_2, \cdots, x_i, x_{i+1}, \cdots, x_n)}{F(x_1, x_2, \cdots, x_i, x_{i+1}, \cdots, x_n)}}{\frac{\Delta x_i}{x_i}},$$

where $F(x_1, x_2, \cdots, x_i, x_{i+1}, \cdots, x_n)$ denotes the simulation outputs function for all the parameters. In general, a slight increase or decrease of $\Delta x_i = \frac{x_i}{10}$ was assumed.

Also, the *Sobol Index* was used to assess the sensitivity of a given model to slight changes in its set of parameters. This index for parameter x_j is defined by:

$$IS_j = Var_{prior}\left[E_{prior}\left(F(x) / x_j \right) \right],$$

where F represents the simulation outputs function, and variables Var_{prior} and E_{prior} denote, respectively, the variance and the mean of the supposed distribution of the set of parameter x.

For the WCT model, for instance, the rainfall-to-mosquitoes constant (μ), the proportion of mosquitoes feeding on humans (h), the indoor-outdoor temperature adjustment factor (l), the probability of the vector surviving each gonotrophic cycle in a population not covered by an IRS campaign (α),the probability of the vector becoming infected per infectious meal (k), the probability of the vector becoming infectious with the malaria parasite (v), the length of the period required by the adult mosquito to search for a suitable water body, lay the cohort of eggs, find a new host and bite again (υ),the human host recovery probability (r), the total number of degree-days needed to complete a successful development of mosquito's ovaries (f_u), the threshold temperature below which ovaries development ceases (g_u), the number of degree-days needed to complete parasite development within the mosquito (f_N), the temperature threshold below which parasite development ceases (g_N), and the proportion of humans that are infectious (x) were all included in the analysis of WCT sensitivity.

Uncertainty. The fifth set of simulations explored the role of uncertainty in the predictability of malaria outbreaks. Numerical simulations generated distributions of monthly cases or *P. falciparum* malaria prevalence by taking into account uncertainty in parameter values (i.e. introducing parameter ranges in simulation runs). 25%, 50% and 95% percentiles of the distributions of simulated primary cases or malaria prevalence were plotted for each month and compared to actual positive cases or *P. falciparum* malaria incidence. Simulations also included time lags of 0, 1 and 2 months.

The sixth and last set of simulations focused on the analysis of nonlinear changes in the mean duration of host's infectivity to vectors, from the first to the final present of infective gametocytes, due to increased resistance to anti-malarial drugs (Rapuoda et al., 1996; Shanks et al., 2000) and the influence of higher transmission on its spread (Artzy-Randrup et al., 2010). Although chloroquine resistance was first reported in Kenya in the late 1970s (Masaba et al., 1985), only by 1996 clear signs of increased resistance were reported in Kericho (Rapuoda et al., 1996). The recovery rate was thus set to reflect high sensitivity of malaria parasites to chloroquine in the mid-1980s, and low to moderate sensitivity by the mid- to late-1990s. The proposed nonlinear fashion allows representing that approximately half of clinical infections did not clear thoroughly by the end of the available historical period (Rapuoda et al., 1996). A single simulation run was compared with the 25%, 50% and 95% percentiles of the distributions of monthly *P. falciparum* malaria prevalence suggested by the multi-model ensemble for time lags with the highest R^2-values.

4.4.3. Analysis of climatic data

Annual cycles of observed rainfall and minimum and maximum temperatures were calculated and compared with the annual cycle of *P. falciparum* malaria incidence. Annual values of several climatic variables, see Table 2, were then computed. As presented in the table, climate variables included the diurnal temperature range, which has been suggested to be important in the analysis of malaria transmission dynamics (Paaijmans et al., 2009). Total December-January-February, March-April-May, June-July-August, and September-October-November rainfall amounts, dry days and maximum dry spells were also processed to support

the analyses. A total number of 24 climatic variables were analyzed: 12 for rainfall, 4 for minimum temperature, 4 for maximum temperature, and 4 for the diurnal temperature range.

ECHAM4.5 grid points located along the Eastern African highlands were obtained by masking the quality controlled NOAA NGDC GLOBE gridded 1-km global Digital Elevation Model (Hastings and Dunbar, 1999) with the ECHAM4.5 grid. The resulting dataset thus comprised a matrix of 18 latitudinal grid points by 9 pressure levels per month. ECHAM4.5 mean annual free air temperatures for each grid box were obtained by averaging the corresponding T_a monthly values.

Long-term linear trends in observed and simulated annual time series were identified using simple regression analysis, and trend magnitudes were calculated by the method of least squares. Upper and lower confidence limits were also computed for the simple linear regression models. Confirmatory analyses were implemented to assess the statistical significance of the observed trends. Four hypothesis tests, namely the Student's t-test, the Hotelling-Pabst test, the non-parametric Mann-Kendall test (Kendall 1975), and the aligned rank Sen's t-test (Sen 1968), were all used to assess the null hypothesis of statistically significant (at a α=0.05) linear trends in annual time series. Serially independent yearly time series were assumed when implementing the non-parametric Mann-Kendall test. A historical time series was considered to have a statistically significant trend at a α=0.05 significance level when at least three of the implemented hypothesis tests accepted the null hypothesis of a trend in the mean.

Wavelet analysis (Lau and Weng, 1995; Torrence and Compo, 1998) was conducted to assess the dominant periodic signals in observed monthly time series of minimum temperature, maximum temperature and total rainfall. Monthly one-dimensional series were decomposed into

two-dimensional time-frequency space using the Interactive Wavelet Plot available online at: http://ion.researchsystems.com/. Seasonality, interannual variability associated with the El Niño-Southern Oscillation (ENSO), and longer interdecadal fluctuations were studied in global wavelet plots. Long-term linear trends and dominant periodic signals were then removed from historical time series to compare, in anomalies plots, actual malaria morbidity profiles with simulated malaria incidence.

4.5. Results

Seasonality and interannual variability. Figures 1(B) and 1(C) show the historical annual cycles of observed rainfall, minimum temperature and maximum temperature observed in Kericho over the period 1979-2009. Rainfall amounts exhibit a seasonal cycle that fits long rains and short rains climatology. The highest peak commonly occurs during the months of April and May, whose monthly values reach about 250-260 mm. A dry season usually takes place during the quarter December-January-February with rainfall amounts ranging from 90 to 115 mm/month. Minimum temperatures exhibit a bimodal annual cycle with peaks of 11.6°C and 11.1°C occurring during the months of April and November, respectively, and historical low values of about 10.6°C usually taking place in September. Maximum temperatures show an annual cycle with a historical peak in February of about 26.2°C and a minimum value of 22°C in July. Mean temperatures exhibit, in turn, a seasonal distribution with a peak in the months of February and March of about 18.5°C and a minimum value in July of 16.7°C. Figure 1(B) also shows the historical annual cycle of *P. falciparum* malaria incidence observed in Plantation 1 over the period spanning from January, 1970 through October, 2004. *P. falciparum* malaria

exhibits a bimodal annual cycle peaks in the months of February and June-July of about 3.8 and 5.3-5.0 positive cases per 1,000 inhabitants. Minimum malaria incidence values are commonly observed during the months of October-November-December with values reaching 2.0 positive cases per 1,000 inhabitants. The June-July peak in malaria incidence follows the maximum monthly rainfall amounts with a 2-month time delay. It also shows to follow the peak in mean temperatures with a 4-month time delay. Lastly, wavelet analysis results (not shown here) suggest the following dominant periodic signals in the historical monthly time series of minimum and maximum temperatures: 6 months, 12 months, 40 to 48 months, and 64 to 96 months; the latter, however, is beyond the cone of influence in the wavelet power spectra. The time series of monthly rainfall shows 6-month, 12-month and 32- to 64-month clear periodic signals in its global wavelet; the remainder signals are also beyond the cone of influence. Therefore, the dominant interannual variability could be represented by a 3.4-year period sinusoid.

Long-term linear trends. Table 2 presents the historical annual values of the set of observed climatic variables under study. The historical annual rainfall (R1) reaches 1,986 mm/year with a 95% confidence interval of ±94.2 mm. Historical annual average minimum (ATmin) and maximum (ATmax) temperatures reach 11.0±0.1°C [95%] and 24.1±0.1°C [95%], respectively. Table 2 also summarizes the long-term trends observed in annual time series. Among rainfall variables only the total number of dry days per year (R2) exhibited a statistically significant (at α=0.05) long-term linear trend of about +7.4 days per decade. Minimum temperatures on the warmest days (MTmin), annual minimum temperatures (ATmin) and day-to-day standard deviation of minimum temperatures (SDTmin) showed increasing trends of +0.4, +0.2 and +0.1 °C per decade, respectively. Maximum temperatures on the warmest days

(MTmax), annual maximum temperatures (ATmax) and maximum temperatures on the coldest days (mTmax2) exhibited increasing trends of +0.2, +0.3 and +0.2 °C per decade, respectively. The rest of the annual historical time series did not show statistically significant trends at α=0.05. Mean annual temperatures thus likely increased at a rate of +0.25°C per decade over the period 1979-2009. This rate of change is consistent with trends reported by previous studies (Waweru et al., 2011). Such an increasing trend is also suggested by ECHAM4.5 ensemble simulation runs. Long-term linear trends in mean annual air temperatures in the latitudinal range where Kericho District is located (ECHAM4.5 grid boxes centered at 1.3953°S and 1.3953°N) reached +0.16, +0.16, +0.19, and +0.22 °C per decade over the period 1950-2010 at pressure levels of 1000, 950, 850, and 700 mb.

Base scenarios. Figure 3 depicts the MAC, AM, WCT, and ABP simulation outputs for the historical annual cycles of mean temperature and rainfall. For the set of parameters defined in the analysis of base scenarios (see caption), models overestimate the historical *P. falciparum* malaria incidence in 0.7 to 4.0 positive cases per 1,000 inhabitants. They also exhibit, in average, a unimodal annual cycle with a peak in the months of May and June, compared to the observed bimodal seasonal distribution of malaria incidence. Moreover, process-based models show different abilities to fit the baseline seasonality that are likely to come from the way they describe different aspects of the *P. falciparum* malaria transmission cycle. The MAC, AM and WCT models are driven by the combined effects of mean monthly temperature and total monthly rainfall, whereas the ABP model is influenced by the dynamics of the force of infection and its two main components (the local transmission and the external force of infection), as well as the fluctuations of the larvae carrying capacity, which is turn are controlled by the total rainfall

amount. Figure 3 also displays the WCT results for various mean durations of infectivity. Changes in the infectivity from 40 to 95 days (equivalent to changes in the human host recovery probability from 0.7500 to 0.3158 month^{-1}) increase simulated *P. falciparum* malaria prevalence from 2.3 to 5.2 positive cases per 1,000 inhabitants in the months of September and October, and from 5.7 to 13.3 positive cases in March; i.e. changes in the mean duration of infectivity have a strong impact on malaria prevalence particularly after the February and March peak of mean temperatures.

Models' outputs and accuracies. Figure 4(a) depicts the monthly *P. falciparum* malaria incidence observed in Kericho along with the monthly *P. falciparum* malaria prevalence simulated by the four-model ensemble for the actual climatic conditions observed over the full retrospective period 1979-2009, and assuming full certainty in the best set of parameters. Figures SM-1 to SM-4 in the online supplementary material show the individual MAC, AM, WCT, and ABP model simulation outputs for actual conditions and detrended mean temperature time series. The four-model ensemble explains approximately 33% of the variance of *P. falciparum* malaria incidence in Kericho, with a mean square error of about 1E-05. Individual simulation outputs explain from 20 to 30% of the variance, and thus are below the R^2-value obtained by the four-model ensemble. Figure 4(b) presents the correlation coefficients between the monthly *P. falciparum* malaria incidence and the monthly malaria prevalence simulated by the multi-model ensemble for the actual climatic conditions, and for +0.15, +0.25 and +0.35°C per decade detrended time series. The total variance explained by the four-model ensemble decreases from 33% to 24.3%, 14.4% and 4.0%, respectively, when the +0.15, +0.25 and +0.35°C/decade long-term linear trends are removed from the actual climatic time series. The mean square error

remains constant. Table 3 shows the percentage of the variance (R^2-value) of the actual *P. falciparum* malaria morbidity that is explained by MAC, AM, WCT, and ABP simulation outputs when the +0.25°C/decade long-term trend and the 3.4-year cycle are removed from the actual climatic time series. MAC and AM simulation outputs suggest that almost all the correlation between simulated malaria prevalence and actual malaria incidence is explained by the long-term trend and the interannual dependency. ABP and WCT simulation outputs indicate that the seasonal cycle explains most of the variance of the observed *P. falciparum* malaria incidence. Lastly, figure 4(a) also depicts the monthly malaria prevalence simulated by the four-model ensemble for the actual climatic conditions observed over the period 2005-2009. Ensemble simulation outputs suggest that *P. falciparum* malaria prevalence reduced from 13.8 positive cases per 1,000 inhabitants to almost 5.1 primary cases over the last 5 years of the retrospective period. Climatic conditions have likely been less favorable to malaria transmission in the highlands under study in recent years.

Models' sensitivity. Figure 5 depicts the discrete gradient value obtained for each parameter x_i of the WCT model. For a slight change $\Delta x_i = \frac{x_i}{10}$, parameters g_N, α, f_u, and f_N have strong impact on final simulation outputs, suggesting that the WCT tool is highly sensitive to changes in the duration of the sporogonic and gonotrophic cycles, as well as in the survival probability of the mosquito vector. The Sobol Index (results not shown) suggests, in turn, that the WCT model is also highly sensitive to changes in the probability of the vector becoming infected per infectious meal (IS_k=4465302 compared to IS_μ=0.0028, IS_h=1307.9, and IS_l=0.000032).

Uncertainty. Figure 6(a) shows the 25%, 50% and 95% percentiles of the distributions of monthly *P. falciparum* malaria prevalence simulated by the MAC, AM, WCT, and ABP models, for the actual climatic conditions, and for 1-, 1-, 2-, and 0-month time lags, respectively. These lags exhibited the highest correlation coefficients between observed malaria incidence and simulated prevalence. Simulation outputs for uncertainty in parameter values included, respectively, 90, 142, 131, and 131 runs of these models (a grand total of 494 set of parameters were simulated). R^2-values of the 50% percentiles reached 30.9%, 31.6%, 20.7%, and 22.2%, respectively, as presented in the scatter plots in figure 6(b). The highest R^2-values of the MAC and AM 50% percentiles (35.7% and 32.7%, respectively) were obtained in the quarter December-January-February (DJF) (see figures SM-5 (a) and (b) in the online supplementary material), suggesting that these models can capture the February peak in the historical bimodal annual cycle of *P. falciparum* malaria. The highest R^2-values of the WCT and ABP models (26.9% and 46.3%, respectively) were obtained in the trimesters March-April-May (MAM) and September-October-November (see figures SM-5 (c) and (d) in the online supplementary material), indicating that these models most likely represent the periods of minimum malaria incidence. Lastly, figure 6(c) depicts the 25%, 50% and 95% percentiles of the distributions of monthly *P. falciparum* malaria prevalence simulated by the multi-model ensemble (MME). 31.8% of the variance of *P. falciparum* malaria incidence in Kericho is explained by the median of MME. However, if individual simulation outputs are merged at a monthly timescale, the median of the ensemble explains 36.7% of the variance of the observed *P. falciparum* malaria. Also, MME simulation runs showed their highest R^2-values of 32.5% and 31.2% in the quarters DJF and MAM, respectively. Figure 6(c) also depicts the monthly *P. falciparum* malaria prevalence suggested by the MME for nonlinear changes in the mean duration of host's

infectivity to vectors. In this case, 37.7% of the variance of malaria incidence in Kericho is explained by simulation outputs.

4.6. Discussion

The climate forecasting community has used multi-model ensembles to overcome challenges resulting from initial conditions and parameter and structural uncertainties in model design (Palmer et al., 2004). Ensemble approaches have been used to quantify uncertainty in future climate and its impacts (for example on malaria incidence) in a probabilistic way (Thomson et al., 2006). Building on the experiences of the climate forecasters this paper describes our recent advances in the effort to implement an ensemble framework of various mathematical process-based malaria models. The 2012 executive version of the multi-model ensemble (composed of four well-known dynamical models) explained from 32 to 38% of the variance of *Plasmodium falciparum* malaria incidence observed in Tea Plantation 1 of Kericho district, Kenyan highlands, over the historical period 1979-2004. R^2-values obtained by the four-model ensemble were above the results achieved with individual model simulation outputs. Since the executive ensemble framework merges four process-based models that are highly sensitive to changes in the duration of the sporogonic cycle, the gonotrophic cycle, and the survival probability of the mosquito vector, which are all strongly affected by ambient temperatures, the tool mostly allows the assessment of the impacts of changes in climatic conditions on malaria morbidity profiles. In the foreseeable future the multi-model ensemble can be, however, easily expanded to assess the role of changes in non-climatic factors.

Malaria, as several other climate-sensitive diseases, is highly sensitive to even small variations in ambient temperatures. Previous studies (e.g. Rogers and Randolph, 2000; Patz et al., 2002; Tanser et al., 2003; Martens et al., 1995; Zhou et al., 2004; Pascual et al., 2006; and Protopopoff et al., 2009; Waweru et al., 2011) suggest that changes in climatic conditions cannot be ruled out as potential drivers of the observed increases in *P. falciparum* malaria in the highlands of Western Kenya. Multi-model ensemble simulation runs presented here suggest that from 8.7 to 18.6% of the variance of *P. falciparum* malaria incidence observed in the site under study over the period 1979-2004 could be attributed to the +0.19 to +0.25°C per decade statistically significant long-term linear trend in near-surface air temperatures that took place over the period 1950-2009. Ensemble simulation outputs also suggest that climatic conditions have likely been less favorable to malaria transmission in Kericho in recent years.

Even though the four-model ensemble overestimates the historical *P. falciparum* malaria incidence when the annual cycles of mean temperature and rainfall are assumed in base scenario experiments, simulation outputs for actual climatic conditions (assuming certainty and uncertainty in parameter values) observed over the selected retrospective period do not fully capture the magnitude of the peaks in malaria incidence. Simulation runs indicate that on top of the aforementioned 8.7 to 18.6% increase in the variance of *P. falciparum* malaria incidence that could be attributed to the long-term trend in ambient temperatures, at least 6% of such variability or over 10 positive cases per 1,000 inhabitants during recent peaks in the incidence should be related to the increased resistance to anti-malarial drugs. Hence, long-term changes in climatic conditions and nonlinear changes in the mean duration of host's infectivity should be synergistically driving the increasing incidence of *Plasmodium falciparum* malaria in the highlands of Western Kenya.

Health authorities must be starting to implement simple, open source tools such as the ones discussed here to make better decisions regarding malaria control investments, particularly now that our planet is likely to get back on track of the long-term warming trend after a recent cooling period. Instead of using individual process-based models in isolation, however, authorities may gain more useful insights by developing 'ensembles' of different models, where biases in one tool may be compensated by biases in other models. The approach presented herein is to use different sets of parameter values and initial conditions for each model and for all the proposed dynamical tools, and present combined simulation outputs as probability distributions. These experiments are robust in the sense that each process-based model has been subjected to several control simulations, including base scenarios and stability conditions, as well as multiple sets of runs for different choices of parameter values. As mentioned above, results suggest that the mean and the median of the multi-model ensemble outputs outperformed individual model simulation runs. Results also incorporated the level of uncertainty associated with modeling outputs.

But which models should be considered in the multi-model ensemble? Intuitively, one should pick those that better represent the most relevant aspects of the *P. falciparum* malaria transmission cycle, and that exhibit high accuracy and predictive power. From an operative point of view, one would also prefer to include those tools that show a high skill level using a short list of parameters and exogenous variables, which can be easily measured in the field or under controlled laboratory conditions. Also, one would prefer those models that are consistent with other related tools, that are not complicated, and that in the general sense are useful for routine activities of health services. How should we combine the results of the best malaria transmission models? Simulation runs in this set of experiments were combined using equally weighted

models. In a perfect world, models with higher reliability and consistency should weigh more than those with lower skill level (Tebaldi and Knutti, 2007). Future work will therefore address the need to consider R^2-values between simulated malaria cases and actual positive cases, mean square errors, a function of likelihood, or the 'bias' and 'convergence' criteria (Giorgi and Mearns, 2002) for deriving differential model weighting.

There are various limitations in the use of a malaria process-based multi-model ensemble. Models usually describe different aspects of the transmission cycle of *P. falciparum* malaria. As a consequence, some dynamical models are driven by ambient temperature while others are strongly influenced by rainfall. Hence, there is a need to initially judge, subjectively and based on pure expertise, which model is suitable for a specific application. Also, simulation experiments cannot span the full range of possible combinations of parameter values and initial conditions due to time and computational capacity constraints. That is why many times the fine-tuning process of model parameters involves purely subjective judgment, making it hard to guarantee the proper identification of the 'optimum location' in the parameter space (Tebaldi and Knutti, 2007).

Acknowledgments

The research team acknowledges Samuel M. Waweru from the Kenya Meteorological Department for providing quality controlled daily records of maximum temperatures, minimum temperatures and rainfall totals gathered at Kericho meteorological station. D. Ruiz was partially supported by the Department of Earth and Environmental Sciences at Columbia University in the

City of New York, the International Research Institute for Climate and Society, Lamont-Doherty Earth Observatory, and the Antioquia School of Engineering (Colombia).

References

Alonso, D., M.J. Bouma, and M. Pascual, 2011. Epidemic malaria and warmer temperatures in recent decades in an East African highland. Proc Biol Sci 278(1712):1661-9.

Anderson, R.M. and R.M. May, 1991. Infectious diseases of humans: dynamics and control. London: Oxford University Press.

Artzy-Randrup, Y., D. Alonso, and M. Pascual, 2010. Transmission intensity and drug resistance in malaria population dynamics: implications for climate change. PLoS ONE 5(10): e13588. doi:10.1371/journal.pone.0013588.

Charlwood, J.D., M.H. Birley, H. Dagoro, R. Paru, and P.R. Holmes, 1985. Assessing survivial rates of *Anopheles farauti* (Diptera: Culicieae) from Papua New Guinea. Journal of Applied Ecology 54:1003-1016.

Chaves L.F., and C.J.M. Koenraadt, 2010. Climate change and highland malaria: fresh air for a hot debate. Quarterly Review of Biology 85(1): 27–55.

Collins, W.E., and G.M. Jeffery, 1999. A retrospective examination of the patterns of recrudescence in patients infected with *Plasmodium falciparum*. Am J Trop Med Hyg 61:44-48.

Detinova, T.S., 1962. Age-grouping methods in Diptera of medical importance with special reference to some vectors of malaria. No. 47 in Monograph Series, WHO. 1962.

Eichner, M., H.H. Diebner, L. Molineaux, W.E. Collins, G.M. Jeffery, and K. Dietz, 2011. Genesis, sequestration and survival of *Plasmodium falciparum* gametocytes: parameter estimates from fitting a model to malariatherapy data. Trans R Soc Trop Med Hyg 95:497-501.

Ermert, V., A.H. Fink, A.E. Jones, and A.P. Morse, 2011. Development of a new version of the Liverpool Malaria Model. I. Refining the parameter settings and mathematical formulation of basic processes based on a literature review. Malaria Journal 2011, 10:35.

Giorgi, F. and L. Mearns, 2002. Calculation of average, uncertainty range and reliability of regional climate changes from AOGCM simulations via the 'reliability ensemble averaging' (REA) method. J. Clim. 15, 1141–1158. (doi:10.1175/1520-0442(2002)015!1141:COAURAO2.0.CO;2).

Graves, P.M., T.R. Burkot, A.J. Saul, R.J. Hayes, and R. Carter, 1990. Estimation of Anopheline survival rates, vectorial capacity and mosquito infection probability from malaria vector infection rates in villages near Madang, Papua New Guinea. Journal of Applied Ecology 27(1):134-147.

Hastings, D.A., and P.K. Dunbar, 1999. Global land one-kilometer base elevation (GLOBE) digital elevation model, Documentation, Volume 1.0. Key to Geophysical Records Documentation (KGRD) 34. National Oceanic and Atmospheric Administration, National Geophysical Data Center, 325 Broadway, Boulder, Colorado 80303, USA.

Hay, S.I., J. Cox, D.J. Rogers, S.E. Randolph, D.I. Stern, G.D. Shanks, M.F. Myers, and R.W. Snow, 2002a. Climate change and the resurgence of malaria in the East African highlands. Nature 415: 905-909.

Hay, S.I., A.M. Noor, M. Simba, M. Busolo, H.L. Guyatt, S.A. Ochola, and R.W. Snow, 2002b. Clinical epidemiology of malaria in the highlands of western Kenya. Emerg Infect Dis. 8:543–8.

Hay, S.I., D.J. Rogers, S.E. Randolph, D.I. Stern, J. Cox, G.D. Shanks, and R.W. Snow, 2002c. Hot topic or hot air? Climate change and malaria resurgence in East African highlands. Trends in Parasitology 18(12): 530–534.

Hay, S.I., M. Simba, M. Busolo, A.M. Noor, H.L. Guyatt, S.A. Ochola SA, and R.W. Snow, 2002d. Defining and detecting malaria epidemics in the highlands of western Kenya. Emerg Infect Dis. 8:555–62.

Hay, S.I., E.C. Were, M. Renshaw, A.M. Noor, S.A. Ochola, I. Olusanmi, N. Alipui, and R.W. Snow, 2003. Forecasting, warning, and detection of malaria epidemics: a case study. Lancet. 2003;361:1705–6.

Hay, S.I., G.D. Shanks, D.I. Stern, R.W. Snow, S.E. Randolph, and D.J. Rogers, 2005. Climate variability and malaria epidemics in the highlands of East Africa. Trends Parasitol 21:52–53.

Hii, J.L., M.H. Birley, and V.Y. Sang, 1990. Estimation of survival rate and oviposition interval of *Anopheles balabacensis* mosquitoes from mark-recaputre experiments in Sahah, Malaysia. Medical and Veterinary Entomology 4:135-140.

Jepson, W.F., A. Moutia, and C. Courtois, 1947. The malaria problem in Mauritius: the binomics of Mauritian anophelines. Bull Entomol Res 1947, 38:177-208.

Kiszewski, A., A. Mellinger, A. Spielman, P. Malaney, S.E. Sachs, and J. Sachs, 2004. A global index representing the stability of malaria transmission. Am J Trop Med Hyg 70:486-498.

Lau, K.-M. and H.-Y. Weng, 1995. Climate signal detection using wavelet transform: how to make a time series sing. Bull. Am. Meteor. Soc. 76: 2391-2402.

Lindsay S.W., and W.J. Martens, 1998. Malaria in the African highlands: past, present and future. Bull World Health Organ 76: 33–45.

Macdonald, G., 1957. The epidemiology and control of malaria. Oxford University Press, Oxford, U.K.

Macdonald, G., and G.W. Göckel, 1964. The malaria parasite rate and interruption of transmission. Bull World Health Org 31:365-377.

Magesa, S.M., T.J. Wilkes, A.E. Mnzava, K.J. Njunwa, J. Myamba, M.D. Kivuyo, N. Hill, J.D. Lines, and C.F. Curtis, 1991. Trial of pyrethroide impregnated bednets in an area of Tanzania holoendemic for malaria. Part 2. Effects on the malaria vector population. Acta Tropica 49:97-108.

Martens, W.J., L.W. Niessen, J. Rotmans, T.H. Jetten, and A.J. McMichael, 1995. Potential impact of global climate change on malaria risk. Environ Health Perspect 103: 458–464.

Masaba, S., D. Anyona, and D. Chepkwoni, 1985. In vitro response of *Plasmodium falciparum* to chloroquine in the Nandi district, Kenya. Bull World Health Organ 63: 593–595.

Murphy, J.R., S. Baqar, J.R. Davis, D.A. Herrington, and D.F. Clyde, 1989. Evidence for a 6.5-day minimum exoerythrocytic cycle for *Plasmodium falciparum* in humans and confirmation that immunization with a synthetic peptide representative of a region of the circumsporozoite protein retards infection. J Clin Microbiol 27:1434-1437.

Mutero, C.M., and M.H. Birley, 1987. Estimation of the survival rate and oviposition cycle of field populations of malaria vectors in Kenya. Journal of Applied Ecology 24:853-863.

Nikolaev, B.P., 1935. On the influence of temperature on the development of malaria plasmodia in the mosquito. Leningrad Pasteur Institute of Epidemiology and Bacteriology 2:108-109.

Okiro, E.A., A. Al-Taiar, H. Reyburn, R. Idro, J.A. Berkley, and R.W. Snow, 2009. Age patterns of severe paediatric malaria and their relationship to *Plasmodium falciparum* transmission intensity. Malaria Journal 8: 4.

Omumbo, J.A., B. Lyon, S.M. Waweru, S.J. Connor, and M.C. Thomson, 2011. Raised temperatures over the Kericho tea estates: revisiting the climate in the East African highlands malaria debate. Malaria Journal 10: 12.

Paaijmans, K.P., A.F. Read, and M.B. Thomas, 2009. Understanding the link between malaria risk and climate. PNAS 106(33): 13844-13849.

Palmer, T.N., U. Andersen, P. Cantelaube, M. Deque, F.J. Doblas-Reyes, H. Feddersen, R.Graham, S. Gualdi, J.-F Gueremy, R. Hagedorn, M. Hoshen, N. Keenlyside, A. Lazar, V. Marletto, A.P. Morse, B. Orfila, P. Rogel, J.-M. Terres, and M.C. Thomson, 2004. Development of a European ensemble system for seasonal to inter-annual prediction. Bulletin of the American Meteorology Society 85(6): 853–872.

Pascual, M., J.A. Ahumada, L.F. Chaves, X. Rodó, and M. Bouma, 2006. Malaria resurgence in the East African highlands: temperature trends revisited. Proc Natl Acad Sci USA 103:5829–5834.

Pascual, M., B. Cazelles, M.J. Bouma, L.F. Chaves, and K. Koelle, 2008. Shifting patterns: malaria dynamics and rainfall variability in an African highland. Proc. R. Soc. B 275: 123–132.

Patz, J.A., M. Hulme, C. Rosenzweig, T.D. Mitchell, R.A. Goldberg, A.K. Githeko, S. Lele, A.J. McMichael, and D. Le Sueur, 2002. Climate change: regional warming and malaria resurgence. Nature 420: 627–628.

Protopopoff, N., W. Van Bortel, N. Speybroeck, J.P. Van Geertruyden, D. Baza, U. D'Alessandro, and M. Coosemans, 2009. Ranking malaria risk factors to guide malaria control efforts in African highlands. PLoS ONE 4(11): e8022. doi:10.1371/journal.pone.0008022.

Rapuoda, B.A., J.H. Ouma, K. Njiagi, B. Khan, and S. Omar, 1996. Status of antimalarial drugs sensitivity in Kenya. Malaria and Infectious Diseases in Africa 8:25–43.

Reiter, P., 2008. Global warming and malaria: knowing the horse before hitching the cart. Malaria Journal 2008, 7(Suppl 1):S3 doi:10.1186/1475-2875-7-S1-S3.

Roeckner, E., K. Arpe, L. Bengtsson, M. Christoph, M. Claussen, L. Dümenil, M. Esch, M. Giorgetta, U. Schlese, and U. Schulzweida, 1996. The atmospheric general circulation model ECHAM4: Model description and simulation of present-day climate. Max-Planck-Institut fur Meteorologie Rep. 218, Hamburg, Germany, 90 pp.

Rogers D.J., and S.E. Randolph, 2000. The global spread of malaria in a future, warmer world. Science 289: 1763–1766.

Ross, R., 1911. The prevention of malaria. Murry, London, U.K.

Ruiz, D. and G. Yan, 2004. Modeling malaria transmission for Kisii District in the highlands of Western Kenya. Part I: analysis of base scenarios. Department of Biological Sciences, State University of New York at Buffalo, 45 pp.

Ruiz, D., S. Connor and M.C. Thomson, 2008. A multimodel framework in support of malaria surveillance and control. Pages 101-125 in: Seasonal Forecasts, Climatic Change, and Human Health – Health and Climate / Advances in Global Change Research Vol. 30; Madeleine C. Thomson, Ricardo Garcia Herrera and Martin Beniston (ed.), Springer Science + Business Media, Dordrecht; Springer Netherlands, ISBN 978-1-4020-6876-8, The Netherlands.

Ruiz, D., M.C. Thomson, S.J. Connor, R. Cousin, and C. Brun, 2012. Process-based modeling of malaria transmission dynamics. Grupo 'Investigación en Gestión Ambiental'-Escuela de Ingeniería de Antioquia (Colombia) and International Research Institute for Climate and Society-Columbia University in the City of New York (USA), 72 pages.

Schneider, P., L. Wolters, G. Schoone, H. Schallig, P. Sillekens, R. Hermsen, and R. Sauerwein, 2005. Real-time nucleic acid sequence-based amplification is more convenient than real-time PCR for quantification of *Plasmodium falciparum*. J Clin Microbiol 43:402-405.

Shanks, G.D., K. Biomndo, S.I. Hay, and R.W. Snow, 2000. Changing patterns of clinical malaria since 1965 among a tea estate population located in the Kenyan highlands. Trans R Soc Trop Med Hyg 94:253-255.

Shanks, G.D., S.I. Hay, D.I. Stern, K. Biomndo, and R.W. Snow, 2002. Meteorologic influences on *Plasmodium falciparum* malaria in the highland tea estates of Kericho, western Kenya. Emerg Infect Dis. 8:1404–8.

Shanks, G.D., K. Biomndo, H.L. Guyatt, and R.W. Snow, 2005a. Travel as a risk factor for uncomplicated *Plasmodium falciparum* malaria in the highlands of western Kenya. Trans R Soc Trop Med Hyg. 99: 71–4.

Shanks, G.D., S.I. Hay, J.A. Omumbo, and R.W. Snow, 2005b. Malaria in Kenya's western highlands. Emerging Infectious Diseases 11(9): 1425-1432.

Shute, P.G., and M. Maryon, 1951. A study of gametocytes in a West African strain of *Plasmodium falciparum*. Trans R Soc Trop Med Hyg 44:421-438.

Sinden, R., 1983. Sexual development of malarial parasites. Adv Parasitol 22:153-216.

Sutherland, C.J., A. Alloueche, J. Curtis, C.J. Drakeley, R. Ord, M. Duraisingh, B.M. Greenwood, M. Pinder, D. Warhurst, and G.A. Targett, 2002. Gambian children successfully treated with chloroquine can harbor and transmit *Plasmodium falciparum* gametocytes carrying resistance genes. Am J Trop Med Hyg 67:578–85.

Stern D.I., P.W. Gething, C.W. Kabaria, W.H. Temperley, A.M. Noor, E.A. Okiro, G.D. Shanks, R.W. Snow, and S.I. Hay, 2011. Temperature and malaria trends in highland East Africa. PLoS ONE 6(9): e24524. doi:10.1371/journal.pone.0024524.

Tanser, F.C., B. Sharp, and D. Le Sueur, 2003. Potential effect of climate change on malaria transmission in Africa. Lancet 362: 1792–1798.

Tebaldi, C. and R. Knutti, 2007. The use of the multi-model ensemble in probabilistic climate projections. Phil. Trans. R. Soc. A 2007 365: 2053–2075, doi: 10.1098/rsta.2007.2076.

Thomson, M.C., F.J. Doblas-Reyes, S.J. Mason, R. Hagedorn, S.J. Connor, T. Phindela, A.P. Morse, and T.N. Palmer, 2006: Malaria early warnings based on seasonal climate forecasts from multi-model ensembles. Nature 439: 576-579.

Torrence, C. and G.P. Compo, 1998. A practical guide to Wavelet Analysis. Bull. Amer. Meteor. Soc. 79: 61-78.

Waweru, S.M., J.A. Omumbo, B. Lyon, M.C. Thomson, and S.J. Connor, 2011. Revisiting the East African malaria debate. World Meteorological Organization Bulletin Volume 60(1). Available online at: http://www.wmo.int/pages/publications/bulletin_en/archive/60_1_en/60_1_Waweru_en.html

Worrall, E., S.J. Connor and M.C. Thomson, 2007. A model to simulate the impact of timing, coverage and transmission intensity on the effectiveness of indoor residual spraying (IRS) for malaria control. Tropical Medicine & International Health 12(1): 75-88.

Zhou, G., N. Minakawa, A. Githeko, and G. Yan, 2004. Association between climate variability and malaria epidemics in the East African Highlands. PNAS USA 101(8): 2375–2380.

Table 1(a). Parameters and exogenous variables – community-based, malaria parasite and human host

Component	Parameter/exogenous variable		Process-based model				Note[%]
			MAC	AM	WCT	ABP	
Community-based	Total human population at risk		d	d	d	N	(1)
	Human natural birth		--	--	--	$B=\delta_H*N$	--
	Human natural mortality rate	Assuming a given average lifetime	--	μ_1	--	--	(1)
		Individual losses due to mortality or more generally, population turnover	--	--	--	δ_H	(1)
	Proportion of total population at risk covered with IRS program campaign		--	--	C	--	(1)
	Proportion of positive cases actually reported to health facilities		--	--	λ	--	(1)
Malaria parasite	Parasite species		*P. falciparum*				--
	Sporogony/malaria parasites incubation period		n	$n=f_N/(T+l-g_N)$	$n=f_N/(T+l*(U-\upsilon)/U-g_N)$	$\gamma_P=f(T)^{\&}$	--
	Number of degree-days needed to complete parasite development		--	f_N	f_N	--	(1)
	Temperature threshold below which parasite development ceases		--	g_N	g_N	--	(1)
	Latency of infection in mosquito vectors		--	t_m	--	--	(2)
Human host	Reciprocal of the average duration of the "affected state"		r=1/(HD+WN)	r=1/[HD+wn(t)]	--	--	--
	Average time in the exposed phase		--	--	--	$1/\gamma$	(2)
	Host delay for infectivity; length of the interval between infection/sporozoite inoculation and the onset of infectivity/gametocyte maturation (*HD*) or latency of infection (t_h)		HD	t_h	--	--	(2)
	External force of infection		--	--	--	β_e	(2)
	Probability that an infectious bite results in infection		--	--	--	b	(1)
	Host window for immunity; duration of a host's infectivity to vectors, from the first to the final present of infective gametocytes		WN	wn(t)	--	--	(2)
	Loss of immunity basal rate		--	--	--	σ_0	(2)
	Human recovery	Assuming a given mean duration of infectivity	--	--	r	--	(2)
		C to S clearance rate	--	--	--	ρ	(1)
		Fraction of infections in humans that fully develops severe malaria symptoms and then receive clinical treatment	--	--	--	ξ	(2)
		Factor that decreases the per-capita transmission rate when asymptomatic but infectious individuals -I- can present a relapse of severe malaria symptoms if they are bitten again	--	--	--	η	(2)
		I to R recovery basal rate	--	--	--	r_0	(2)
		C to I recovery rate	--	--	--	ν	(2)

[&] See supplementary material; [%] (1) chosen from literature and fixed constant, and (2) chosen from literature and fitted.

Table 1(b). Parameters and exogenous variables – *Anopheles* mosquito population and environment

Component	Parameter/exogenous variable		Process-based model				Note[%]
			MAC	AM	WCT	ABP	
Mosquito population	Vector natality: rainfall-to-mosquitoes constant (μ), mosquito fecundity factor (F), and number of eggs per oviposition event (n)		μ	μ	μ	F, n	(2)
	Vector survivorship: daily survival probability (p)		p=α^(1/U)	p=α^(1/U)	p=[α*(1-C)+ α*β*C]^(1/U)	$\langle\lambda\rangle = f(T)$ [&]	--
	Probability of surviving each gonotrophic cycle in an unsprayed population (not covered by the IRS campaign)		α	α	α	--	(1)
	Reduction in α in the population covered by the spray program immediately after spraying		--	--	β	--	(1)
	Gonotrophic cycle		$U=\upsilon+(f_U/(T+l-g_U))$	$U=\upsilon+(f_U/(T+l-g_U))$	$U=\upsilon+(f_U/(T+l-g_U))$	--	--
	Total number of degree days needed to complete development of the ovaries		f_u	f_u	f_u	--	(1)
	Minimum temperature needed to complete development of ovaries		g_u	g_u	g_u	--	(1)
	Length of a part of gonotrophic cycle to find a water body and a new human host		υ	υ	υ	--	(1)
	Vector feeding		$a=0.091678*T_e-1.7982$	$a=0.091678*T_e-1.7982$	a=h/U	$a=0.091678*T_e-1.7982$	--
	Human blood index (proportion of mosquitoes feeding on humans)		--	--	h	--	(1)
	Mortality rate	Assuming a given average lifespan	--	μ_2	--	--	(1)
		Larvae mortality caused by temperature- or rain-independent processes, such as predation	--	--	--	δ_0	(2)
		Per-capita larvae death rate - inverse of the larval average life time- at temperatures of 14, 16, 18, and 20°C	--	--	--	$\delta_L(14)$, $\delta_L(16)$, $\delta_L(18)$, $\delta_L(20)$	(1)
		Death factor introduced to represent the washout effect for the larvae	--	--	--	δ_R	(2)
	Vector infectivity: probability of becoming infected per infectious meal (k), probability of becoming infectious with malaria parasites (v)		--	--	k and v	--	(1)
	Proportion of *Anopheles* mosquitoes with sporozoites in their salivary glands which are actually infective		b	b	--	--	(1)
	Vector susceptibility or human host-to-mosquito probability of transmission		--	c	--	c	(1)
Environment	Daily effective temperature		$T_e=T+(1-x_p)*l$	$T_e=T+(1-x_p)*l$	--	$T_e=T+(1-x_p)*\Delta T$	--
	Daily ambient temperature		T	T	T	T	--
	Temperature weighting parameter		x_p	x_p	--	x_p	(1)
	Difference between indoor and outdoor temperatures (l) or maximum allowed difference between the maximum temperature adult mosquitoes can experience and outdoor temperature (ΔT)		l	l	l	ΔT	(1)
	Daily/monthly rainfall		P	P	P	P and $\langle P\rangle_{12}$ [&]	--
	Larvae carrying capacity	Conversion factor	--	--	--	k_A	(2)
		Loss rate	--	--	--	k_E	(2)

[&] See supplementary material; [%] (1) chosen from literature and fixed constant, and (2) chosen from literature and fitted.

Table 2. Historical values and long-term trends in observed weather data

Climate variable [units]			Historical value	C.I. [95%]	Trend [units/decade] α=0.05
Rainfall (R)	R1	Total annual R [mm]	1,986.4	94.2	N/S
	R_{DJF}	Total DJF R [mm]	291.3	60.5	N/S
	R_{MAM}	Total MAM R [mm]	674.4	50.8	N/S
	R_{JJA}	Total JJA R [mm]	510.7	45.1	N/S
	R_{SON}	Total SON R [mm]	505.5	42.8	N/S
	R2	Total number of dry days per year [number]	140.4	6.3	7.4
	$R2_{DJF}$	Total dry days over DJF trimester [number]	56.6	3.7	N/S
	$R2_{MAM}$	Total dry days over MAM trimester [number]	28.6	2.3	N/S
	$R2_{JJA}$	Total dry days over JJA trimester [number]	27.3	3.0	N/S
	$R2_{SON}$	Total dry days over SON trimester [number]	27.9	2.7	N/S
	R3	Maximum daily R [mm]	35.4	1.9	N/S
	$R4_{DJF}$	Maximum dry spell over the DJF trimester [days]	16.4	3.1	N/S
Minimum temperature (Tmin)	MTmin	Annual Tmin on the warmest days [°C]	13.9	0.2	0.4
	ATmin	Annual Tmin [°C]	11.0	0.1	0.2
	mTmin2	Annual Tmin on the coldest days [°C]	7.9	0.1	N/S
	SDTmin	Day-to-day standard deviation of Tmin [°C]	1.6	0.1	0.1
Maximum temperature (Tmax)	MTmax	Annual Tmax on the warmest days [°C]	26.5	0.1	0.2
	ATmax	Annual Tmax [°C]	24.1	0.1	0.3
	mTmax2	Annual Tmax on the coldest days [°C]	20.8	0.2	0.2
	SDTmax	Day-to-day standard deviation of Tmax [°C]	1.4	0.0	N/S
Diurnal temperature range (DTR)	MDTR	Maximum annual DTR [°C]	17.6	0.2	N/S
	ADTR	Annual DTR [°C]	13.1	0.1	N/S
	mDTR2	Minimum annual DTR [°C]	7.9	0.2	N/S
	SDDTR	Day-to-day standard deviation of DTR [°C]	2.4	0.1	N/S

C.I.: confidence interval; α: significance level; DJF: December-January-February; MAM: March-April-May; JJA: June-July-August; SON: September-October-November; N/S: non-significant

Table 3. Percentage of the variance (R^2-value) of the actual *Plasmodium falciparum* malaria morbidity that is explained by the MAC, AM, WCT, and ABP simulation outputs

Model	**R^2-value**		
	Actual climatic conditions	Long-term trend removed	Long-term trend and 3.4-year cycle removed
MAC	0.231	0.067	0.000
AM	0.229	0.104	0.019
WCT	0.087	0.085	0.084
ABP	0.298	0.285	0.238

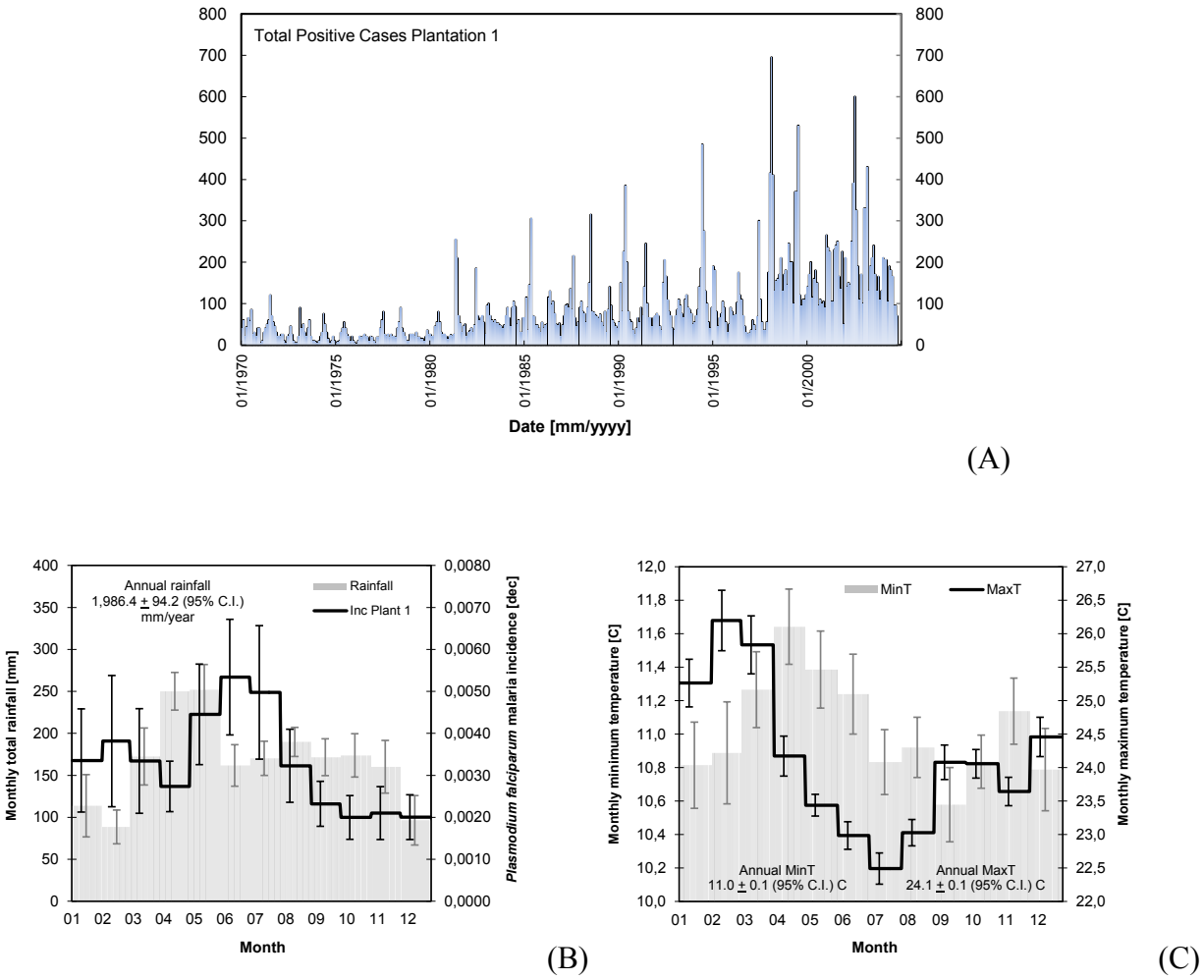

Figure 1. (A) Monthly malaria positive cases at Tea Plantation 1 in Kericho, Kenya, over the period spanning from January, 1970 through October, 2004. (B) and (C) Annual cycles of rainfall (gray bars in panel B), minimum temperature (gray bars in panel C), and maximum temperature (black solid line in panel C) observed in Kericho District, Kenyan highlands, over the period 1979-2009. Error bars depict the confidence intervals for a 0.05 significance level. See also the *Plasmodium falciparum* malaria incidence (black solid line in panel B) observed in Plantation 1 over the period spanning from January, 1970 through October, 2004. The total annual rainfall amount is presented on the top left hand side of panel B. The average minimum and maximum annual temperatures are presented on the bottom left hand

side and bottom right hand side of panel C. See also rainfall and temperature confidence intervals for a 95% confidence level.

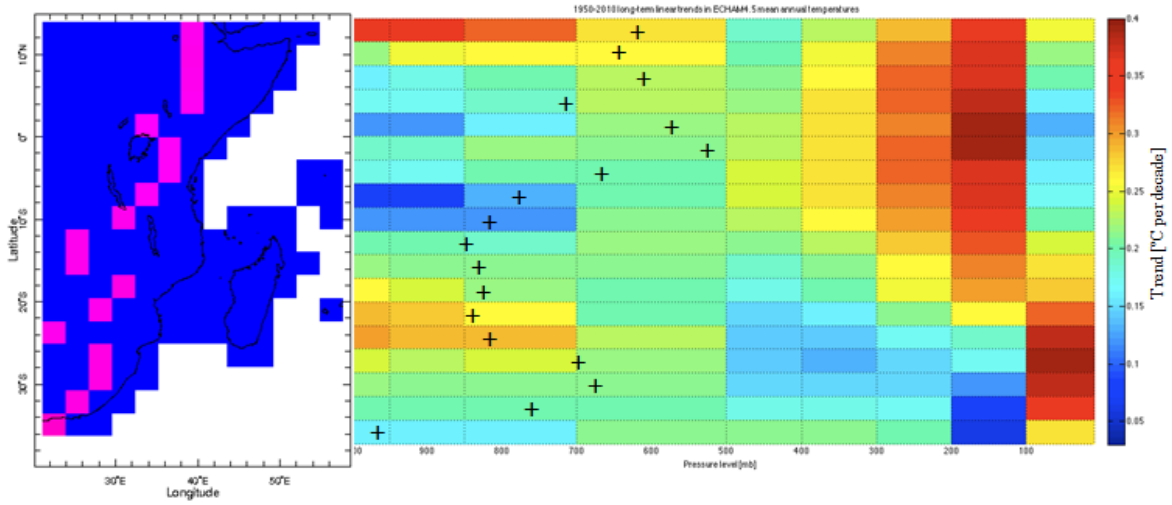

Figure 2. 1950-2010 long-term linear trends in ECHAM4.5 mean annual air temperatures (T_a) along the African Eastern highlands (see pink 2.8125°pixels on plan view - left panel), for the latitudinal range [35°S-15°N], and for 9 pressure levels [1000, 950, 850, 700, 500, 400, 300, 200, and 100 mb; see vertical profile - right panel]. T_a values are obtained through ECHAM4.5 ensemble simulation runs. Long-term linear trends, expressed in °C per decade (see color scale), are statistically significant at α=0.05 significance level. Crosses depict the maximum altitudes (expressed in atmospheric pressures) of the NOAA NGDC GLOBE gridded 1-km, quality controlled global Digital Elevation Model (Hastings and Dunbar, 1999) in the ECHAM4.5 model gridpoints.

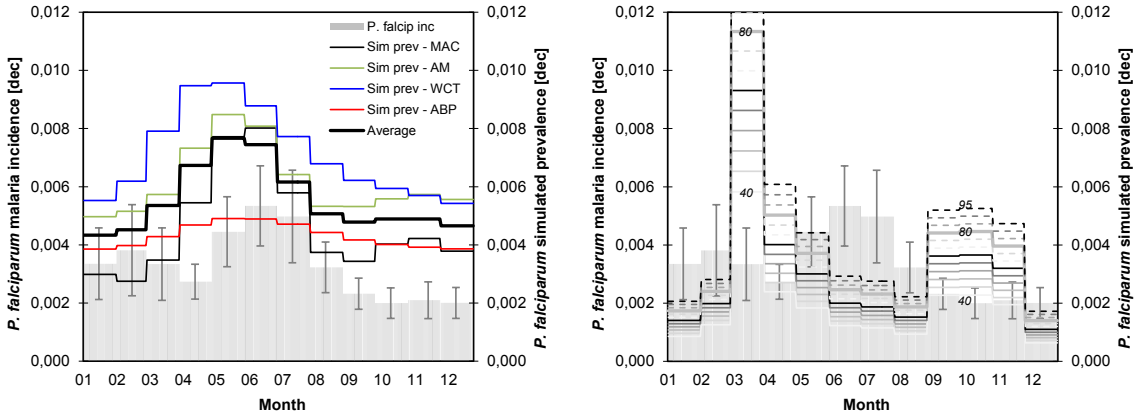

Figure 3. Simulation outputs for base scenarios. Left panel: actual *Plasmodium falciparum* malaria incidence observed in Tea Plantation 1 in Kericho, Kenya, over the period spanning from January, 1970 through October, 2004 (grey solid bars), along with malaria prevalence simulated by the MAC (black solid line labeled Sim prev – MAC), AM (green solid line labeled Sim prev – AM), WCT (blue solid line labeled Sim prev – WCT), and ABP (red solid line labeled Sim prev – ABP) models for the historical annual cycles of mean temperature and rainfall. The black thick line depicts the annual cycle of *P. falciparum* malaria prevalence obtained by averaging all models' simulation outputs. The following parameter values were assumed for the MAC model: b=0.01; HD=20 days; WN=20 days; r=1/(HD+WN); α=exp(-1/1.229); υ=1.26 days; f_U=36.5°C-days; l=5°C; g_U=9.9°C; U=υ + (f_U/(T+l-g_U)); p=α^(1/U); x_p=0.01; T_e=T+(1-x_p)*l; a=0.091678*T_e-1.7982; and d=27,000 individuals. For the AM model (besides the set of parameters proposed for the MAC model): f_N=116°C-days; g_N=16°C; n=f_N/(T+l-g_N); t_h=13 days; t_m=10 days; μ_1=(1/(70*365)) days^{-1}; μ_2=(1/21) days^{-1}; and c=1.0. For the WCT model (besides the set of parameters proposed for the MAC and AM models): μ=6,500; C=0.24; β=exp(-1/0.4); x=0.1; h=0.8; k=1; v=0.4; r_{WCT}=1/(80/30) month^{-1}; and λ=1.00. And for the ABP model (besides the set of parameters proposed for the MAC, AM and WCT models): δ_H=1/20*(1/135); b_{ABP}=0.5; β_e=0.0000257; σ_0=0.0805; ρ=0.428; r_0=0.00555; γ=0.0486; ξ=0.825; η=0.0346; ν=0.05; F=66; k_A=695; k_E=0.198;

δ_0=0.0329; c_{ABP}=0.365; x_{ABP}=0.01; and ΔT=4.2°C. A full description of all these parameters is presented in Ruiz et al. (2012); see the online supplementary material. Right panel: actual *P. falciparum* malaria incidence (grey solid bars) along with malaria prevalence simulated by the WCT model for various mean durations of infectivity, $1/r_{WCT}$ (from 40 to 95 days).

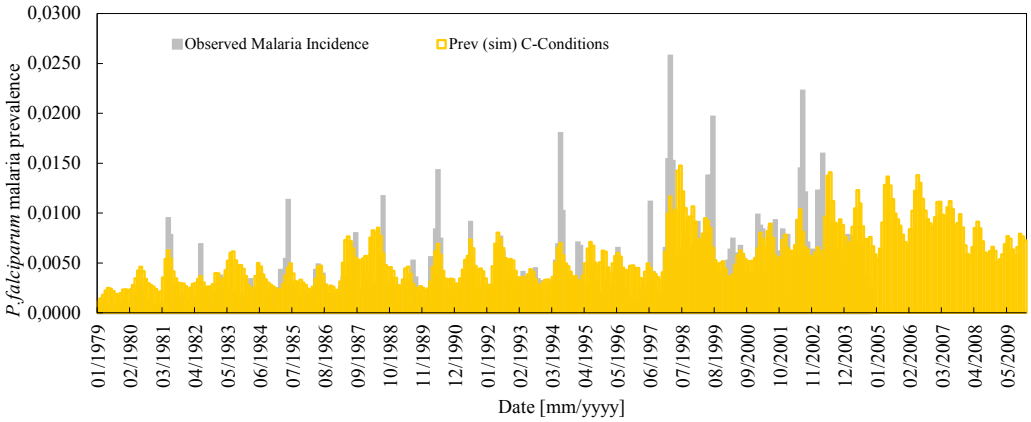

Figure 4(a). Monthly *Plasmodium falciparum* malaria incidence observed in Kericho District, Kenyan highlands, over the period spanning from January, 1979 through October, 2004 (grey solid bars), along with monthly *P. falciparum* malaria prevalence simulated by the multi-model ensemble for the actual climatic conditions (C-conditions; yellow solid bars), for the period spanning from January, 1979 through December, 2009, and for 0-month time lags. Daily mean temperatures were estimated as an average of daily minimum and maximum temperatures. Full certainty in the set of parameters of the four-model ensemble is assumed in this simulation run. R^2=0.33; MSE=1E-05.

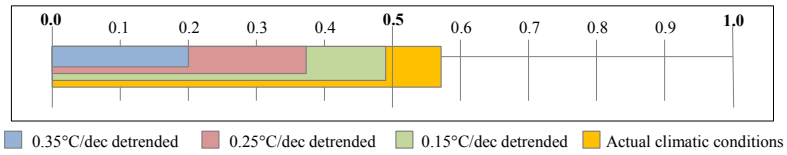

Figure 4(b). Correlation coefficients (R-values) between the monthly *Plasmodium falciparum* malaria incidence observed in Kericho over the period spanning from January, 1979 through October, 2004, and the monthly *P. falciparum* malaria prevalence simulated by the multi-model ensemble for the actual climatic conditions, for +0.15, +0.25 and +0.35°C per decade detrended time series, and for 0-month time lags. Full certainty in the set of parameters of the four-model ensemble is assumed in these simulation runs.

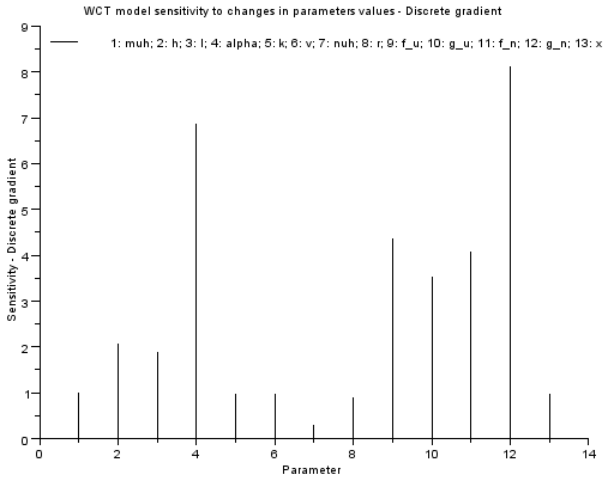

Figure 5. WCT model sensitivity (discrete gradient) to changes in its set of thirteen parameters: μ=6,500; h=0.8; l=5.0°C; α=exp(-1/1.229); k=1; v=0.4; υ=1.26 days; r_{WCT}=1/(80/30); f_U=36.5°C-days; g_U=9.9°C; f_N=116°C-days; g_N=16°C; and x=0.1.

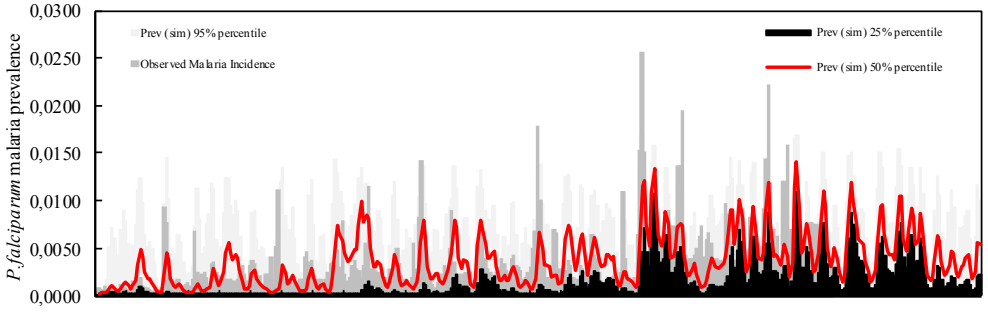
0,0300
0,0250
0,0200
0,0150
0,0100
0,0050
0,0000
P. falciparum malaria prevalence
Prev (sim) 95% percentile
Observed Malaria Incidence
Prev (sim) 25% percentile
Prev (sim) 50% percentile

(A)

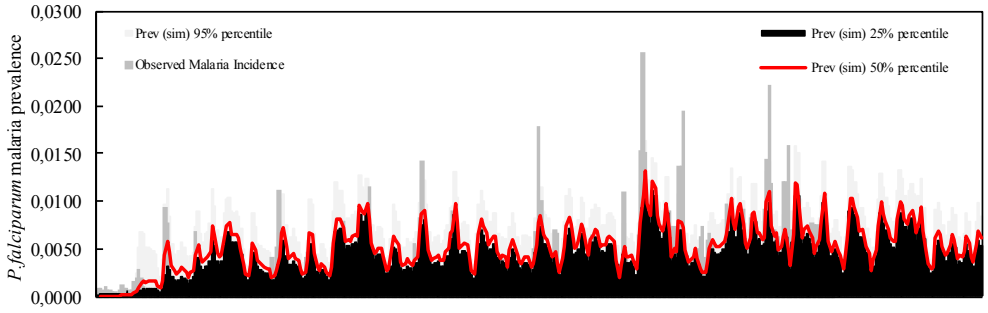
0,0300
0,0250
0,0200
0,0150
0,0100
0,0050
0,0000
P. falciparum malaria prevalence
Prev (sim) 95% percentile
Observed Malaria Incidence
Prev (sim) 25% percentile
Prev (sim) 50% percentile

(B)

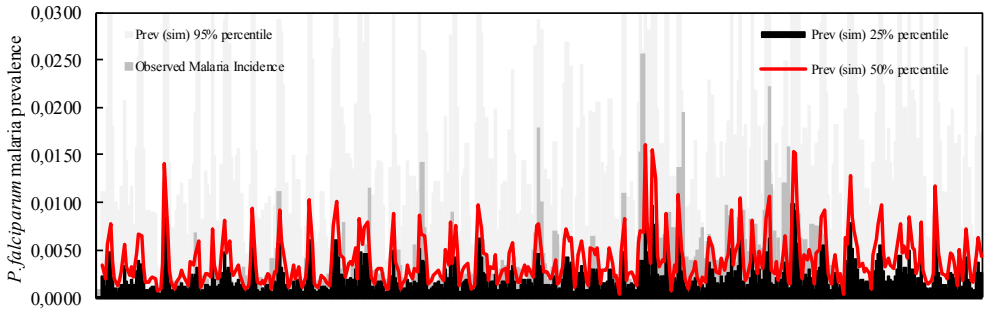
0,0300
0,0250
0,0200
0,0150
0,0100
0,0050
0,0000
P. falciparum malaria prevalence
Prev (sim) 95% percentile
Observed Malaria Incidence
Prev (sim) 25% percentile
Prev (sim) 50% percentile

(C)

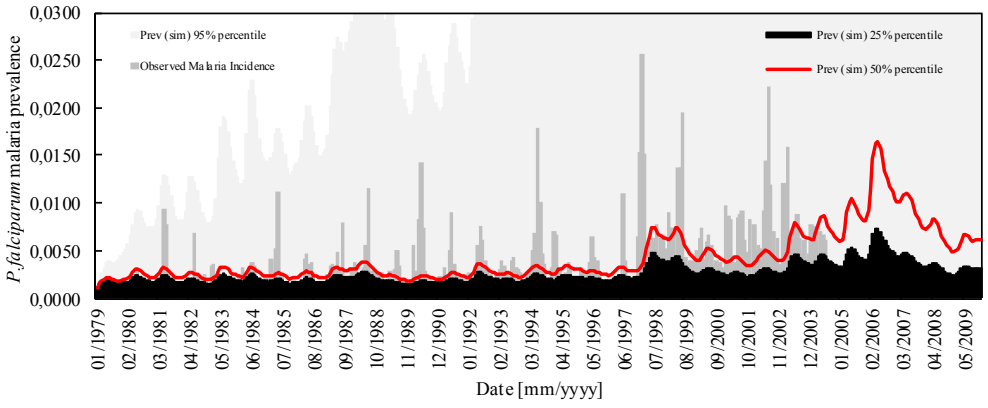
0,0300
0,0250
0,0200
0,0150
0,0100
0,0050
0,0000
P. falciparum malaria prevalence
Prev (sim) 95% percentile
Observed Malaria Incidence
Prev (sim) 25% percentile
Prev (sim) 50% percentile
01/1979
02/1980
03/1981
04/1982
05/1983
06/1984
07/1985
08/1986
09/1987
10/1988
11/1989
12/1990
01/1992
02/1993
03/1994
04/1995
05/1996
06/1997
07/1998
08/1999
09/2000
10/2001
11/2002
12/2003
01/2005
02/2006
03/2007
04/2008
05/2009
Date [mm/yyyy]

(D)

Figure 6(a). Monthly *Plasmodium falciparum* malaria incidence observed in Kericho District, Kenyan highlands, over the period spanning from January, 1979 through October, 2004 (grey solid bars), along with the 25%, 50% and 95% percentiles of the distributions of monthly *P. falciparum* malaria prevalence simulated by the MAC (A), AM (B), WCT (C), and ABP (D) models, for the actual climatic conditions, for the period spanning from January, 1979 through December, 2009, and for 1-, 1-, 2-, and 0-month time lags, respectively. The following parameter ranges were assumed for the MAC model: b=[0.001;0.010] (10 values); HD=[11;26 days] (9 values); WN=[12;30 days] (10 values); α=[0.4;0.6] (11 values); υ=[0.5;4.0 days] (9 values); f_U=[36.5;37.1 °C-days] (7 values); l=[1;10 °C] (10 values); g_U=[7.7;9.9 °C] (12 values); x_p=[0.00;1.00] (12 values); and d=[fixed constant]. For the AM model (besides the set of parameters proposed for the MAC model): f_N=[111.0;204.4 °C-days] (11 values); g_N=[14.2;19.0 °C] (11 values); t_h=[5.5;16 days] (12 values); t_m=[8;30 days] (8 values); μ_1=[(1/(60*365));(1/(80*365)) days^{-1}] (5 values); μ_2=[(1/30);(1/11.2) days^{-1}] (5 values); and c=[unknown; fixed constant]. For the WCT model (besides the set of parameters proposed for the MAC and AM models): μ=[2,000;10,000] (10 values); C=[0.00;0.50] (7 values); β=[unknown; fixed constant]; x=[0.0;0.3] (7 values); h=[0.5;1.0] (6 values); k=[0.0;1.0] (10 values); v=[0.0;1.0] (10 values); r_{WCT}=[1/(666.66/30);1/(25.97/30) month^{-1}] (10 values); and λ=[unknown; fixed constant]. And for the ABP model (besides the set of parameters proposed for the MAC, AM and WCT models): δ_H=[fixed constant]; b_{ABP}=[0.01;0.50] (6 values); β_e=[0;10^{-4}] (12 values); σ_0=[0.00;0.10] (12 values); ρ=[0.00;1.00] (11 values); r_0=[0.00;0.01] (12 values); γ=[0.0475;0.1435] (11 values); ξ=[fixed constant]; η=[0.00;0.10] (12 values); ν=[0.2;1.0] (10 values); F=[fixed constant]; k_A=[0;3*103] (8 values); k_E=[0;0.3] (7 values); δ_0=[fixed constant]; c_{ABP}=[0.00;0.379] (9 values); x_{ABP}=[0;1] (12 values); and ΔT=[2.2;5.0°C] (8 values). Literature ranges are reported in Alonso et al., 2011; Charlwood et al., 1985; Collins and Jeffery, 1999; Detinova, 1962; Eichner et al., 2011; Ermert et al., 2011; Graves et al., 1990; Hii et al., 1990; Jepson et al., 1947; Kiszewski et al., 2004; Macdonald and Göckel, 1964; Magesa et al., 1991; Murphy et al., 1989; Mutero and Birley, 1987; Nikolaev, 1935; Schneider et al., 2005; Shute and Maryon, 1951; Sinden, 1983; and Worral et al. 2007.

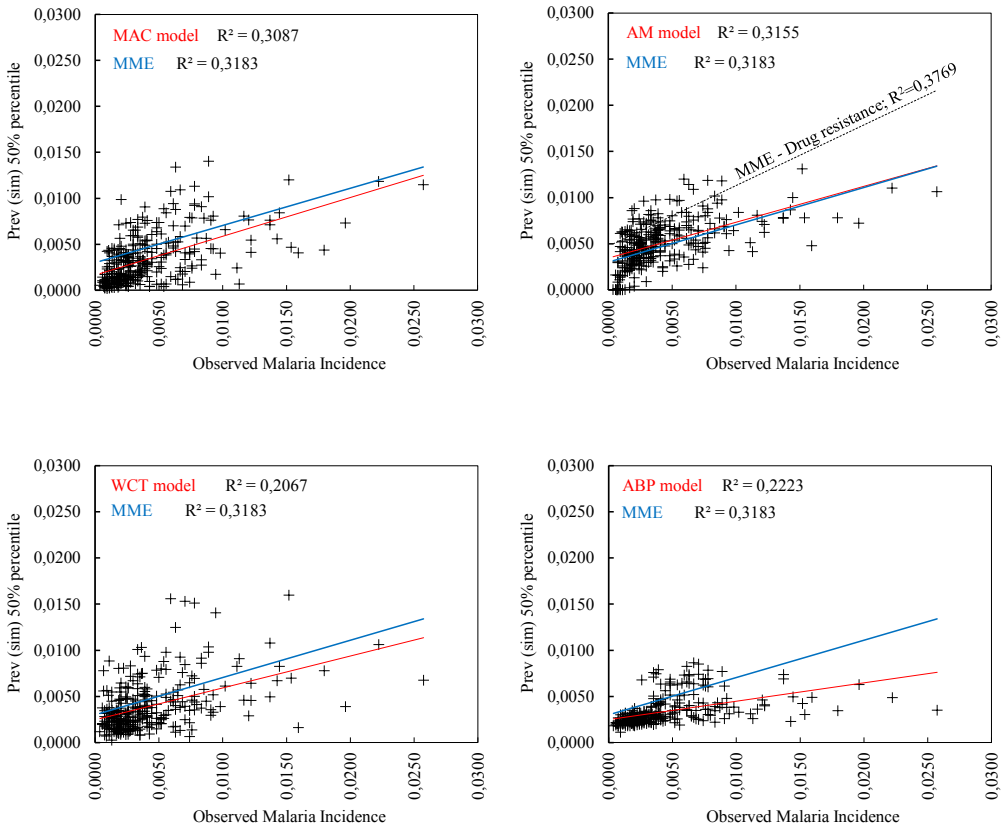

Figure 6(b). Monthly *Plasmodium falciparum* malaria incidence observed in Kericho District, Kenyan highlands, over the period spanning from January, 1979 through October, 2004 (x-axes) versus the 50% percentile of the distributions of monthly *P. falciparum* malaria prevalence (y-axes) simulated by the MAC (upper left panel), AM (upper right), WCT (lower left), and ABP (lower right) models, for the actual climatic conditions, for the period spanning from January, 1979 through December, 2009, and for 1-, 1-, 2-, and 0-month time lags, respectively. Red and blue solid lines represent the adjusted linear trends (see R^2-values on each panel) for each model and for the four-model ensemble (MME), respectively. Dashed black line in the upper right panel depicts the adjusted linear trend for the MME when nonlinear changes in the mean duration of host's infectivity to vectors are considered. Simulation runs for the quarters December-January-February, March-April-May, June-July-August, and September-October-November are presented in figures SM-5 (a-d) in the online supplementary material.

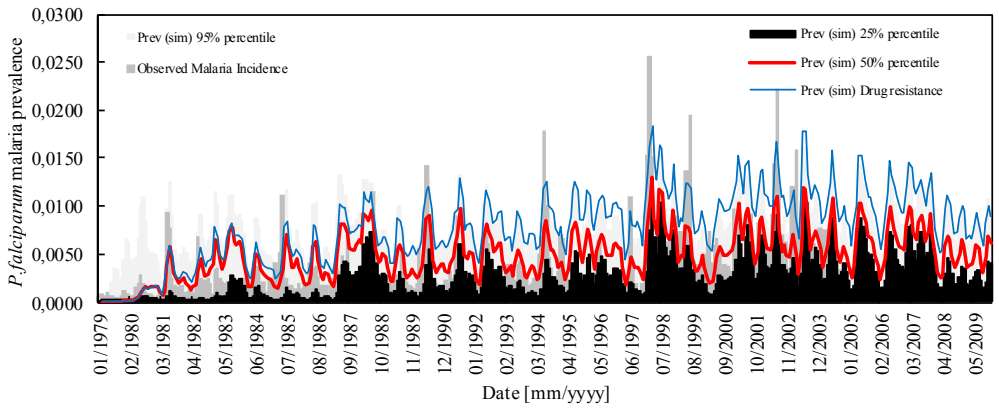

Figure 6(c). Monthly *Plasmodium falciparum* malaria incidence observed in Kericho District, Kenyan highlands, over the period spanning from January, 1979 through October, 2004 (grey solid bars), along with the 25%, 50% and 95% percentiles of the distributions of monthly *P. falciparum* malaria prevalence suggested by the multi-model ensemble for the actual climatic conditions and for the period spanning from January, 1979 through December, 2009. Simulations of the MAC, AM, WCT, and ABP models include 1-, 1-, 2-, and 0-month time lags, respectively. See also the monthly *P. falciparum* malaria prevalence suggested by the multi-model ensemble for nonlinear changes in the mean duration of host's infectivity to vectors (blue solid line). MME simulation runs for the quarters December-January-February, March-April-May, June-July-August, and September-October-November are presented in figures SM-5 (a-d) in the online supplementary material.

Chapter 5[14]

Implementation of malaria dynamical models in municipality-level Early Warning Systems in Colombia – Part I: description of study sites

Abstract

As part of the Integrated National Adaptation Pilot project and the Integrated Surveillance and Control System, the Colombian National Institute of Health is working on the design and implementation of a Malaria Early Warning System framework supported on seasonal forecasting capabilities, weather and environmental monitoring, and malaria statistical and dynamical models. In this article we provide an overview of the local eco-epidemiological settings where various malaria process-based mathematical models are currently being implemented at a municipal level. The description includes general characteristics (location and natural resources), malaria situation (predominant type of infection, malaria positive cases data, malaria incidence, and seasonality), entomological conditions (primary and secondary vectors, mosquito densities and feeding frequencies), climatic conditions (climatology and long-term

[14] Note: This chapter will be submitted to the American Journal of Tropical Medicine and Hygiene as:

Daniel Ruiz[1,2,3], Viviana Cerón[4], Adriana María Molina[1], Martha Lucía Quiñónes[5], Mónica Marcela Jiménez[6], Martha Ahumada[4], Patricia Gutiérrez[4], Salua Osorio[4], Gilma Mantilla[2], Stephen J. Connor[7], and Madeleine C. Thomson[2]

[1]Grupo 'Investigación en Gestión Ambiental – IGEA', Escuela de Ingeniería de Antioquia, Colombia
[2]International Research Institute for Climate and Society, Columbia University in the City of New York, USA
[3]Department of Earth and Environmental Sciences, Columbia University in the City of New York, USA
[4]Subdirección de Vigilancia y Control en Salud Pública, Instituto Nacional de Salud, Colombia
[5]Facultad de Medicina, Universidad Nacional de Colombia Sede Bogotá, Colombia
[6]Instituto Colombiano de Medicina Tropical, Universidad CES, Colombia
[7]School of Environmental Sciences, University of Liverpool, United Kingdom

trends), inferred stability of disease transmission, key drivers of epidemic outbreaks, and non-climatic factors (populations at risk, control campaigns and socioeconomic conditions). Selected pilot sites exhibit different eco-epidemiological settings that challenge the implementation of the integrated surveillance and control system.

Keywords: malaria-prone municipalities, malaria Early Warning System, malaria surveillance and control, Colombian eco-epidemiological conditions, climate and human health

5.1. Introduction

The malaria research community has stated that short-, medium- and long-term climate-based predictions should be merged with routine surveillance and control activities in order to better predict patterns of malaria risks in time and space, as well as to improve malaria epidemic early detection and response (World Health Organization, 2004, 2009 and 2010; Pan American Health Organization, 2006). As part of the Integrated National Adaptation Pilot project, the Colombian National Institute of Health – CNIH is working on the design and implementation of a proactive, collaborative, multidisciplinary, Integrated Surveillance and Control System – ISCS (Ruiz et al., 2008). The aim of this initiative is to improve risk assessments of malaria transmission in order to facilitate effective allocation of health resources and more cost-effective preventive responses. One of the key components of the ISCS is a Malaria Early Warning System Framework (Thomson and Connor, 2001; Poveda et al., 2001; Thomson et al., 2006; Ruiz et al., 2006; Poveda et al., 2008), in which the CNIH is proposing several mathematical models as a means to predict changes in the risk of malaria in specified populations. Dynamical

models, i.e. those that employ the established biological mechanisms of the transmission cycle of malaria parasites (Aron and May, 1982), are being used to integrate climatic variables with demographic, epidemiological, entomological, and non-climatic factors in order to simulate malaria transmission dynamics. This article provides a description of the local eco-epidemiological settings in Colombia where several malaria process-based mathematical models are currently being implemented. The main goal of our activities is to provide a framework for the implementation of dynamical models in routine activities of state and municipal health services, and in a more general sense, for strengthening the institutional capacity of the Colombian malaria surveillance and control program.

Colombia provides a perfect setting for the implementation of the ISCS given the following reasons: (i) *Plasmodium falciparum* and *P. vivax* malaria infections in Colombia, which are responsible for, respectively, 36% and 64% of the current national malaria burden, are still a major public health concern in the Americas as their official morbidity profiles account for almost 15% of the total primary cases observed in the region (Pan American Health Organization, 2006). A successful malaria surveillance and control campaign in a single country could thus have a significant regional-scale impact; (ii) even though nearly 85% of the Colombian rural territory has environmental conditions suitable for malaria transmission, only two states (from a total of thirty two states) concentrate 50% of malaria cases, and 75% of the national reported cases occur in only 44 municipalities (Mantilla et al., 2009). Malaria interventions could then be targeted at those localities hardest-hit by malaria infections in order to control the nationwide disease burden; (iii) malaria in Colombia experiences unstable/epidemic periods that have been strongly linked to the occurrence of the warm phase of El Niño-Southern Oscillation-ENSO, particularly in lowland regions along the Pacific and

Atlantic coasts (Bouma et al., 1997; Poveda and Rojas, 1997; Poveda et al., 2001; Gagnon et al., 2002; and Mantilla et al., 2009). ENSO-based predictions could then be used to predict high and low-risk years for malaria transmission with sufficient lead time to mobilize resources in order to reduce the impact of epidemics (Bouma et al., 1997); (iv) in its two official national communications to the United Nations Convention on Climate Change, the Colombian government has identified malaria as one of the two climate-sensitive diseases of primary concern. As a result of this political will an adaptation research and implementation agenda plan has already been proposed in response to the recommendations of the Intergovernmental Panel on Climate Change (World Bank, 2006); (v) in recent years a lot of resources has been invested in strengthening the solid institutional arrangements of the national, state and municipal health services, in an attempt to build the capacity for a routine evaluation of the spatio-temporal risk of malaria infections and the implementation of locally-adapted malaria control strategies (World Bank, 2006; Mejia, 2007). They include cooperative agreements, development projects and initiatives such as the Global Fund's Multi-Country Malaria Project – PAMAFRO, the Centro Latino-Americano de Investigación en Malaria – CLAIM and the Integrated National Adaptation Pilot project/Human Health Component, just to mention a few; and (vi) the steep increasing trend in the overall malaria morbidity that was observed over the period 1960-1998 is now showing a moderate decline (Mantilla et al., 2009). The overall malaria mortality, which reached about 130 to 150 deaths per year over the most recent decade, has also significantly decreased and the trend continues. All these characteristics, current patterns and timing could then bring elements for a successful case of malaria surveillance and control, and potential future elimination (Roll Back Malaria, 2008).

5.2. Study sites

Four malaria pilot sites distributed throughout the country (see figure 1) were selected through a multi-criteria analysis that considered, amongst others, the level of endemicity, primary and secondary mosquito vectors, sectorial and territorial decentralization, easy access, and political will. Even though these localities exhibit historical *hypoendemic* conditions according to world's malaria clinical endemicity profiles (Bruce-Chwatt, 1980), they are the municipalities with the highest morbidity and transmission levels in Colombia. They include the municipalities of Montelibano and Puerto Libertador, both located in the Department of Cordoba, on the Colombian Caribbean Coast, and whose surface areas reach 1,900 and 2,060 km^2, respectively; the municipality of San José del Guaviare, in the Department of Guaviare, located in a transition region between the Colombian grassland plains to the northeast and the tropical rainforests of the Amazon to the south. San José has a total area of about 16,200 km^2, of which 84% is an indigenous reserve and protected forest. Also selected was the municipality of Buenaventura, the most important maritime port on the Colombian Pacific Coast, located in the Department of Valle del Cauca, and whose total area reaches 6,297 km^2. The Pacific Coast, an area of about 72,000 km^2 and with almost 2.2 million inhabitants, is amongst the Colombian regions with the highest transmission rates; 51% of *P. falciparum* infections are reported in this region. All these pilot sites are located at altitudes below 200 m above sea level and have historical mean annual temperatures in the range from 27 to 28°C. Their main natural resources include numerous water sources, highly diverse flora and fauna, vast savannahs, and gold, silver, platinum, coal, manganese, and copper reserves, as well as various pristine rainforests protected by law in several natural parks.

5.3. Data

Malaria, entomological, climatic, and socio-economic data were gathered to characterize the malaria situation in each of the pilot sites. Data included predominant type of infection, malaria positive cases, primary and secondary vectors, mosquito densities and feeding frequencies, rainfall, temperature and relative humidity data from appropriate meteorological stations, populations at risk along with information on interventions reducing adult biting rates and larval breeding sites, as well as social and economic factors in each of the study sites. A brief description of the datasets used is presented below.

5.3.1. Malaria positive cases data

Colombia has experienced various major institutional health system regimes over the past five decades (Kroeger et al., 2002; Valero, 2006; Mantilla et al., 2009). Initially, an institutional program running independently, the so-called Malaria Eradication Service (MES), was in charge of malaria surveillance and control activities until 1974. From that year up to 1992, the Colombian government carried on surveillance activities through the Ministry of Health, whose arrangement followed the MES' framework and approach, and whose control campaigns were conducted on the ground through the so-called Direct Campaign Special Units. In 1993, the Colombian health sector changed again to function under a thoroughly reformed National Health Care System. The change included the decentralization of decision-making processes and required that each state and/or municipality was in charge of responding with control and intervention measures for any health issue, including malaria. More recently, in the early 2000s, malaria surveillance activities were in charge of the CNIH through a passive Public Health

Surveillance System, the so-called SIVIGILA. Currently, malaria surveillance programs are based on blood tests conducted at both private clinics and public health facilities, and they do not include clinical follow-up of positive cases. In summary, surveillance activities in Colombia have shifted from state collective notification to locality-level individual report. All these changes in malaria control policy and institutional arrangements play a role in changes in malaria morbidity profiles observed over the available long-term historical period 1960-to present (see figure 1 in Mantilla et al., 2009).

In order to consider a single source of malaria cases data, *Plasmodium falciparum* and *P. vivax* malaria morbidity profiles reported by SIVIGILA over a 540-epidemiological week (EW) period, spanning from the first EW of 2000 through the eighteenth EW of 2010, were processed for each of the malaria pilot sites. Case data are available as single data points for each EW, for each age class, and for each pilot site. See figures SM-I-1 and SM-I-2 in the online supplementary material – Part I for aggregated data. There is no information available, up to date, on the proportion of cases reporting at health facilities and changes in the reporting rate may result in differences between sites as well as changes in observed cases over time. Between 9 and 19% of the total number of epidemiological weeks are ‘blanks’ (either missing or null records) in the provided datasets. Also, historical data exhibit strong changes in the mean and various inconsistent records, particularly in the datasets of the municipalities of Puerto Libertador and San José del Guaviare.

5.3.2. Entomological data

The variables required for an in-depth understanding of local entomological conditions, such as mosquito density, natality, survivorship, feeding frequency, infectivity, and susceptibility (see the summary of exogenous variables in Ruiz et al., 2011), were gathered from a number of sources including the literature, field collections and via laboratory experiments. The international literature search (e.g. Bruce-Chwatt, 1980; Garrett-Jones, 1964) resulted in the quantification of several mosquito exogenous variables, such as the rate of oviposition, the natural and induced (for instance, by insecticides) mortality rates, and the human blood index, just to mention a few. Local literature search lead to the analysis of secondary information, previously documented by the Malaria Eradication Service of the former Colombian Ministry of Health (SEM, 1957) and published papers (e.g. Olano et al., 2001), on the nationwide presence of *Anopheles* mosquito species. See figure 1. In addition, a series of field entomological collections were conducted over the period 2008-2011 at the different pilot sites which resulted in the collection of over 5,040 adult female mosquitoes and the analysis of primary and secondary vectors incriminated in malaria transmission locally, as well as in preliminary estimates of mosquito densities (detailed information is presented in Ruiz et al., 2011). And lastly, experiments conducted under controlled laboratory conditions with over 1,240 adult female mosquitoes resulted in the assessment of *Anopheles darlingi* feeding frequencies. See figure 2. It is worth noting that this is one of the first set of experiments designed to estimate the feeding frequency of this *Anopheles* species. We were unable to get satisfactory information on some exogenous variables such as vector resistance against insecticides, seasonality of local breeding sites, and mosquito feeding and resting habits.

5.3.3. Climate data

Historical records of daily minimum, mean and maximum temperatures, total daily rainfall, and mean daily relative humidity, provided by the Colombian Institute of Hydrology, Meteorology and Environmental Studies (IDEAM) through the CNIH, were processed for each of the pilot sites. One nearby weather station per municipality, chosen amongst moderately dense hydrometeorological networks, was selected for the analysis (see table 1). Criteria included records availability, observational time periods, and quality and homogeneity of historical records. Selected weather stations are manually-operated and have long, although discontinuous (on a daily timescale, climate variables have numerous missing records), historical climatic datasets. The longest historical time period spans back almost 65 years (January, 1946-October, 2010), whereas the shortest dataset covers the period December, 1982 through December, 2009. A detailed description of these datasets can be found in Ruiz et al. (2011).

5.3.4. Non-climatic factors

The characterization of non-climatic factors followed the structure proposed in the summary of exogenous variables discussed by Ruiz et al. (2011). Hence, for a partial level of understanding of malaria transmission, non-climatic exogenous variables included: (i) the total human populations at risk (only rural communities) and their population growth rates, all based on previous demographic census and projections published online at http://www.dane.gov.co/ by the Colombian National Administrative Department of Statistics (DANE); (ii) the descriptions of spray programs, activities blocking adult female-human host interactions, activities controlling immature mosquitoes, and environmental interventions, all based on reports of intervention

campaigns conducted by state and municipal health services (e.g. Cordoba State Health Service, 2007); and (iii) the description of socioeconomic conditions prevailing in the communities at risk, particularly economic quantitative variables, cultural quantitative factors and cultural qualitative potential drivers, taking into account 39 non-published local reports and datasets provided (physically or digitally) by the state health services: 13 files in total for the municipalities of Montelibano and Puerto Libertador; and 15 and 11 files for the municipalities of San José del Guaviare and Buenaventura, respectively.

5.4. Methodology

Plasmodium falciparum and *P. vivax* malaria positive cases were aggregated to obtain data points for each epidemiological period – EP, which comprises four epidemiological weeks, and for each municipality. Malaria incidence per EP and per type of infection were calculated with the historical total human populations at risk, and then compared to the annual cycles of climatic variables as discussed below. In order to define primary and secondary vectors in each malaria pilot site, maps of historical spatial distributions (presence/absence) of *Anopheles albimanus*, *An. darlingi*, *An. nuneztovari*, *An. punctimacula*, *An. pseudopunctipennis*, *An. neivai*, and *An. lepidotus* in Colombia were generated on a Geographic Information System platform. See figure 1. To confirm primary vector species at a local level, adult mosquitoes were collected in the study sites through the Human Landing Capture technique. Mosquito species were identified by morphological characteristics, except *An. nuneztovari*, *An. oswaldoi* and *An. rangeli* mosquitoes which were identified by the polymerase chain reaction-restriction fragment length polymorphism (PCR-RFLP) assay. Indoor and outdoor mosquito densities were estimated

through human biting rates (HBRs) assessed in the pilot sites during dry and wet seasons. Field activities did not include tests to assess mosquitoes' blood preference (anthropophilic versus zoophilic mosquitoes). Lastly, the duration of the gonotrophic cycle of *Anopheles darlingi* mosquitoes was estimated at the Entomology Laboratory of the CNIH, under controlled temperatures of 24, 27 and 30°C, controlled relative humidity above 80%, and a constant 12-hour photoperiod. See figure 2.

Climatic records were organized in Microsoft Office Excel 2007® spreadsheets and shared with municipal health authorities, and were also posted on the Data Library of the International Research Institute for Climate and Society (http://iridl.ldeo.columbia.edu/index.html). Kandel-Last (Last and Kandel, 2001), Grubbs' (Grubbs, 1969) and normal range statistical tests were initially implemented to detect inconsistencies and anomalous records in daily minimum, mean and maximum temperatures. Outlying observations, i.e. those that were not reflecting the very nature of the climatic variable, were expunged from climatic datasets before calculating monthly values (see caption in table 1). Annual cycles of temperature, rainfall and relative humidity were then calculated and compared to the historical annual distributions of malaria incidence. See figure 3 and discussion below. Mean annual values of temperature and relative humidity, total annual rainfall amounts, and their confidence intervals for a 95% confidence level were also calculated. Exploratory analysis, including time series and box plots, were performed to detect changes in the mean, changes in the variance and long-term linear trends in annual (free of seasonality) historical time series (see table 1). The T-test for detection of linear trends and the Hotelling-Pabst, Mann-Kendall and Sen hypothesis tests were applied to assess the statistical significance (α=0.05) of observed long-term linear trends. Slope parameters, calculated by the method of least squares, were determined for

those historical time series showing statistically significant trends in the mean and were used to define future medium-term changing climate scenarios. Upper and lower confidence limits were also assessed for the simple linear regression models.

In order to quantify cultural quantitative and qualitative non-climatic factors, an analysis of critical conditions was performed at a local level for specific counties within three of the pilot sites: the counties of No Hay Como Dios and Alcides Fernandez in Montelibano; the county of Juan José in the municipality of Puerto Libertador; and the counties of Citronela and Zacarias in Buenaventura. See figure 4. This criticality analysis, to be presented in depth in a forthcoming publication, was conducted using structured surveys applied to a representative sample of households in each area. Non-climatic factors were grouped into six representative groups (see black solid bars in figure 4, plotted on the left y-axis): (I) variables related to the level of immunity of human populations, such as previous malaria infections, people under age of five and pregnancy; (II) those related to the risk of contact between mosquito populations and human hosts: age, gender, occupation, walls (if present) in household and their material, ceiling (if present) and its material, windows and screens, doors and screens, crop type, sanitary services and their location; (III) variables related to local installed capacity: participation in malaria control programs, and education level of head of household; (IV) variables representative of disease knowledge, attitudes, customs, practices and beliefs, in particular those related to malaria symptoms, malaria treatment, infection with malaria parasites, auto-medication, self-protection, mosquitoes breeding sites, timing of malaria outbreaks, communication and education; (V) those describing the access to health services: health insurance and access to malaria treatment; and (VI) variables related to interventions: bed net use and spraying frequency.

Lastly, in order to ground the effort at the scale of actual decision making, an assessment of local capacity in state health authorities (to implement malaria dynamical models) was initially conducted. See figure 5. The assessment included six workforce-related aspects such as entomological surveillance, epidemiological surveillance, vector-borne diseases coordination, decision-making planning, social expertise, and collaborative/cooperative efforts, as well as six installed/available tools-related aspects: continuous AC power supply, computer access, Internet access, text editor software, at least Microsoft Office Excel 2007, and simulation software such as Powersim Constructor Version 2.51® or Powersim Studio 8 Academic®. Various in-person and online workshops on the development and implementation of dynamical models were then held at state and municipal health services. Concepts of general systems theory, process-based (biological) modeling, malaria dynamical modeling, experimentation-validation-analysis processes, and malaria integrated surveillance and control activities were discussed with public health and tropical medicine experts. Lectures were supported on a recently created online course entitled 'Simulating Malaria Transmission Dynamics-SMTD' (http://saber.eia.edu.co/eiadigital/), which now includes two major sessions: a six-module conceptual session and a five-module practical simulation experiment.

5.5. Results

5.5.1. Total primary cases, malaria incidence and seasonality

Primary cases. Total *Plasmodium falciparum* and *P. vivax* malaria primary cases observed in the pilot sites over the historical period 2000-2010 are presented in table 2 and figures SM-I-1 and SM-I-2 in the online supplementary material. In average, the total number of

P. falciparum malaria infections reported annually ranged from 700 positive cases in San José del Guaviare to almost 1,800 cases in the municipalities of Montelibano and Buenaventura. *P. vivax* malaria infections reached, in turn, average annual values in the range from 1,200 positive cases in San José del Guaviare to almost 4,000 primary cases in Montelibano and Puerto Libertador. A maximum number of about 730 cases per epidemiological period of *P. falciparum* malaria were reported in Buenaventura in 2004, whereas over 950 positive cases of *P. vivax* malaria were observed in Puerto Libertador in 2007. Available malaria records (not shown here) also suggest that infections tend to affect people in the 15 to 44 age group.

Malaria incidence and seasonality. *P. falciparum* and *P. vivax* malaria incidence and seasonality for each of the pilot sites are presented in figure 3. *P. falciparum* malaria in the municipality of Montelibano (not the predominant type of infection) reaches an average incidence of 4 positive cases per 1,000 inhabitants and shows to be stable all year round (incidence ranges from 3 to 6 positive cases per 1,000 inhabitants). *P. vivax* malaria, the predominant infection, reaches an average incidence of 15 positive cases per 1,000 inhabitants and also shows to be stable all year round. In the municipality of Puerto Libertador, located in the same region, *P. falciparum* malaria incidence reaches 4 positive cases per 1,000 inhabitants and shows peaks in the months of February and June of 6 and 8 positive cases, respectively. *P. vivax* malaria reaches, in turn, almost 17 positive cases but shows a bimodal intraannual distribution with minimum and maximum values of about 7 and 23 positive cases in December and July, respectively. Mean temperatures in these two pilot sites and their surroundings are favorable for both mosquito survival and the successful incubation of malaria parasites (i.e. >21.5°C) all year round. Monthly rainfall is suitable for breeding sites productivity (i.e. >100 mm/month) only over the period April through November.

Comparisons of malaria incidence with intraannual cycles of climatic variables suggest that, in the municipality of Montelibano, *P. falciparum* and *P. vivax* malaria incidence follow, although not that closely, the annual cycle of mean temperature. *P. vivax* infection, in particular, exhibits a peak in its incidence over the period December through March when rainfall amounts are limited. In Puerto Libertador, both malaria infections seem to respond to a combination (or synergistic effects) of rainfall and temperature: in February and March, when rainfall is limited (i.e. monthly values in the range from 100 to 300 mm), increases in mean temperature seem to drive the increases in malaria incidence. In June-July-August, when temperatures reach lower values, increases in monthly rainfall amounts could favor the increase in vector densities and hence in malaria incidence.

In the municipality of San José del Guaviare, *P. falciparum* malaria (not the predominant type of infection, see figure 3) reaches an average incidence of 3 positive cases per 1,000 inhabitants, with a peak of 5 cases in May. The predominant infection, *P. vivax*, shows an average incidence of almost 5 positive cases and a unimodal distribution with a peak in May of about 9 positive cases. The mean temperature is favorable all year round and monthly rainfall shows to be suitable only over the period March through December. Historical *P. vivax* and *P. falciparum* malaria incidence follow the annual cycle of rainfall: for total monthly rainfall in the range [0-200 mm], *P. falciparum* and *P. vivax* malaria infections exhibit average incidence of 2 and 3 to 4 positive cases per 1,000 inhabitants, respectively. For amounts greater than 200 mm per month, *P. falciparum* malaria increases at a rate of 0.7 to 1 positive cases per 1,000 inhabitants per 100 mm increase in rainfall. *P. vivax* malaria increases, in turn, at a rate of 1 primary case per 1,000 inhabitants per 100 mm increase in rainfall.

Lastly, in municipality of Buenaventura *P. falciparum* malaria has been the critical burden. See figure 3. It exhibits a unimodal distribution with an average incidence of 4 positive cases and a peak of 7 positive cases in April. *P. vivax* malaria incidence is also unimodal, has an average value of 3 positive cases and a peak of 5 positive cases is usually reached in April. Even though both mean temperature and monthly rainfall in this locality are favorable all year round, *P. vivax* and *P. falciparum* malaria incidence mainly follow the annual cycle of temperature: their incidence increase at rates of about +5.6 and +3.8 positive cases per 1,000 inhabitants per 1°C increase in mean monthly temperature, respectively.

5.5.2. Vector species, mosquito densities and feeding frequencies

Vector species incriminated in malaria transmission. Fifteen (15) species in total were identified in the study sites, including *Anopheles albimanus*, *An. darlingi*, *An. nuneztovari*, *An. punctimacula*, *An. pseudopunctipennis*, *An. neivai*, *An. lepidotus*, *An. oswaldoi*, *An. rangeli*, *An. marajoara* (or *An. albitarsis*), and *An. neomaculipalpus* species. Species collected in Montelibano included *An. nuneztovari* (87.8% of the total number of collected mosquitoes), *An. rangeli* (8.4%) and *An. darlingi* (3.3%); in Puerto Libertador, mosquito species included *An. nuneztovari* (72.7%), *An. darlingi* (15.7%) and *An. rangeli* (10.8%); in San José del Guaviare, *An. marajoara* (45.6%), *An. braziliensis* (19.2%), *An. oswaldoi* (18.1%), and *An. darlingi* (15.0%); lastly, in Buenaventura 99.5% of the total number of collected mosquitoes were *An. nuneztovari* species. These proportions are consistent with previous mosquito collection campaigns conducted by municipal and state health services (e.g. Cordoba State Health Service, 2007), except for the case of Buenaventura, where *An. albimanus* has been frequently

incriminated in malaria transmission (Quiñones et al., 1987; Olano et al., 1997). For the sake of representing malaria transmission dynamics in Montelibano, Puerto Libertador and San José del Guaviare, an anthropophilic mosquito vector (e.g. *An. darlingi*) is assumed to be incriminated in local transmission, whereas in the municipality of Buenaventura a zoophilic vector (e.g. *An. albimanus* or *An. nuneztovari*) is considered to be responsible of malaria infections.

Vector densities. In the municipalities of Montelibano and Puerto Libertador, *An. darlingi* showed almost constant (throughout the sampling period) HBRs ranging from 0.3 to 2.4 mosquitoes per human host per night. In San José del Guaviare, this *Anopheles* species reached HBRs of about 1.6 to 8.6 mosquitoes per human host per night primarily during the wet seasons of the sampling period. *An. nuneztovari* showed, in turn, very high HBRs ranging from 28 to almost 72 mosquitoes per human host per night in Montelibano and Puerto Libertador, and from 21 to 66 mosquitoes per host per night in the municipality of Buenaventura, primarily during dry seasons. Roughly speaking, a significant difference between indoor and outdoor mosquito densities was not observed in the selected pilot sites.

Feeding frequency. Experiments conducted under controlled laboratory conditions suggest that the anthropophilic *An. darlingi* feeds on humans every 5.0 and 3.7 days at ambient temperatures of 24 and 30°C, respectively. See figure 2. Previous studies also conducted in Colombia (Rúa et al., 2005) suggest that *An. albimanus* mosquitoes have less anthropophilic habits but more frequent blood meals: every 3.6 and 2.8 days at temperatures of 24 and 30°C, respectively. In order to reflect these inferred feeding intervals, the total number of degree-days required for the digestion of a portion of ingested blood and the minimum temperature required for the digestion of a blood meal were then set to 67°C-day and 11°C for *An. darlingi*, and 53°C-day and 10°C for *An. albimanus*.

5.5.3. Annual values of climate variables, climatology and long-term trends

Annual values and climatology. In the surroundings of the municipalities of Montelibano and Puerto Libertador, rainfall records reach an historical average annual value of 2,383 ± 160.5 mm (β=95%) and exhibit an unimodal intraannual distribution with a peak of 350 mm in August and a minimum value of about 20 mm in January. Historical rainfall does not exceed 70 mm per month over the dry period December-January-February (DJF). See figure 3. Mean temperatures reach, in turn, an average annual value of 27.2 ± 0.2 °C (β=95%), maxima of 27.5°C in March and April, and minima of about 27.0°C during the period September-October-November. In the municipality of San José del Guaviare, rainfall records reach an historical average annual value of 2,796 ± 151 mm (β=95%) and also exhibit an unimodal intraannual distribution but with a peak of 380 mm in May and a minimum value of about 70 mm in January. Over the period DJF rainfall records do not exceed 125 mm per month. Mean temperature reaches an average annual value of 25.3 ± 0.2 °C (β=95%), with maximum and minimum values of about 26.5 and 24.1°C in February and July, respectively. Lastly, in the municipality of Buenaventura the historical average annual rainfall reaches 6,532 ± 248 mm (β=95%) and its annual cycle is bimodal with two peaks commonly occurring in the months of May (630 mm) and October (820 mm). The long 'dry season' is usually observed during the trimester January-February-March, when monthly rainfall amounts do not exceed 400 mm per month. Mean temperatures in this locality reach average annual values of about 26.0 ± 0.2 °C (β=95%), with maximum and minimum values of about 26.4 and 25.7°C in April and November, respectively.

Long-term trends. Annual rainfall amounts and annual minimum temperatures observed in the surroundings of the pilot sites of Montelibano and Puerto Libertador increased at rates of approximately +7.0% and +0.2°C per decade over the periods 1973-2008 and 1978-2008, respectively. In the municipality of San José del Guaviare, annual minimum temperatures increased at a rate of +0.4°C per decade over the period 1982-2007. In the area of the municipality of Buenaventura, rainfall also increased over the past 40 years but at a lower rate of +3.4% per decade. The rest of the historical time series did not exhibit increasing/decreasing statistically significant long-term trends.

5.5.4. Non-climatic factors

Total human populations at risk and growth rates. The total number of inhabitants living in the selected malaria pilot sites as of 2008 reached values in the range from 38,700 individuals in Puerto Libertador to almost 349,000 people in Buenaventura. Their estimated total populations at risk, i.e. people living in rural areas, were of about 23,800 and 35,300 inhabitants, respectively (see figure 1). Population growth rates over the period 2000-2010 ranged from 23 newborns per 1,000 inhabitants per year in Montelibano and San José del Guaviare, to almost 39 new susceptible individuals per year in Puerto Libertador. Information on differential (disease-induced) mortality rates or case-fatality rates and individual (economic-driven) migration patterns are not available. Massive forced (displaced) human migrations recently increased the total number of inhabitants in Montelibano and San José del Guaviare by almost 16 and 4%, respectively. That information is, however, limited to the period 2007-2008, despite the multiple

coerced displacements (particularly in those two pilot areas) that have characterized the Colombian conflict over recent decades.

Control campaigns. Vector control activities such as annual Indoor Residual Spraying (IRS) campaigns, blocking and screening programs, and breeding site control were available for just a few interventions. According to municipal health authorities, in the municipalities of Montelibano and Puerto Libertador the highest percentage coverage achieved by K-OTRINE SC-50 IRS campaigns reached 2.7% over the period 2005-2008. The distribution of long lasting insecticide (K-OTAB)-treated bed nets has, in turn, achieved 47% of the total populations at risk in these pilot sites. Lastly, a maximum percentage of 78.6% of productive breeding sites was intervened (e.g. with *Bacillus sphaericus* and *Bacillus thuringiensis* bacteria) over the period 2007-2008. In the municipality of San José del Guaviare, the highest percentage coverage achieved by IRS campaigns reached 3.2% of the total population at risk in 2007, and the distribution of long lasting insecticide-treated bed nets reached a maximum coverage of 11% in 2008. As for intervened breeding sites in this municipality, information is only limited to the product used in control campaigns (i.e. there is no information on achieved coverage). Lastly, in the municipality of Buenaventura, the highest percentage coverage achieved by IRS campaigns reached 1.8% and 1.9% of the total population at risk in 2008 and 2009, respectively, and the distribution of long lasting insecticide-treated bed nets reached 0.1% and 1.2% in 2006 and 2009, respectively. Similar to the case of San José del Guaviare, there is no information on intervened productive breeding sites in Buenaventura.

Socioeconomic conditions. Information on economic variables, such as access to municipal and state health services, coverage of malaria treatment, living conditions, and employment, is very limited. It can be argued, however, that despite the fact that numerous

economic activities are conducted in these municipalities, such as agriculture, fisheries, gold and coal mining, cattle grazing, handcrafting and even ecotourism, human populations in rural areas have unsatisfied basic needs that reach 72.0% in Montelibano and Puerto Libertador, 77.4% in San José del Guaviare, and 47.5% in Buenaventura. Public services such as water and energy distribution networks, sewage systems, landfills, primary and secondary schools, and hospitals have also very low coverage levels or are even absent in their rural areas, as observed in many places throughout rural Colombia. Lastly, information on institutional arrangements, political and public interests, and social organizations or non-institutional arrangements is not available.

Information on cultural quantitative and qualitative factors is also very scarce, disperse and non-homogeneous in the selected pilot sites. Based on the analysis of the proposed household samples in the municipalities of Montelibano, Puerto Libertador and Buenaventura, it can be argued that non-climatic factors related to the level of immunity of human populations, disease knowledge, access to health services, and malaria interventions lie in the very-low to low intervals of the proposed levels of criticality. See figure 4. Non-climatic factors describing the risk of contact between mosquito populations and human hosts, and the local installed capacity in, particularly, the municipalities of Montelibano and Puerto Libertador, lie in the moderate to high intervals of the proposed levels of criticality, and could be the socioeconomic drivers behind the low to moderate prevalence of *Plasmodium vivax* malaria in their populations at risk (see shaded bars and confidence intervals in figure 4, plotted on the right y-axis).

Local capacity of health authorities. Currently, state and municipal health authorities have moderate to high workforce levels (from 4 to 5 points in a desired 6-level scale) for the implementation of malaria dynamical models. See figure 4. Their installed technological capacities range, in turn, from 2.5 points in San José del Guaviare to 5 point at the CNIH. In

general, their major constraints include the lack of expertise in social aspects, restricted knowledge in decision-making approaches and tools, limited collaborative and cooperative efforts, and unavailable simulation platforms.

5.6. Discussion and conclusions

This article described the local climatic, demographic, entomological and socioeconomic settings of four *hypoendemic* malaria-prone municipalities where malaria process-based mathematical models are currently being implemented as part of the activities of the Colombian Integrated Surveillance and Control System (ISCS). The selected malaria pilot sites exhibit different eco-epidemiological settings, particularly cultural diversity and socioeconomic conditions, that challenge the implementation of not only the ISCS but many other initiatives. Two of the sites also have displaced populations due to the armed conflict that make the characterization of their eco-epidemiological profiles particularly difficult. The health services of all malaria pilot sites show, however, favorable workforce and technological conditions that could allow a successful implementation of malaria dynamical models in their routine activities at the municipality level.

A qualitative index was explored by the research group to assess the level of understanding (low, moderate or good) of local epidemiological settings, taking into account the different determinants of malaria transmission. Roughly speaking, research activities provided our group with moderate to high levels of understanding of the malaria situation of malaria pilot sites, as well as their entomological and climatic conditions. In particular, our first set of experiments conducted under controlled laboratory conditions resulted in the assessment of the

gonotrophic cycle length of *Anopheles darlingi* mosquitoes, filling gaps in the Colombian entomological records. Along with previous assessments for *An. albimanus* (Rúa et al., 2005 and 2006), state health services now have good estimates of the feeding frequencies of the two Colombian primary vectors. Research activities also provided our group with a better understanding (although is still limited) of the non-climatic factors of malaria pilot sites. In particular, non-climatic variables describing spray programs, activities blocking adult female-human host interactions, and activities controlling immature mosquitoes, lack continuous and homogenous records over the available observational period of malaria cases or are limited to only a few set of interventions. We suggest that these gaps, along with the detected missing data, inconsistent records and strong changes in the historical time series of malaria primary cases, need to be reviewed before assessing the skill levels of process-based malaria mathematical models. Also, we suggest that current state and municipal epidemiological surveillance systems should be improved in order to collect information on malaria interventions, socioeconomic factors and primary cases systemically, routinely and confidently.

Malaria is a highly complex multi-factorial disease whose relationship to constantly changing, internal and external entomological, climatic and socioeconomic drivers varies according to local eco-epidemiological settings. In order to understand such a complexity, several malaria process-based models have been proposed by the scientific community and are currently available to public health decision-makers. Models can provide numerous advantages to understand the underlying processes and factors that drive the malaria transmission cycle and can also offer useful information on the role of current surveillance activities (Roll Back Malaria, 2010). In this context, we believe that malaria transmission mathematical models could play a significant role in effectively guiding municipal and state decision-makers and health

practitioners in improved risk assessments, malaria control investments and choice of environmentally-sound interventions. The practical implementation of such models in operational surveillance is presented in the second part of this study, where preliminary results using observed weather and seasonal climate forecasts are discussed in detail.

Acknowledgments

The authors would like to thank the Instituto Nacional de Salud de Colombia (INS), the Departamento Administrativo de Salud de Guaviare, the Laboratorio de Salud Pública de Córdoba, the Laboratorio de Salud Pública del Valle, and the Instituto de Hidrología, Meteorología y Estudios Ambientales (IDEAM) for all their support throughout the project. We also acknowledge the participation and support of research assistants Maria Elena Gutiérrez, Paula Andrea Zapata, Catalina López, and Adelaida Londoño, and the helpful suggestions made by Hugo Oliveros (International Research Institute for Climate and Society) and three anonymous peer-reviewers who read and commented this manuscript. Analyses conducted here have been funded by Conservation International Colombia, as part of the Integrated National Adaptation Pilot project. Daniel Ruiz has been partially funded by the Unidad Académica Civil, Ambiental e Industrial – Escuela de Ingeniería de Antioquia, the International Research Institute for Climate and Society (IRI) and the Department of Earth and Environmental Sciences, Columbia University in the City of New York (USA).

Authors' detailed addresses:

[1] Grupo 'Investigación en Gestión Ambiental – IGEA', Unidad Académica Civil, Ambiental e Industrial, Escuela de Ingeniería de Antioquia (www.eia.edu.co), km 02+000 Vía al Aeropuerto José María Córdova, Municipio de Envigado, Antioquia, Colombia. Phone number: +57(4) 354-9090; Fax number: +57(4) 331-7851; E-mails: pfcarlos@eia.edu.co and pfamolina@eia.edu.co

[2] International Research Institute for Climate and Society (http://portal.iri.columbia.edu), Lamont-Doherty Earth Observatory, Columbia University in the City of New York, 61 Route 9W - PO Box 1000, Palisades, NY 10964-8000, USA. Phone number: +1(845) 680-4465; Fax number:+1(845) 680-4864; E-mails: pfcarlos@iri.columbia.edu, mthomson@iri.columbia.edu, sjconnor@iri.columbia.edu, and mantilla@iri.columbia.edu

[3] Department of Earth and Environmental Sciences, Columbia University in the City of New York, 1200 Amsterdam Avenue, 556-7 Schermerhorn Extension, New York, NY 10027, USA.

[4] Subdirección de Vigilancia y Control en Salud Pública, Instituto Nacional de Salud, Avenida Calle 26 No. 51-20, Zona 6 CAN, Bogotá, D.C., Colombia. Phone number: +57(1) 220-7700; Fax number: +57(1) 220-0901; E-mails: vceron@ins.gov.co, mahumada@ins.gov.co, pgutierrezduenas@gmail.com, and sosorio@ins.gov.co

[5] Facultad de Medicina, Universidad Nacional de Colombia Sede Bogotá, Carrera 30 No 45-03, Edificio 471, Ciudad Universitaria, Bogotá D.C., Colombia. Phone number: +57(1) 316-5000 ext. 15136; E-mail: mlquinonesp@unal.edu.co

[6] Instituto Colombiano de Medicina Tropical, Universidad CES, Calle 10 A No. 22 – 04, Medellín, Colombia. Phone number: +57(4) 444-0555; E-mail: mmjimenez@ces.edu.co

[7] School of Environmental Sciences, University of Liverpool, Liverpool L69 3BX, United Kingdom, E-mail: sjconnor@liv.ac.uk

Shipping address for reprints:

Escuela de Ingeniería de Antioquia, km 02+000 Vía al Aeropuerto José María Córdova, Municipio de Envigado, Antioquia, Colombia. Phone number: +57(4) 354-9090; Fax number: +57(4) 331-7851

References

Bouma, M,J., G. Poveda, W. Rojas, D. Chavasse, M. Quiñones, J. Cox, and J. Patz, 1997. Predicting high risk years for malaria in Colombia using parameter of El Niño Southern Oscillation. Tropical Medicine and International Health 2(12): 1122-1227.

Bruce-Chwatt, L.J., 1980. Essential malariology. London: Heinemann.

Cordoba State Health Service, 2007. Informe de acciones desarrolladas por el Grupo de Entomología del Laboratorio Departamental de Salud Pública, Departamento de Córdoba. 30 pages.

Gagnon, A., K. Smoyer-Tomic and A. Bush, 2002. The El Niño-Southern Oscillation and malaria epidemics in South America. Int J Biometeorol 46: 81-89.

Garrett-Jones, C., 1964. The human blood index of malaria vectors in relation to epidemiological assessment. Bulletin of the World Health Organization 30: 241–261.

Grubbs, F., 1969. Procedures for detecting outlying observations in samples, Technometrics 11(1): 1-21.

Kroeger, A., J. Ordoñez-Gonzalez, and A.I. Aviña, 2002. Malaria control reinvented: health sector reform and strategy development in Colombia. Tropical Medicine and International Health 7(5): 450–458.

Last, M. and A. Kandel, 2001. Automated detection of outliers in real-world data. Proceedings of the 2nd International Conference on Intelligent Technologies 2001.

Mantilla, G., H. Oliveros, and A. Barnston, 2009. The role of ENSO in understanding changes in Colombian's annual malaria burden by region, 1960-2006. Malaria Journal 2009, 8:6.

Mejia, L.E., 2007. Adapting to the impacts of climate change on health via the Integrated National Adaptation Project. Environment Matters - Annual Review 2007: 12-13.

Olano, V.A., G. Carrasquilla, and F. Méndez, 1997. Transmisión de la malaria urbana en Buenaventura, Colombia: aspectos entomológicos. Revista Panamericana Salud Pública 1: 287.

Olano, V.A., H.L. Brochero, R. Sáenz, M.L. Quiñones, and J.A. Molina, 2001. Mapas preliminares de la distribución de especies de *Anopheles* vectores de malaria en Colombia. Biomédica 21: 402-408.

Pan American Health Organization, 2006. Regional strategic plan for malaria in the Americas 2006-2010. Washington, D.C., 85 pages.

Poveda, G., and W. Rojas, 1997. Evidencias de la asociación entre brotes epidémicos de malaria en Colombia y el fenómeno El Niño-Oscilación del Sur. Revista de la Academia Colombiana de Ciencias 21(81): 421-429.

Poveda, G., W. Rojas, M.L. Quiñones, I.D. Vélez, R.I. Mantilla, D. Ruiz, J.S. Zuluaga and G.L. Rúa, 2001. Coupling between annual and ENSO timescales in the malaria-climate association in Colombia. Environmental Health Perspectives 109: 489-493.

Poveda, G., M.L. Quiñones, I.D. Vélez, W. Rojas, G.L. Rúa, D. Ruiz, J.S. Zuluaga, L.E. Velásquez, M.D. Zuluaga, and O. Hernández, 2008. Desarrollo de un Sistema de Alerta Temprana para la malaria en Colombia. Universidad Internacional de Andalucía. 182 p.

Quiñones, M.L., M. Suárez, and G. Fleming, 1987. Distribución y bionomía de los anofelinos de la Costa Pacífica de Colombia. Colombia Médica 1987: 18:19.

Roll Back Malaria, 2008. The global malaria action plan: for a malaria free world. The Roll Back Malaria Partnership, 274 pages.

Rúa, G.L., M.L. Quiñones, I.D. Vélez, J.S. Zuluaga, W. Rojas, G. Poveda, and D. Ruiz, 2005. Laboratory estimation of the effects of increasing temperatures on the duration of gonotrophic cycle of *Anopheles albimanus* (Diptera: Culicidae). Mem Inst Oswaldo Cruz 100(5): 515-520.

Rúa, G., M.L. Quiñones, I.D. Vélez, G. Poveda, D. Ruiz, W. Rojas, and J.S. Zuluaga, 2006. Diagnostics and prediction of climate variability and human health impacts in the Tropical Americas. Universidad Nacional de Colombia-Universidad de Antioquia-Corporación para

Investigaciones Biológicas. Final Report-Collaborative Research Network/Inter-American Institute for Global Change Research, 250 pages.

Ruiz, D., G. Poveda, I.D. Vélez, M.L. Quiñones, G.L. Rúa, L.E. Velásquez, and J.S. Zuluaga, 2006. Modelling entomological-climatic interactions of *Plasmodium falciparum* malaria transmission in two Colombian endemic-regions: contributions to a National Malaria Early Warning System. Malaria Journal 5:66, doi:10.1186/1475-2875-5-66.

Ruiz, D., S. Connor, and M. Thomson, 2008. A multimodel framework in support of malaria surveillance and control. Chapter VII, pages 101-125 in: Seasonal Forecasts, Climatic Change, and Human Health – Health and Climate / Advances in Global Change Research Vol. 30; Madeleine C. Thomson, Ricardo Garcia Herrera and Martin Beniston (ed.), Springer Science + Business Media, Dordrecht; Publisher: Springer Netherlands, ISBN 978-1-4020-6876-8, The Netherlands.

Ruiz, D., A.M. Molina, M.L. Quiñónes, M.M. Jiménez, M. Thomson, S. Connor, M.E. Gutiérrez, P.A. Zapata, C. López, and A. Londoño, 2011. Simulating malaria transmission dynamics in the pilot areas of the Colombian Integrated National Adaptation Pilot project. Escuela de Ingeniería de Antioquia, 374 pages.

Servicio de Erradicación de Malaria, 1957. Plan de erradicación. Ministerio de Salud, Bogotá, Colombia.

Thomson, M.C. and S.J. Connor, 2001. The development of Malaria Early Warning Systems for Africa. Trends in Parasitology 17(9): 438-445.

Thomson, M.C., F.J. Doblas-Reyes, S.J. Mason, R. Hagedorn, S.J. Connor, T. Phindela, A.P. Morse, and T.N. Palmer, 2006. Malaria early warnings based on seasonal climate forecasts from multi-model ensembles. Nature 439: 576-579.

Valero, M., 2006. Malaria in Colombia: retrospective glance during the past 40 years. Rev Salud Pública 8: 141-149.

World Bank - Latin America and the Caribbean, 2006. Colombia: Integrated National Adaptation Program (Available online at: http://web.worldbank.org/external/projects/).

World Health Organization, 2004. Malaria epidemics: forecasting, prevention, early detection and control: from policy to practice. World Health Organization, Geneva, 48 pages.

World Health Organization, 2009. Protecting health from climate change: Global research priorities. World Health Organization, Geneva, 24 pages.

World Health Organization, 2010. Mathematical modelling to support malaria control and elimination. Roll Back Malaria - Progress & Impact Series No. 5, 48 pages.

Table 1. Weather stations available for the analysis of local climatic conditions in the INAP malaria pilot sites

ID	Type[$]	Name and municipality(ies)	Lat [N]	Long [W]	Alt (m)	Climatic variable[&]	Available period (monthly timescale)	Statistically significant long-term trend in annual time series
2502516	CO	CUBA HDA (Montelibano and Puerto Libertador)	08°00'	75°25'	50	R	05/1973-11/2009	+6.9 %/decade
						MinT*	01/1978-11/2009	+0.2 °C/decade
						MaxT*	01/1978-11/2009	--
						MeanT*	01/1978-11/2009	--
						RH	01/1978-09/2006	N/A
3101501	CO	TRUENO EL (San José del Guaviare)	02°24'	72°43'	150	R	08/1982-12/2009	--
						MinT[$]	08/1982-12/2009	+0.4 °C/decade
						MaxT[$]	08/1982-12/2009	--
						MeanT[$]	12/1982-12/2009	--
5311501	SP	APTO BUENAV (Buenaventura)	03°51'	76°58'	14	R	01/1946-10/2010	+3.4 %/decade
						MinT[#]	04/1983-10/2010	--
						MaxT[#]	04/1983-10/2010	--
						MeanT[#]	04/1983-10/2010	--

[$] CO: ordinary climatological weather station; SP: primary synoptic weather station.

[&] R: Total monthly rainfall, expressed in mm; MinT: Minimum monthly temperature in °C; MaxT: Maximum monthly temperature in °C; MeanT: Mean monthly temperature in °C; and RH: Mean monthly relative humidity in %.

[*] Daily minimum temperatures gathered at the weather station Cuba Hda exhibit a historical mean value of 22.4°C and a standard deviation of 1.3°C. Only three potential outlying records exceeding 26°C were

expunged from climatic datasets. Daily maximum temperatures exhibit, in turn, a historical mean value of 33.1°C and a standard deviation of 1.5°C. Two records exceeding 39.0°C and one observation below 25°C were considered true outliers. Lastly, daily mean temperatures exhibit a mean value and a standard deviation of about 27.2°C and 1.1°C, respectively. Three daily temperatures of about 22.1-22.5°C, one record of 6.5°C, and two observations exceeding 32.0°C were expunged from historical datasets.

[$] Daily minimum temperatures gathered at the weather station Trueno El show a historical mean value of 21.1°C and a standard deviation of 1.4°C. Four records of about 25°C and above, as well as seven observations below 15°C were expunged from climatic datasets. Daily maximum temperatures exhibit, in turn, a historical mean value of 31.4°C and a standard deviation of 2.2°C. Two records exceeding 38.0°C were considered true outliers. Lastly, daily mean temperatures exhibit a mean value and a standard deviation of about 25.2°C and 1.4°C, respectively. Five daily temperatures exceeding 30.5°C were expunged from historical datasets.

[#] Daily minimum temperatures gathered at the weather station Apto Buenaventura exhibit a historical mean value of 22.8°C and a standard deviation of 0.9°C. Only one potential outlying record of 16.9°C was expunged from the available dataset. Daily maximum temperatures exhibit, in turn, a historical mean value of 30.4°C and a standard deviation of 1.7°C. Only one record of 24.0°C was considered a true outlier. Lastly, daily mean temperatures exhibit a mean value and a standard deviation of about 26.0°C and 0.9°C, respectively. Three daily temperatures exceeding 29.0°C and two observations around 22.7°C were expunged from historical datasets.

Table 2. *Plasmodium falciparum* and *P. vivax* malaria positive cases observed over the historical period 2000-2010

Study site	***Plasmodium falciparum* infection**				***Plasmodium vivax* infection**			
	Approx. average annual value	Maximum annual value and (year of occurrence)	Maximum value per EP* and (EP)	Maximum value per EW	Approx. average annual value	Maximum annual value and (year of occurrence)	Maximum value per EP and (EP)	Maximum value per EW
Montelibano	1,800	2,600 (2001)	Over 500 (sixth EP of 2001)	About 180	4,000	7,000 (2007)	Over 860 (sixth EP of 2001)	About 280
Puerto Libertador	1,400	2,800 (2002)	Over 420 (seventh EP of 2003)	About 170	4,000	6,600 (2007)	Over 950 (third EP of 2007)	About 430
San José del Guaviare	700	850 (2000)	Over 180 (fifth EP of 2000)	About 95	1,200	1,800 (2008)	Over 340 (fifth EP of 2008)	About 200
Buenaventura	1,800[&]	4,900 (2002)	Over 730 (fifth EP of 2004)	About 260	1,500	3,400 (2004)	Over 560 (fourth EP of 2004)	About 320

[*] One epidemiological period (EP) = four epidemiological weeks (EWs)

[&] Strong difference between the periods 2001-2005 and 2006 to present

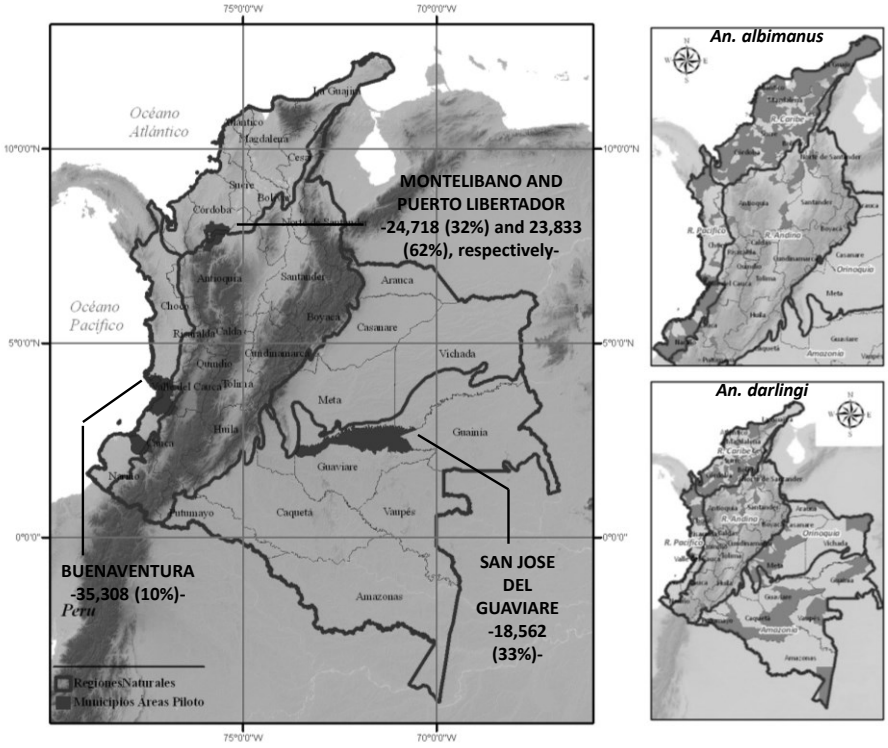

Figure 1. Pilot sites of the Integrated National Adaptation Pilot project (left panel) and spatial distributions of *Anopheles albimanus* and *An. darlingi* primary vectors (top and bottom right panels). See also the total number of individuals living in their rural areas as of 2008 and the proportions (in parentheses) with respect to the total number of individuals living in the municipality. In top and bottom right panels, municipalities with reports of *Anopheles* are shaded – source: Malaria Eradication Service of the former Colombian Ministry of Health (1957) and published papers (e.g. Olano et al., 2001).

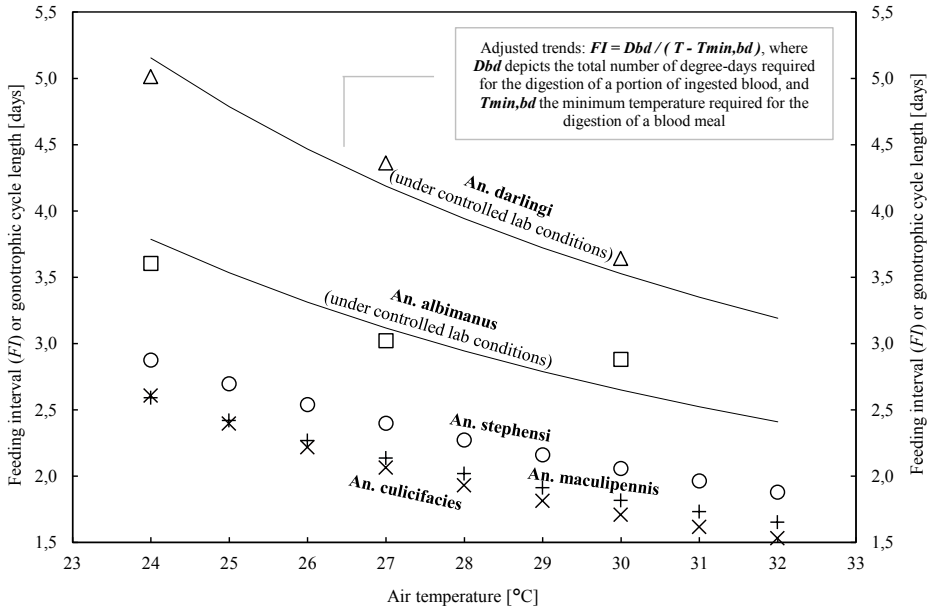

Figure 2. Gonotrophic cycle lengths of Colombian primary vectors, *Anopheles darlingi* and *An. albimanus*, compared to feeding intervals of *An. stephensi*, *An. maculipennis* and *An. culicifacies* mosquito vectors. Feeding intervals of the African vectors are based on scientific literature. The following sample sizes were used to assess the gonotrophic cycle length of *An. darlingi*: n=66 at 24°C; n=170 at 27°C; and n=87 at 30°C. The duration of gonotrophic cycle of *An. albimanus* was estimated under controlled laboratory conditions during previous research projects carried out in Colombia (Rua et al., 2005 and 2006).

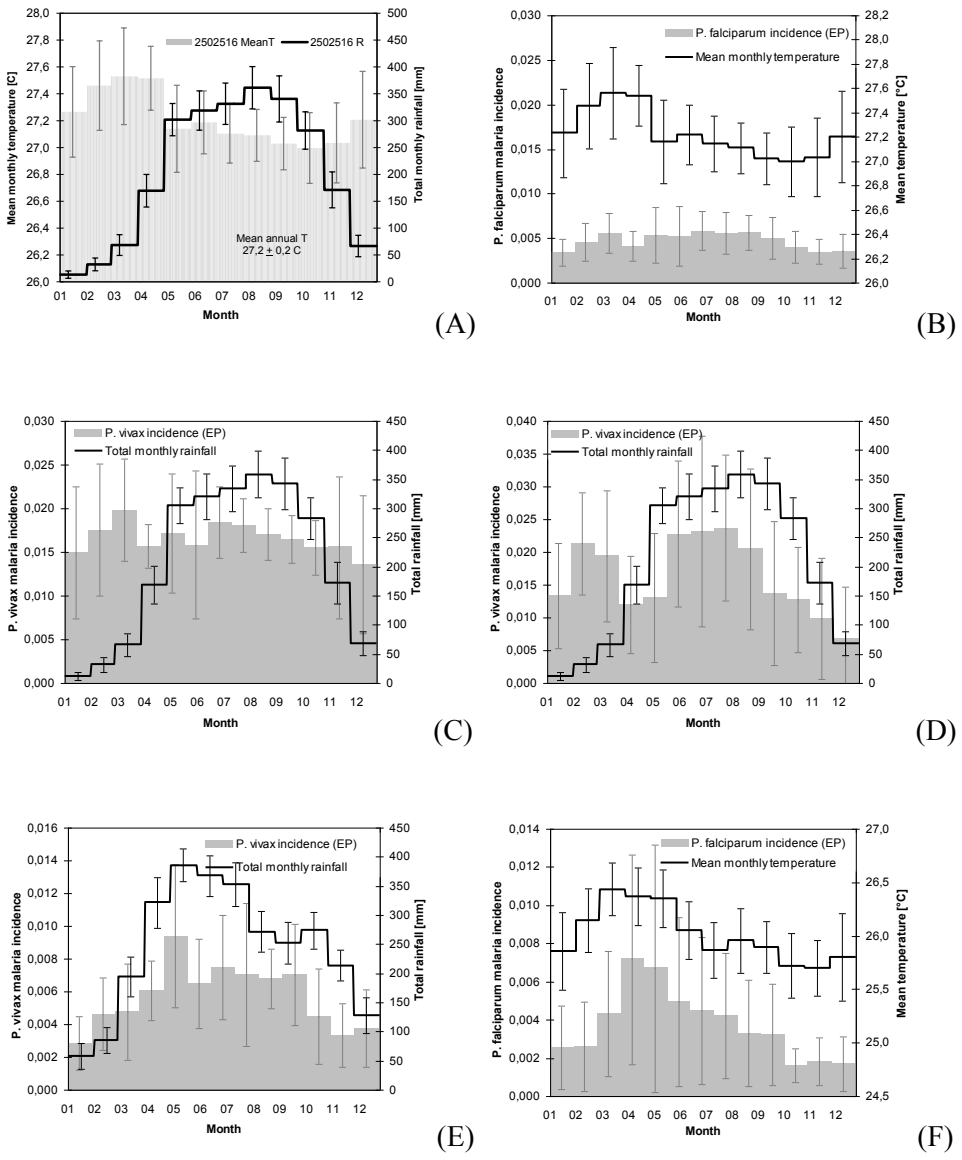

Figure 3. Annual cycles of temperature, rainfall, *Plasmodium falciparum* and *P. vivax* malaria observed in the selected pilot sites. The grey solid bars in panel (A) and the black solid line in panel (B) depict the historical mean monthly temperatures observed in the surroundings of the municipalities of Montelibano and Puerto Libertador, according to available climatic records gathered at the weather station 2502516 Cuba Hda over the period 1978-2009. The black solid lines in panels (A), (C) and (D) show the total monthly rainfall observed at the same weather station over the period 1973-2009. The black solid line in

panel (E) denotes the total monthly rainfall observed in the municipality of San José del Guaviare, according to records gathered at the weather station 3101501 Trueno El over the period 1982-2009. The black solid line in panel (F) shows the mean monthly temperatures observed at the synoptic weather station 5311501 Apto Buenaventura over the period 1983-2009. See also the annual cycles of *Plasmodium falciparum* and *P. vivax* malaria incidence per epidemiological period (EP) observed in the municipalities of Montelibano (panels (B) and (C)), Puerto Libertador (panel (D)), San José del Guaviare (panel (E)), and Buenaventura (panel (F)), according to malaria data provided by the passive Colombian Public Health Surveillance System. Error bars indicate confidence intervals for a α=0.05 significance level.

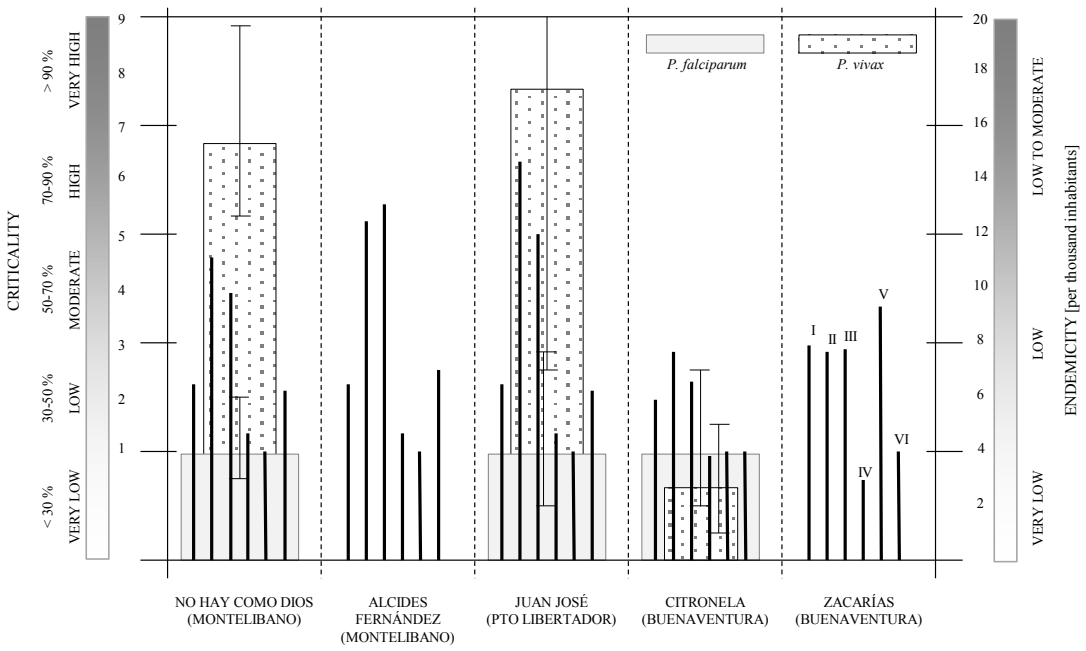

Figure 4. Criticality of local conditions. Black solid bars depict the representative groups of non-climatic factors, such as: (I) immunity of human populations; (II) risk of contact; (III) local installed capacity; (IV) disease knowledge, customs and beliefs; (V) access to health services; and (VI) malaria interventions (their levels of criticality are plotted on the left y-axis). Solid and shaded bars depict, respectively, the historical *Plasmodium falciparum* and *P. vivax* malaria incidence (plotted on the right y-axis); see also their confidence intervals. Malaria incidence in Montelibano are only plotted on purpose in the box of 'No Hay como Dios' county; similarly, malaria incidence in the municipality of Buenaventura are only plotted in the box of 'Citronela' county.

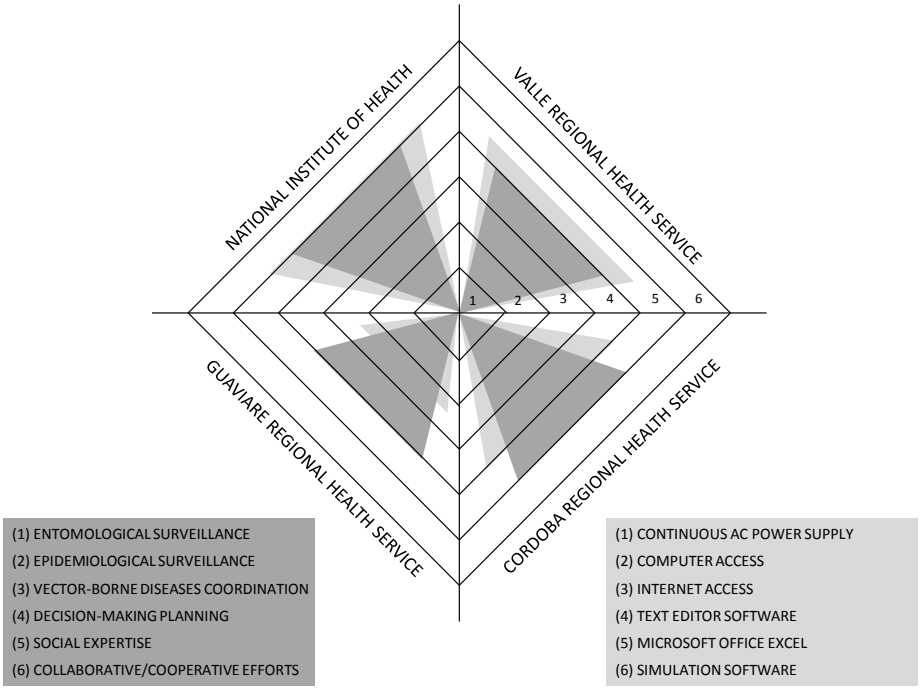

Figure 5. Capacity in state and municipal health authorities to implement malaria dynamical models. Workforce-related aspects are represented by the grey solid triangles; installed/available tools-related aspects are represented by the light grey solid triangles.

Chapter 5[15]

Implementation of malaria dynamical models in municipality-level Early Warning Systems in Colombia – Part II: preliminary results using observed weather and seasonal climate forecasts

Abstract

One of the key components of the Colombian Integrated Surveillance and Control System (ISCS) is a Malaria Early Warning System framework, in which several mathematical models have been proposed as a means to predict changes in malaria transmission risk. Process-based biological models, in particular, are being used to integrate climatic variables with demographic, entomological and socioeconomic factors in order to simulate malaria transmission dynamics. In this article we summarize the preliminary results of the implementation of various malaria dynamical models in four Colombian pilot sites where the ISCS is being implemented. Numerical simulations included several retrospective experiments over at least 8-year historical periods using observed weather data. They also comprised short- to long-term future changing

[15] Note: This second part will be submitted to the American Journal of Tropical Medicine and Hygiene as:

Daniel Ruiz[1,2,3], Viviana Cerón[4], Adriana María Molina[1], Martha Lucía Quiñónes[5], Mónica Marcela Jiménez[6], Martha Ahumada[4], Patricia Gutiérrez[4], Rémi Cousin[2], Salua Osorio[4], Gilma Mantilla[2], Stephen J. Connor[7], and Madeleine C. Thomson[2]

[1]Grupo 'Investigación en Gestión Ambiental – IGEA', Escuela de Ingeniería de Antioquia, Colombia
[2]International Research Institute for Climate and Society, Columbia University in the City of New York, USA
[3]Department of Earth and Environmental Sciences, Columbia University in the City of New York, USA
[4]Subdirección de Vigilancia y Control en Salud Pública, Instituto Nacional de Salud, Colombia
[5]Facultad de Medicina, Universidad Nacional de Colombia Sede Bogotá, Colombia
[6]Instituto Colombiano de Medicina Tropical, Universidad CES, Colombia
[7]School of Environmental Sciences, University of Liverpool, United Kingdom

scenarios using: (i) individual and multi-model ensemble seasonal climate forecasts; (ii) potential impacts of Indoor Residual Spraying (IRS) campaigns; (iii) statistically significant long-term linear trends observed in historical climatic records; (iv) likely occurrence of the warm phase of El Niño-Southern Oscillation; (v) expected changes in climatic conditions under several emission scenarios; and (vi) potential long-term changes in socioeconomic conditions. Up to 28% of the variance of *Plasmodium falciparum* malaria incidence observed in the pilot sites over the period January 3, 2000 through January 3, 2010 was explained by the implemented process-based models, particularly when local climatic, entomological and socioeconomic conditions were all considered concurrently. Mathematical tools also predicted malaria prevalence that was consistent with observed malaria incidence in the simulation of short-term future scenarios, except for worst-case scenario experiments, but predict malaria positive cases that tend to be above the observed primary cases. A better understanding of the impacts of IRS campaigns and the weight of uncertainty in seasonal forecasts is needed for an improved skill level of short-term future malaria predictions. Simulation runs of medium-term future scenarios suggest that by 2015 increases in the highest monthly *Plasmodium falciparum* malaria incidence could be expected in the municipalities under study. Simulation outputs of long-term climatic scenarios indicate that the critical part in terms of malaria control in the pilot sites will likely take place during the third and fourth decades of this century. Lastly, outreach activities included the design of interactive platforms and the implementation of the proposed tools in environment-informed systems at municipal level. In general, simulation experiments improved our understanding of malaria complexity, allowed us to estimate previous malaria outbreaks, and helped us to investigate decision-making processes.

5.1. Introduction

Mathematical modeling plays a critical role in investigating research questions or testing ideas within multifactorial infectious diseases, as well as in navigating complex public health decisions (Roll Back Malaria, 2010). Malaria transmission mathematical models, in particular, could play a significant role in effectively guiding local and regional decision-makers and health practitioners in improved risk assessments, malaria control investments and choice of environmentally-sound interventions. Hence, malaria dynamical models can significantly contribute to the reduction of the burden of this disease in endemic- and epidemic-prone regions. Previous studies have in fact shown that malaria dynamical models reach satisfactory predictability and high problem-adapted skill scores when their simulation outputs are compared to actual malaria morbidity profiles, transmission rates or seasonality (e.g. Alonso et al., 2011; Ermert et al., 2011). Many of these studies have been conducted for Africa, whereas for South America published literature on the implementation of malaria dynamical models is restricted to a set of simulation exercises in Colombia (Ruiz et al., 2002, 2003 and 2006) and theoretical simulation experiments such as those conducted in Brazil by Yang and Ferreira (2000) and in Ecuador by Muñoz et al. (2010). Although moderate to high level skills were obtained in Ruiz et al. simulations (based on validations with field data), the practical and tangible implementation of malaria process-based models in operational surveillance was not explored in detail. In this article we summarize the preliminary results of the implementation of various malaria dynamical models in four Colombian pilot sites at a municipal level, an activity that was conducted in close collaboration with state and municipal health services.

Modeling and simulation activities constitute one of the main efforts of the Malaria Early Warning System Framework that has been proposed for the Colombian Integrated Surveillance

and Control System (ISCS). This article complements a previous publication in which we provide a description of the local eco-epidemiological settings of four *hypoendemic* malaria-prone localities under study. In this publication we describe the set of simulation exercises that were proposed to: (i) compare simulation outputs with actual malaria morbidity profiles in order to assess models' skill levels; (ii) incorporate skill levels along with seasonal forecasting capabilities into malaria control plans at a local level (Thomson et al., 2006; Jones and Morse, 2010); (iii) conduct prospective analyses in order to explore potential medium- (interannual) to long-term changes in malaria morbidity profiles; and (iv) provide a framework for the implementation of mathematical models in routine activities of state and municipal health services, and in a more general sense, for strengthening the institutional capacity of the Colombian malaria control program.

5.2. Study sites

Simulation experiments were conducted in four *hypoendemic* malaria pilot sites distributed throughout Colombia. They include the municipalities of Montelíbano and Puerto Libertador, on the Colombian Caribbean Coast; the municipality of San José del Guaviare, on the Colombian Eastern Plains; and the municipality of Buenaventura, on the Colombian Pacific Coast. These malaria-prone localities exhibit different eco-epidemiological settings, particularly cultural diversity and socioeconomic conditions, that challenge the implementation of the ISCS. A detailed description of their epidemiological profiles was presented in the first part of this publication.

5.3. Data

Data included *Plasmodium falciparum* and *P. vivax* malaria positive cases, primary and secondary *Anopheles* mosquito species, human biting rates and feeding frequencies, minimum, mean and maximum temperature, rainfall and relative humidity records, total human populations at risk and their population growth rates, intervention campaigns conducted by health services (where available), and socioeconomic conditions prevailing in the communities at risk. A detailed description of the observed local settings was presented in the first part of this publication.

5.4. Methods

A set of simulation experiments (see figure 1), including retrospective analyses and future changing scenarios, has been proposed to integrate climatic variables with demographic, entomological and socioeconomic factors in order to simulate malaria transmission dynamics, and to confirm or disconfirm models' skill levels and predictive powers. Retrospective experiments and short-term future changing scenarios, in particular, allow a recursive revision of dynamical models to reflect new data and include improved understanding or evolving needs.

5.4.1. Dynamical models

Dynamical models are available in a thirteen process-based multi-model ensemble, the so-called multi-model platform MME09, which has been previously described by Ruiz et al. (2008a and b). The 2011 version of the MME09 platform includes the following eleven malaria

transmission process-based models: the Ross-Macdonald's model (Ross, 1911 and Macdonald, 1957; hereafter called MAC), the Martens' model (1997, hereafter called MAR), the classic differential-equation and differential-delay-equation compartment models discussed by McKenzie et al. (1998), the Yang's model (Yang, 2000; Yang and Ferreira, 2000), the SimulMal model (Ruiz et al. 2002, 2003, 2006), the weather-driven model proposed by Hoshen and Morse (2004), the mathematical model suggested by Worrall, Connor, and Thomson (2007, hereafter called WCT), the transmission model of endemic human malaria proposed by Chiyaka, Garira and Dube (2007), the Gomero's malaria-sickle-cell model (2008), and the coupled mosquito-human model of malaria proposed by Alonso, Bouma and Pascual (2011). The multi-model platform also contains the tool for decision makers proposed by Githeko and Ndegwa (2001) and the non-spatial malaria epidemiology model suggested by Ruiz and Yan (2003). The systems of ordinary differential equations, schematic diagrams, stock-flow models (or Forrester diagrams), and level and exogenous variables of all these tools, as well as some of their crucial aspects and simulation results are presented in the online supplementary material. The MAC, MAR, SimulMal, and WCT models were later merged in an executive version (MME10EXE) of the multi-model ensemble. Experiments presented here include only simulation outputs of this MME10EXE platform. Community-based, environmental, mosquito population, parasite, and human host exogenous variables were gathered from published literature, directly calculated from field records or local data, and measured in laboratory experiments. Numerical simulations were run using the computer software Powersim Constructor® Version 2.51, Powersim Studio 8 Academic®, and Microsoft Office Excel 2007®.

5.4.2. Models' outputs, predictive powers, sensitivity, and uncertainty

Retrospective analyses were proposed to assess how well dynamical models describe malaria infections in the populations at risk. Simulations included analyses of base scenarios, changes in initial conditions, local settings, sensitivities, and uncertainties (see left panel in figure 1) over a 3,654-day simulation period spanning from January 3, 2000 through January 3, 2010, or from the first epidemiological week of 2000 through the 52nd epidemiological week of 2009. Base scenarios and changes in initial conditions comprised experiments assuming constant mean annual temperatures, constant monthly rainfall amounts (annual rainfall homogeneously distributed throughout the year), and historical annual cycles of mean temperature and rainfall. Initial populations of infected, infectious and immune individuals were assumed to be equal to 1%, 1% and 10% of the total populations at risk, respectively. The initial proportions of infectious and immune individuals were also set to 0.1, 1.0 and 10.0% of the total populations at risk in order to assess changes in equilibrium points. Vector densities, rainfall to mosquito ratios, human blood indices, daily survival probabilities, and probabilities of surviving a feeding cycle were held constant in these model simulations. Modeling outputs were compared to the historical annual cycles of Plasmodium falciparum malaria infections, as shown in figure 2, in order to assess how well the dynamical models simulate historical (observed) malaria incidence.

Simulations of local settings included the following three experiments: (i) *only local climatic conditions*; i.e. models were run with homogenous and continuous actual (observed) mean monthly temperatures and total monthly rainfall records. Local entomological and socioeconomic conditions were assumed to be equal to those variables reported in the literature. (ii) *Local climatic and entomological conditions*; i.e. entomological variables proposed in the literature for *Anopheles maculipennis* and *An. stephensi* were replaced with those values

estimated for the primary vectors incriminated in malaria transmission in the pilot sites. Vector densities and daily survival probabilities were assumed to be functions of rainfall amounts (and in turn, availability of breeding sites) and mean ambient temperatures, respectively. Local socioeconomic conditions were assumed to be equal to those variables reported in the literature. And (iii) *local climatic, entomological and socioeconomic conditions*; non-climatic factors included the conditions of acquired immunity of local populations, the descriptions of IRS programs, and the activities blocking adult female-human host interactions. Immunity was represented with the average infectious period and the probability of recovery of human populations. Spray programs were represented with the variable depicting the percentage coverage achieved by IRS campaigns, which in turn affect the probability of a vector surviving each gonotrophic cycle. Blocking activities were represented in the percentage coverage achieved by the bed-net program, which controls the probability of mosquito vectors becoming infected. In all runs, initial populations of infected, infectious and immune individuals were assumed to be equal to 1%, 1% and 10% of the total populations at risk, respectively. Simulated prevalence per epidemiological period (EP) were compared to the actual *Plasmodium falciparum* malaria morbidity profiles in time series plots (see figure 3) and anomaly plots (see figure SM-II-1 in the online supplementary material) in order to assess how well simulation outputs agree with field observations. They were also compared graphically on weekly timescale (epidemiological week, EW; see figures SM-II-2 (a) and (b) in the online supplementary material) or statistically (see correlation coefficients and mean square errors in figure 4).

Sensitivity analyses comprised the simulation of potential impacts of small changes (±1%, ±5% and ±10%) in several parameters on *P. falciparum* malaria prevalence profiles. Variables of interest included, in particular, the probability of human recovery, *r*, which is a

function of the average infectious period; the probability of a vector surviving each gonotrophic cycle in an unsprayed population (α); the probability of a mosquito surviving through one whole day; and the human blood index (h). Moderate scenarios considered a 10% decrease in α, a 10% increase in r, and a 10% decrease in h (see figure SM-II-1 in the online supplementary material). Conversely, critical scenarios assumed a 10% increase in α, a 10% decrease in r, and a 10% increase in h.

Uncertainty analyses included the simulation of changes in the relationship between the total number of mosquitoes emerging per month in each pilot site and the total rainfall amount. Various linear functions (with different slopes and origins) and a 2^{nd}-order polynomial function were explored. Thus, the rainfall-to-mosquito constant parameter of the WCT model was increased or reduced in 10%. These changes were supported on entomological data from previous field campaigns conducted on the Colombian Pacific Coast over a 44-month research period (Rúa et al. 2006).

5.4.3. Integration of short-, medium- and long-term climate-based predictions

Simulations also included short-, medium- and long-term future changes in epidemiological conditions. See right panel in figure 1. Short-term scenarios included the analysis of changes in near-surface mean temperatures and rainfall amounts suggested by individual and multi-model ensemble seasonal forecasts, as well as potential impacts of IRS campaigns. Seasonal near-surface air temperature and precipitation skill maps (observations vs. model outputs anomaly correlations over the period 1950-2000; source: International Research Institute for Climate and Society – IRI, Model Skill Comparison,

http://iri.columbia.edu/forecast/climate/skill/Skill_comp.html) of six climate models were initially consulted to define the model that provides consistent simulation outputs for the Colombian territory. Individual ECHAM4.5 model predictions (http://iri.columbia.edu/climate/forecast/ncp) and net assessment probability forecasts (http://iri.columbia.edu/climate/forecast/net_asmt) were then used to define the short-term climate scenarios (one to two seasons ahead of a given forecast issued date). Likely climatic conditions for eleven trimesters starting in the quarter December, 2009 through February, 2010 (D/09-JF/10), and extending to June through August, 2012 (JJA/12) were defined to estimate *Plasmodium falciparum* malaria prevalence. Simulation outputs were later compared to the observed *P. falciparum* malaria incidence, gathered over the period December, 2009 through December, 2011, once malaria positive cases records became available. Each of the simulations of short-term changes in climatic conditions included three experiments derived from the suggested anomalies in mean temperature and total rainfall. See for instance figure SM-II-3 in the online supplementary material for the forecast horizon spanning from December 1, 2009 through May 31, 2010, and for the pilot municipalities of Montelíbano and Puerto Libertador. Simulations of the period D/09-JF/10 through JJA/12 also included the recursive revision of dynamical models to reflect new climate data. See figure 5.

Medium-term changes in climatic conditions for a 5-year forecast period were defined by extrapolating the statistically significant long-term linear trends observed in historical records of local annual rainfall and mean temperature, and by considering a likely occurrence of a warm phase (El Niño event) of El Niño-Southern Oscillation, which has been suggested to have a strong impact on malaria outbreaks in Colombia (Bouma et al., 1997; Poveda and Rojas, 1997; Poveda et al., 2001; Gagnon et al., 2002; and Mantilla et al., 2009). Experiments comprised in

this case simulations of a 5,842-day time period spanning from January 3, 2000 through December 31, 2015. Similar to the analysis of future short-term scenarios, each of the simulations of medium-term changes in climatic conditions included three experiments. See figure 6. Simulations were initially based on the °C/decade and %/decade historical changes in mean annual temperatures and total annual rainfall observed in the local historical climatic records. In particular, for the municipalities of Montelíbano and Puerto Libertador, +0.1, +0.2 and +0.3°C increases per decade in mean annual temperature and +3, +5 and +9% increases per decade in total annual rainfall were assumed for the analyses. In San José del Guaviare, only increases in mean annual temperature of +0.2, +0.4 and +0.6°C per decade were considered. In Buenaventura, only increases in total annual rainfall of +2, +4 and +6% per decade were assumed for simulating medium-term climatic conditions.

Medium-term future scenarios also considered temperature and rainfall anomalies expected by 2015 due to the potential occurrence of weak, average and strong El Niño-like conditions. Temperature and precipitation probabilities (below-, near- and above-normal conditions; IRI, ENSO Probability Maps, http://iri.columbia.edu/climate/forecast/enso/) for the trimesters December-January-February, March-April-May, June-July-August, and September-October-November associated with El Niño were initially studied for each of the Colombian hydroclimatic regions. +0.3, +0.5 and +0.7°C anomalies in DJF and MAM seasonal temperatures, and -5%, -10% and -15% anomalies in DJF and JJA seasonal rainfall amounts, associated with weak, average and strong El Niños, respectively, were assumed for the analyses of medium-term climatic conditions. See figure 6.

Long-term changes in climatic conditions included the analysis of changes in mean annual temperature and total annual rainfall expected, with respect to the base period 1961-1990,

for the IPCC (2001) emission scenarios. IPCC-2007 scenarios (Meehl et al., 2007) were not used because their downscaling results were not available at a local scale. By 2050, mean annual temperatures in the region of the municipalities of Montelíbano and Puerto Libertador are likely to increase from +1.0 to +2.8°C (DG-UNAL, 2005), with respect to the base period 1961-1990, under the emission scenarios B1, B2, A1, and A2. Total annual rainfall could, in turn, have decreases in the range from -1% to -4% (DG-UNAL, 2005). In the municipalities of San José del Guaviare and Buenaventura, increase in temperature could range from +1.1 to +3.0°C and from 1.0 to +2.9°C, respectively (DG-UNAL, 2005). Annual rainfall could increase from +1 to +4% and from +4 to +10%, respectively (DG-UNAL, 2005). Experiments included simulations of the dynamical model proposed by Martens (1997, MAR) over a 108-year retrospective time period (1900-2008), and comparisons to the annual parasite indices observed in the states where malaria pilot sites are located (see, for instance, the *Plasmodium falciparum* and *P. vivax* malaria incidence observed in the Department of Córdoba over the period 1960-2008 in figure SM-II-4 of the online supplementary material). Simulations also include experiments for 42-year (2009-2050) and 72-year (2009-2080) forecast periods.

Analyses of long-term future scenarios also included potential changes in socioeconomic conditions. A set of simulations were conducted to analyze the impacts on malaria morbidity profiles of future changes in average infectious periods of *Plasmodium falciparum* infections in human hosts. Three favorable scenarios (decreases in the average infectious period of -1, -5 and -10%) and three unfavorable socioeconomic scenarios (increases of +1, +5 and +10%) were considered in the simulations of opposite emission scenarios B1 and A2.

5.5. Results

Previous modeling efforts to represent *P. falciparum* malaria transmission in Colombia (Ruiz et al., 2006) were focused on two endemic-prone areas: the locality of Nuquí on the Pacific coast, and the municipality of El Bagre, on the north-western plains. In Nuquí, *P. falciparum* malaria positive cases showed to be statistically correlated with mean monthly ambient temperatures for a 1-month time lag (R=+0.827) and with total monthly rainfall for a 3-month time lag (R=-0.447). In El Bagre, *P. falciparum* malaria was statistically correlated with mean ambient temperatures for a time lag of one epidemiological period, EP (R=+0.487), and with total rainfall for a time lag of four EPs (R=-0.496). The analysis of base scenarios over 2,252-day and 3,282-day historical periods (6 and 9 years, respectively, or simulation periods November 1, 1997 – December 31, 2003 and 1st EP, 1994 – 13th EP, 2002) yielded correlation coefficients between observed and modeled incidences of about +0.727 and +0.455 for the municipalities of Nuquí and El Bagre, respectively. The mean square errors reached 60E-05 and 100E-05, respectively.

Simulation exercises conducted here suggest that dynamical models were also able to qualitatively reproduce historical malaria morbidity profiles in the selected malaria pilot sites. Outputs of base scenarios, changes in initial conditions, local settings, sensitivity, and uncertainty suggest that the WCT model better represented *Plasmodium falciparum* malaria incidence observed over the period January 3, 2000 through January 3, 2010 in the municipalities of Montelíbano, San José del Guaviare and Buenaventura, whereas the SimulMal model did so in the locality of Puerto Libertador. Best correlation coefficients and mean square errors between simulated prevalence per epidemiological period and actual *Plasmodium falciparum* malaria morbidity profiles reached, however, values in the range from +0.288 to +0.533, and from 6E-05

to 26E-05, respectively. See figure 4. Thus, from 8 to 28% of the variance of *P. falciparum* malaria incidence was explained by the implemented process-based models. Results improved when local climatic, entomological and socioeconomic conditions were all taken into account, as shown in figure 4.

In the analysis of short-term future scenarios, WCT and SimulMal results suggest that these two mathematical tools predicted values that were consistent with observed malaria incidence, except for worst-case scenario experiments. Simulation results for the period December 1, 2009 through May 31, 2010 suggested that *P. falciparum* malaria incidence in the municipality of Montelíbano could have reached an incidence in the range from 6 to 24 positive cases per 1,000 inhabitants in May, 2010 (forecast issued in November, 2009) if no IRS control campaigns were conducted. Actual positive cases provided by the CNIH in September, 2010 indicate that *P. falciparum* malaria incidence in May, 2010 reached 5 positive cases per 1,000 inhabitants. In the municipality of Puerto Libertador, simulation results suggested that malaria incidence could have reached from 6 to 30 positive cases per 1,000 inhabitants by the end of the MAM/10 trimester if no IRS control campaigns were conducted. Observed malaria positive cases reached slightly over 14 cases per 1,000 inhabitants, i.e. in the range of predicted incidence. Lastly, in the municipality of Buenaventura simulation experiments suggested that malaria positive cases per epidemiological week could have reached over 67 and 89 cases during the fourth and second weeks of March and May, 2010, respectively, if no IRS campaigns were conducted. Actual malaria positive cases provided by the CNIH indicate that peaks in transmission reached 35 positive cases per week, two weeks before the increases suggested by simulations. Experiments for the trimesters MAM/11 and June-July-August, 2011 (JJA/11) suggested that *P. falciparum* malaria positive cases in Buenaventura could have reached peaks of

about 152 and 147 cases per week. Total MAM/11 and JJA/11 positive cases could have decreased to 143 and 139 primary cases, respectively, with IRS campaigns reaching 0.5, 1.0, 1.5, and 2.0% of the total population at risk, which are consistent with historical 0.3%, 1.8% and 1.9% coverage.

A closer look at the simulation outputs for the forecast period spanning from January 4, 2010 through April 19, 2012 suggest that models predict malaria positive cases that tend to be above the observed incidence. For instance, see figure 5 for the *P. falciparum* malaria primary cases simulated by the WCT model. The WCT tool underestimated malaria positive cases observed in Montelíbano (and Puerto Libertador) in the first three months of the forecast period, and overestimated malaria morbidity in the remainder twelve months. Weekly differences during the peak months of August, 2010 and June, 2011 reached 52 (67) and 127 (172) positive cases, respectively. Similarly, the WCT tool overestimated *P. falciparum* malaria positive cases in San José del Guaviare during almost the full forecast period. Weekly differences during the peak months of June, 2010 and May, 2011 reached 36 and 40 positive cases, respectively. In Buenaventura, differences between simulated malaria and actual positive cases reached 85 and 91 in September, 2010 and September, 2011, respectively. These overestimations could be explained by two voluntary omissions: (i) in the analysis of short-term future scenarios, the impacts of IRS campaigns were not included; and (ii) uncertainty in monthly mean temperatures and total rainfall amounts suggested by ECHAM4.5 individual seasonal forecasts for years 2010 and 2011 were not considered; see figures SM-II-5 (a) and (b) in the online supplementary material. Comparisons with actual (observed) monthly mean temperatures and total rainfall amounts gathered at the weather station Cuba Hda in the same years indicate that temperature forecasts for the municipalities of Montelíbano and Puerto Libertador were in average 0.8°C

above the actual monthly temperature, particularly in 2010. In Buenaventura, however, such a strong difference was not observed, according to the records gathered at the weather station Apto Buenaventura.

WCT and SimulMal results of medium-term future scenarios suggest that, by 2015, long-term trends in climatic conditions and seasonal anomalies in temperature and rainfall associated with an El Niño event could combined increase the highest monthly *Plasmodium falciparum* malaria incidence in the municipalities of Montelíbano, Puerto Libertador, San José del Guaviare, and Buenaventura in almost 8, 7, 2, and 4 positive cases per 1,000 inhabitants, respectively. Simulation results of long-term climatic scenarios suggest that, by the end of the 2020s *P. falciparum* malaria in the region of the municipalities of Montelíbano and Puerto Libertador could reach inflection points followed by steep slopes that increase incidence, by 2040, to values in the range 35-85 positive cases per 1,000 inhabitants. They also indicate that malaria incidence could reach, by 2050, almost 110 positive cases per 1,000 inhabitants under the A2 emission scenario. After 2050 morbidity profiles seem to stabilize, indicating that the critical part in terms of malaria control will likely take place during the third and fourth decades of this century. Simulation results also suggest that, by 2080, a 10% decrease in the duration of the infectious period of human hosts could reduce the expected *Plasmodium falciparum* malaria incidence under the emission scenario B1 in almost 40 positive cases per 1,000 inhabitants. Conversely, a 10% increase in the duration of the infectious period could add additional 50 positive cases per 1,000 inhabitants to the expected 2080 incidence. Thus, increases in historical mean annual temperatures and increases in average infectious periods in human hosts could drive *Plasmodium falciparum* malaria incidence in the region of the municipalities of Montelíbano and Puerto Libertador to unprecedented values around 10% of the total population at risk.

5.6. Interactive platforms and environment-informed systems at local level

Outreach activities included the design of interactive and online platforms, and the implementation of environment-informed systems at municipal level. Interactive modeling platforms using Powersim Constructor Version 2.51® for Microsoft Windows XP-Home Edition Version 2002®, Powersim Studio 8 Academic® for Microsoft Windows 7 Enterprise®, and Microsoft Office Excel 2007 for Microsoft Windows Vista Home Basic® were designed to build regional and local capacity. Up to date they include the following tools:

- The Powersim Studio 8 Academic® for Microsoft Windows 7 Enterprise® individual platforms of the SimulMal and WCT models, the Breeding Places Availability Model – BPAM Version 2010, and the vector ecology (immature stages) VEC – Version 2010, as well as the executive version of the multi-model ensemble platform (MME10EXE).
- The Microsoft Office Excel 2007 for Microsoft Windows Vista Home Basic® individual platform of the WCT model.
- The Powersim Constructor Version 2.51® for Microsoft Windows XP-Home Edition Version 2002® full version of the multi-model ensemble platform (MME09) and the individual platform of the MAR model.

Interactive platforms currently require from 5 to 75 seconds for running 3,654-day simulation periods on a Intel(R) Core™2 Duo CPU T6670 @ 2.20 GHz personal laptop with 4.00 GB RAM. Importantly, models were structured in such a way that inputs and outputs are relevant to the needs of end-users within state and municipality health services. They also

integrate the key epidemiological dimensions and assess interventions' effectiveness in a single framework. Simple Microsoft Excel® for Microsoft Windows 7 Enterprise spreadsheets were also proposed to organize exogenous variables and parameters of dynamical models for each of the selected pilot sites. Furthermore, an online version of the WCT model individual platform, currently available in the Data Library of the International Research Institute for Climate and Society (IRI) is being developed to support monthly to seasonal planning of malaria control activities (http://iridl.ldeo.columbia.edu/home/.remic/.maproom/.Health/.Regional/.S_America/.Malaria/.WCT_Model). Lastly, detailed protocols for installing, compiling and executing the aforementioned platforms were socialized with the National Institute of Health.

5.7. Discussion and conclusions

Simulation outputs for the pilot sites of the Colombian Integrated National Adaptation Plan suggest that the implementation of *Plasmodium falciparum* malaria dynamical models is a very promising, although not yet fully convincing approach for an early detection of malaria outbreaks. As mentioned before, simulation outputs suggest that process-based models are able to qualitatively reproduce the observed malaria incidence, but the obtained low to moderate correlation coefficients and mean square errors indicate that their skill level is still limited. However, we argue that this partial predictability is influenced by the discontinuous, non-homogenous and inconsistent records of malaria positive cases observed over the available 540-week base period. As mentioned in the first part of this study, up to 19% of the total number of epidemiological weeks is missing in the provided datasets: 18.5, 17.6, 8.9, and 10.0% of the total

number of available weeks of *Plasmodium falciparum* malaria cases observed in the municipalities of Montelíbano, Puerto Libertador, San José del Guaviare, and Buenaventura, respectively; and 12.2, 11.3, 5.2, and 8.7% of the total number of available weeks of *P. vivax* malaria cases, respectively. State and municipal epidemiological surveillance systems should be improved in order to collect information on malaria primary cases routinely and confidently.

Simulation activities have promoted the integration of and regional cooperation between several institutions on the adaptation strategy to climate change in Colombia. They have also linked what had previously been largely separate analytical domains: vector-borne diseases, traditionally dominated by entomologists and tropical medicine health practitioners; malaria epidemiology, dominated by public health experts; and climatology and modeling, usually lead by engineers and environmental science experts. We will continue to weave together the threads between the academia and regional and local health authorities so as to build local capacity that could facilitate the assessment of the impacts of changes in climatic conditions on malaria morbidity profiles. We perceive that significant efforts are required to translate modeling outputs into useful results for decision-makers.

Final note

Our project entitled '*Simulating malaria transmission dynamics in the pilot areas of the Colombian Integrated National Adaptation Pilot project*' has been documented in the following five chapters (Ruiz et al, 2011): (Chapter 1) Malaria transmission models; (Chapter 2) Main characteristics of malaria pilot areas; (Chapter 3) Simulation results; (Chapter 4) Complementary activities: building local capacity, interactive and online operative platforms, and exogenous

variables and parameters; and (Chapter 5) Complementary activities: spatial risk assessment, conceptual framework for the analysis of non-climatic drivers, descriptions of the vulnerability of populations at risk, conclusions and recommendations. As mentioned in the main text, Chapter 1 contains the systems of ordinary differential equations, schematic diagrams, stock-flow models (or Forrester diagrams), and level and endogenous variables of the studied process-based models. It also contains some of the crucial aspects and simulation results of malaria dynamical models, as well as their community-based, environmental, mosquito population, parasite, and human host exogenous variables. Chapter 1 has been posted on the online course entitled '*Simulating Malaria Transmission Dynamics-SMTD*' (http://saber.eia.edu.co/eiadigital/) and is also available in the online supplementary material.

Acknowledgments

The authors would like to thank the Instituto Nacional de Salud de Colombia (INS), the Departamento Administrativo de Salud de Guaviare, the Laboratorio de Salud Pública de Córdoba, the Laboratorio de Salud Pública del Valle, and the Instituto de Hidrología, Meteorología y Estudios Ambientales (IDEAM) for all their support throughout the project. We also acknowledge the participation and support of research assistants Maria Elena Gutiérrez, Paula Andrea Zapata, Catalina López, and Adelaida Londoño, and the helpful suggestions made by the anonymous peer-reviewers who read and commented this manuscript. Analyses conducted here have been funded by Conservation International Colombia, as part of the Integrated National Adaptation Plan project. Daniel Ruiz has been partially funded by Unidad Académica Civil, Ambiental e Industrial – Escuela de Ingeniería de Antioquia, the International Research

Institute for Climate and Society (IRI) and the Department of Earth and Environmental Sciences, Columbia University in the City of New York (USA). The retrospective forecasts produced at the International Research Institute for Climate and Society (IRI) have been performed largely using computing grants from the multi-agency CSL computing program, David G. DeWitt, PI.

Authors' detailed addresses:

[1] Grupo 'Investigación en Gestión Ambiental – IGEA', Unidad Académica Civil, Ambiental e Industrial, Escuela de Ingeniería de Antioquia (www.eia.edu.co), km 02+000 Vía al Aeropuerto José María Córdova, Municipio de Envigado, Antioquia, Colombia. Phone number: +57(4) 354-9090; Fax number: +57(4) 331-7851; E-mails: pfcarlos@eia.edu.co and pfamolina@eia.edu.co

[2] International Research Institute for Climate and Society (http://portal.iri.columbia.edu), Lamont-Doherty Earth Observatory, Columbia University in the City of New York, 61 Route 9W - PO Box 1000, Palisades, NY 10964-8000, USA. Phone number: +1(845) 680-4465; Fax number:+1(845) 680-4864; E-mails: pfcarlos@iri.columbia.edu, mthomson@iri.columbia.edu, sjconnor@iri.columbia.edu, remic@iri.columbia.edu, and mantilla@iri.columbia.edu

[3] Department of Earth and Environmental Sciences, Columbia University in the City of New York, 1200 Amsterdam Avenue, 556-7 Schermerhorn Extension, New York, NY 10027, USA.

[4] Subdirección de Vigilancia y Control en Salud Pública, Instituto Nacional de Salud, Avenida Calle 26 No. 51-20, Zona 6 CAN, Bogotá, D.C., Colombia. Phone number: +57(1) 220-7700; Fax number: +57(1) 220-0901; E-mails: vceron@ins.gov.co, mahumada@ins.gov.co, pgutierrezduenas@gmail.com, and sosorio@ins.gov.co

[5] Facultad de Medicina, Universidad Nacional de Colombia Sede Bogotá, Carrera 30 No 45-03, Edificio 471, Ciudad Universitaria, Bogotá D.C., Colombia. Phone number: +57(1) 316-5000 ext. 15136; E-mail: mlquinonesp@unal.edu.co

[6] Instituto Colombiano de Medicina Tropical, Universidad CES, Calle 10 A No. 22 – 04, Medellín, Colombia. Phone number: +57(4) 444-0555; E-mail: mmjimenez@ces.edu.co

[7] School of Environmental Sciences, University of Liverpool, Liverpool L69 3BX, United Kingdom, E-mail: sjconnor@liv.ac.uk

Shipping address for reprints:

Escuela de Ingeniería de Antioquia, km 02+000 Vía al Aeropuerto José María Córdova, Municipio de Envigado, Antioquia, Colombia

References

Alonso, D., M.J. Bouma, M. Pascual, 2011. Epidemic malaria and warmer temperatures in recent decades in an East African highland. Proc Biol Sci 278(1712):1661-9.

Aron, J.L., and R.M. May, 1982. The population dynamics of malaria. In: Anderson, R.M. (ed.). The population dynamics of infectious disease: theory and applications. London, Chapman and Hall, 139–179.

Bouma, M., G. Poveda, W. Rojas, M.L.Quiñones, J. Cox, and J. Patz, 1997. Predicting high-risk years for malaria in Colombia using parameters of El Niño-Southern Oscillation. Trop Med Int Health 2:1122-1127.

Bruce-Chwatt, L.J., 1980. Essential malariology. London: Heinemann.

Chiyakaa, C., W. Garira, and S. Dube, 2007. Transmission model of endemic human malaria in a partially immune population. Mathematical and Computer Modelling 46: 806–822, doi:10.1016/j.mcm.2006.12.010.

Departamento de Geografía – Universidad Nacional de Colombia, 2005. Escenarios de cambio climático para el territorio colombiano. Fase PDF-B, Integrated National Adaptation Pilot (INAP) - Informe Ejecutivo. Bogotá, Colombia, 19 pp.

Ermert, V., A. H. Fink, A. E. Jones, and A. P. Morse, 2011. Development of a new version of the Liverpool Malaria Model. II. Calibration and validation for West Africa. Malaria Journal 2011, 10:62.

Gagnon, A., K. Smoyer-Tomic and A. Bush, 2002. The El Niño-Southern Oscillation and malaria epidemics in South America. Int J Biometeorol 46: 81-89.

Githeko, A.K. and W. Ndegwa, 2001. Predicting malaria epidemics in the Kenyan highlands using climate data: a tool for decision makers. Global Change and Human Health 2: 54-63.

Gomero, B., 2008. A deterministic mathematical model to study control measures for malaria. Honor thesis, 32 pages.

Hoshen, M.B. and A.P. Morse, 2004. A weather-driven model of malaria transmission. Malaria Journal 3:32, doi:10.1186/1475-2875-3-32.

IPCC, 2001. Climate Change 2001: The Scientific Basis. Contribution of Working Group I to the Third Assessment Report of the Intergovernmental Panel on Climate Change [Houghton, J.T.,Y. Ding, D.J. Griggs, M. Noguer, P.J. van der Linden, X. Dai, K. Maskell, and C.A. Johnson (eds.)]. Cambridge University Press, Cambridge, United Kingdom and New York, NY, USA, 881 pp.

Jones, A.E. and A.P. Morse, 2010. Application and validation of a seasonal ensemble prediction system using a dynamic malaria model. J Clim 23:4202-4215.

Macdonald, G., 1957. The epidemiology and control of malaria. Oxford University Press, Oxford, U.K.

Mantilla, G., H. Oliveros, and A. Barnston, 2009. The role of ENSO in understanding changes in Colombian's annual malaria burden by region, 1960-2006. Malaria Journal 2009, 8:6.

Martens, W.J.M., 1997. Health impacts of climate change and ozone depletion. An eco-epidemiological modelling approach. Maastricht, Netherlands.

Meehl, G.A., T.F. Stocker, W.D. Collins, P. Friedlingstein, A.T. Gaye, J.M. Gregory, A. Kitoh, R. Knutti, J.M. Murphy, A. Noda, S.C.B. Raper, I.G. Watterson, A.J. Weaver, and Z-C. Zhao, 2007. Global Climate Projections. In: Climate Change 2007: The Physical Science Basis. Contribution of Working Group I to the Fourth Assessment Report of the Intergovernmental Panel on Climate Change [Solomon, S., D. Qin, M. Manning, Z. Chen, M. Marquis, K.B. Averyt, M. Tignor and H.L. Miller (eds.)]. Cambridge University Press, Cambridge, United Kingdom and New York, NY, USA, pp. 764-765.

McKenzie, F.E., R.C.Wong and W.H. Bossert, 1998. Discrete-event simulation models of *Plasmodium falciparum* malaria. Simulation 71(4): 213-217.

Muñoz, A.G., D. Ruiz, and C. Recalde, 2010. Malaria biological models and dynamical downscaling for northwestern South America in the Observatorio Andino framework. ICID+18 / 2nd International Conference: Climate, Sustainability and Development in Semi-arid Regions, Fortaleza, Ceara (Brazil).

Poveda, G. and W. Rojas, 1997. Evidencias de la asociación entre brotes epidémicos de malaria en Colombia y el fenómeno El Niño-Oscilación del Sur. Revista de la Academia Colombiana de Ciencia 21:421-429.

Poveda, G., W. Rojas, M.L. Quiñones, I.D. Vélez, R.I. Mantilla, D. Ruiz, J.S. Zuluaga and G.L. Rúa, 2001. Coupling between annual and ENSO timescales in the malaria-climate association in Colombia. Environmental Health Perspectives 109: 489-493.

Poveda, G., M.L. Quiñones, I.D. Vélez, W. Rojas, G.L. Rúa, D. Ruiz, J.S. Zuluaga, L.E. Velásquez, M.D. Zuluaga, and O. Hernández, 2008. Desarrollo de un Sistema de Alerta Temprana para la malaria en Colombia. Universidad Internacional de Andalucía. 182 p.

Roll Back Malaria, 2010. Mathematical modelling to support malaria control and elimination. Progress & impact series 5, 48 pages.

Ross, R., 1911. The prevention of malaria. Murry, London, U.K.

Ruiz, D., G. Poveda, M.L. Quiñones, I.D. Vélez, G.L. Rúa, W. Rojas and J.S. Zuluaga, 2002. Modelación sistémica para el diagnóstico de la interacción clima-malaria en Colombia.

Aplicación durante El Niño 1997–1998 y La Niña 1998–2000. Meteorología Colombiana 5: 41-48.

Ruiz, D., G. Poveda, R.I. Mantilla, M.L. Quiñones, I.D. Vélez, G.L. Rúa, W. Rojas and J.S. Zuluaga, 2003. Modelación de la interacción entomológica-climática de la transmisión de la malaria mediante Dinámica de Sistemas. Revista Colombiana de Entomología 29: 191-201.

Ruiz, D. and G. Yan, 2003. Biology of African Highland Malaria: report. Department of Biological Sciences, State University of New York at Buffalo, USA, 60 pages.

Ruiz, D., G. Poveda, I.D. Vélez, M.L. Quiñones, G.L. Rúa, L.E. Velásquez, and J.S. Zuluaga, 2006. Modelling entomological-climatic interactions of *Plasmodium falciparum* malaria transmission in two Colombian endemic-regions: contributions to a National Malaria Early Warning System. Malaria Journal 5:66, doi:10.1186/1475-2875-5-66.

Ruiz, D., S. Connor, and M. Thomson, 2008a. A multimodel framework in support of malaria surveillance and control. Chapter VII, pages 101-125 in: Seasonal Forecasts, Climatic Change, and Human Health – Health and Climate / Advances in Global Change Research Vol. 30; Madeleine C. Thomson, Ricardo Garcia Herrera and Martin Beniston (ed.), Springer Science + Business Media, Dordrecht; Publisher: Springer Netherlands, ISBN 978-1-4020-6876-8, The Netherlands.

Ruiz, D., S. Connor, and M. Thomson, 2008b. Malaria modelling and Integrated Surveillance and Control Systems. Chapter XIII, Part III (Aplicaciones en Política Pública), online publication 'Dinámica de Sistemas: casos y aplicaciones en Latino-América', LatinAmerican Chapter, System Dynamics Society.

Ruiz, D., A.M. Molina, M.L. Quiñónes, M.M. Jiménez, M. Thomson, S. Connor, M.E. Gutiérrez, P.A. Zapata, C. López, and A. Londoño, 2011. Simulating malaria transmission dynamics in the pilot areas of the Colombian Integrated National Adaptation Pilot project. Escuela de Ingeniería de Antioquia, 374 pages.

Thomson, M.C. and S.J. Connor, 2001. The development of Malaria Early Warning Systems for Africa. Trends in Parasitology 17(9): 438-445.

Thomson, M.C., F.J. Doblas-Reyes, S.J. Mason, R.Hagedorn, S.J. Connor, T. Phindela, A.P. Morse, and T.N. Palmer, 2006. Malaria early warnings based on seasonal climate forecasts from multi-model ensembles. Nature 439: 576-579.

Worrall, E., S.J. Connor and M.C. Thomson, 2007. A model to simulate the impact of timing, coverage and transmission intensity on the effectiveness of indoor residual spraying (IRS) for malaria control. Tropical Medicine & International Health 12(1): 75-88.

Yang, H., 2000. Malaria transmission model for different levels of acquired immunity and temperature-dependent parameters (vector). Rev. Saúde Pública 34 (3): 223-231.

Yang, H. and M. Ferreira, 2000. Assessing the effects of global warming and local social and economic conditions on the malaria transmission. Rev. Saúde Pública 34(3): 214-222.

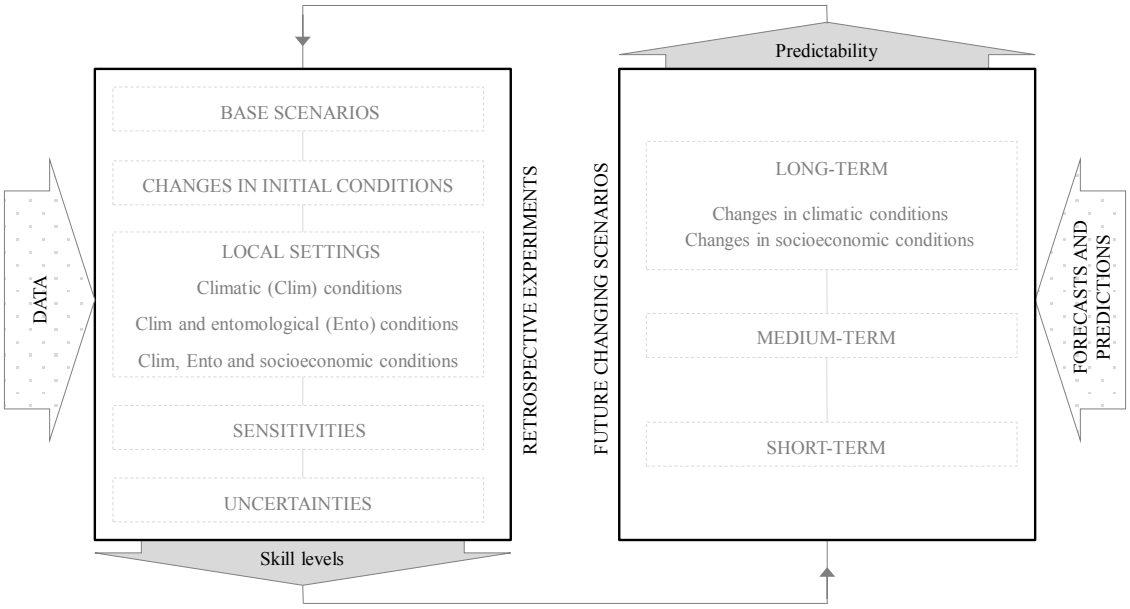

Figure 1. Proposed set of experiments for a recursive revision of malaria dynamical models (see counterclockwise loop). Retrospective experiments include simulations of base scenarios, changes in initial conditions, analysis of local settings, sensitivities, and uncertainties. Future changing scenarios include simulations of short-, medium- and long-term future changes in epidemiological conditions.

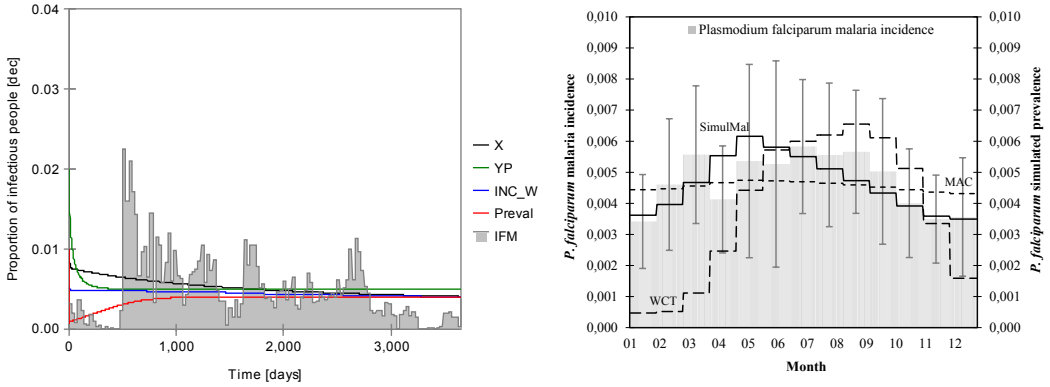

Figure 2. *Plasmodium falciparum* malaria incidence observed in the municipality of Montelíbano, on the Colombian Caribbean Coast, along with malaria prevalence simulated by the MAC, MAR, WCT and SimulMal models for the proposed base scenarios. Left panel: grey solid bars represent the actual *P. falciparum* malaria morbidity profile observed over the 3,654-day simulation period. Solid lines show the *P. falciparum* malaria prevalence simulated by the MAC (black solid line labeled X), MAR (green solid line labeled YP), WCT (blue solid line labeled INC_W), and SimulMal (red solid line labeled Preval) models for the constant mean annual temperature and the constant monthly rainfall (annual rainfall homogeneously distributed throughout the year) of the municipality of Montelíbano. Only the MAC model requires longer periods to reach the equilibrium prevalence when the initial total number of infectious individuals is increased from 1 to 10% of the total population at risk. Right panel: grey solid bars represent the historical annual cycle of *P. falciparum* malaria incidence observed over the selected base period. Solid lines show the *P. falciparum* malaria prevalence simulated by the MAC (black dashed thin line), WCT (black shaded line) and SimulMal (black solid line) models for the historical annual cycles of mean temperature and rainfall.

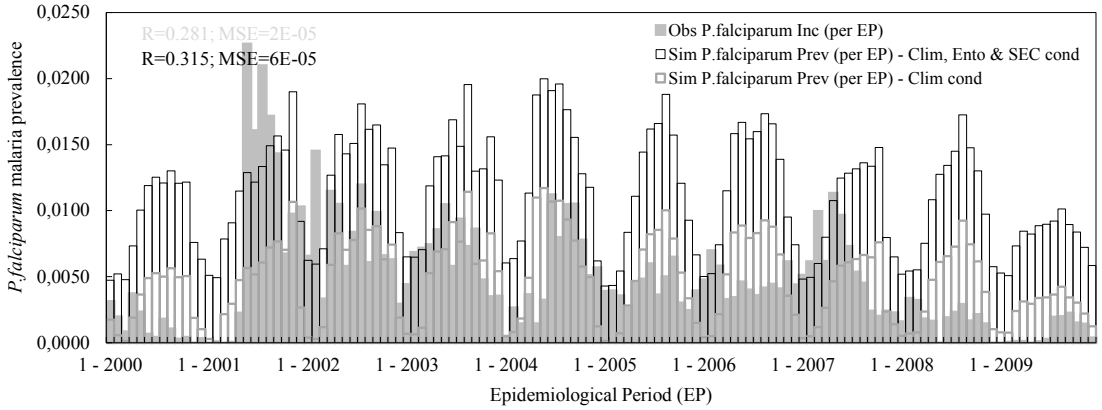

Figure 3. *Plasmodium falciparum* malaria incidence observed in the municipality of Montelíbano over the 3,654-day simulation period, along with *P. falciparum* malaria prevalence simulated by the WCT model for the observed climatic conditions (*Clim cond*) and the observed climatic, entomological and socioeconomic conditions (*Clim, Ento & SEC cond*). WCT simulation outputs and the actual *P. falciparum* malaria morbidity profile are compared over a 3,157-day simulation period that spans from May 14, 2001 (daily time step t=498) through January 3, 2010 (t=3,654), or EW 20 / 2001 through EW 52 / 2009, and on an epidemiological period (EP) time scale. The grey solid bars depict the actual *P. falciparum* malaria incidence per epidemiological period; the pale grey and black bars represent the *P. falciparum* malaria prevalence per epidemiological period simulated by the WCT model (see correlation coefficient R and mean square error MSE on the top left corner) for the observed *Clim cond* and the observed *Clim, Ento & SEC cond*, respectively.

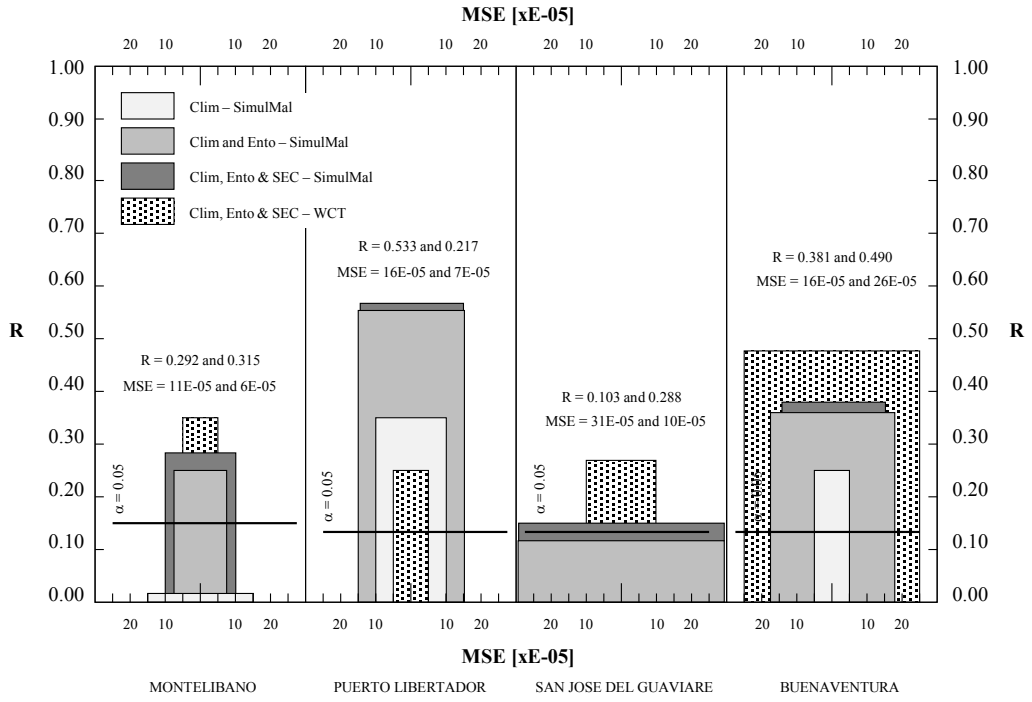

Figure 4. SimulMal and WCT *Plasmodium falciparum* malaria simulation results. From left to right: municipalities of Montelíbano, Puerto Libertador, San José del Guaviare, and Buenaventura. Correlation coefficients between actual *Plasmodium falciparum* malaria morbidity profiles and simulated prevalence are plotted on primary and secondary y-axes. α=0.05 represents the threshold above which correlation coefficients are statistically significant at 95% confidence level. Mean square errors (MSE) are displayed on primary and secondary x-axes. SimulMal model results for local climatic (Clim - SimulMal), local climatic and entomological (Clim and Ento - SimulMal), and local climatic, entomological and socioeconomic conditions (Clim, Ento & SEC - SimulMal) are plotted with pale grey, full grey, and dark grey bars, respectively. WCT model results are only shown for local climatic, entomological and socioeconomic conditions (grey shaded bars labeled Clim, Ento & SEC - WCT).

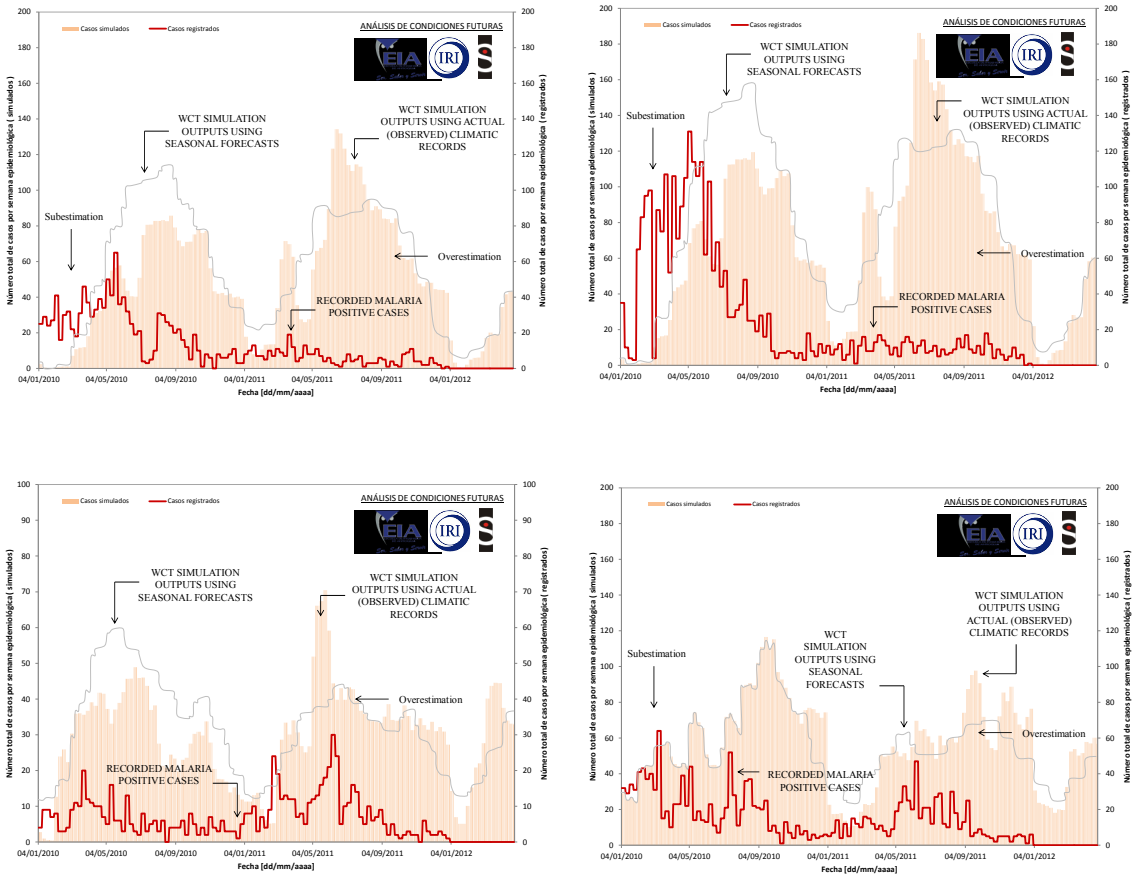

Figure 5. *Plasmodium falciparum* malaria positive cases (red solid line) observed in the municipalities of Montelíbano (top left panel), Puerto Libertador (top right), San José del Guaviare (bottom left), and Buenaventura (bottom right) per epidemiological week, along with malaria primary cases simulated by the Microsoft Office Excel 2007® version of the WCT model for the forecast horizon spanning from January 4, 2010 through April 19, 2012. Simulations include outputs using seasonal forecasts (grey solid line) and actual climatic records (orange solid bars).

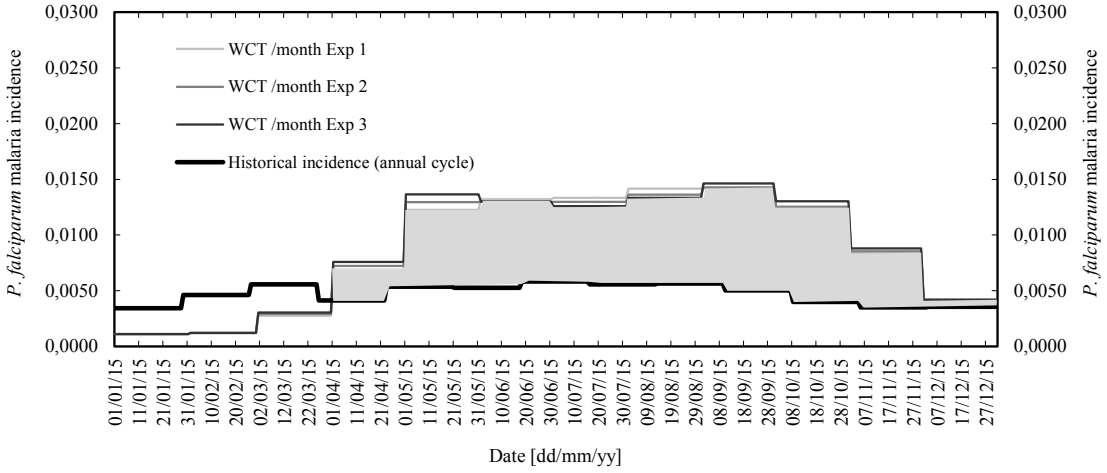

Figure 6. Monthly *Plasmodium falciparum* malaria incidence suggested by the WCT model for the medium-term forecast horizon spanning from January 01, 2015 through December 31, 2015, and for the pilot municipality of Montelíbano. Exp 1, 2 and 3 represent the proposed medium-term climate forecast experiments. Only changes in climatic conditions are considered in these simulations. Shadow area depicts the suggested increase in malaria incidence.

Chapter 6[16]

General conclusions, final remarks and future work

6.1. General conclusions and final remarks

This PhD thesis described my research activities recently conducted in the field of 'climate studies in service to society'. A balance between the two multifactorial systems under study was proposed by dedicating two chapters to each area of interest. In the analysis of climatic stress on high-altitude Andean ecosystems my attempt was to integrate the study of near-term climate change trends derived from weather stations, simulation, reanalysis, sea surface temperature, and satellite data, with the analysis of changes in hydrological regimes, the extent of life zones, and the increased occurrence and rapid spread of high-altitude fires. The goal was to provide some elements for the study of potential impacts on the integrity of páramo environments (and in general for their ecosystem goods and services) of the self-reinforcing cycle resulting from changes in atmospheric instability. My research contributes with climate trends obtained from high quality weather station data, particularly important for a region with a sparse hydrometeorological network, as well as from ensemble simulation runs of a general circulation model with the highest skill level in the tropical Andes. Results documented herein agree with the rapid and sustained increasing trend (with faster rates in the last two decades) of minimum and maximum temperatures observed over the Andes. Results also suggest increases in

[16] This chapter uses elements from the book chapter 'Risk management at the Latin American Observatory' by Muñoz et al. (2012) and from the outreach article 'Five-tiered integrated climate-related biodiversity vulnerability assessment in the Tropical Andes' by Ruiz et al. (2012). Copies of these manuscripts are available in the digital backup of this thesis.

the occurrence of unusually heavy rainfall events and give some insights into the differences in precipitation trends between the northern and southern tropical Andes. They also document differences with altitude in sunshine and rainfall records, particularly in the study conducted for the northern Andes. My research also provides continuous and homogeneous easy accessible temperature and humidity data logger data from several high-Andean regions, which could contribute to improve our understanding of convection processes in areas with complex orography such as the Andean region.

As for the dynamics of *Plasmodium falciparum* malaria infections, my research activities focused on the analysis of various malaria process-based models and the creation of a multi-model ensemble. I proposed an experimentation-validation-analysis process to assess the role that climatic and non-climatic factors (and confounders) play in the transmission dynamics of *P. falciparum* malaria. Such a process could improve our understanding of the nonlinearities, time-delays and feedbacks behind the complexity of this disease. It could also allow us to assess the potential key drivers of malaria epidemics and the potential consequences of long-term changes in climatic conditions for the timing and severity of malaria outbreaks. My research findings suggest that increases in near-surface temperatures and nonlinear changes in the mean duration of host's infectivity could be synergistically driving the increasing incidence of *P. falciparum* malaria in epidemic-prone regions. They also fill in an important gap in entomological studies and provide a better understanding of the role of non-climatic factors in malaria transmission. I also studied current decision-making processes and the role of control interventions in specific pilot sites with different eco-epidemiological settings, and helped to set up environment-informed systems by building local capacity. In Colombia, in particular, the process required me to promote the cooperation between several institutions and multiple experts working on the

adaptation strategy to climate change. Lastly, I explored some key aspects of uncertainty and sensitivity in the dynamics of this important vector-borne disease. I believe that with this work I have established the preliminary basis for a Malaria Early Warning System framework supported on seasonal forecasting capabilities, weather and environmental monitoring, and malaria dynamical models.

I hope that my research findings in these two fields could contribute to the ongoing adaptation efforts in the Tropics, particularly those efforts related to conservation planning of hotspot protected areas and malaria integrated surveillance systems. The academic exercise required me to reach six milestones along the way, which were socialized in my PhD thesis proposal: 'Exploring evidence'; 'Formulating hypothesis and causality'; 'Instrumenting and processing data'; 'Creating mathematical tools'; 'Documenting'; and 'Socializing and building capacity'. A brief description of these key aspects is presented below.

Exploring evidence. Evidence of long-term changes in the dynamics of high-altitude Andean ecosystems and *Plasmodium falciparum* malaria infections were explored during the first stages of this research. For instance, see in figure 1: (top panel) El Niño warm event riding on top of the long-term trend in the total number of days per year when near-surface ambient temperatures (weather data observed at 1,310 m above sea level) were above the temperature threshold of 21.5°C, which is considered critical for the successful development of numerous pests and pathogens. And (bottom panel) long-term trends in malaria incidence in the Americas observed over the period 1959-2000.

Formulating hypothesis and causality. In the analysis of the ongoing radiative positive feedback mechanism and the concomitant increase in climatic stress on high-altitude Andean environments (see figure 11 in chapter 3), the suggested driving mechanisms explored here included: faster upper-tropospheric warming, particularly in the tropical belt; rapid upward shifts in freezing levels; and decreases in the amount of fog and cloud cover in high-altitude environments and upper levels. For the analysis of increases in the incidence of *Plasmodium falciparum* malaria, potential culprits included: global long-term climate change, increased antimalarial drug resistance, and depletion of malaria control interventions.

Instrumenting and processing data. Total twenty-nine (29) U23-001 HOBO® temperature and relative humidity (T/RH) data loggers/digital sensors were installed in the study sites of this dissertation. In the surroundings of the Claro River high-altitude basin, five (5) (T/RH) data loggers were installed on its headwaters in the main transitions between life zones. Hourly temperature, relative humidity and dew point records from this altitudinal transect span back to mid-December, 2008. In the Colombian-Ecuadorian and Bolivian-Peruvian altitudinal ecotransects at least twelve (T/RH) data loggers were installed in each of the study areas, at elevational intervals of 500 meters across two ca. 4,500 m altitudinal gradients and in as many ecosystems as possible. Hourly records from these transects are available for the historical period spanning from early August, 2011 through date. Records are being shared with all the main institutions involved in research activities in text files and MS Excel spreadsheets.

Creating mathematical tools. Fifteen (15) malaria process-based (biological/dynamical) models were revisited and built in five platforms: Powersim Constructor® Version 2.51, Powersim Studio 8 Academic®, Microsoft Office Excel 2007®, Scilab® (free open source software), and IRI Data Library. Ingrid codes for the IRI Data Library expert mode were also created for the analysis of coupled ocean-atmosphere climate models simulation outputs along the axis of the Andes Cordillera (see chapter 3 for, specifically, the ECHAM4.5 model ensemble simulation runs), specifically, mean annual near-surface and free air temperatures, environmental lapse rates, dew points, specific humidity, squared moist and dry Brunt-Väisälä frequencies, lifting condensation levels, and convective available potential energies.

A Geographic Information System platform has also been created to integrate and analyze all the components and functional relationships of high-altitude environments at local scale. Secondary information and up-to-date data gathered during field campaigns have been incorporated into the tool. The framework includes the following georreferenced features and primary data: (i) main characteristics of high-altitude watersheds, including topography, drainage network, life zones, and vegetative cover; (ii) key sites of areas under study including snowlines, water bodies and wetlands; (iii) tracks, Global Positioning System marks and photographic records; (iv) hydrological information, meteorological records and field data including streamflow measurements, water quality assessments, water bodies perimeters, and experimental vegetation plots.

Documenting. Research projects (conducted and ongoing) have been documented in five (5) final reports[17]. One (1) in-press outreach article, four (4) to-be-submitted research articles, three (3) already-published research articles, and seven (7) already-published book chapters (see footnotes on first page of each chapter) resulted from the research activities described here.

Socializing and building capacity. Total fourteen (14) peer-reviewed talks in congresses, seminars and scientific events, thirteen (13) lectures in seminars and congresses, and twenty-five (25) training workshops (see full list in my online public profiles) were given over the past 5 years of research activities. Two (2) short video clips on the work on Andean high-altitude environments, one (1) virtual catalog of páramo flora, and one (1) online course on the analysis of malaria transmission dynamics were also prepared and widely distributed.

---

[17] 2010-2011 and 2011-2012 annual narrative reports of the project 'Impacts of climate change on biodiversity in the tropical Andes: climate-related risk, vulnerability, and decision making tools for conservation planning', 13 and 16 pages in total, respectively.

Simulating malaria transmission dynamics in the pilot sites of the Integrated National Adaptation Pilot Project – Second phase. Contents: I – Malaria transmission models; II – Description of pilot sites; III – Simulation outputs; IV – Complementary activities I: capacity building, operative platform and exogenous datasets; V – Complementary activities II: risk analysis, non-climatic factors, conclusions and recommendations; VI – Comments by National Institute of Health and supplementary material. Antioquia School of Engineering, National University of Colombia – Bogotá, and CES University, 2011, 338 pages.

Simulating malaria transmission dynamics in the pilot sites of the Integrated National Adaptation Pilot Project. Contents: I – Malaria transmission models; II – Description of pilot sites; III – Simulation outputs; IV – Complementary activities, conclusions and recommendations. Antioquia School of Engineering, National University of Colombia – Bogotá, and CES University, 2010, 312 pages.

Signals of climate variability and change in surface water supply of high-mountain watersheds. Case study: high mountain basins of the Claro and Otun rivers, Los Nevados Natural Park, Andean Central Mountain Range, Colombia. Contents: 1 – Introduction; 2 – Methodology; 3 – GIS platform; 4 – Water balance; 5 – Life zones; 6 – Ecosystems integrity; 7 – Analysis of climatic conditions. Antioquia School of Engineering, 2010, 92 pages.

Signals of climate variability and change in surface water supply of high-mountain watersheds. Case study: Claro River high mountain basin, Los Nevados Natural Park, Andean Central Mountain Range, Colombia. Contents: Introductory chapter: Summary for Policy-Makers; 1 – Lifting Condensation Level; 2 – Water balance; 3 – Life zones; 4 – High mountain fires; 5 – Ecosystem integrity and importance; 6 – Analysis of climatic conditions; Final chapter: Conclusions and final remarks. Antioquia School of Engineering, 2008, 250 pages.

6.2. Future work

As a direct result of the various activities conducted in this thesis, four research projects have been formulated (and are currently underway). A brief description of our research interests is presented below.

6.2.1. Dendrochronological potential of *Polylepis* and *Espeletia* in the high-altitude ecosystems of the Colombian Central Cordillera, South America

The most recent paleoclimate reconstructions for the Tropical Andes have been carried out in Peru, Bolivia and northern Chile (e.g. Thompson et al., 2003), with relatively coarse temporal resolution. In the surroundings of El Ruiz-Tolima volcanic massif, the paleoecological history of the last 6,000 to 50,000 years was reconstructed through volcanic soil sequences, glacial geomorphology, mineralogy, sediments, and pollen deposits (Kuhry et al., 1983; Bakker and Salomons, 1989; Cleef et al., 1995; Thouret et al., 1997). There are no high-resolution paleoclimatic reconstructions in the area under study. To fill in the gap, I have recently joined efforts with Dr. Laia Andreu Hayles, who is currently a Postdoctoral Research Scientist at the Tree Ring Lab, Columbia University in the City of New York (USA), in order to explore the dendrochonrological potential of some tree species in the El Ruiz-Tolima volcanic massif, and to develop more creative approaches that could help the research group to extract the climatic signal from other plant species. These research activities represent the first step forward of our long-term research interests in reconstructing, through ring-width or isotope chronologies, the past climate variability in high-altitude environments with annual resolution for the Holocene.

Two species in particular, namely *Polylepis sericea* and *Espeletia hartwegiana*, are drawing the interests of these activities.

Polylepis sericea (see left picture in figure 2) can be found in rainy subpáramo, wet subpáramo and rainy páramo, in the altitudinal range 3,200-4,300 m. The suitability of the genus *Polylepis* for dendrochronological studies has been successfully demonstrated with *Polylepis australis* in Central Argentina (Suarez et al., 2008) and with *Polylepis tarapacana* in two different sites. One study was conducted in the high-elevation alpine dry land (at around 4,750 m) in the subtropical mountains of northwestern Argentina (Morales et al., 2004) and the other in the Bolivian plateau at 4,000 and 5,200 m (Argollo et al., 2004). The longest tree-ring series were found in the latter study ranging from 98 to 705 years. Although several studies on the ecology and physiology of *Polylepis sericea* have been published in the Venezuelan Andes (Rada et al., 1996; Azocar et al., 2007; Rada et al., 2009), a systemic dendrochronolgical work with this species has not been carried out yet.

Espeletia hartwegiana (see right picture in figure 2), can be found in rainy subpáramo, wet subpáramo, rainy páramo, and rainy superpáramo, at altitudes that range from 3,200 m to slightly above 4,300 m. The inner part of the *Espeletia hartwegiana* stem is empty, making the classical dendrochronological approach impossible. However, the leaves from this species remain on the stem after their death making possible an innovative approach to obtain a paleoclimatic record. This original approach is based on analyzing the isotope signatures of the dead leaves from the different layers of the stem. A similar idea was successfully performed using isotope ratios of *saguaro* cactus spines (English et al., 2007). The isotopic records obtained from the chronosequence of cactus spines demonstrated the potential of this type of tissues to record past physiological and climatic variation.

The development of *Polylepis sericea* tree-ring width chronology will include sampling 15 trees approximately, with at least 2 samples per tree. The standard dendrochonrological techniques will be performed at the Tree Ring Lab in order to cross-date the collected samples and to build a master tree-ring chronology of this stand. The stable isotope pilot study of *Espeletia hartwegiana* will involve a detailed study of the stem and leaves of this species in the field. This visual analysis will allow the research group to carefully collect and classify the leaves formed in the different layers of the stem obtaining a chronosequence of *Espeletia* leaves. The leaves will be analyzed by means of a mass spectrometer in order to determine the isotopic signature of $\delta^{13}C$ and $\delta^{18}O$. Response functions will be performed with the *Polylepis* ring-width chronology and *Espeletia* isotopic records versus local meteorological data, in order to evaluate the climatic signal contained in these records.

6.2.2. Reconstructing Late Quaternary tropical glacier change through He-3 surface-exposure dating

As previously stated, mountain glaciers in the area of Los Nevados Natural Park (as in all mountain ranges in Colombia) are rapidly melting. In order to support a larger investigation into tropical climate led by scientists at Columbia's Lamont-Doherty Earth Observatory (LDEO) of the Earth Institute, Columbia University in the City of New York (USA) (for further information see http://blogs.ei.columbia.edu/tag/peru-glaciers/), I will join research activities proposed for the ice-capped mountains of the Colombian Andes. I have recently teamed up with Dr. Gordon Bromley, who is currently a Postdoctoral Research Scientist at LDEO, to study rocks that record the ebb and flow of ice in the Santa Isabel Nevado and Sierra Nevada del Cocuy, in the

Colombian Central and Eastern Cordilleras, respectively. The general objective is to study a detailed record of Late Quaternary glacier change since the last ice age.

Glacier mass balance is controlled primarily by temperature, particularly in the humid tropics. Therefore, the research group is reconstructing both the timing and magnitude of past glacial advances so as to build a long-term record of temperature change from the northern tropical Andes. Specifically, we are interested in the last 30,000 years, a period encompassing the last glacial maximum, late-glacial period, and Holocene. Field work will involve detailed mapping of glacial deposits and landforms in the Colombian cordilleras and collection of samples from moraines for He-3 surface-exposure dating. We anticipate that this investigation will provide a northern hemisphere counterpart to existing datasets from the Peruvian Andes.

6.2.3. Impacts of climate change on biodiversity in the Tropical Andes

Climate change and vulnerability analyses at a local scale – the scale most relevant to decision makers and land-use planners – are virtually non-existent in the Andes. With regard to biodiversity, large-scale patterns and gradients of species richness are fairly well established in the region for a handful of selected taxonomic groups, but vast knowledge gaps exist at smaller spatial scales and for the great majority of taxonomic groups. Local biological inventory data, where available, have not been integrated into multidisciplinary analyses. Furthermore, although recent advances in the mapping and classification of Andean ecosystems represent immense progress, how vulnerable these ecosystems are to climate change can only be crudely guessed in the most general terms. Thus, an integration of all this available information and approaches into local-scale analyses represents a novel approach in the Andes.

I have recently joined a five-tiered research project in which the team group is studying near-term climate change trends, land-use patterns, biodiversity patterns and gradients, the vulnerability of species and ecosystems to changes in historical climatic conditions, as well as local perceptions of climate variability and change in two binational transboundary study areas: on the Pacific slope of the northern Andes in the border region between Colombia (Nariño department) and Ecuador (Carchi province), and on the Amazonian slope of the central Andes in the border region between Bolivia and Peru, in the Madidi – Apolobamba – Bahuaja-Sonene – Tambopata protected area complex (see chapter 3). These regions are renowned for their exceptional biodiversity and endemism and have been considered key Andean biodiversity hotspots. Results will then be integrated to pinpoint high-risk areas and ecosystems that are particularly vulnerable to the synergistic effects of long-term climatic changes and land-use change. The objective is to assist the four Tropical Andean countries (Bolivia, Colombia, Ecuador, and Peru) in the implementation of a standard methodology for estimating climate change risks for biodiversity at a local scale that could subsequently be expanded to other strategic areas. The overall goal is to support and guide adaptation measures and sustained conservation programs for key tropical environments.

The ongoing research project has five main components: climate, biodiversity, social, land use/cover, and outreach and capacity building. The main objective of the climate component is to develop knowledge on local climate gradients and to determine short- to medium-term climate scenarios (10-20 years ahead) by combining observed and projected climate trends derived from computer modeling, climatological field stations (ground-truth data), climate change indices, local temperature and humidity records from digital sensors, and reconstructions of pre-instrumental periods through classical dendrochronological techniques (tree-ring records).

Spatial scales of analysis include local and regional conditions. Analyses of the former include case studies in the two binational transboundary areas specifically examining historical minimum temperatures, maximum temperatures, and daily rainfall. Analyses of regional conditions are based on evidence from near-term historical climate models' simulation runs (reanalysis data) and comprise the full length of the Andes Cordillera and all pressure levels (see chapter 3).

As previously mentioned, at least 12 data loggers/digital sensors measuring temperature and relative humidity at hourly intervals have been installed in each of the study areas to complement the available hydrometeorological networks, which include 75 and 17 weather stations in the Colombian-Ecuadorian and Bolivian-Peruvian transboundary regions, respectively. Data loggers have been deployed at elevational intervals of 500 meters across two ca. 4,500 m altitudinal gradients (see figure 3) and in as many ecosystems as possible. Gathered data are improving our understanding of the physical processes taking place along the altitudinal transects such as conditions of atmospheric instability, and local seasonal temperature and precipitation anomalies. A better understanding of local mechanisms and their relationships with interannual (El Niño-Southern Oscillation events) to multi-decadal phenomena will provide elements for the analysis of long-term changes and for better simulation and validation efforts. Digital sensor data are currently being combined with weather station records, whose historical periods span over 50 years, to build a set of climate change indices and to assess near-term historical conditions of atmospheric instability and moist convection in the two study areas.

The dendrochronological work, in turn, aims to reconstruct the past ca. 100-200 years along the upper portion of the elevational gradients. A long list of Andean tree species has been analyzed to identify key species with sufficiently wide elevational ranges, distinctive annual rings, and long life spans. The result, a short list of tree species with dendrochronological

potential currently includes 5 species for the analysis of páramo environments and high-Andean forests (such as *Polylepis incana* and *Weinmannia cochensis*) and 5 species in upper cloud forests (such as *Symplocos carmencitae*, *Ocotea* sp. and *Cedrela montana*). The oldest individuals of the selected tree species have been georeferenced, initially in the Colombia-Ecuador border area, in relatively well preserved environments. To date the group has sampled 64 increment cores of *W. cochensis*, 139 of *P. incana*, 76 of *S. carmencitae*, 65 of *Ocotea*, and 64 of *C. montana*. Tree-ring width chronologies are currently under construction and radiocarbon analyses will be used to assess periodicity (i.e. annual) of tree rings in different species.

6.2.4. Risk management at the Latin American Observatory

The Observatorio Latinoamericano de Eventos Extraordinarios (OLE^2), or Latin American Observatory, is a collaborative network that aims to increase the efficiency of regional and local decision-making processes, by providing more accurate environmental information and exchanging experiences on data, methodologies and scientific products. Activities are being conducted through a standardized methodology and a Web-sharing service. The goal of the OLE^2 is to monitor and forecast key environmental variables and develop accurate products based on different scientific tools, in order to help decision makers improve risk management and set up efficient early warning systems. Since the OLE^2 aims to provide model outputs for, among others, climate and health applications, I am using several of the mathematical tools discussed herein to improve the decision-making processes of some regional health services. Specifically, I have joined efforts with the OLE^2 initiative to strengthen the malaria integrated surveillance and control system in Colombia, and to set up the Dengue Early Warning System in Ecuador.

Malaria integrated surveillance and control system in Colombia. As mentioned before, the Colombian National Institute of Health (INS) recently teamed up with the Institute of Hydrology, Meteorology and Environmental Studies (IDEAM) and several universities and research centers to design and implement a proactive, collaborative, multidisciplinary, Integrated Surveillance and Control System (ISCS). This initiative is part of a set of measures and policy options that the Colombian adaptation strategy to climate change proposed for three areas of primary concern: the high-altitude Andean ecosystems, the insular and coastal areas, and human health.

The aim of the adaptation strategy for the health sector is to have a better-prepared institutional arrangement for increased exposure to malaria and dengue fever, two climate-sensitive, vector-borne diseases that are still considered human health burdens in Colombia. The potential increase in the incidence of these two diseases is likely to occur not only in the already endemic malaria and dengue fever prone areas, but also on the fringes with the Andean regions where local communities have not been exposed to pathogens before. The approach has been to assist the health sector to better cope with current climate variability and climate-related events, as a means to make it better prepared against future climatic conditions likely to be brought by the ongoing long-term global climate change. As a result, Colombia has been working on reducing people's vulnerabilities to the negative impacts of malaria and dengue outbreaks, as well as on developing an Early Warning System framework (already described in chapter 5), supported by seasonal forecasting capabilities, weather and environmental monitoring, and statistical and dynamic models.

The implementation of the ISCS has required, among many other activities, analyzing the local eco-epidemiological settings of various malaria- and dengue fever-prone pilot sites,

implementing process-based biological and statistical models, and strengthening the local capacity of health authorities. It has also required strengthening the IDEAM capability to routinely and systemically produce and disseminate, relevant, continuous, homogenous, and reliable climate information that could support the decision-making process of health authorities. Such information includes ground-truth historical records, modeling simulation outputs, seasonal forecasts, El Niño Southern Oscillation forecasts, and climate change predictions. All this information, along with disease morbidity profiles, entomological conditions, socio-economic drivers, and impacts of interventions and control campaigns, is now steadily becoming a core part of routine activities and disease control plans of health services at regional, municipal and local levels, and is starting to facilitate a better allocation of health resources and more cost-effective preventive responses. On a broader scale, measures proposed as part of the adaptation plan have been mainstreamed into the Colombian political agenda to ensure their sustainability. They have reached, for instance, the 2010-2014 National Development Plan, the 2010-2014 Environmental Action Plan, the Colombia's Poverty Reduction Plan, and the Public Health National Plan.

Climate and dengue fever in Ecuador. The Ecuadorian National Institute of Meteorology and Hydrology (INAMHI) has conducted various research activities on the analysis of potential increases in the incidence of malaria and dengue fever in key lowland provinces (Muñoz et al., 2010; Muñoz and Recalde, 2011). Activities have included the implementation and coupled analysis of the 30 km WRF (Weather Research and Forecasting) dynamic downscaling regional climate model, and the Ross-Macdonald malaria infectious disease process-based model, to reproduce the spatio-temporal variability of primary positive cases reported by the National Malaria Eradication Service over a recent 13-year historical period. Activities have also included

a first design of an Early Warning System for malaria and dengue fever outbreaks, which is now developing into an integrated surveillance and climate modeling for malaria and dengue fever predictability in rural and urban settings. The INAMHI has also joined efforts with several research groups to broaden the understanding of the complex transmission dynamics (in both space and time) of these vector-borne diseases, in order to improve decision-making processes in regional and local health authorities and, in a more general sense, to strengthen the already solid surveillance and control activities of infectious diseases conducted by the Ecuadorian health sector.

References

Argollo, J., C. Soliz, and R. Villalba, 2004. Dendrochronological potential of *Polylepis tarapacana* in the Central Andes. Ecología en Bolivia 39(1): 5-24.

Azocar, A., F. Rada, and C. Garcia-Nunez, 2007. Functional characteristics of the arborescent genus *Polylepis* along a latitudinal gradient in the high Andes. Interciencia 32(10): 663-668.

Bakker, J.G.M. and J.B. Salomons, 1989. A palaeoecological record of a volcanic soil sequence in the Nevado del Ruiz area, Colombia. Review of Palaeobotany and Palynology 60:149-163.

Cleef, A.M., G.W. Noldus, and T. van der Hammen, 1995. Estudio palinológico del Pleniglacial Medio de la sección Río Otoño-Manizales Enea (Cordillera Central, Colombia). In: T. van der Hammen and A.G. dos Santos, editors. Studies on Tropical Andean Ecosystems. Volume 4. Pages 441-449. Cramer (Borntraeger), Berlin/Stuttgart, Germany.

English, N.B., D.L. Dettman, D.R. Sandquist, and D.G. Williams, 2007. Past climate changes and ecophysiological responses recorded in the isotope ratios of *saguro* cactus spines. Oecologia 154: 247-258.

Kuhry, P., J.B. Salomons, P.A. Riezebos, and T. Van der Hammen, 1983. Paleoecología de los últimos 6,000 años en el área de la Laguna de Otún-El Bosque. In: T. van der Hammen, P.A. Perez and P. Pinto (ed.). Studies on Tropical Andean Ecosystems. Volume 1. Pages 227-261. Cramer (Borntraeger), Berlin/Stuttgart, Germany.

Méndez-Galván, J.F., 2006. Programa de control de la malaria en México: ¿es posible su eliminación?. Los vínculos entre investigación y políticas en salud colectiva, Rio de Janeiro, Brazil.

Morales, M.S., R. Villalba, H.R. Grau, and L. Paolini, 2004. Rainfall-controlled tree growth in high-elevation subtropical treelines. Ecology 85(11): 3080-3089.

Muñoz, A.G., D. Ruiz, and C. Recalde, 2010. Malaria biological models and dynamical downscaling for northwestern South America in the Observatorio Andino framework. ICID+18 / 2nd International Conference: Climate, Sustainability and Development in Semi-arid Regions, Fortaleza, Ceara (Brazil).

Muñoz, A.G., and C. Recalde, 2011. Reporte metodológico sobre el experimento de predicibilidad de malaria en el Litoral Ecuatoriano. Proyecto INAMHI-MAE-SCNPRAA-PACC. 52 pages.

Muñoz, A.G., D. Ruiz, P. Ramírez, G. León, J. Quintana, A. Bonilla, W. Torres, M. Pastén, and O. Sánchez, 2012. Risk management at the Latin American Observatory. Chapter 22 in Risk Management - Current Issues and Challenges, Nerija Banaitiene (Ed.), ISBN: 978-953-51-0747-7, InTech, available online at: http://www.intechopen.com/books/risk-management-current-issues-and-challenges/risk-management-at-the-latin-american-observatory.

Pan American Health Organization, 2006. Regional strategic plan for malaria in the Americas 2006-2010. Washington, D.C., ISBN 92 75 12641 0, 85 pages.

Rada, F., A. Azocar, B. Briceno, J. Gonzales, and C. Garcia-Nunez, 1996. Carbon and water balance in *Polylepis sericea*, a tropical treeline species. Trees 10(4): 218-222.

Rada, F., C. Garcia-Nunez, and S. Rangel, 2009. Low temperature resistance in saplings and ramets of *Polylepis sericea* in the Venezuelan Andes. Acta Oecologica 35(5): 610-613.

Ruiz, D., S.K. Herzog, P.M. Jørgensen, T.H. Larsen, R. Martínez, J.J. Nieto, S.V. Poats, and M. Ohira, 2012. Five-tiered integrated climate-related biodiversity vulnerability assessment in the Tropical Andes. Mountain Research Initiative Newsletter 7: 7-11. Available online at: http://mri.scnatweb.ch/es/global-news/mri-newsletter.

Suarez, M.L., D. Renison, P. Marcora, and I. Hensen, 2008. Age-size-habitat relationships for *Polylepis australis*: dealing with endangered forest ecosystems. Biodiversity and Conservation 17(11): 2617-2625.

Thompson, L.G., E. Mosley-Thompson, M.E. Davis, P.N. Lin, K. Henderson, and T.A. Mashiotta, 2003. Tropical glacier and ice core evidence of climate change on annual to millennial timescales. Climatic Change 59: 137-155.

Thouret, J.C., T. van der Hammen, B. Salomons, and E. Juvigné, 1997. Late quaternary glacial stages in the Cordillera Central, Colombia, based on glacial geomorphology, tephra-soil stratigraphy, palynology, and radiocarbon dating. J. Quaternary Science 12(5): 347-369.

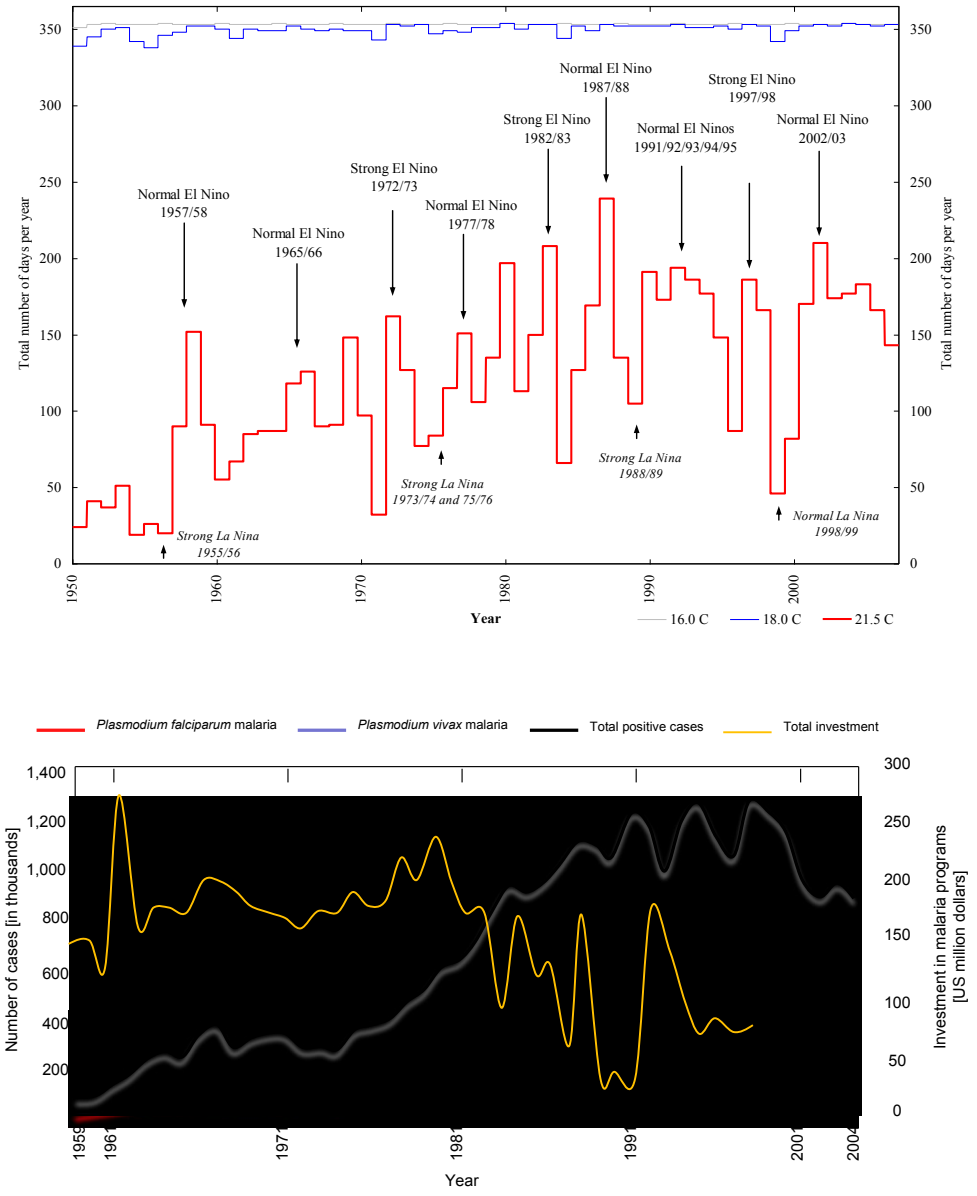

Figure 1. Potential evidence of long-term changes in the dynamics of high-altitude Andean ecosystems and *Plasmodium falciparum* malaria infections. Top panel: total number of days per year when mean ambient temperatures, gathered at the weather station Cenicafé located at 1,310 m in the surroundings of the El Ruiz-Tolima volcanic massif, on the Colombian Central Cordillera, were above 16.0°C (grey solid line), 18.0°C (blue solid line), and 21.5°C (red solid line). Bottom panel: malaria in the Americas over the period 1959–2004 (source: Regional Strategic Plan for Malaria in the Americas 2006-2010 (Pan

American Health Organization) and Malaria Control in the Americas 1958–1999 (Méndez-Galván, 2006)).

Figure 2. *Polylepis sericea* and *Espeletia hartwegiana* individuals.

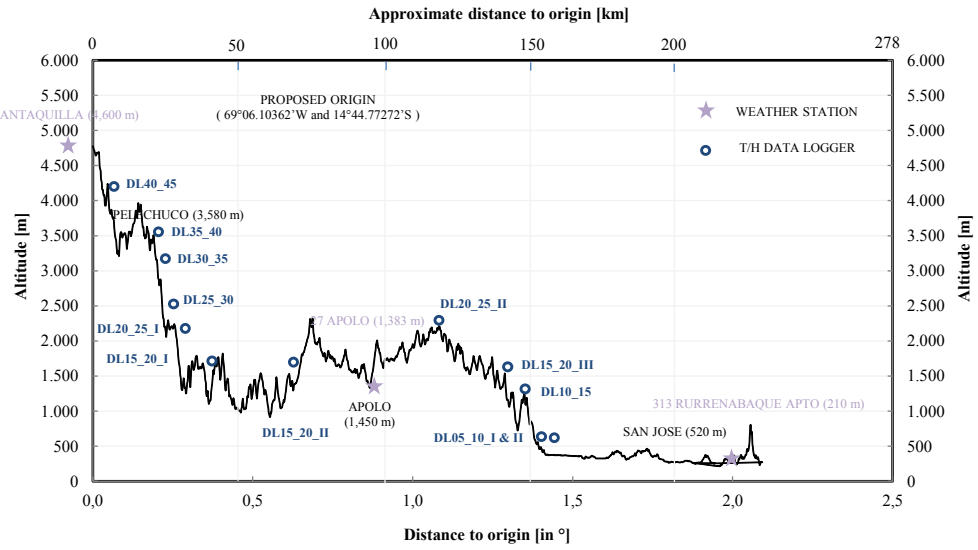

Figure 3. Vertical profile of the 4,500 m altitudinal ecotransect and location of the temperature/relative humidity data loggers on the Amazonian slope of the Central Andes, in the border region between Bolivia and Peru.

Appendices - Supplementary material

Chapter 2 - Climatic stress on high-altitude Andean ecosystems

Available historical periods of weather station data. As presented in the main text, a total number of 37 weather stations, located in the spatial domain 04°25'N-05°15'N and 75°00'W-76°00'W, were considered to assess local changing climatic conditions. Their datasets comprise daily, monthly and annual records of sunshine, rainfall, minimum and maximum temperatures, relative humidity, and diurnal temperature range. Sunshine variables include: total sunshine (SR1, in hours), total number of foggy days (SR2, in days), total number of sunny days (TSD, in days), daily maximum sunshine (SR4, in hours), daily mean sunshine (SR5, in hours), daily minimum sunshine (SR6, in hours), and day-to-day standard deviation of daily sunshine (SR7, in hours). Rainfall variables include: total amount (R1, in mm), total number of dry days (R2, in days), and maximum daily rainfall (R3, in mm). Minimum temperature variables include: minimum temperatures on the warmest days (MTmin, in °C), average minimum temperatures (ATmin, in °C), minimum temperatures on the coldest days (mTmin2, in °C), and day-to-day standard deviation of minimum temperatures (SDTmin, in °C). Maximum temperature variables include: maximum temperatures on the warmest days (MTmax, in °C), average maximum temperatures (ATmax, in °C), maximum temperatures on the coldest days (mTmax2, in °C), and day-to-day standard deviation of maximum temperatures (SDTmax, in °C). Relative humidity variables include: maximum relative humidity (MRH, in %), mean relative humidity (ARH, in

%), minimum relative humidity (mRH2, in %), and day-to-day standard deviation of relative humidity (SDRH, in %). Lastly, diurnal temperature range variables include: maximum diurnal temperature range (MDTR, in °C), mean diurnal temperature range (ADTR, in °C), minimum diurnal temperature range (mDTR2, in °C), and day-to-day standard deviation of diurnal temperature range (SDDTR, in °C). The available historical periods of all these variables are presented in Table A.1. A detailed description of these records can be found in Ruiz (2009).

Table A.1. Available historical periods of weather station data. The longest historical time periods are highlighted with brackets. Temperature variables in this table include minimum temperature, maximum temperature and diurnal temperature range.

#	ID	Altitude [m]	Sunshine	Rainfall	Temperature	Relative humidity
1	2613510	1,020	N.A.	1963-2005	N.A.	N.A.
2	2614503	1,670	N.A.	1981-2004	N.A.	N.A.
3	2615517	2,200	N.A.	1992-2005	N.A.	N.A.
4	2121002	1,765	N.A.	1981-2005	N.A.	N.A.
5	2125011	2,960	N.A.	1960-2007	N.A.	N.A.
6	2125050	1,585	N.A.	1962-1979	N.A.	N.A.
7	2614009	1,520	N.A.	1981-2005	N.A.	N.A.
8	2614018	900	N.A.	1979-2005	N.A.	N.A.
9	2615006	890	N.A.	1963-2005	N.A.	N.A.
10	2302501	1,420	N.A.	N.A.	N.A.	N.A.
11	2615511	2,080	1970-2007	1968-2006	1969-2006	1969-2006
I	2615515	4,150	1982-2005	1981-2003	1981-2003	1981-2003
II	2125512	2,029	1979-1994	1975-2005	1978-2005	1977-2005
III	WMO 8014902	1,360	N.A.	1951-1970	N.A.	N.A.

#	ID	Altitude [m]	Sunshine	Rainfall	Temperature	Relative humidity
IV	WMO 8014904	1,360	N.A.	1950-1979	N.A.	N.A.
V	WMO 8014911	1,310	N.A.	1971-1980	N.A.	N.A.
VI	2613504	1,342	N.A.	1947-2005	1959-1995	1948-1995
VII	2612506	1,204	N.A.	1949-2007	1978-2007	N.A.
VIII	WMO 8021101	3,264	N.A.	1950-1979	N.A.	N.A.
IX	WMO 8021400	928	N.A.	1955-1993	N.A.	N.A.
X	CHEC 6-9009	2,600	N.A.	1963-2006	N.A.	N.A.
XI	City of Manizales	2,150 m	N.A.	N.A.	N.A.	N.A.
XII	2615502	1,310	1961-2007	[1942-2006]	[1950-2007]	[1950-2007]
XIII	2613505	1,381	1956-2007	1956-2006	1956-2007	1990-2007
XIV	2615505	2,088	[1955-2005]	1956-2005	1956-2005	1990-2005
XV	2615509	1,026	[1955-2005]	1963-2006	1956-2005	1990-2005
XVI	2613507	2,120	1961-2006	1961-2006	1961-2006	1990-2006
XVII	2612524	1,321	1987-2007	1986-2007	1987-2007	1990-2006
XVIII	2613506	1,635	1961-2007	1960-2007	1975-2006	1990-2006
XIX	2125513	1,453	1976-2006	1972-2006	1976-2006	1990-2006
XX	2613511	1,684	1978-2006	1977-2006	1978-2006	1978-2006
XXI	2613516	2,000	N.A.	1987-2005	1994-2006	1989-2006
XXII	2613514	4,000	N.A.	1994-2004	1994-2002	1997-2002
XXIII	2124509	3,250	N.A.	1987-2002	1984-1996	2001-2002
XXIV	2615016	3,240	N.A.	1970-2007	N.A.	N.A.
XXV	2302013	3,580	N.A.	1973-1994	N.A.	N.A.
XXVI	2615015	2,220	N.A.	1970-2007	N.A.	N.A.

N.A.: Not available

Inconsistencies and outliers in historical time series. As mentioned in the main text, daily time series were checked for inconsistencies, and potential outliers were detected through simple run sequence plots. Erroneous records that were found in daily data are summarized below.

Anomalous data were not detected in the available historical series of sunshine and relative humidity. As for total rainfall, the weather station XVII (ID 2612524) reported null daily rainfall records (not rain at all) throughout 1986. As for minimum temperatures, only two weather stations exhibited potential outliers: the met stations 11 (ID 2615511) and II (ID 2125512). The former reported a minimum temperature of 1.3°C in October, 2004, despite the fact that over the period spanning from July, 1970 through April, 2006, this weather station recorded minimum temperatures on the coldest days with a sample mean of 9.9°C, a standard deviation of 1.1°C, a minimum value of 6.0°C, and a maximum value of 12.4°C. The weather station II (ID 2125512), in turn, reported minimum temperatures of 1.4°C on July 20, 2002 and November 18, 2002. Over the period 1978-2005, the average minimum temperature on the coldest days gathered at this weather station in July reached 11.6°C, with a standard deviation of 1.1°C. In November, these records reached values of 12.3 and 1.3°C, respectively. As for maximum temperatures, the weather station XVII (ID 2612524) reported a temperature of 15.3°C on April 16, 2007, lower than the average minimum temperature on the coldest days in April, which reached 15.8°C±0.9°C. The weather station XXI (ID 2613516) reported a maximum temperature of 37.8°C in April, 1995, very unusual for a met station located at 2,000 m above sea level.

Year-to-year changes in seasonal conditions. December-January-February (DJF), March-April-May (MAM), June-July-August (JJA), and September-October-November (SON) time series were also processed to support the analysis. In this supplementary material only results pertaining to the total sunshine and minimum temperatures on the coldest days are included. Tables A.2 to A.5 present the main results of the hypothesis tests that were implemented to detect long-term linear trends in the DJF, MAM, JJA, and SON total sunshine, respectively. Only weather stations with available data are presented. ITT, IHP, IMK, and ISN depict the results of the Student's t-test, the Hotelling-Pabst test, the non-parametric Mann-Kendall test, and the aligned rank Sen's t-test, respectively. Letter 'R' denotes when the null hypothesis of a zero slope parameter is rejected at a 95% confidence level (i.e. there is a statistically significant long-term trend in the time series). Letter 'A' denotes when the null hypothesis was accepted. The highest slope parameters or trend magnitudes among seasons are highlighted with brackets. Based on the results of those weather stations that recorded statistically significant trends in total sunshine, it can be argued that the strongest changes in this climatic variable occurred during the DJF season.

Table A.2. Long-term linear trends (statistically significant at a α=0.05) in DJF total sunshine

#	Altitude [m]	ITT	IHP	IMK	ISN	Trend [hours/decade]	Average total sunshine [hours]
11	2,080	A	A	A	A	Not significant	449
I	4,150	A	R	R	R	[+14.4]*	257
II	2,029	A	A	A	A	Not significant	352
XII	1,310	R	R	A	R	[-20.9]	491

XIII	1,381	R	R	A	R	[-20.3]	493
XV	1,026	R	R	A	R	[-38.9]	459
XVI	2,120	A	A	A	A	Not significant	247
XVII	1,321	A	A	A	A	Not significant	447
XVIII	1,635	R	R	A	R	[-36.9]	411
XIX	1,453	A	A	A	A	Not significant	364
XX	1,684	A	A	A	A	Not significant	385

*Only DJF total sunshine exhibited a statistically significant long-term trend

Table A.3. Long-term linear trends (statistically significant at a α=0.05) in MAM total sunshine

#	Altitude [m]	ITT	IHP	IMK	ISN	Trend [hours/decade]	Average total sunshine [hours]
11	2,080	A	R	A	R	Not significant	335
I	4,150	A	A	A	A	Not significant	174
II	2,029	A	A	A	A	Not significant	338
XII	1,310	R	R	A	R	-19.1	397
XIII	1,381	R	R	A	R	-16.6	402
XV	1,026	R	R	A	R	-24.4	361
XVI	2,120	R	R	A	R	-12.9	202
XVII	1,321	A	A	A	A	Not significant	363
XVIII	1,635	R	R	A	R	-35.9	334
XIX	1,453	A	A	A	A	Not significant	314
XX	1,684	A	A	A	A	Not significant	304

Table A.4. Long-term linear trends (statistically significant at a α=0.05) in JJA total sunshine

#	Altitude [m]	ITT	IHP	IMK	ISN	Trend [hours/decade]	Average total sunshine [hours]
11	2,080	A	A	A	R	Not significant	416
I	4,150	A	A	A	A	Not significant	271
II	2,029	A	A	A	A	Not significant	511
XII	1,310	R	R	A	R	-13.3	468
XIII	1,381	R	R	A	R	-16.7	482
XV	1,026	R	R	A	R	-28.0	425
XVI	2,120	R	R	A	R	[-15.9]	301
XVII	1,321	A	A	A	A	Not significant	458
XVIII	1,635	R	R	A	R	-30.6	420
XIX	1,453	A	A	A	A	Not significant	516
XX	1,684	A	A	A	A	Not significant	377

Table A.5. Long-term linear trends (statistically significant at a α=0.05) in SON total sunshine

#	Altitude [m]	ITT	IHP	IMK	ISN	Trend [hours/decade]	Average total sunshine [hours]
11	2,080	A	A	A	A	Not significant	326
I	4,150	A	A	R	R	Not significant	161
II	2,029	A	A	A	A	Not significant	363
XII	1,310	R	R	A	R	-13.2	400
XIII	1,381	R	A	A	A	Not significant	401
XV	1,026	R	R	A	R	-25.0	362
XVI	2,120	R	R	A	R	-7.3	206

XVII	1,321	R	R	R	R	[27.9]*	387
XVIII	1,635	R	R	A	R	-22.9	335
XIX	1,453	A	A	A	A	Not significant	370
XX	1,684	A	A	A	A	Not significant	318

*Only SON total sunshine exhibited a statistically significant long-term trend

Tables A.6 to A.9 show the main results of the hypothesis tests that were implemented to detect long-term linear trends in the DJF, MAM, JJA, and SON minimum temperatures on the coldest days, respectively. Only weather stations with available data are presented. The highest slope parameters or trend magnitudes among seasons are highlighted with brackets. Based on the results of those weather stations that recorded statistically significant trends in minimum temperatures on the coldest days, it can be argued (although I cannot be that conclusive) that the strongest changes in this climatic variable occurred during the DJF and JJA dry seasons.

Table A.6. Long-term linear trends (statistically significant at a α=0.05) in DJF minimum temperature on the coldest days

#	Altitude [m]	ITT	IHP	IMK	ISN	Trend [°C/decade]	Average minimum temperature [°C]
11	2,080	R	R	R	R	[+0.5]	9.4
I	4,150	R	R	R	R	[+1.2]	-1.5
II	2,029	R	R	R	R	[+0.8]	12.1
VI	1,342	R	R	R	R	[+0.9]	14.4

VII	1,204	R	R	R	R	+0.5	14.7
XII	1,310	R	R	R	R	[+0.3]	14.7
XIII	1,381	R	R	R	R	+0.3	14.5
XV	1,026	R	R	R	R	[+0.2]	11.2
XVI	2,120	A	A	A	A	Not significant	9.1
XVII	1,321	A	A	A	A	Not significant	15.4
XVIII	1,635	R	R	R	R	+0.4	13.6
XIX	1,453	R	R	R	R	[+0.5]	14.4
XX	1,684	R	R	R	R	[+1.5]	12.0

Table A.7. Long-term linear trends (statistically significant at a α=0.05) in MAM minimum temperature on the coldest days

#	Altitude [m]	ITT	IHP	IMK	ISN	Trend [°C/decade]	Average minimum temperature [°C]
11	2,080	A	A	A	A	Not significant	10.1
I	4,150	R	A	R	A	Not significant	-0.2
II	2,029	R	R	R	R	+0.5	12.5
VI	1,342	R	R	R	R	+0.8	14.6
VII	1,204	A	A	A	A	Not significant	14.9
XII	1,310	R	R	R	R	+0.2	15,0
XIII	1,381	R	R	R	R	+0.2	14.8
XV	1,026	A	A	A	A	Not significant	11.7
XVI	2,120	A	A	A	A	Not significant	9.8
XVII	1,321	A	A	A	A	Not significant	15.5
XVIII	1,635	R	R	A	A	+0.3	13.7

XIX	1,453	R	R	R	R	+0.3	15.0
XX	1,684	A	A	A	A	Not significant	12.9

Table A.8. Long-term linear trends (statistically significant at a α=0.05) in JJA minimum temperature on the coldest days

#	Altitude [m]	ITT	IHP	IMK	ISN	Trend [°C/decade]	Average minimum temperature [°C]
11	2,080	R	R	R	R	+0.3	10.1
I	4,150	A	A	R	R	Not significant	-1.3
II	2,029	R	R	R	R	+0.6	11.9
VI	1,342	R	R	R	R	+0.8	14.1
VII	1,204	R	R	R	R	[+0.8]	14.4
XII	1,310	R	R	R	R	+0.2	14.7
XIII	1,381	R	R	R	R	[+0.4]	14.5
XV	1,026	R	R	R	A	+0.1	11.6
XVI	2,120	A	A	A	A	Not significant	9.8
XVII	1,321	A	A	A	A	Not significant	15.4
XVIII	1,635	R	R	R	R	+0.4	13.6
XIX	1,453	R	R	R	R	+0.3	13.9
XX	1,684	R	R	R	R	+0.8	12.4

Table A.9. Long-term linear trends (statistically significant at a α=0.05) in SON minimum temperature on the coldest days

#	Altitude [m]	ITT	IHP	IMK	ISN	Trend [°C/decade]	Average minimum temperature [°C]
11	2,080	R	R	R	R	+0.4	9.8
I	4,150	R	R	R	R	+0.7	-0.7
II	2,029	R	R	R	R	[+0.8]	12.1
VI	1,342	R	R	R	R	+0.6	13.9
VII	1,204	R	R	R	R	+0.6	14.3
XII	1,310	R	R	R	R	+0.2	14.4
XIII	1,381	R	R	R	R	+0.3	14.2
XV	1,026	R	R	R	R	+0.1	11.3
XVI	2,120	A	A	A	A	Not significant	9.5
XVII	1,321	A	A	A	A	Not significant	15.1
XVIII	1,635	R	R	R	R	[+0.5]	13.1
XIX	1,453	R	R	R	R	+0.3	14.5
XX	1,684	R	R	R	R	+0.9	12.0

Long-term linear trends in monthly time series. Monthly records of sunshine, rainfall, minimum, mean and maximum temperature, diurnal temperature range, and relative humidity gathered at the weather station XII (ID 2615502) were also processed to support the analysis. As presented before, sunshine, rainfall, temperature, and relative humidity records at this weather station span the historical periods 1961-2007, 1942-2006, 1950-2007, and 1950-2007, respectively. Almost all these observational periods span the longest historical periods in the

available dataset. Table A.10 summarizes the results of the Student's t-test (in this case for monthly time series).

Table A.10. Long-term linear trends (statistically significant at a α=0.05) in monthly time series recorded at the weather station XII (ID 2615502)

Climatic variable		Decision (α = 0.05)	Slope parameter (in units/decade)
Sunshine	SR1	R	-5.64
	SR2	R	+0.12
	TSD	A	--
	SR4	R	-0.12
	SR5	R	-0.24
	SR6	R	-0.12
	SR7	A	--
Rainfall	R1	A	--
	R2	A	--
	R3	A	--
Minimum temperature	MTmin	R	+0.24
	ATmin	R	+0.24
	mTmin2	R	+0.24
	SDTmin	R	+0.05
Maximum temperature	MTmax	R	+0.24
	ATmax	R	+0.12
	mTmax2	A	--
	SDTmax	R	+0.05
Relative humidity	MRH	A	--

	ARH	R	+0.72
	mRH2	R	+1.20
	SDRH	R	-0.24
Diurnal temperature range	MDTR	A	--
	ADTR	R	-0.12
	mDTR2	R	-0.12
	SDDTR	R	+0.04
Mean temperature	MTmean	R	+0.24
	ATmean	R	+0.24
	mTmean2	R	+0.12
	SDTmean	R	+0.02

Chapter 3 - Atmospheric instability, feedback mechanisms and climatic stress on high-altitude Andean ecosystems

Table SM-1(a). Historical periods of weather station data available on the Colombian side of the Colombian/Ecuadorian transboundary region. The longest historical time periods are highlighted with brackets. Temperature variables in this table include minimum temperature, maximum temperature and diurnal temperature range.

#	ID	Altitude [m]	Sunshine	Rainfall	Temperature	Relative humidity
1	5102501	16	N.A.	1968-2011	1968-2011	N.A.
2	5204501	2,710	N.A.	1953-2011	1953-2011	N.A.
3	5205504	2,820	N.A.	1979-2011	1979-2011	N.A.
4	4701508	1,550	N.A.	1983-2011	1983-2011	N.A.
5	5204504	1,875	N.A.	1972-2011	1972-2011	N.A.
6	5205502	3,120	N.A.	1968-2011	1968-2011	N.A.
7	5205503	1,493	N.A.	1968-2011	1968-2011	N.A.
8	5205506	1,500	N.A.	1972-2011	1972-2011	N.A.
9	5205510	3,000	N.A.	1990-2011	1990-2011	N.A.
10	5206502	32	N.A.	1972-2011	1972-2011	N.A.
11	5102502	1,181	N.A.	1968-1993	1968-1993	N.A.
12	5102505	1,010	N.A.	1993-2011	1993-2011	N.A.
13	5103502	1	N.A.	1991-2011	1991-2011	N.A.
14	5205509	2,800	N.A.	1987-2011	1987-2011	N.A.
15	5203502	1,400	N.A.	1986-2011	1986-2011	N.A.
16	5102001	950	N.A.	1963-2011	N.A.	N.A.

#	ID	Altitude [m]	Sunshine	Rainfall	Temperature	Relative humidity
17	5206004	1,770	N.A.	1983-2011	N.A.	N.A.
18	5102004	100	N.A.	1983-2011	N.A.	N.A.
19	5102005	100	N.A.	1983-2011	N.A.	N.A.
20	5103002	20	N.A.	1983-2011	N.A.	N.A.
21	5201002	1,700	N.A.	1971-2011	N.A.	N.A.
22	5201003	1,700	N.A.	1990-2011	N.A.	N.A.
23	5201006	650	N.A.	1972-2011	N.A.	N.A.
24	5201014	500	N.A.	1970-2011	N.A.	N.A.
25	5202004	350	N.A.	1965-2011	N.A.	N.A.
26	5204007	2,590	N.A.	1958-2011	N.A.	N.A.
27	5205001	1,620	N.A.	1965-2011	N.A.	N.A.
28	5205002	1,700	N.A.	1958-2011	N.A.	N.A.
29	5205004	2,000	N.A.	1963-2011	N.A.	N.A.
30	5205005	2,834	N.A.	1972-2011	N.A.	N.A.
31	5205006	2,693	N.A.	1965-2011	N.A.	N.A.
32	5205008	2,420	N.A.	1957-2011	N.A.	N.A.
33	5205009	2,550	N.A.	1957-2011	N.A.	N.A.
34	5205010	2,830	N.A.	1972-2011	N.A.	N.A.
35	5205011	3,092	N.A.	1958-2011	N.A.	N.A.
36	5205012	2,817	N.A.	1971-2011	N.A.	N.A.
37	5205013	3,100	N.A.	1972-2011	N.A.	N.A.
38	5205014	1,480	N.A.	1980-2011	N.A.	N.A.
39	5206005	840	N.A.	1984-2011	N.A.	N.A.
40	5207001	100	N.A.	1983-2011	N.A.	N.A.
41	5207003	340	N.A.	1987-2011	N.A.	N.A.
42	5208001	350	N.A.	1966-2011	N.A.	N.A.
43	5302002	80	N.A.	1983-2011	N.A.	N.A.
44	5103501	3	N.A.	1948-2011	1948-2011	N.A.
45	5204502	1,796	N.A.	1957-2011	1957-2011	N.A.

#	ID	Altitude [m]	Sunshine	Rainfall	Temperature	Relative humidity
46	5205501	2,961	N.A.	[1941-2011]	[1941-2011]	N.A.

N.A.: Not available

Table SM-1(b). Historical periods of weather station data available on the Ecuadorian side of the Colombian/Ecuadorian transboundary region. The longest historical time periods are highlighted with brackets. Temperature variables in this table include minimum temperature, maximum temperature and diurnal temperature range.

#	ID	Altitude [m]	Sunshine	Rainfall	Temperature	Relative humidity
1	M003	3,058	N.A.	1965-2005	1965-2005	N.A.
2	M004	2,628	N.A.	1976-2006	1976-2006	N.A.
3	M005	60	N.A.	1964-2005	1964-2005	N.A.
4	M006	120	N.A.	[1962-2006]	[1962-2006]	N.A.
5	M007	205	N.A.	N.A.	N.A.	N.A.
6	M008	960	N.A.	1965-2006	1965-2006	N.A.
7	M025	360	N.A.	1964-2005	1964-2005	N.A.
8	M026	260	N.A.	1964-2004	1964-2004	N.A.
9	M027	554	N.A.	1964-1984	1964-1984	N.A.
10	M031	3,083	N.A.	1963-2005	1963-2005	N.A.
11	M033	2,160	N.A.	1963-2006	1963-2006	N.A.
12	M036	4	N.A.	N.A.	N.A.	N.A.
13	M037	13	N.A.	N.A.	N.A.	N.A.
14	M038	50	N.A.	1966-1999	1966-1999	N.A.
15	M039	480	N.A.	N.A.	N.A.	N.A.
16	M051	7	N.A.	1981-2005	1981-2005	N.A.

#	ID	Altitude [m]	Sunshine	Rainfall	Temperature	Relative humidity
17	M056	5	N.A.	N.A.	N.A.	N.A.
18	M072	4	N.A.	1966-1989	1966-1989	N.A.
19	M103	2,860	N.A.	1965-2005	1965-2005	N.A.
20	M105	2,556	N.A.	1964-2005	1964-2005	N.A.
21	M124	223	N.A.	1964-2005	1964-2005	N.A.
22	M129	350	N.A.	1964-1997	1964-1997	N.A.
23	M138	2,289	N.A.	1964-2006	1964-2006	N.A.
24	M162	20	N.A.	1964-2006	1964-2006	N.A.
25	M166	50	N.A.	1964-2005	1964-2005	N.A.
26	M167	5	N.A.	1964-2005	1964-2005	N.A.
27	M171	220	N.A.	N.A.	N.A.	N.A.
28	M218	35	N.A.	1967-2001	1967-2001	N.A.
29	M466	41	N.A.	N.A.	N.A.	N.A.

N.A.: Not available

Table SM-1(c). Historical periods of weather station data available on the Bolivian side of the Bolivian/Peruvian transboundary region. The longest historical time periods are highlighted with brackets. Temperature variables in this table include minimum temperature, maximum temperature and diurnal temperature range.

#	ID	Altitude [m]	Sunshine	Rainfall	Temperature	Relative humidity
1	Ayo Ayo	3,880	N.A.	1953-2011	1957-2011	N.A.
2	Carabuco	3,815	N.A.	1995-2011	1991-2011	N.A.
3	Collana	3,940	N.A.	1973-2011	1973-2011	N.A.
4	Huarina Cota Cota	3,825	N.A.	1973-2011	1973-2011	N.A.

#	ID	Altitude [m]	Sunshine	Rainfall	Temperature	Relative humidity
5	Central La Paz	3,632	N.A.	[1952-2011]	[1952-2011]	N.A.
6	Tiawuanacu	3,629	N.A.	1973-2011	1973-2011	N.A.
7	Viacha	3,850	N.A.	1987-2011	1987-2011	N.A.

N.A.: Not available

Table SM-1(d). Historical periods of weather station data available on the Peruvian side of the Bolivian/Peruvian transboundary region. The longest historical time periods are highlighted with brackets. Temperature variables in this table include minimum temperature, maximum temperature and diurnal temperature range.

#	ID	Altitude [m]	Sunshine	Rainfall	Temperature	Relative humidity
1	Modelo	137	N.A.	1976-2011	1976-2011	N.A.
2	Jorge Basadre	560	N.A.	1993-2011	1993-2011	N.A.
3	Marcapomacocha	4,479	N.A.	1969-2011	1969-2011	N.A.
4	Lircay	3,150	N.A.	1949-2011	1949-2011	N.A.
5	Candarave	3,415	N.A.	1963-2011	1963-2011	N.A.
6	Requena	128	N.A.	1964-2011	1964-2011	N.A.
7	Pucallpa	160	N.A.	1949-2011	1949-2011	N.A.
8	Puerto Maldonado	256	N.A.	1958-2011	1958-2011	N.A.
9	Piura	49	N.A.	[1932-2011]	[1932-2011]	N.A.
10	Tacna	452	N.A.	1950-2011	1950-2011	N.A.

N.A.: Not available

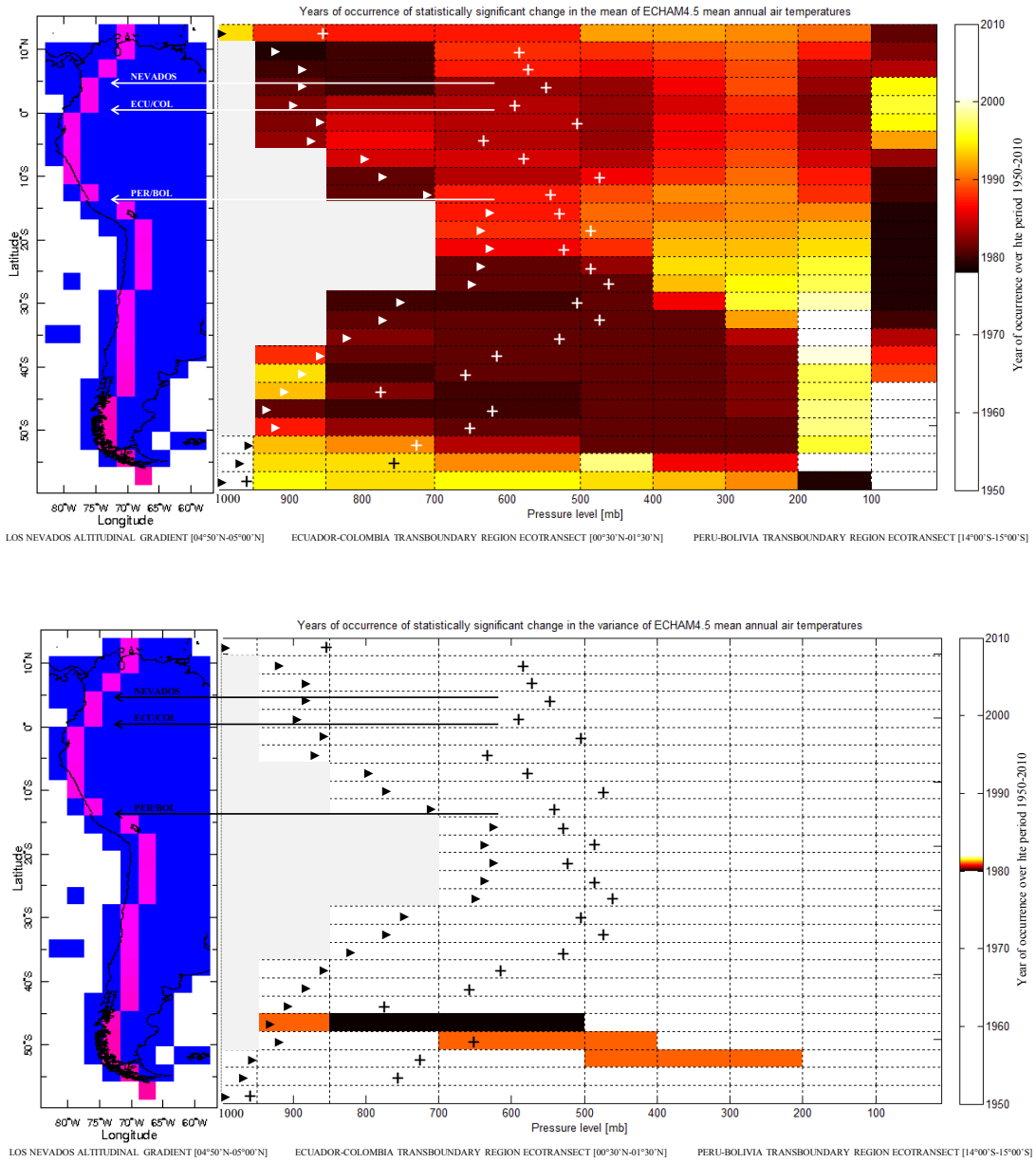

Figure SM-1(a). Years of occurrence of statistically significant changes in the mean (top panel) and the variance (bottom panel) of 1950-2010 ECHAM4.5 mean annual air temperatures along the axis of the Andes Cordillera (see pink 2.8125°pixels on plan views), for the latitudinal range [60°S-15°N], and for 9 pressure levels [1000, 950, 850, 700, 500, 400, 300, 200, and 100 mb; see vertical profiles]. Near-surface and free air temperatures are obtained through ECHAM4.5 ensemble simulation runs. Only statistically

significant (at α=0.05) changes are displayed; i.e. non-significant changes are depicted by white boxes. Proposed ecotransects are highlighted with arrows. Black and white solid triangles and crosses depict, respectively, the average and maximum altitudes (expressed in atmospheric pressures) of the NOAA NGDC GLOBE gridded 1-km, quality controlled global Digital Elevation Model (Hastings and Dunbar, 1999) in the ECHAM4.5 model gridpoints. Areas blocked in grey depict grid boxes below the ground surface. In the latitudes of the Nevados, Ecu/Col and Per/Bol transects, specifically, the abrupt changes in the mean of mean annual air temperatures occurred from 1980 through 1991, according to ECHAM4.5 simulation outputs.

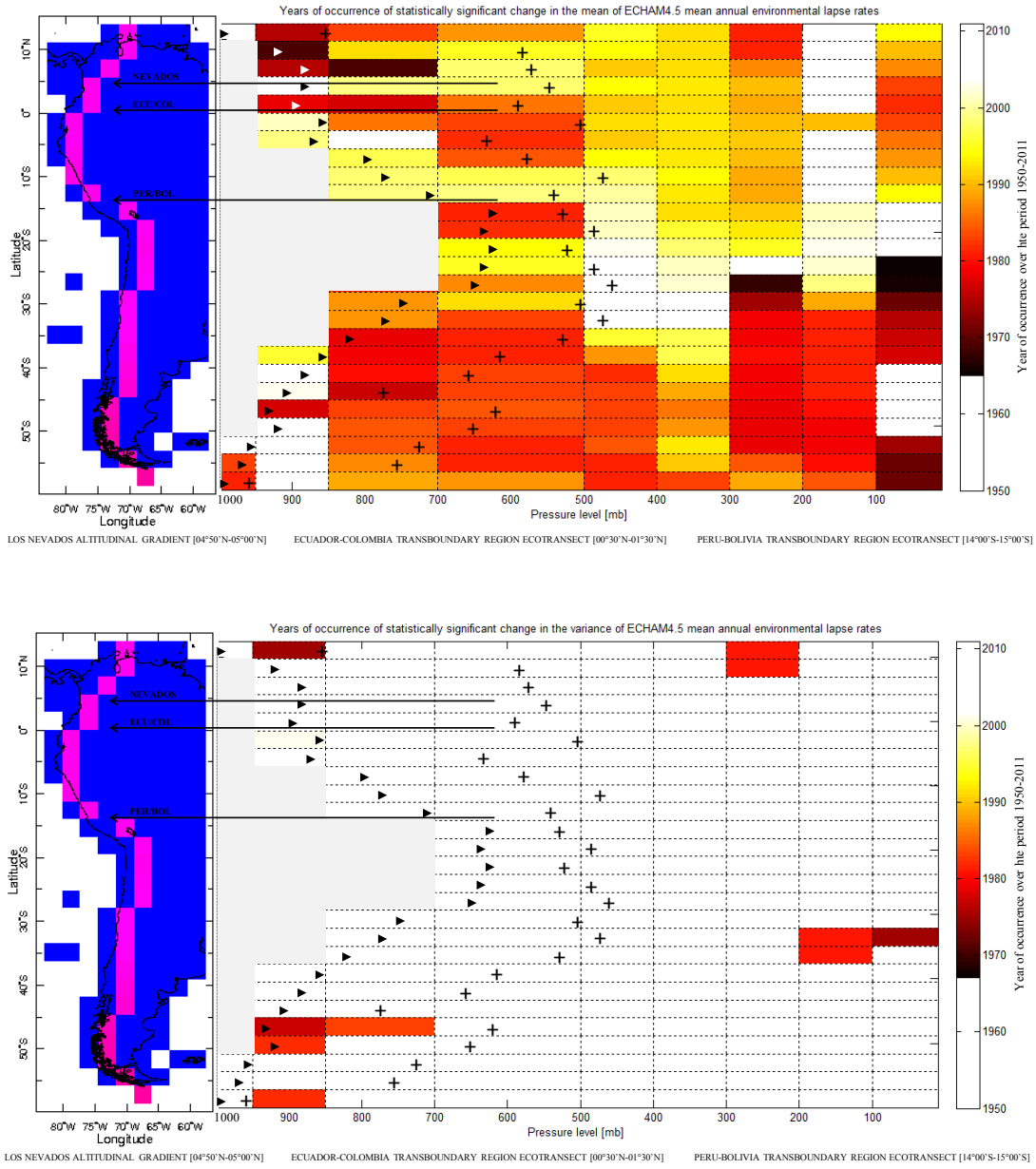

Figure SM-1(b). Years of occurrence of statistically significant changes in the mean (top panel) and the variance (bottom panel) of 1950-2011 ECHAM4.5 mean annual environmental lapse rates along the axis of the Andes Cordillera (see pink 2.8125°pixels on plan views), for the latitudinal range [60°S-15°N], and for 9 pressure levels [1000, 950, 850, 700, 500, 400, 300, 200, and 100 mb; see vertical profiles]. Environmental lapse rates are obtained through ECHAM4.5 ensemble simulation runs. Only statistically

significant (at α=0.05) changes are displayed; i.e. non-significant changes are depicted by white boxes. Proposed ecotransects are highlighted with arrows. Black and white solid triangles and crosses depict, respectively, the average and maximum altitudes (expressed in atmospheric pressures) of the NOAA NGDC GLOBE gridded 1-km, quality controlled global Digital Elevation Model (Hastings and Dunbar, 1999) in the ECHAM4.5 model gridpoints. Areas blocked in grey depict grid boxes below the ground surface.

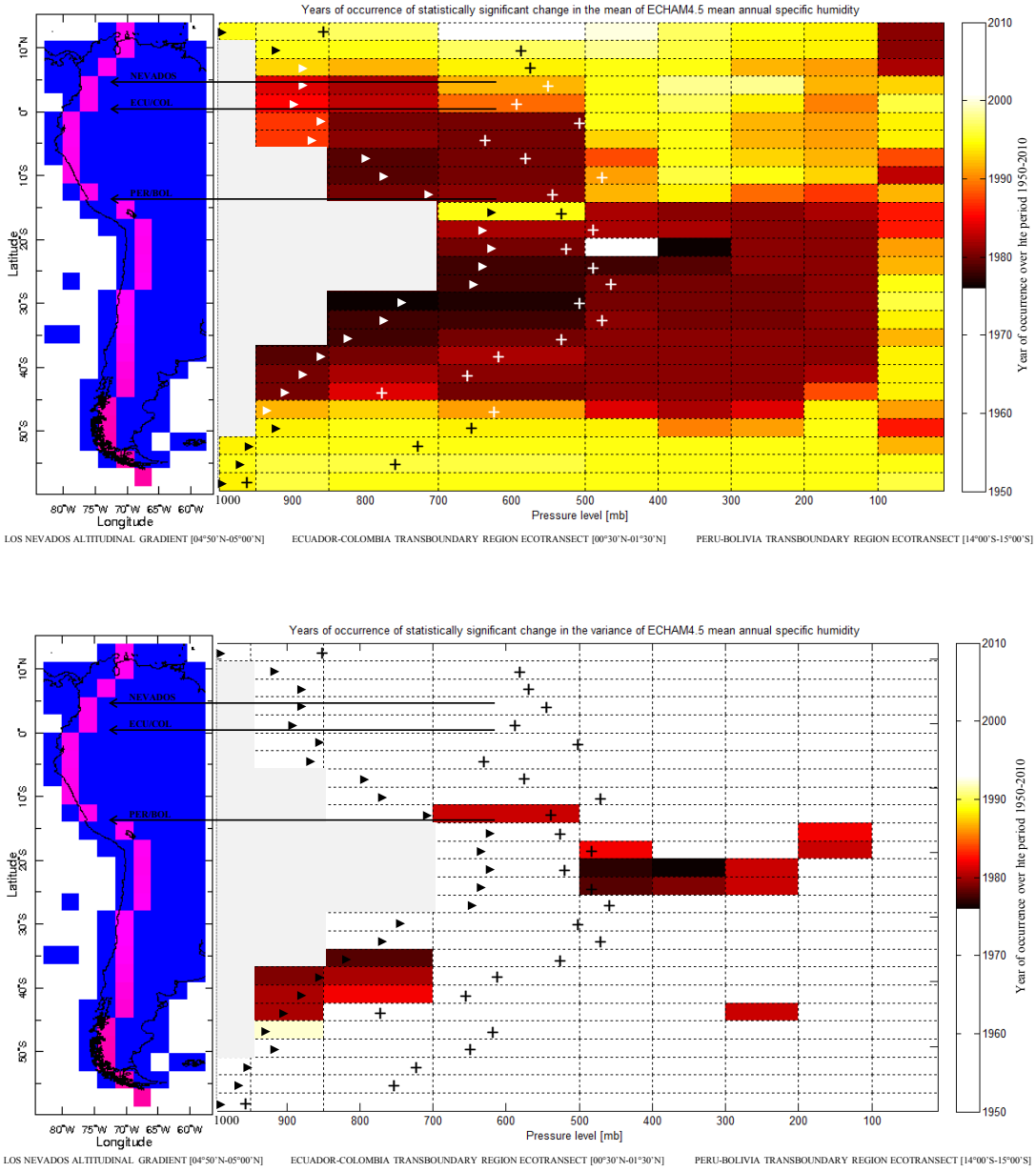

Figure SM-1(c). Years of occurrence of statistically significant changes in the mean (top panel) and the variance (bottom panel) of 1950-2010 ECHAM4.5 mean annual specific humidity along the axis of the Andes Cordillera (see pink 2.8125°pixels on plan views), for the latitudinal range [60°S-15°N], and for 9 pressure levels [1000, 950, 850, 700, 500, 400, 300, 200, and 100 mb; see vertical profiles]. Near-surface and free specific humidity values are obtained through ECHAM4.5 ensemble simulation runs. Only

statistically significant (at α=0.05) changes are displayed; i.e. non-significant changes are depicted by white boxes. Proposed ecotransects are highlighted with arrows. Black and white solid triangles and crosses depict, respectively, the average and maximum altitudes (expressed in atmospheric pressures) of the NOAA NGDC GLOBE gridded 1-km, quality controlled global Digital Elevation Model (Hastings and Dunbar, 1999) in the ECHAM4.5 model gridpoints. Areas blocked in grey depict grid boxes below the ground surface.

Time of occurrence of vertical motions on the west flank of the El Ruiz-Tolima volcanic massif. Figures SM-2(a) to SM-2(d) depict the near-surface air temperatures gathered during the trimesters December-January-February (DJF), March-April-May, June-July-August, and September-October-November (SON) of the historical period 2008-2011, at the T/RH data loggers installed in the headwaters of the Claro River watershed. The 2008 through 2011 period is characterized by the occurrence of El Niño-like, La Niña-like and neutral climatic conditions, one episode each, according to the running 3-month mean of the Oceanic Niño Index (ONI) . Over the period December 1, 2008 through February 28, 2009 (normal conditions), for instance, near-surface air temperatures at the lowest T/RH data logger reached 3.8±1.2°C and 7.8±1.8°C at 06:00 am and noon, respectively. In the highest T/RH data logger near-surface air temperatures averaged 0.1±1.4°C and 6.7±2.0°C at the same times of the day. Over the period December 1, 2009 through February 28, 2010 (El Niño-like conditions), air temperatures in the lowest digital sensor increased to 4.6±1.6°C and 10.0±2.0°C at 06:00 am and 12:00 m, respectively, and to 0.2±1.9°C and 9.7±2.7°C in the highest data logger. Thus, 06:00 am near-surface air temperatures during the 2009-2010 El Niño weak event increased 0.8°C and 0.1°C, with respect to neutral conditions, in the upper and lower levels, respectively, whereas at noon increases in

near-surface temperatures reached 2.2°C and 3.0°C. Conversely, over the period December 1, 2010 through February 28, 2011, which was recognized as La Niña-like conditions, near-surface air temperatures in the lower levels decreased 0.7 and 0.2°C at 06:00 am and noon, respectively, with respect to the 'normal conditions' event. In the upper levels such decreases reached 0.5°C, particularly at 06:00 am.

Temperature records gathered at the installed T/RH data loggers (in the highlands) and available weather stations (in the lowlands) suggest that, over the period 2009-2010 and along the Claro River watershed, environmental lapse rates (Γ) exhibited mean, minimum and maximum values presented in table SM-2. At 06:00, Γ values reached an average rate of about -5.5 K/km with minimum and maximum observed values of -4.3 and -7.3 K/km, respectively. At 14:00, Γ values reached an average rate of about -7.4 K/km with minimum and maximum observed values of -4.9 and -10.7 K/km, respectively.

Over the dry period DJF 2008-2009, the environmental lapse rates at 06:00 am and 02:00 pm ($\Gamma_{06:00}$ and $\Gamma_{14:00}$) reached -5.6 K/km [Min: -4.9; Max: -6.7] and -7.3 K/km [-5.7; -9.8], respectively. See top panel in figure SM-3(a). During the trimester DJF 2009-2010, $\Gamma_{06:00}$ and $\Gamma_{14:00}$ reached -5.7 K/km [-4.6; -6.9] and -7.2 K/km [-5.6; -9.1]. See bottom panel in figure SM-3(a). During the wet seasons SON 2009 and SON 2010, $\Gamma_{06:00}$ and $\Gamma_{14:00}$ reached -5.4 K/km [-4.4; -6.5] and -7.4 K/km [-5.5; -11.1], and -5.6 K/km [-4.6; -6.8] and -7.2 K/km [-4.9; -9.6], respectively. See top and bottom panels in figure SM-3(b).

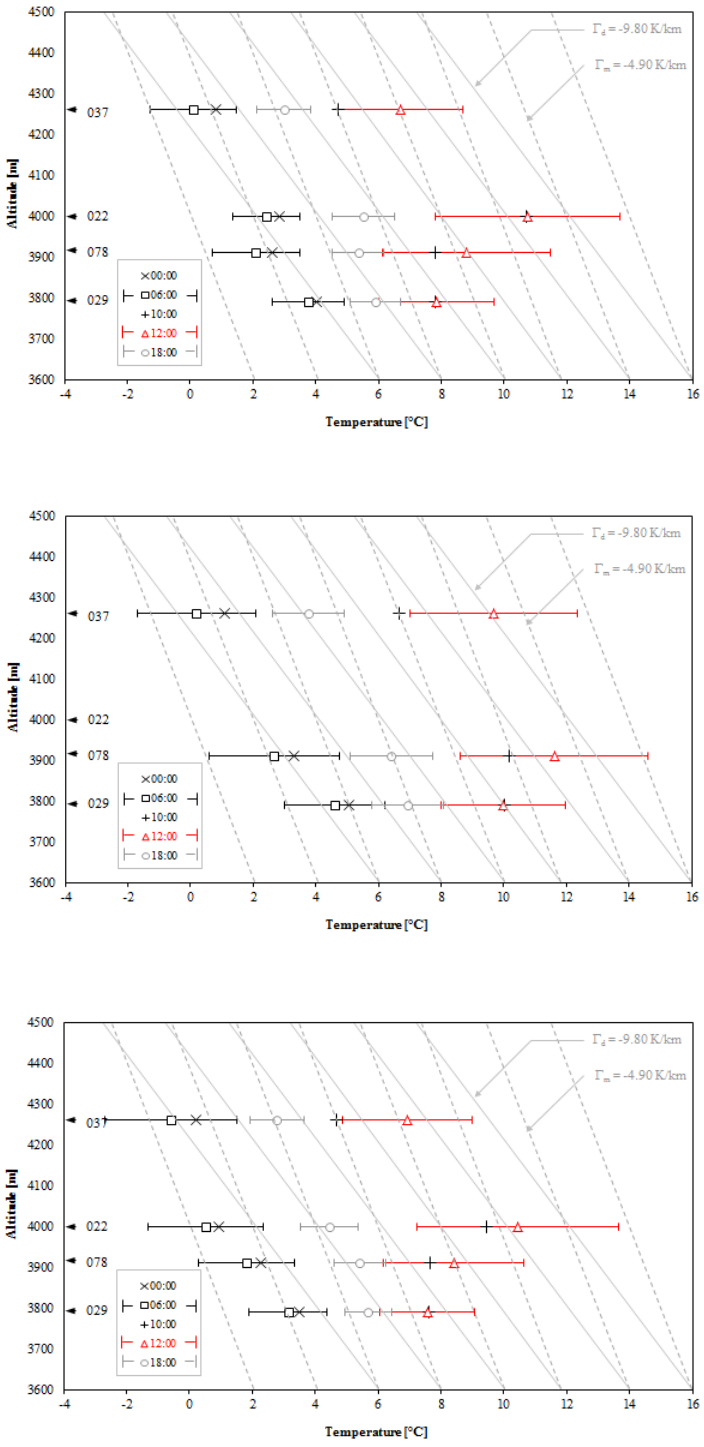

Figure SM-2(a). Near-surface air temperatures [°C] gathered over the periods December 1, 2008 through February 28, 2009 (top panel; normal conditions, according to the running 3-month mean NOAA's ONI

values), December 1, 2009 through February 28, 2010 (middle panel; El Niño-like conditions), and December 1, 2010 through February 28, 2011 (bottom panel; La Niña-like conditions) at the U23-001 HOBO® Temperature/Relative Humidity data loggers 2272886 Salto_Cueva (GPS mark 029; 3,790 m), 2272887 Microcentral (GPS mark 078; 3,910 m), 2272888 El Cisne (GPS mark 022; 4,000 m), and 2272889 Nariz_Diablo (GPS mark 037; 4,260 m). Only five temperatures are presented: 00:00 (black crosses); 06:00 (black squares); 10:00 (black pluses); 12:00 (red triangles); and 18:00 (gray circles). Error bars represent +1.0 standard deviation (error bars for 00:00 and 10:00 temperatures are not displayed). Gray solid lines depict the dry adiabatic lapse rate (Γ_d = -9.80 K/km); gray dashed lines represent the mean annual moist adiabatic lapse rate (Γ_m), which varies from -4.70 to -5.10 K/km in the altitudinal range [3,600 m – 4,500 m] under historical climatic conditions. In this graph only the saturated adiabatic lapse rate of -4.9 K/km is displayed.

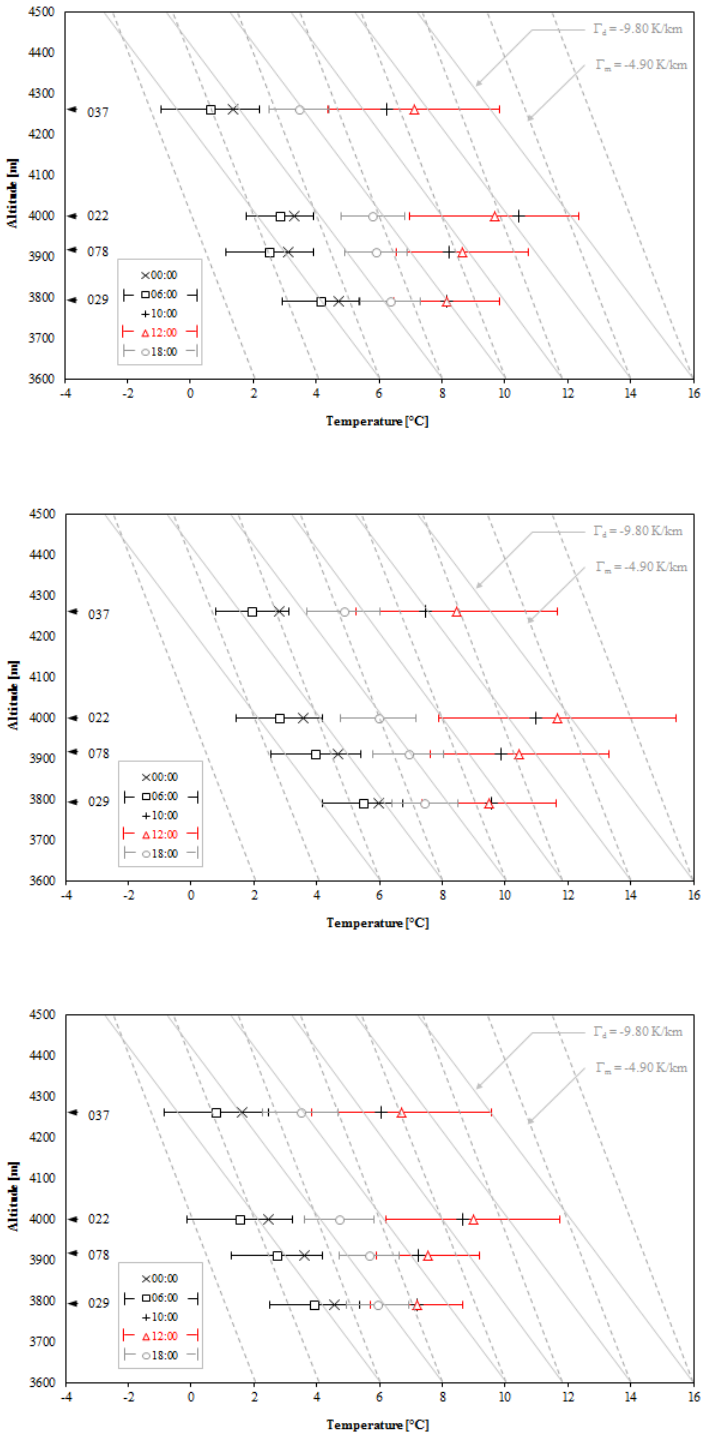

Figure SM-2(b). Near-surface air temperatures [°C] gathered over the periods March 1, 2009 through May 31, 2009 (top panel; normal conditions, according to the running 3-month mean NOAA's ONI

values), March 1, 2010 through May 31, 2010 (middle panel, El Niño-like conditions), and March 1, 2011 through May 31, 2011 (bottom panel; La Niña-like conditions) at the U23-001 HOBO® Temperature/Relative Humidity data loggers 2272886 Salto_Cueva (GPS mark 029; 3,790 m), 2272887 Microcentral (GPS mark 078; 3,910 m), 2272888 El Cisne (GPS mark 022; 4,000 m), and 2272889 Nariz_Diablo (GPS mark 037; 4,260 m). Only five temperatures are presented: 00:00 (black crosses); 06:00 (black squares); 10:00 (black pluses); 12:00 (red triangles); and 18:00 (gray circles). Error bars represent +1.0 standard deviation (error bars for 00:00 and 10:00 temperatures are not displayed). Gray solid lines depict the dry adiabatic lapse rate (Γ_d = -9.80 K/km); gray dashed lines represent the mean annual moist adiabatic lapse rate (Γ_m), which varies from -4.70 to -5.10 K/km in the altitudinal range [3,600 m – 4,500 m] under historical climatic conditions. In this graph only the saturated adiabatic lapse rate of -4.9 K/km is displayed.

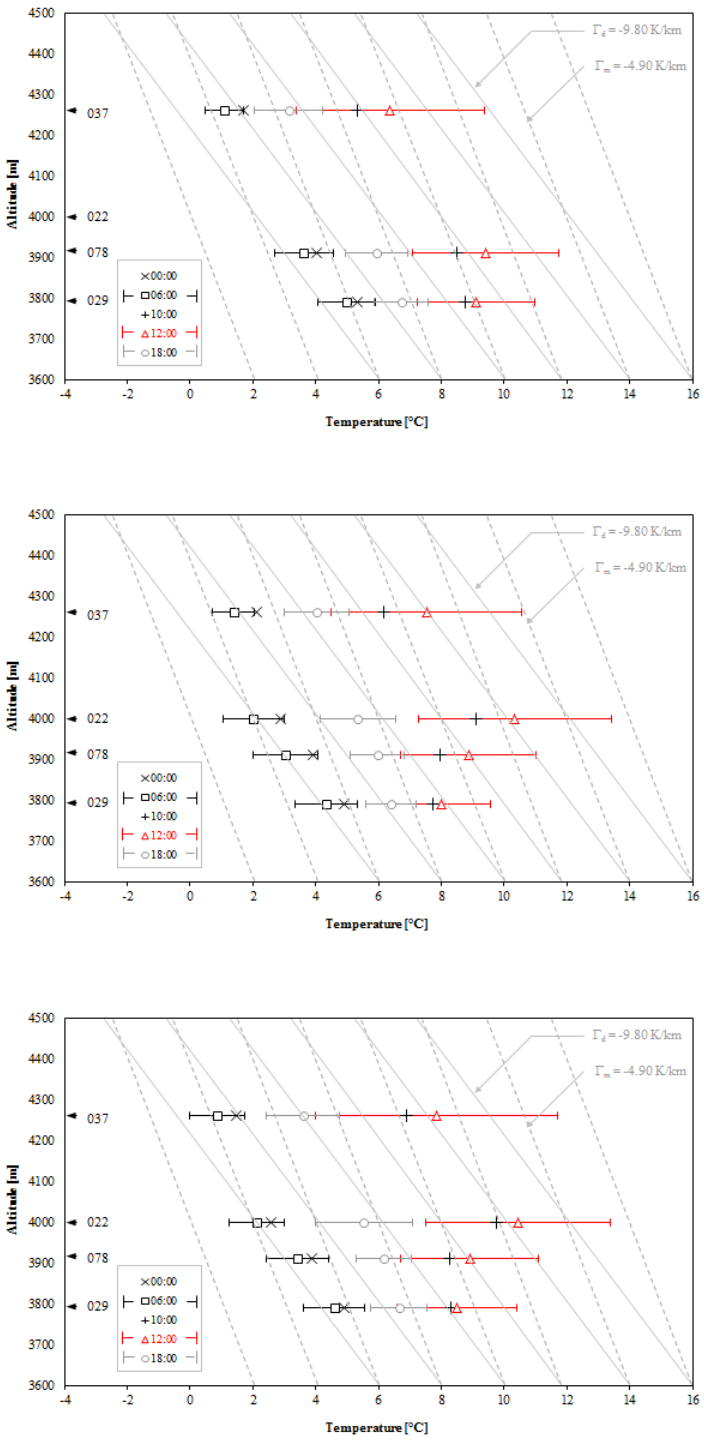

Figure SM-2(c). Near-surface air temperatures [°C] gathered over the periods June 1, 2009 through August 31, 2009 (top panel; El Niño-like conditions, according to the running 3-month mean NOAA's

ONI values), June 1, 2010 through August 31, 2010 (middle panel; La Niña-like conditions), and June 1, 2011 through August 31, 2011 (bottom panel; normal conditions) at the U23-001 HOBO® Temperature/Relative Humidity data loggers 2272886 Salto_Cueva (GPS mark 029; 3,790 m), 2272887 Microcentral (GPS mark 078; 3,910 m), 2272888 El Cisne (GPS mark 022; 4,000 m), and 2272889 Nariz_Diablo (GPS mark 037; 4,260 m). Only five temperatures are presented: 00:00 (black crosses); 06:00 (black squares); 10:00 (black pluses); 12:00 (red triangles); and 18:00 (gray circles). Error bars represent +1.0 standard deviation (error bars for 00:00 and 10:00 temperatures are not displayed). Gray solid lines depict the dry adiabatic lapse rate (Γ_d = -9.80 K/km); gray dashed lines represent the mean annual moist adiabatic lapse rate (Γ_m), which varies from -4.70 to -5.10 K/km in the altitudinal range [3,600 m – 4,500 m] under historical climatic conditions. In this graph only the saturated adiabatic lapse rate of -4.9 K/km is displayed.

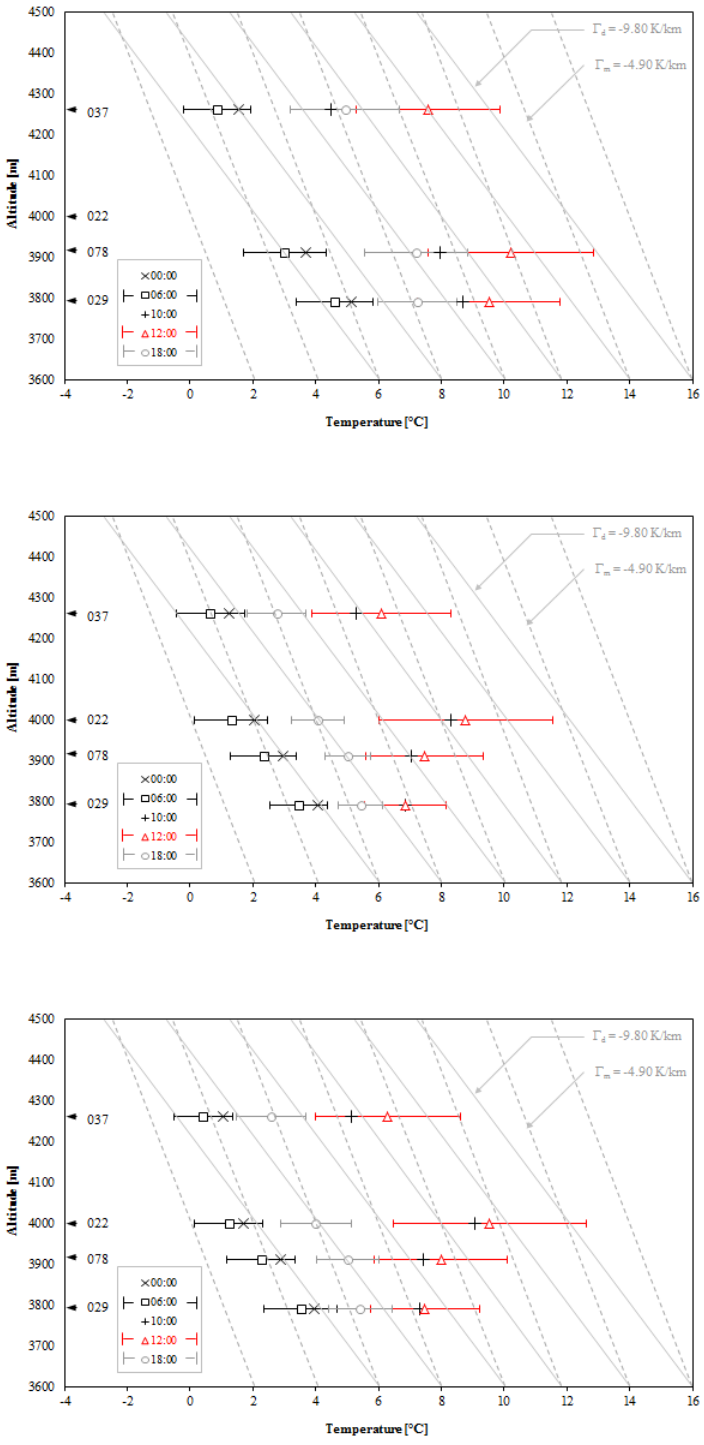

Figure SM-2(d). Near-surface air temperatures [°C] gathered over the periods September 1, 2009 through November 30, 2009 (top panel; El Niño-like conditions, according to the running 3-month mean NOAA's

ONI values), September 1, 2010 through November 30, 2010 (middle panel; La Niña-like conditions), and September 1, 2011 through November 30, 2011 (bottom panel; normal conditions) at the U23-001 HOBO® Temperature/Relative Humidity data loggers 2272886 Salto_Cueva (GPS mark 029; 3,790 m), 2272887 Microcentral (GPS mark 078; 3,910 m), 2272888 El Cisne (GPS mark 022; 4,000 m), and 2272889 Nariz_Diablo (GPS mark 037; 4,260 m). Only five temperatures are presented: 00:00 (black crosses); 06:00 (black squares); 10:00 (black pluses); 12:00 (red triangles); and 18:00 (gray circles). Error bars represent +1.0 standard deviation (error bars for 00:00 and 10:00 temperatures are not displayed). Gray solid lines depict the dry adiabatic lapse rate (Γ_d = -9.80 K/km); gray dashed lines represent the mean annual moist adiabatic lapse rate (Γ_m), which varies from -4.70 to -5.10 K/km in the altitudinal range [3,600 m – 4,500 m] under historical climatic conditions. In this graph only the saturated adiabatic lapse rate of -4.9 K/km is displayed.

Table SM-2. Environmental lapse rates observed over the period January, 2009 through December, 2010, along the Claro River high-altitude basin, Los Nevados Natural Park. [&]: Annual minimum value; [%]: Annual maximum value; Historical minimum and maximum values highlighted in bold

Month	2009						2010					
	06:00			14:00			06:00			14:00		
	Mean	[Min	Max]	Mean	[Min	Max]	Mean	[Min	Max]	Mean	[Min	Max]
January	-5.7	[-4.9	-6.6]	-7.4	[-5.9	-9.0]	-5.6[%]	[-4.7	-6.8[%]]	-7.3	[-5.6	-9.1]
February	-5.6	[-5.0[%]	-6.4]	-7.6	[-6.2	-8.8]	-5.5	[-4.6	-6.7]	-6.9[&]	[-5.9	-8.7]
March	-5.6	[-5.0[%]	-7.3[%]]	-7.6	[-6.3	-10.0]	-5.4	**[-4.3[&]**	-6.7]	-7.2	[-5.4	-9.0]
April	-5.5	[-4.8	-6.6]	-7.5	[-5.4	-8.7]	-5.3[&]	[-4.7	-6.1]	-7.5[%]	[-5.2	-8.9]
May	-5.4	[-4.8	-6.0[&]]	-7.5	[-6.2	-9.4]	-5.3[&]	[-4.6	-6.4]	-7.4	[-5.5	-9.0]
June	-5.2[&]	[-4.5[&]	-6.0[&]]	-7.1[&]	[-5.6	-8.2[&]]	-5.4	[-4.6	-6.1]	-7.1	[-5.5	-8.5]
July	-5.4	[-4.5[&]	-6.0[&]]	-7.9[%]	[-6.3	-9.2]	-5.4	[-4.6	-5.9[&]]	-7.1	[-5.4	-8.7]
August	-5.4	[-4.5[&]	-6.1]	-7.5	[-6.3	-8.8]	-5.4	[-5.0[%]	-6.0]	-6.9[&]	[-5.5	-8.3[&]]
September	-5.4	[-4.5[&]	-6.3]	-7.3	[-5.6	**-10.7[%]]**	-5.5	[-4.9	-6.2]	-7.3	[-6.2[%]	-8.7]
October	-5.4	[-4.6	-6.4]	-7.5	[-4.9[&]	-8.9]	-5.5	[-4.8	-6.7]	-7.5[%]	[-5.0[&]	-9.5[%]]
November	-5.4	[-4.7	-6.6]	-7.8	[-6.6[%]	-9.0]	-5.5	[-4.5	-6.4]	-7.2	[-5.6	-8.8]
December	-5.9[%]	[-4.7	-6.9]	-7.3	[-5.9	-8.7]	-5.6[%]	[-4.6	-6.8[%]]	-7.1	[-6.0	-8.4]

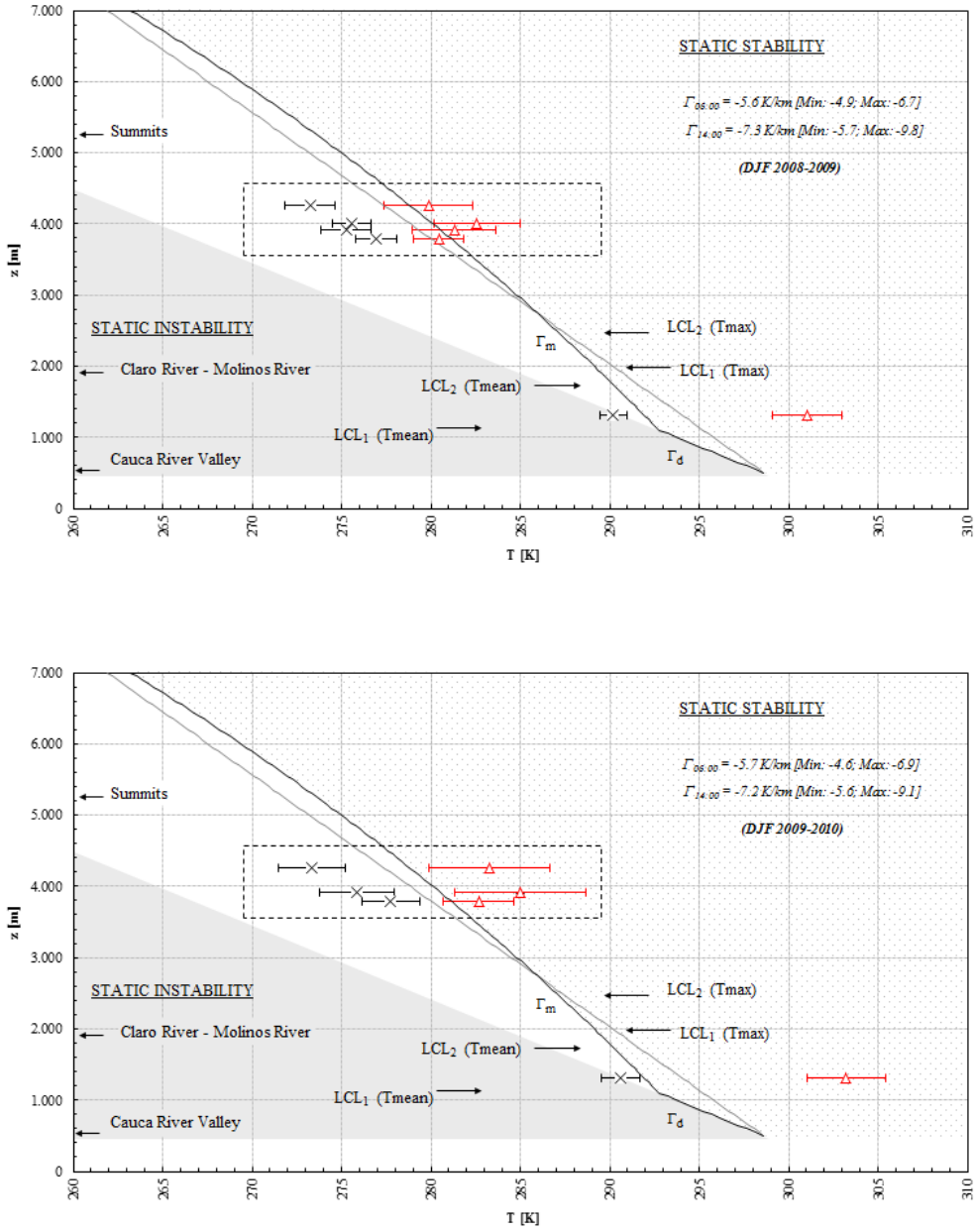

Figure SM-3(a). Regions of static instability, conditional instability, and static stability in the Claro River watershed estimated for the periods December-January-February (DJF) 2008-2009 (top panel) and DJF 2009-2010 (bottom panel). Γ_d and Γ_m represent the dry and moist (saturated) adiabatic lapse rates, respectively. LCL_1 and LCL_2 denote the estimated Lifting Condensation Levels for air parcels located in

the Cauca River inter-Andean valley and in the foothills of the Andean Central Cordillera, respectively, with internal temperatures equal to the mean annual temperature (Tmean) and maximum annual temperature (Tmax) of these initial altitudes. Shaded and dotted areas represent, respectively, the regions of static instability (environmental lapse rate is greater than Γ_d) and static stability (environmental lapse rate is smaller than Γ_d and Γ_m). The white area between the abovementioned areas depicts the region of conditional (in)stability (environmental lapse rate is between Γ_d and Γ_m). In this graph, regions of static instability, conditional instability and static stability are delimited assuming a LCL at an altitude of LCL_1(Tmean). Observed temperatures are represented by box-plots: black crosses for near-surface temperatures gathered in Temperature/Relative Humidity data loggers at 06:00 (daily minimum temperature gathered in Cenicafe weather station (1,310 m) is assumed to take place at 06:00 am); red triangles for near-surface temperatures gathered in Temperature/Relative Humidity data loggers at 14:00 (daily maximum temperature gathered in Cenicafe is assumed to occur at 02:00 pm); confidence intervals represent +1.0 standard deviations.

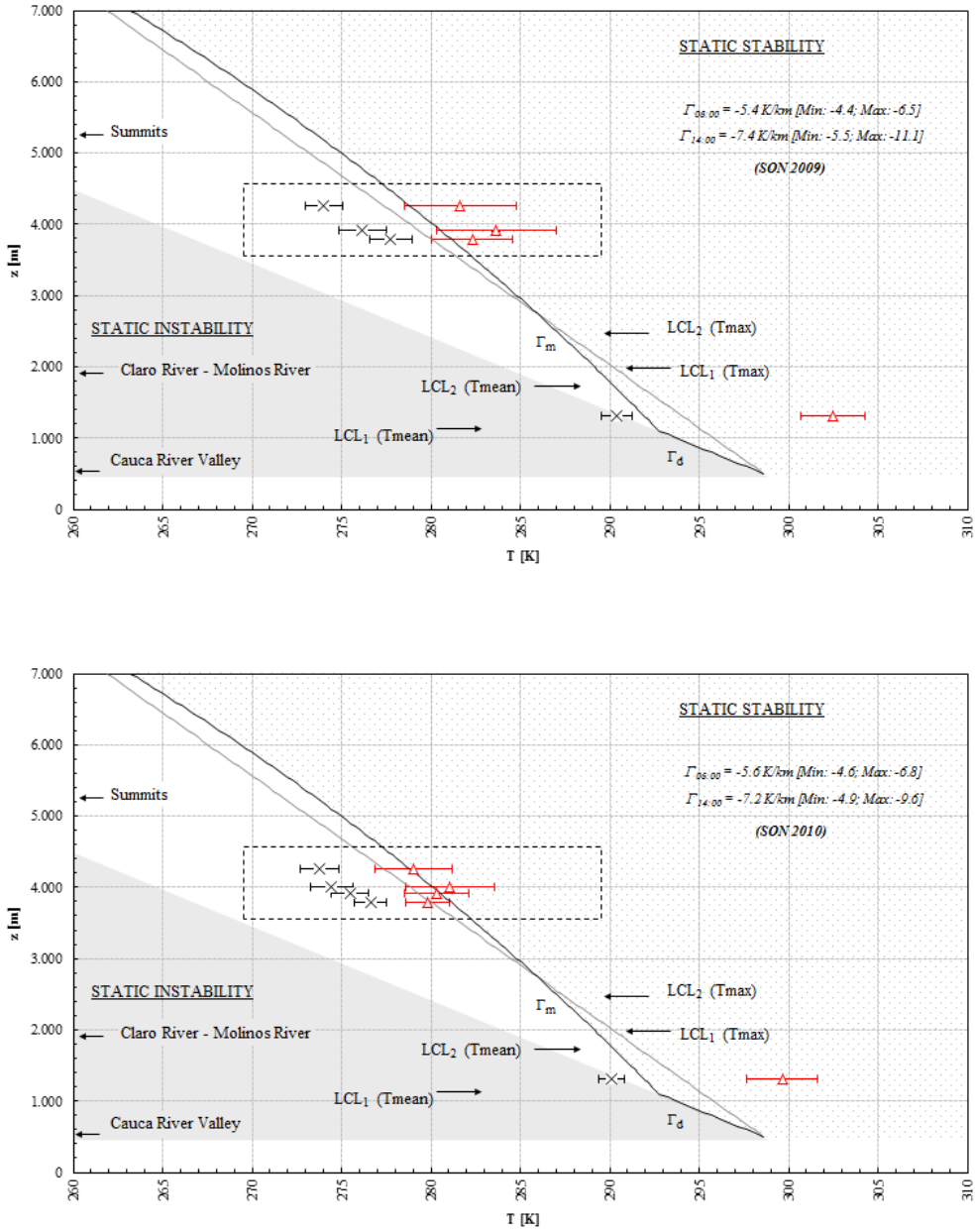

Figure SM-3(b). Regions of static instability, conditional instability, and static stability in the Claro River watershed estimated for the periods September-October-November (SON) 2009 (top panel) and SON 2010 (bottom panel). Γ_d and Γ_m represent the dry and moist (saturated) adiabatic lapse rates, respectively. LCL_1 and LCL_2 denote the estimated Lifting Condensation Levels for air parcels located in the Cauca

River inter-Andean valley and in the foothills of the Andean Central Cordillera, respectively, with internal temperatures equal to the mean annual temperature (Tmean) and maximum annual temperature (Tmax) of these initial altitudes. Shaded and dotted areas represent, respectively, the regions of static instability (environmental lapse rate is greater than Γ_d) and static stability (environmental lapse rate is smaller than Γ_d and Γ_m). The white area between the abovementioned areas depicts the region of conditional (in)stability (environmental lapse rate is between Γ_d and Γ_m). In this graph, regions of static instability, conditional instability and static stability are delimited assuming a LCL at an altitude of LCL_1(Tmean). Observed temperatures are represented by box-plots: black crosses for near-surface temperatures gathered in Temperature/Relative Humidity data loggers at 06:00 (daily minimum temperature gathered in Cenicafe weather station (1,310 m) is assumed to take place at 06:00 am); red triangles for near-surface temperatures gathered in Temperature/Relative Humidity data loggers at 14:00 (daily maximum temperature gathered in Cenicafe is assumed to occur at 02:00 pm); confidence intervals represent +1.0 standard deviations.

Chapter 4 - Multi-model ensemble (MME-2012) simulation experiments: exploring the role of long-term changes in climatic conditions in the increasing incidence of *Plasmodium falciparum* malaria in the highlands of Western Kenya

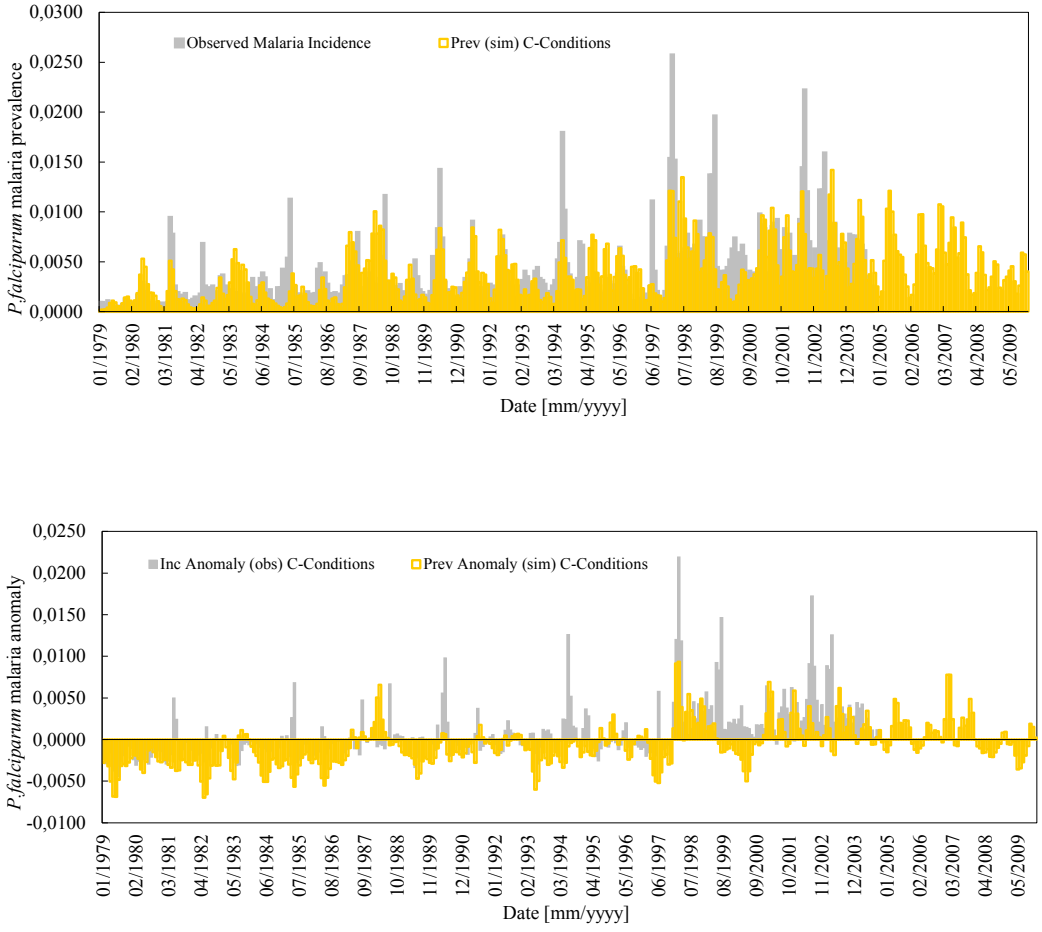

Figure SM-1(a). Monthly *Plasmodium falciparum* malaria incidence (top panel) and anomaly (bottom panel) observed in Kericho District, Kenyan highlands, over the period spanning from January, 1979 through October, 2004, along with monthly *P. falciparum* malaria prevalence (top panel) and anomaly (bottom panel) simulated by the **MAC model** for the actual climatic conditions (C-conditions) and for the

period spanning from January, 1979 through December, 2009. Daily mean temperatures were estimated as an average of daily minimum and maximum temperatures. R^2=0.30; MSE=1E-05.

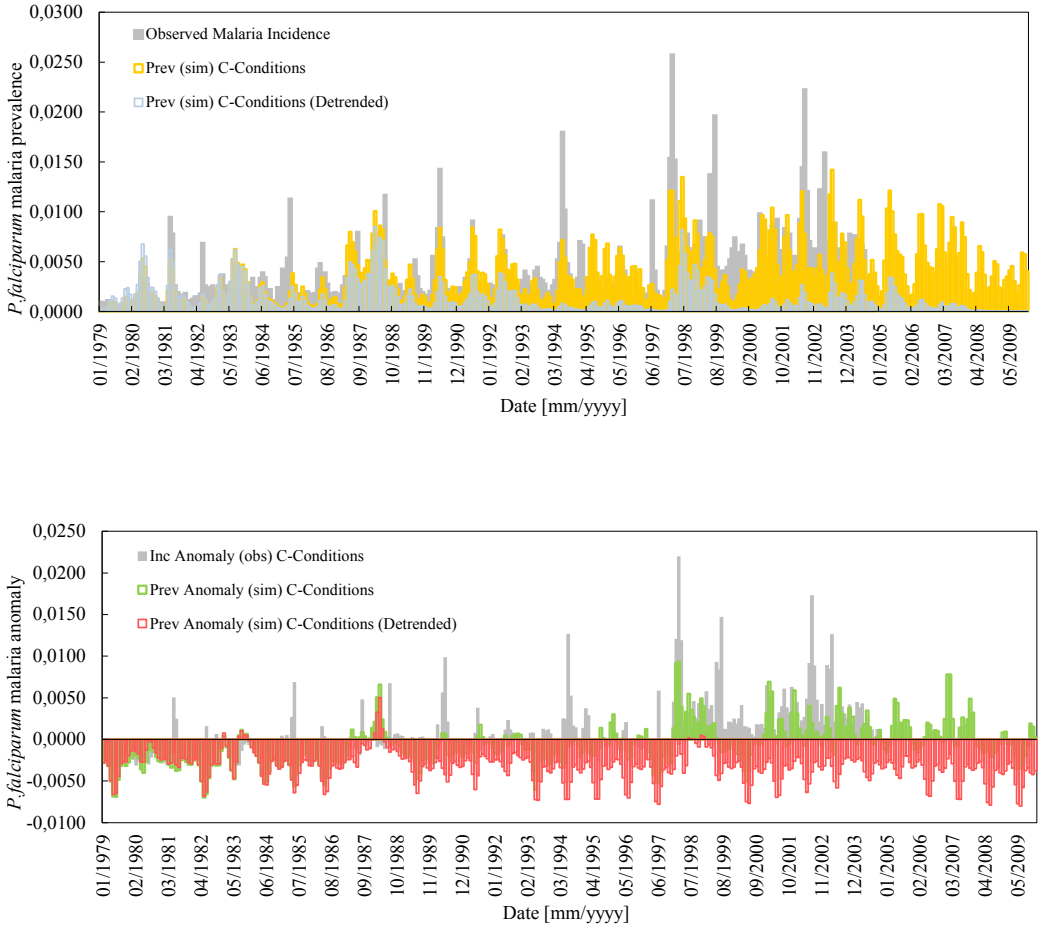

Figure SM-1(b). Monthly *Plasmodium falciparum* malaria incidence (top panel) and anomaly (bottom panel) observed in Kericho District, Kenyan highlands, over the period spanning from January, 1979 through October, 2004, along with monthly *P. falciparum* malaria prevalence (top panel) and anomaly (bottom panel) simulated by the **MAC model** for the actual climatic conditions (C-conditions) and +0.35°C/decade detrended mean temperature conditions (C-conditions Detrended) over the period

spanning from January, 1979 through December, 2009. Daily mean temperatures were estimated as an average of daily minimum and maximum temperatures.

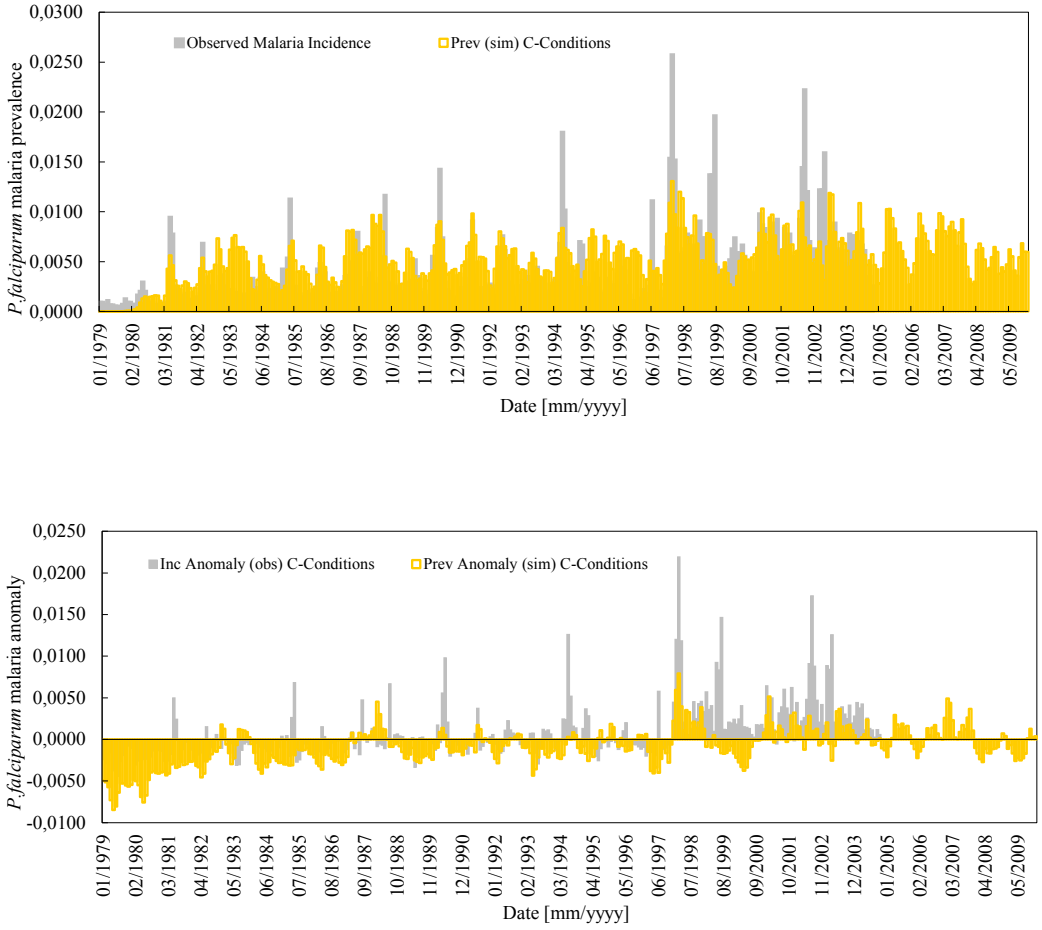

Figure SM-2(a). Monthly *Plasmodium falciparum* malaria incidence (top panel) and anomaly (bottom panel) observed in Kericho District, Kenyan highlands, over the period spanning from January, 1979 through October, 2004, along with monthly *P. falciparum* malaria prevalence (top panel) and anomaly (bottom panel) simulated by the **AM model** for the actual climatic conditions (C-conditions) and for the period spanning from January, 1979 through December, 2009. Daily mean temperatures were estimated as an average of daily minimum and maximum temperatures. R^2=0.28; MSE=1E-05.

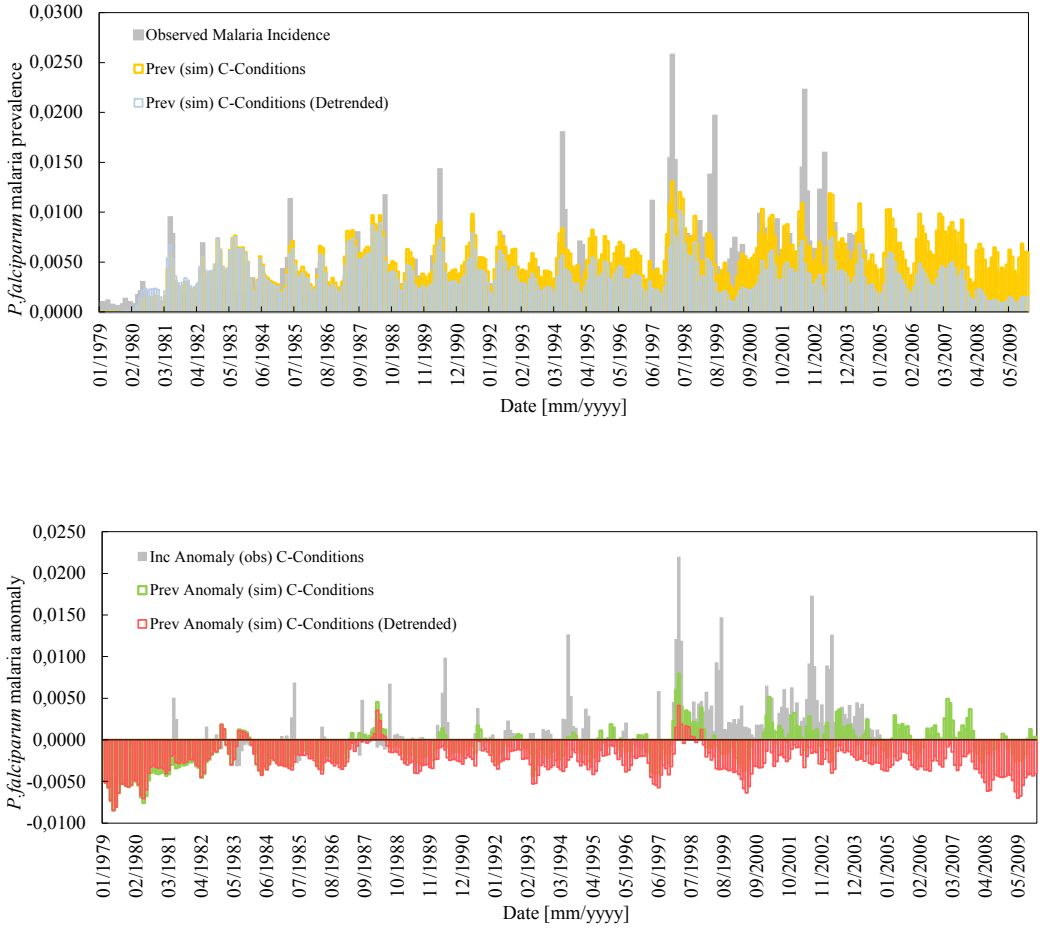

Figure SM-2(b). Monthly *Plasmodium falciparum* malaria incidence (top panel) and anomaly (bottom panel) observed in Kericho District, Kenyan highlands, over the period spanning from January, 1979 through October, 2004, along with monthly *P. falciparum* malaria prevalence (top panel) and anomaly (bottom panel) simulated by the **AM model** for the actual climatic conditions (C-conditions) and +0.35°C/decade detrended mean temperature conditions (C-conditions Detrended) over the period spanning from January, 1979 through December, 2009. Daily mean temperatures were estimated as an average of daily minimum and maximum temperatures.

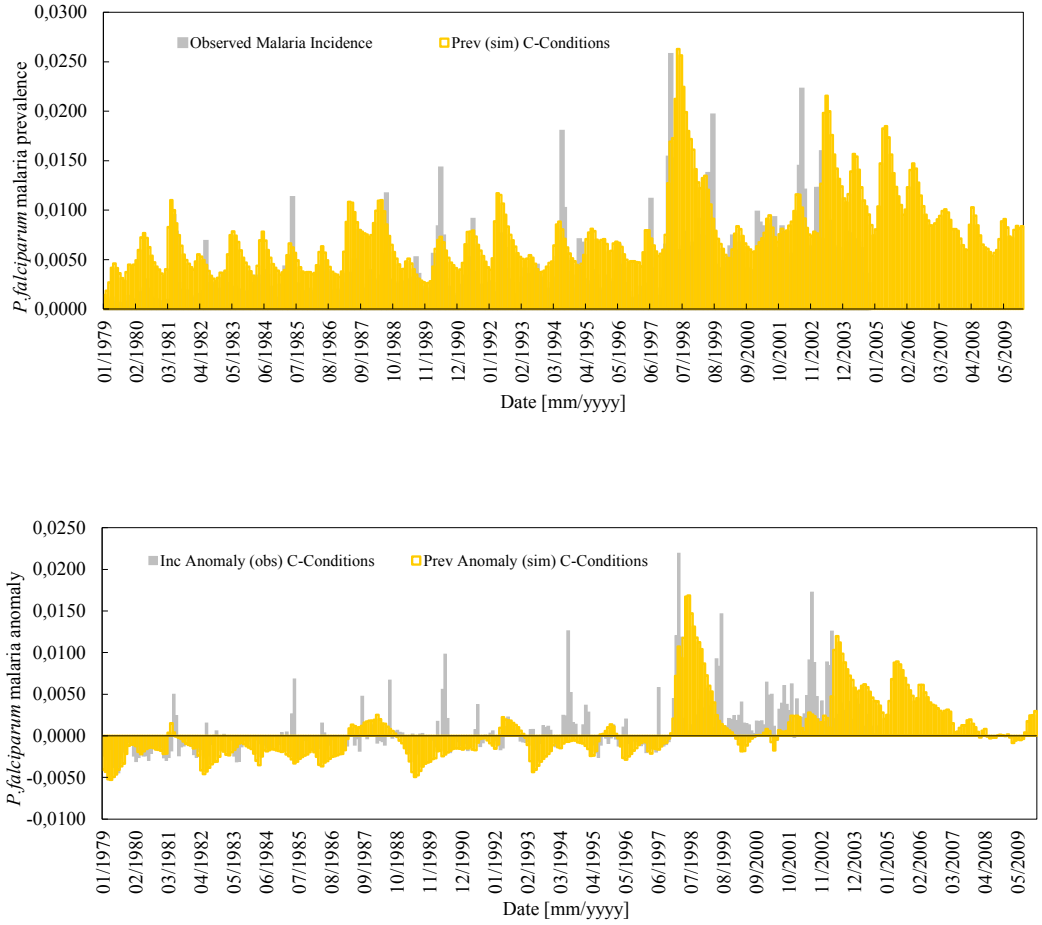

Figure SM-3(a). Monthly *Plasmodium falciparum* malaria incidence (top panel) and anomaly (bottom panel) observed in Kericho District, Kenyan highlands, over the period spanning from January, 1979 through October, 2004, along with monthly *P. falciparum* malaria prevalence (top panel) and anomaly (bottom panel) simulated by the **WCT model** for the actual climatic conditions (C-conditions) and for the period spanning from January, 1979 through December, 2009. Daily mean temperatures were estimated as an average of daily minimum and maximum temperatures. R^2=0.24; MSE=2E-05.

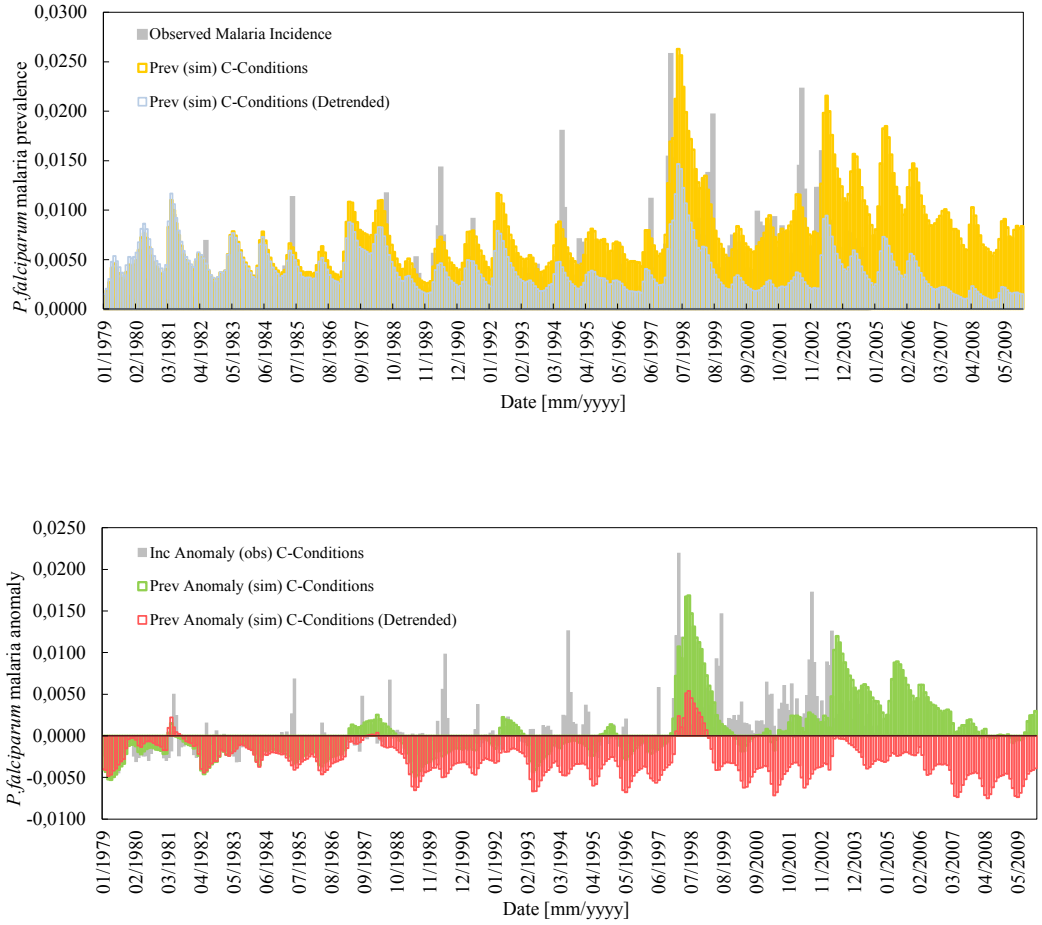

Figure SM-3(b). Monthly *Plasmodium falciparum* malaria incidence (top panel) and anomaly (bottom panel) observed in Kericho District, Kenyan highlands, over the period spanning from January, 1979 through October, 2004, along with monthly *P. falciparum* malaria prevalence (top panel) and anomaly (bottom panel) simulated by the **WCT model** for the actual climatic conditions (C-conditions) and +0.35°C/decade detrended mean temperature conditions (C-conditions Detrended) over the period spanning from January, 1979 through December, 2009. Daily mean temperatures were estimated as an average of daily minimum and maximum temperatures.

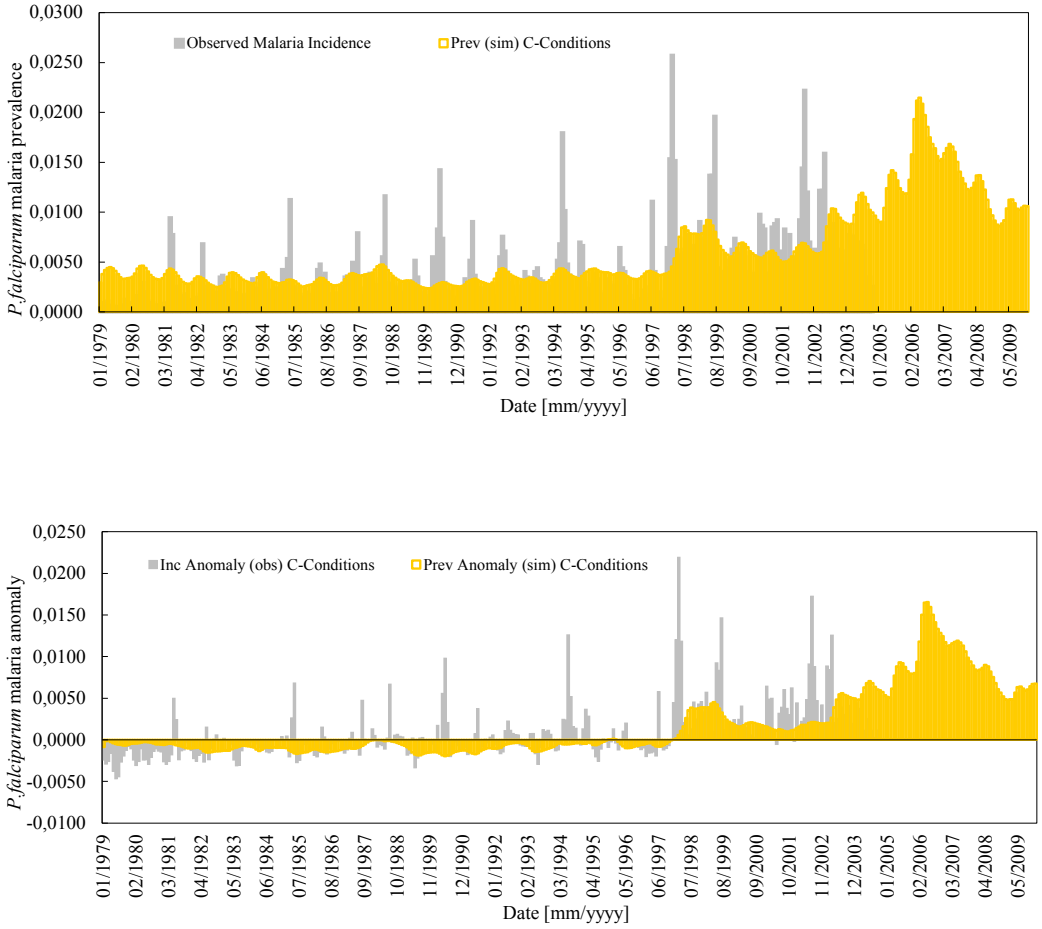

Figure SM-4(a). Monthly *Plasmodium falciparum* malaria incidence (top panel) and anomaly (bottom panel) observed in Kericho District, Kenyan highlands, over the period spanning from January, 1979 through October, 2004, along with monthly *P. falciparum* malaria prevalence (top panel) and anomaly (bottom panel) simulated by the **ABP model** for the actual climatic conditions (C-conditions) and for the period spanning from January, 1979 through December, 2009. Daily mean temperatures were estimated as an average of daily minimum and maximum temperatures. R^2=0.20; MSE=1E-05.

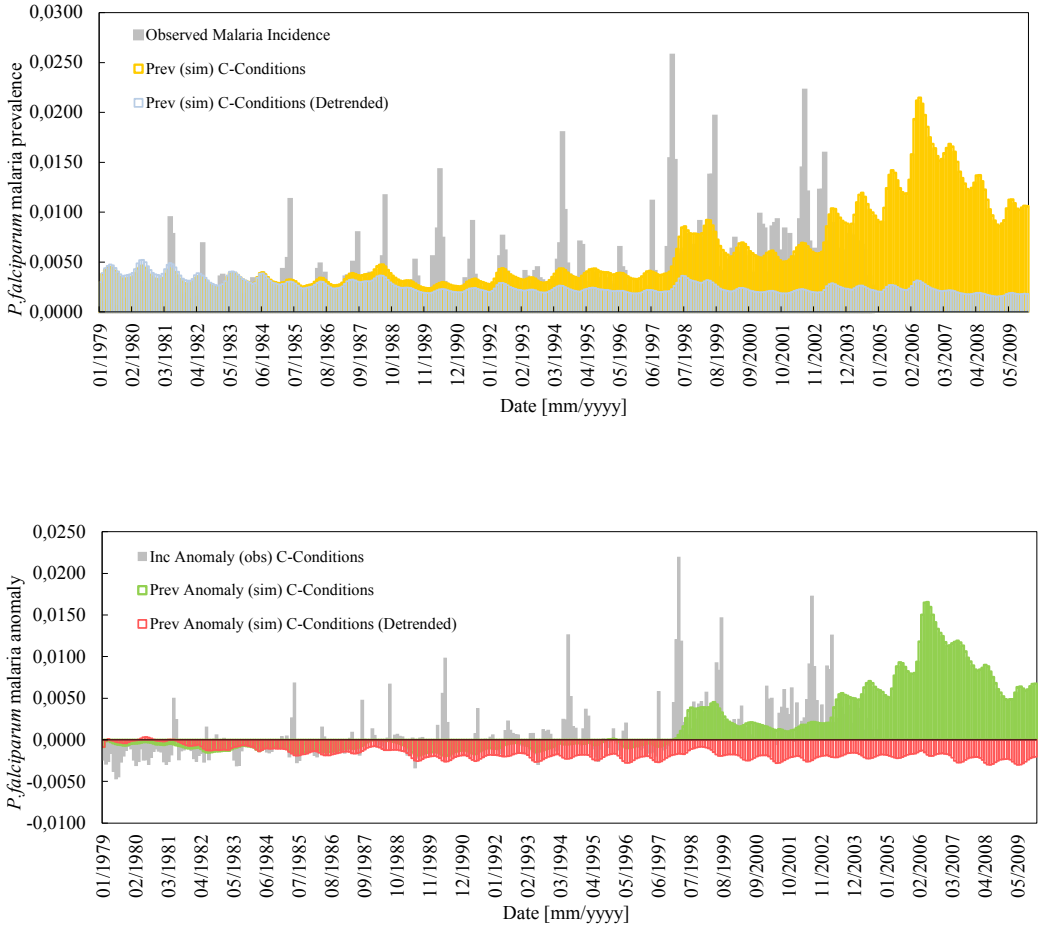

Figure SM-4(b). Monthly *Plasmodium falciparum* malaria incidence (top panel) and anomaly (bottom panel) observed in Kericho District, Kenyan highlands, over the period spanning from January, 1979 through October, 2004, along with monthly *P. falciparum* malaria prevalence (top panel) and anomaly (bottom panel) simulated by the **ABP model** for the actual climatic conditions (C-conditions) and +0.35°C/decade detrended mean temperature conditions (C-conditions Detrended) over the period spanning from January, 1979 through December, 2009. Daily mean temperatures were estimated as an average of daily minimum and maximum temperatures.

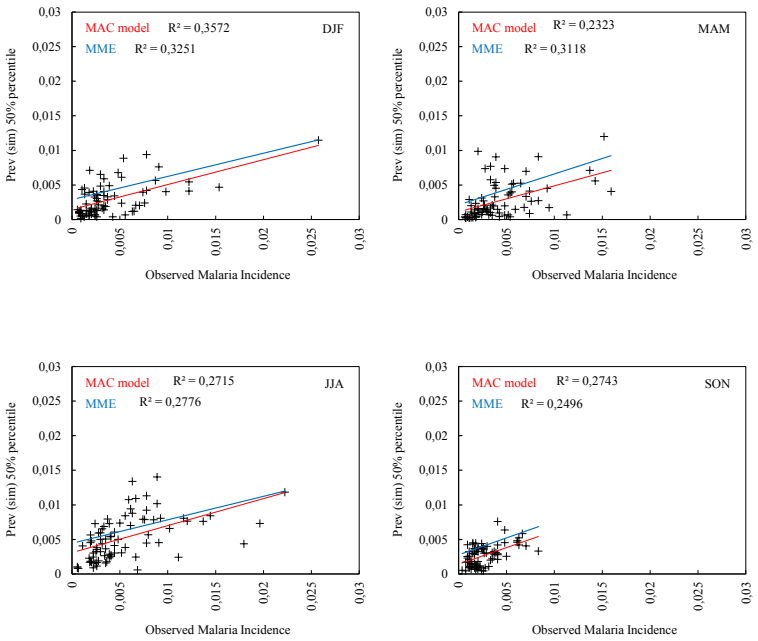

Figure SM-5(a). Monthly *Plasmodium falciparum* malaria incidence observed in Kericho District, Kenyan highlands, over the period spanning from January, 1979 through October, 2004 (x-axes) versus the 50% percentile of the distributions of *P. falciparum* malaria prevalence (y-axes) simulated by the MAC model for the quarters December-January-February (upper left panel), March-April-May (upper right), June-July-August (lower left), and September-October-November (lower right), for the actual climatic conditions observed over the period spanning from January, 1979 through December, 2009, and for a 1-month time lag. Red and blue solid lines represent the adjusted linear trends (see R^2-values on each panel) for each season and for the four-model ensemble (MME), respectively.

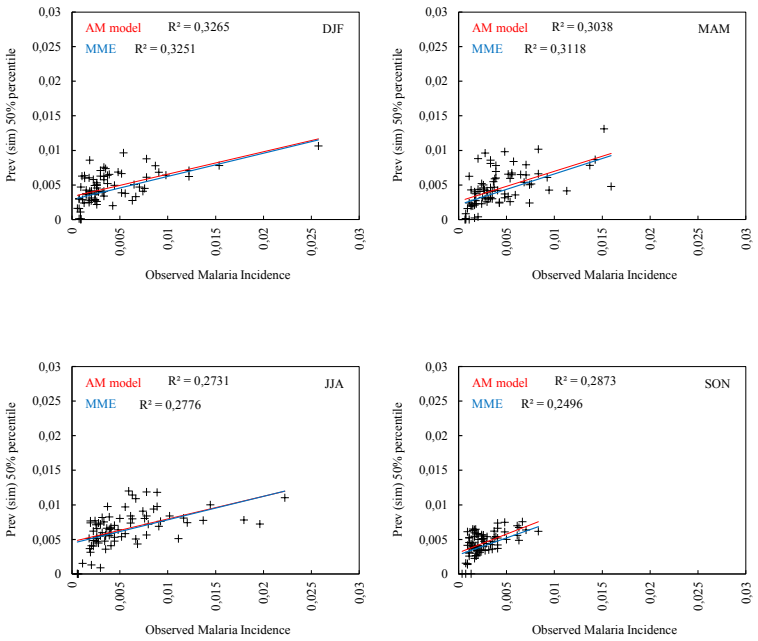

Figure SM-5(b). Monthly *Plasmodium falciparum* malaria incidence observed in Kericho District, Kenyan highlands, over the period spanning from January, 1979 through October, 2004 (x-axes) versus the 50% percentile of the distributions of *P. falciparum* malaria prevalence (y-axes) simulated by the AM model for the quarters December-January-February (upper left panel), March-April-May (upper right), June-July-August (lower left), and September-October-November (lower right), for the actual climatic conditions observed over the period spanning from January, 1979 through December, 2009, and for a 1-month time lag. Red and blue solid lines represent the adjusted linear trends (see R^2-values on each panel) for each season and for the four-model ensemble (MME), respectively.

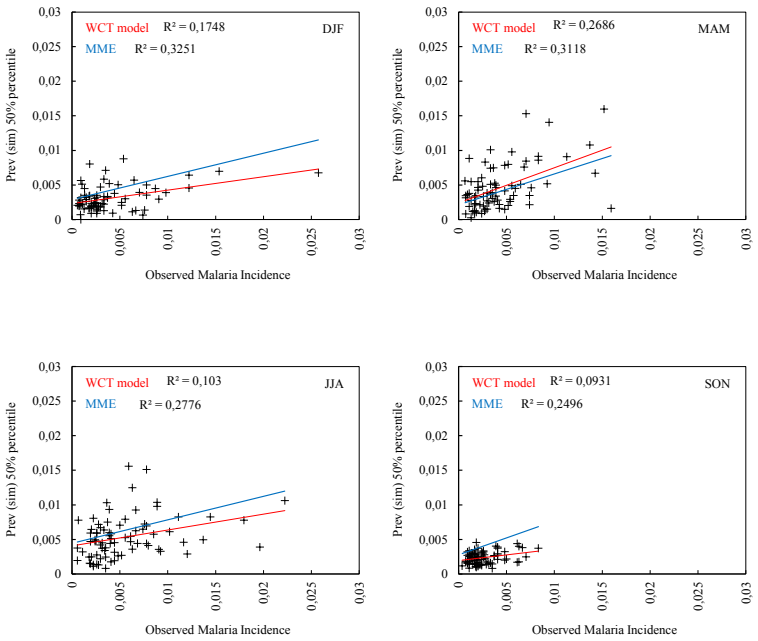

Figure SM-5(c). Monthly *Plasmodium falciparum* malaria incidence observed in Kericho District, Kenyan highlands, over the period spanning from January, 1979 through October, 2004 (x-axes) versus the 50% percentile of the distributions of *P. falciparum* malaria prevalence (y-axes) simulated by the WCT model for the quarters December-January-February (upper left panel), March-April-May (upper right), June-July-August (lower left), and September-October-November (lower right), for the actual climatic conditions observed over the period spanning from January, 1979 through December, 2009, and for a 2-month time lag. Red and blue solid lines represent the adjusted linear trends (see R^2-values on each panel) for each season and for the four-model ensemble (MME), respectively.

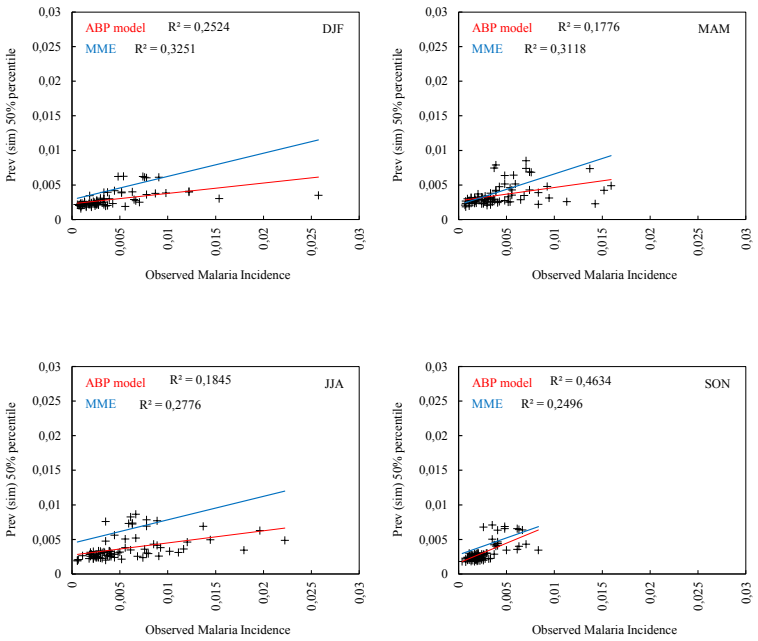

Figure SM-5(d). Monthly *Plasmodium falciparum* malaria incidence observed in Kericho District, Kenyan highlands, over the period spanning from January, 1979 through October, 2004 (x-axes) versus the 50% percentile of the distributions of *P. falciparum* malaria prevalence (y-axes) simulated by the ABP model for the quarters December-January-February (upper left panel), March-April-May (upper right), June-July-August (lower left), and September-October-November (lower right), for the actual climatic conditions observed over the period spanning from January, 1979 through December, 2009, and for a 0-month time lag. Red and blue solid lines represent the adjusted linear trends (see R^2-values on each panel) for each season and for the four-model ensemble (MME), respectively.

Chapter 5 - Implementation of malaria dynamical models in municipality-level Early Warning Systems in Colombia – Supplementary material Part I

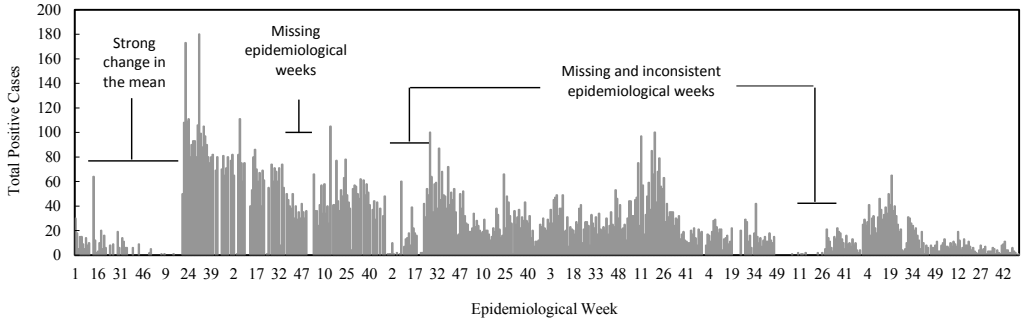

(A)

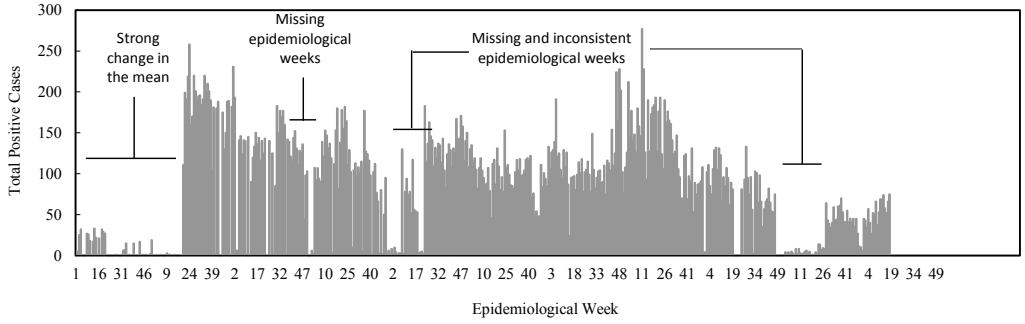

(B)

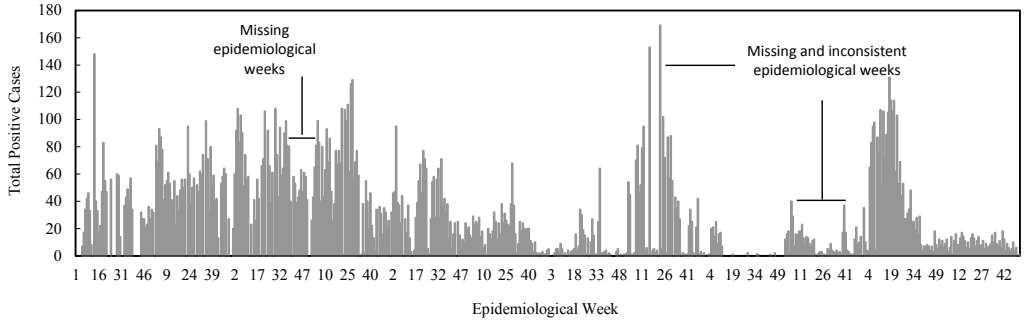

(C)

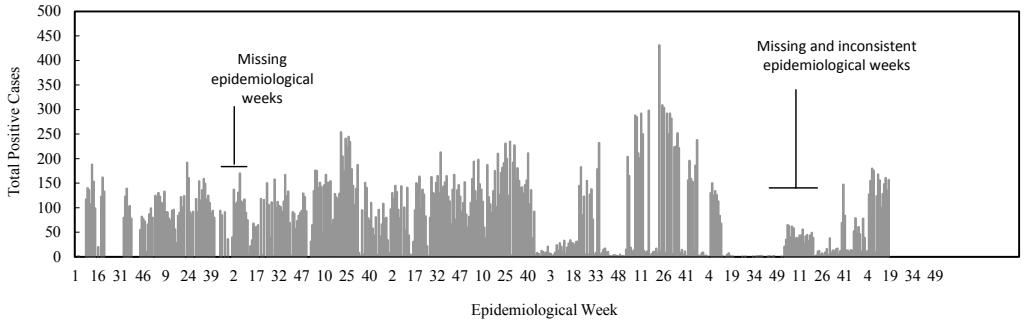

(D)

Figure SM-I-1. Malaria positive cases observed, per epidemiological week-EW, in the municipalities of Montelíbano (top panels A: for *Plasmodium falciparum* and B: for *P. vivax*) and Puerto Libertador (bottom panels C: for *P. falciparum* and D: for *P. vivax*) over the base period spanning from January 3, 2000 through January 1, 2012 (1st EW, 2000 through 52nd EW, 2011).

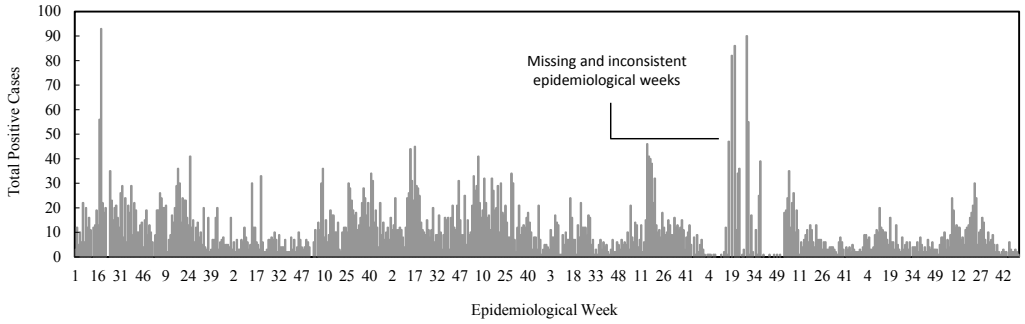

(A)

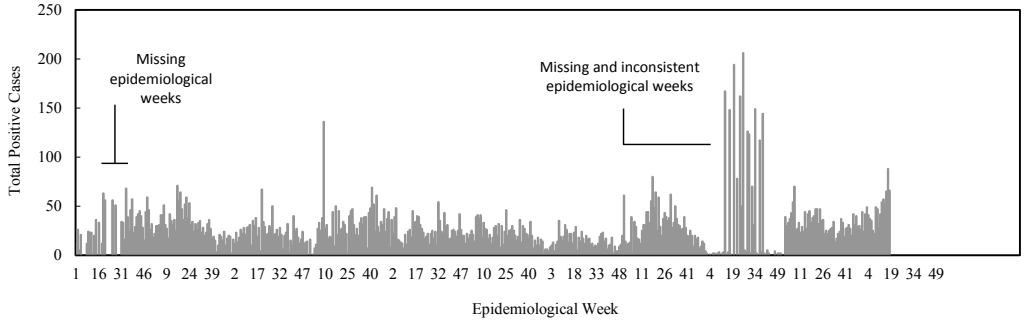

(B)

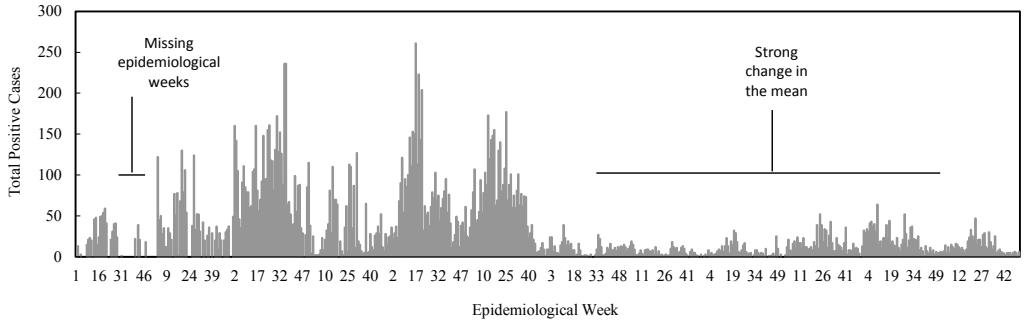

(C)

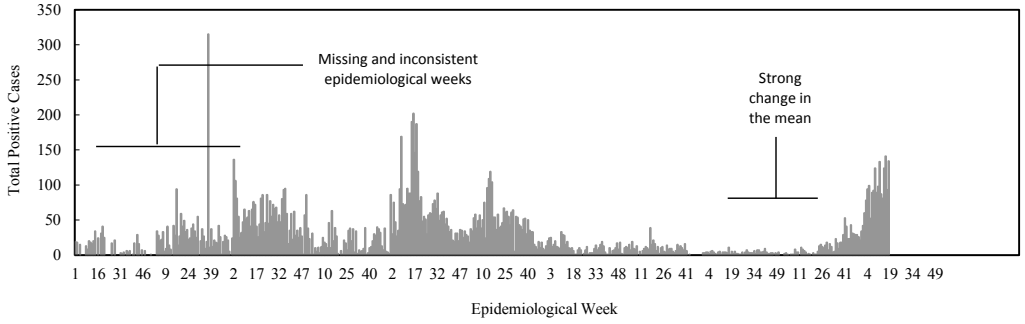

(D)

Figure SM-I-2. Malaria positive cases observed, per epidemiological week-EW, in the municipalities of San José del Guaviare (top panels A: for *Plasmodium falciparum* and B: for *P. vivax*) and Buenaventura (bottom panels C: for *P. falciparum* and D: for *P. vivax*) over the base period spanning from January 3, 2000 through January 1, 2012 (1st EW, 2000 through 52nd EW, 2011).

Chapter 5 - Implementation of malaria dynamical models in municipality-level Early Warning Systems in Colombia – Supplementary material Part II

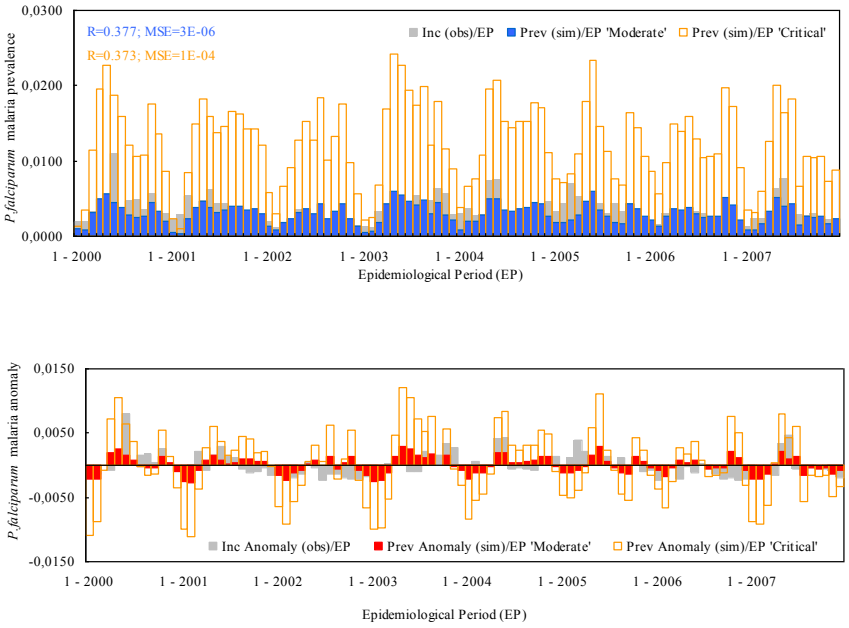

Figure SM-II-1. *Plasmodium falciparum* malaria incidence (grey solid bars) observed in the municipality of San José del Guaviare over a 2,919-day simulation period spanning from January 3, 2000 through December 30, 2007, or Epidemiological Week 01/2000 to EW 52/2007, along with *P. falciparum* malaria prevalence per epidemiological period simulated by the WCT model for moderate (blue and red solid bars in top and bottom panels) and critical (orange bars) conditions. See also correlation coefficients (R) and mean square errors (MSE) on the top left corner of the top panel. In the bottom panel, time series are plotted as anomalies with respect to the *P. falciparum* malaria incidence mean historical value.

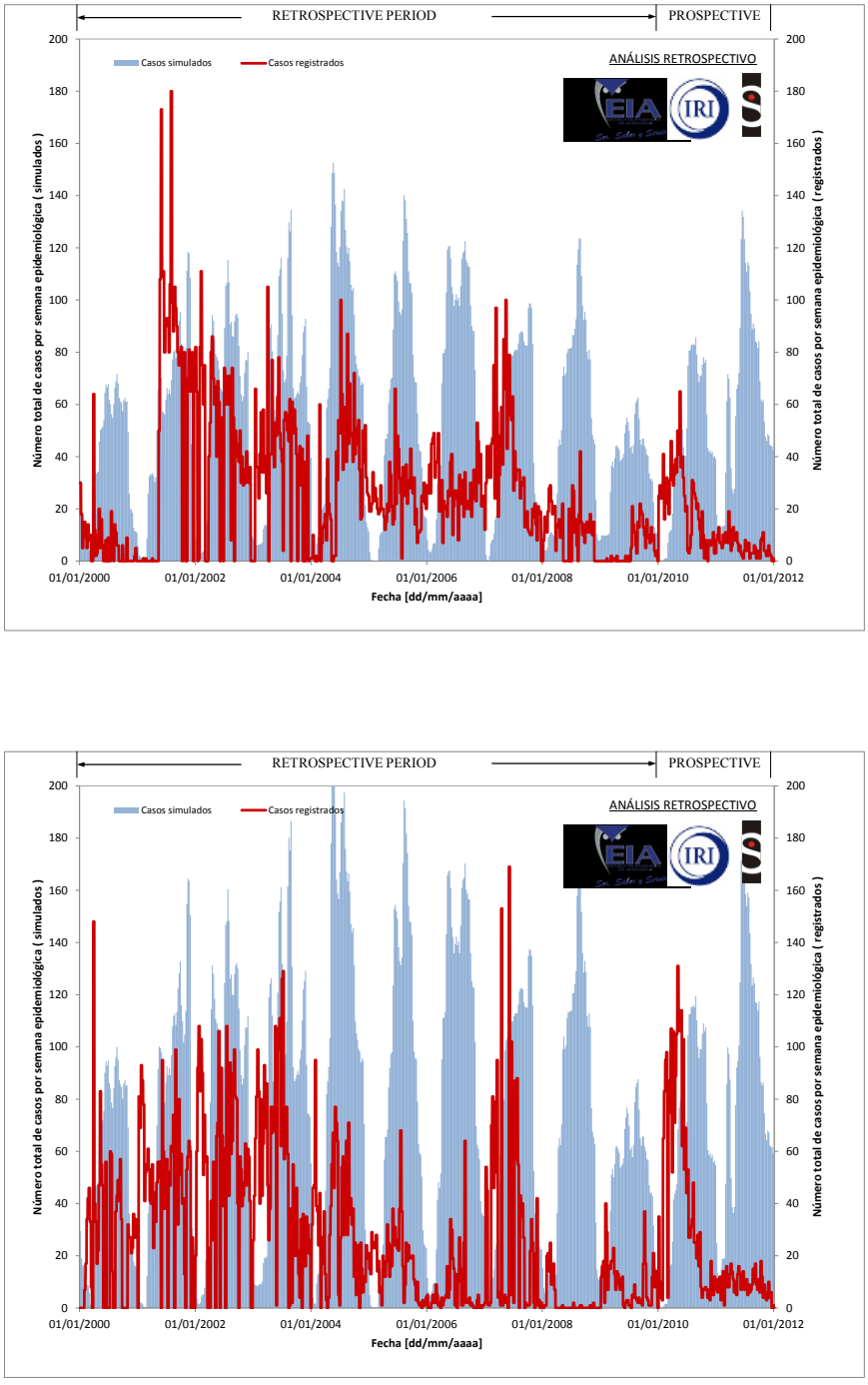

Figure SM-II-2a. Weekly *Plasmodium falciparum* malaria positive cases observed in the municipalities of Montelíbano (top panel) and Puerto Libertador (bottom panel) over the period spanning from January 3,

2000 through January 1, 2012 (epidemiological week EW 01 / 2000 through EW 52 / 2011) – see red solid line, along with weekly *P. falciparum* malaria positive cases simulated by the WCT model (see blue solid bars) for the observed climatic, entomological and socioeconomic conditions.

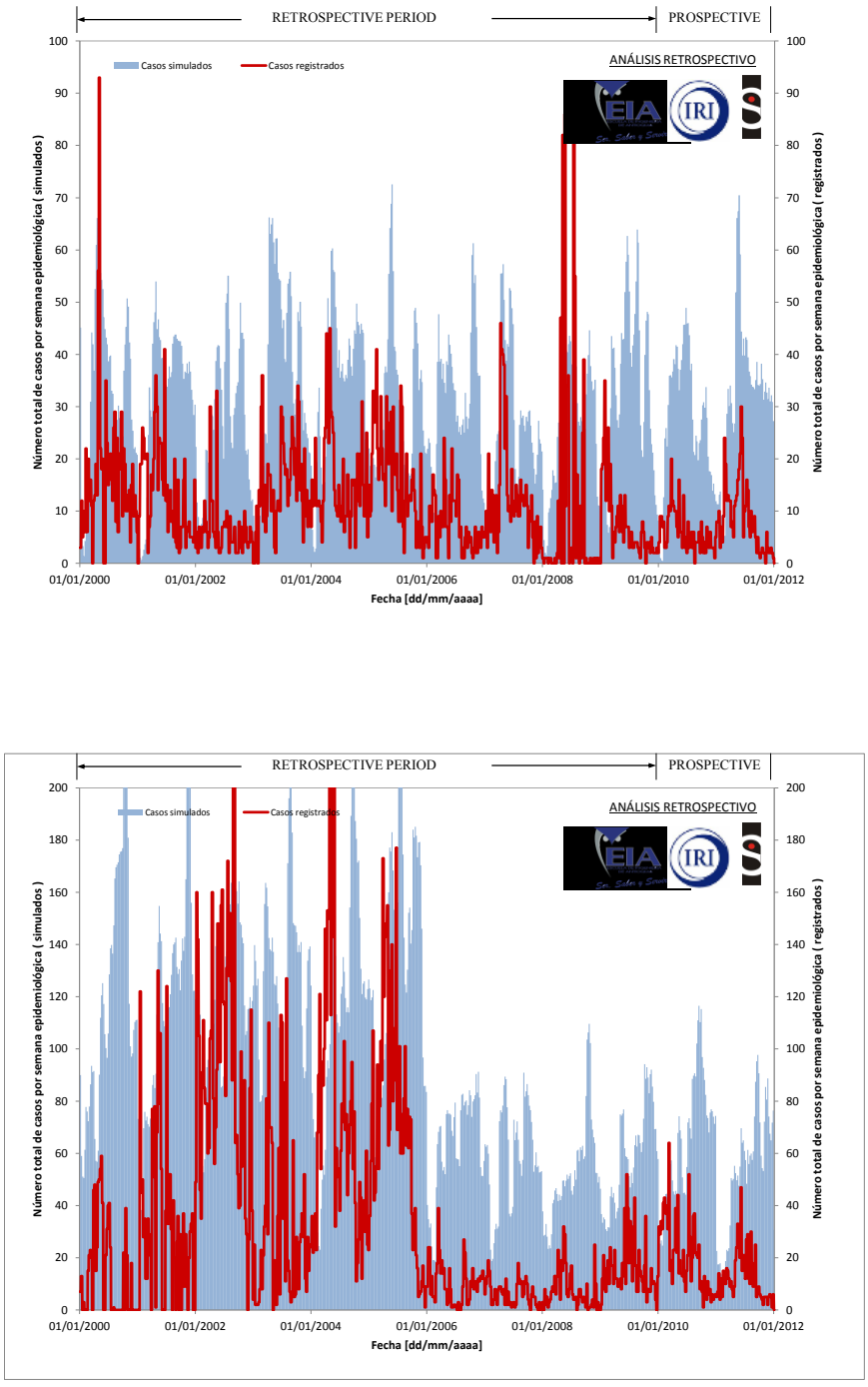

Figure SM-II-2b. Weekly *Plasmodium falciparum* malaria positive cases observed in the municipalities of San José del Guaviare (top panel) and Buenaventura (bottom panel) over the period spanning from

January 3, 2000 through January 1, 2012 (epidemiological week EW 01 / 2000 through EW 52 / 2011) – see red solid line, along with weekly *P. falciparum* malaria positive cases simulated by the WCT model (see blue solid bars) for the observed climatic, entomological and socioeconomic conditions.

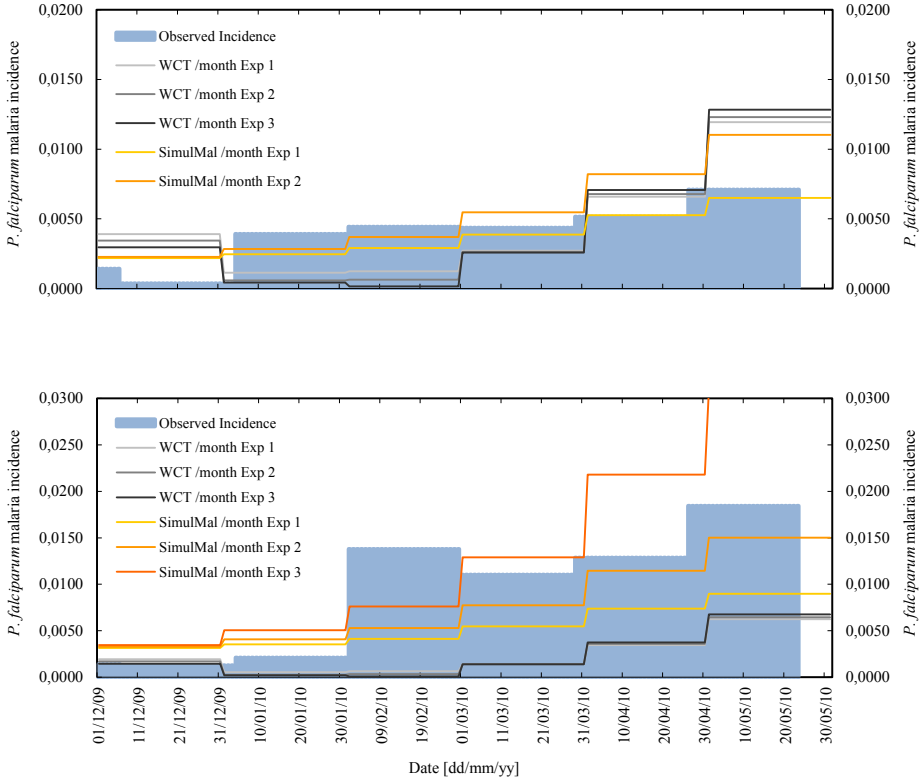

Figure SM-II-3. Monthly *Plasmodium falciparum* malaria incidence suggested by the WCT and SimulMal models for the forecast horizon spanning from December 1, 2009 through May 31, 2010, and for the pilot municipalities of Montelíbano (top panel) and Puerto Libertador (bottom panel). Exp 1, 2 and 3 represent the proposed short-term climate forecast (seasonal forecast) experiments. Only changes in climatic conditions are considered in these simulations.

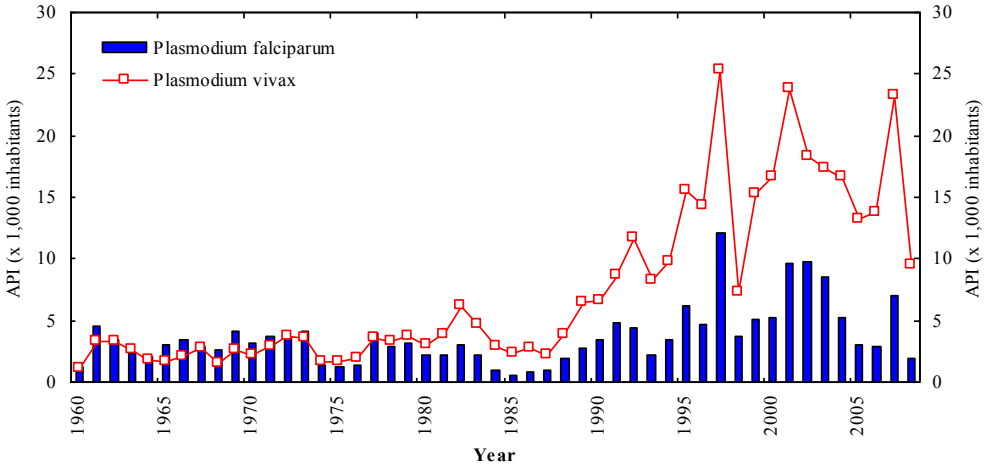

Figure SM-II-4. *Plasmodium falciparum* (blue bars) and *P. vivax* (red solid line) malaria incidence observed in the Department of Córdoba over the period 1960-2008. API stands for Annual Parasite Index and is expressed in total positive cases per 1,000 inhabitants (source of info: Gobernación de Córdoba, Secretaría de Desarrollo de la Salud, Programa Control de Vectores).

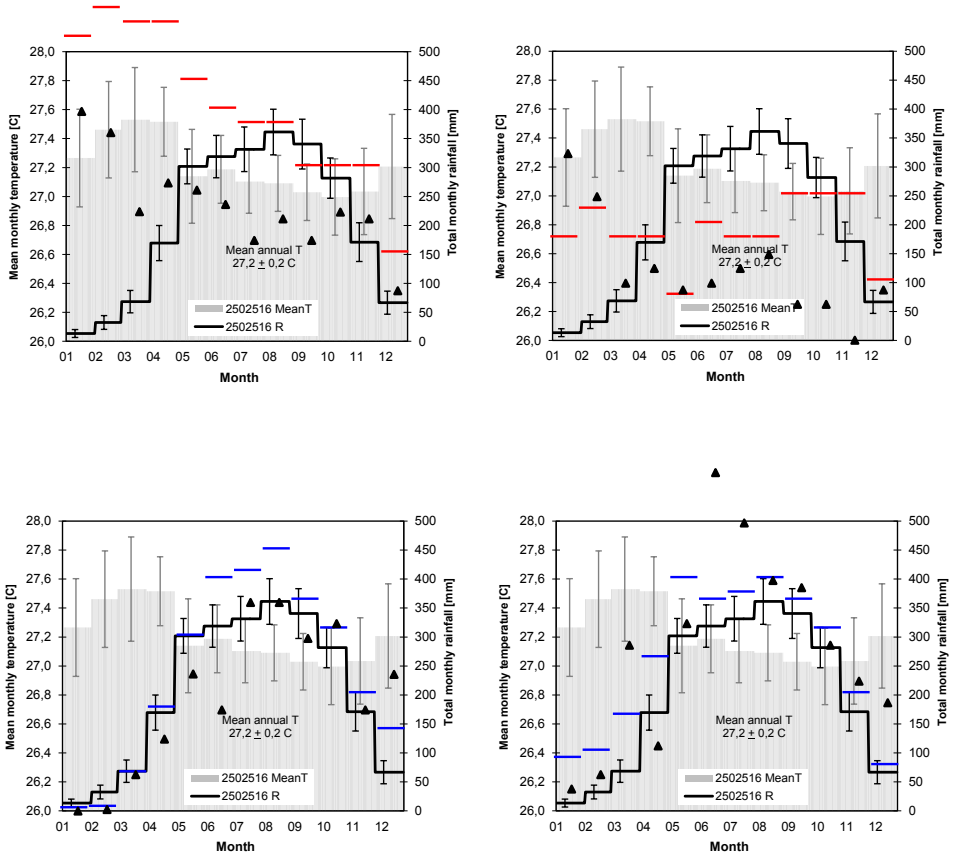

Figure SM-II-5a. Historical annual cycles of mean temperature (grey solid bars) and rainfall (black solid lines) observed in the surroundings of the municipalities of Montelibano and Puerto Libertador, according to available climatic records gathered at the weather station 2502516 Cuba Hda over the periods 1978-2009 and 1973-2009, respectively. Error bars indicate confidence intervals for a α=0.05 significance level. Red and blue short lines depict, respectively, the monthly mean temperatures and total rainfall amounts suggested by ECHAM4.5 individual seasonal forecasts for years 2010 (left panels) and 2011 (right panels). Black solid triangles represent the actual (observed) monthly mean temperatures and total rainfall amounts gathered at the weather station Cuba Hda in the same years (records for the period 2010-to present were provided by the National Institute of Health in July, 2012).

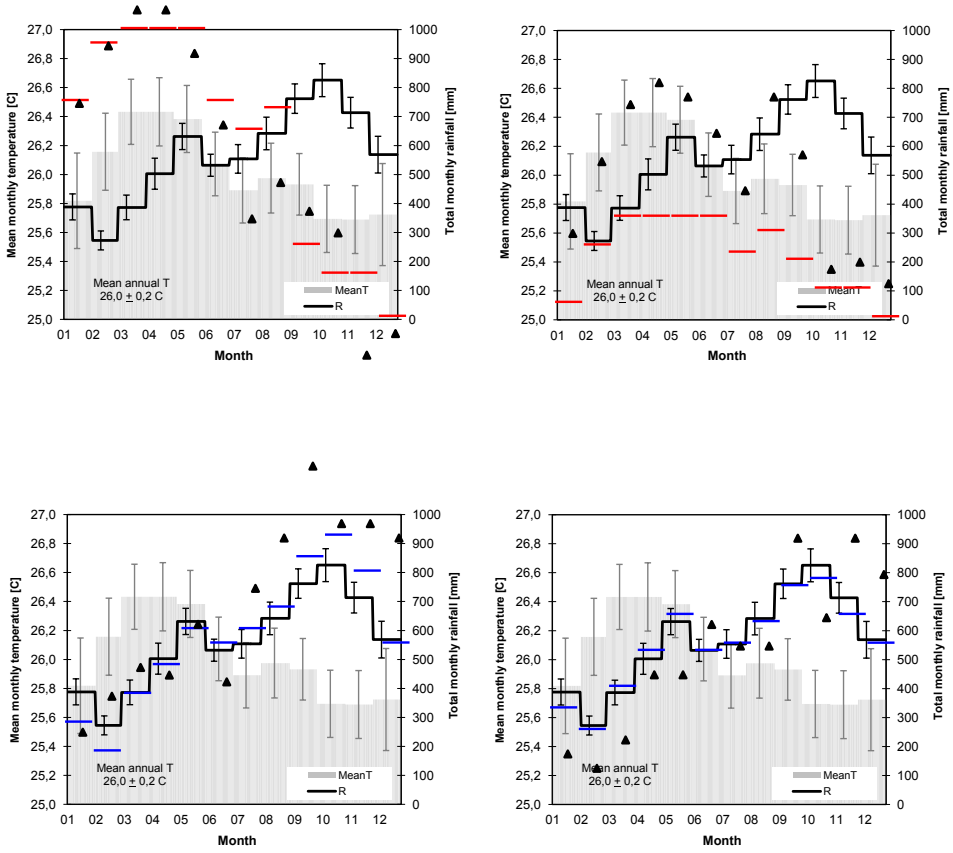

Figure SM-II-5b. Historical annual cycles of mean temperature (grey solid bars) and rainfall (black solid lines) observed in the surroundings of the municipality of Buenaventura, according to available climatic records gathered at the synoptic weather station 5311501 Apto Buenaventura over the periods 1946-2010 and 1983-2010, respectively. Error bars indicate confidence intervals for a α=0.05 significance level. Red and blue short lines depict, respectively, the monthly mean temperatures and total rainfall amounts suggested by ECHAM4.5 individual seasonal forecasts for years 2010 (left panels) and 2011 (right panels). Black solid triangles represent the actual (observed) monthly mean temperatures and total rainfall amounts gathered at the weather station Apto Buenaventura in the same years (records for the period 2010-to present were provided by the National Institute of Health in July, 2012).